The Effects of Cam Femoroacetabular Impingement on Mechanical Hip Joint Loading

Kwan-Ching Geoffrey Ng

A research thesis submitted to the Faculty of Graduate and Postdoctoral Studies
in partial fulfillment of the requirements for the degree of

DOCTOR OF PHILOSOPHY

in Mechanical Engineering

Department of Mechanical Engineering
University of Ottawa
Ottawa, Ontario, Canada

給我的親愛老媽子和婆婆
to my dearest mums and poys

Acknowledgements

This experience taught me that research is no more about seeking the right answers than it is about seeking the right questions. Over the course, I was very privileged and fortunate to have worked with prominent researchers from the areas of mechanical engineering, human kinetics, clinical orthopaedics and biomechanics, and diagnostic imaging. These collaborative efforts and discussions greatly influenced and developed the scope of this multidisciplinary dissertation.

I would first like to express my sincerest appreciation for my supervisors, Prof. Mario Lamontagne and Prof. Michel Labrosse. Not everyone will have the privilege to say that they were supervised by "*The* Mountain" and "*The* Brush". Mario provided me with his valuable guidance, leadership, and continual support, both in and out of the lab. More importantly, it was Mario's confidence and trust in me, as an independent researcher, that enabled me to strive for greater findings. Moreover, Michel has always been ready and willing to go above and beyond to help (especially during the frustrating times with modelling). Michel taught me by way of example and always demonstrated the values of a righteous biomedical engineer.

I would like to express my sincerest gratitude to Dr. Paul Beaulé, for his profound clinical insights, directions, and continual support. With his outstanding leadership, Paul shared his visions and initiatives of early hip joint preservation, which contributed substantially to the foundation of the research program and to the learning objectives of this dissertation.

I would like to thank my Thesis Advisory Committee members, Prof. Hanspeter Frei and Prof. Thomas Blaine Hoshizaki, for their guidance and support. Hanspeter's and Blaine's critical insights helped craft my study designs and contributed to my multidisciplinary research experience. I would like to also thank Prof. Li Jing-Xian and Prof. Daniel Benoit, for their valuable mentoring and, of course, their much needed reminders.

I would like to give special thanks to Dott.ssa Guilia Mantobravi for her insightful inputs and, more importantly, for being an arm's length away (most of the time) for our urgent (de)motivational consultations. I would like to also acknowledge Mr. Hakim Louati, Prof. Andrew Speirs, Mr. Daniel Varin, and Dr. Kawan Rakhra for their valuable insights into many of the technical methods and clinical applications presented in this dissertation. Also, sincere thanks to Teresa Flaxman, Kevin Dwyer, Marshall Kendall, Danilo Catelli, Sarah Reynolds, and Erik Kowalski for their help and input over the course of the dissertation.

Last, but definitely not least, thank you very much to my dearest Anna – my proudest supporter, my harshest reviewer, and my injection of motivation. There are no words to measure my appreciation. Every step of the way, you celebrated my exciting little bits of progress and experienced my most frustrating adversities with me. Thank you for pushing me to always be ambitious, critical, and prepared to compete. Thank you for challenging me to always do better and be better.

Abstract

A major contributing factor to the onset of early hip osteoarthritis is attributed to an enlarged, aspherical femoral head deformity, characterized as cam-type femoroacetabular impingement (FAI). The presence of the cam deformity alone does not explain differences in pathomechanisms and it has been theorized that adverse loading to the subchondral bone may play a predominant mechanical role in early joint degeneration. This doctoral thesis examined the adverse hip joint loading due to cam FAI and characterize mechanical stimuli associated with symptoms. Specifically, this research: 1) examined anatomical and functional characteristics associated with the cam morphology; 2) developed subject-specific finite element hip joint models to examine hip joint stresses, incorporating subject-specific geometries, materials properties, and joint loading; and 3) implemented loading parameters during level walking and squatting to examine hip joint stresses.

First, a classification study was conducted to recruit three participant groups: 1) symptomatic (where participants had the cam deformity and pain); 2) asymptomatic (where participants had the cam deformity, but no pain); and 3) control (where participants did not have the cam deformity or clinical signs). Each participant's CT data were evaluated for multiple anatomical hip joint parameters and then re-classified into their respective subgroups, using a discriminant function analysis, based on the most significant parameters. In addition to the cam deformity, symptomatic individuals had a lower femoral neck-shaft angle and reduced pelvic range of motion.

Second, using the classified participants, hip joint loading was determined for the various severities of cam FAI, with respect to alterations in hip contact forces and anatomical considerations. Hip joint assemblies were segmented and reconstructed from subject-specific CT and MRI data, where bone densities were quantified from CT data. A parametric study was conducted to understand how varying material properties and loading conditions affected the sensitivity of the predictive models, examining the most appropriate modelling parameters to capture relative measurements.

Third, in conjunction with the first two studies, hip contact forces for level walking and squatting tasks were applied to corresponding subject-specific models and simulated. As a cross-sectional analysis, the stress magnitudes and regions described the joint loading in vivo for each

subject group and ascertained the risk of remodeling. For each subgroup (symptomatic, asymptomatic, control), the participants with the largest and smallest femoral neck-shaft angles were selected and compared. The symptomatic model with the lowest femoral neck-shaft angle demonstrated the highest stress on the cartilage, during walking and squatting, and on the subchondral bone, during squatting. The asymptomatic models showed cartilage stresses similar to the control group, but experienced high-risk subchondral bone stresses, similar to the symptomatic group. For both symptomatic and asymptomatic groups, the acetabular subchondral bone stresses coincided with known areas of bone adaptation and proteoglycan depletion.

The outcome of this research program supported that cartilage degradation might not be due to direct contact shear stresses, but perhaps rather attributed to the indirect effects of a stiffer subchondral bone plate. Individuals with a large cam deformity and decreased femoral neck-shaft angles are likely to experience severe subchondral bone stresses during higher amplitudes of hip motion. This provides clinicians with indications of how the pathology exacerbates and where initial cartilage delamination will likely occur, allowing them to perform the correct assessments and proceed with the correct form of care. From a patient's perspective, an early and accurate diagnosis could inhibit cartilage degradation and the progression of osteoarthritis.

Preface

The contents of this dissertation are organized into five parts, with each part arranged into multiple chapters, as follows:

I. *Opening*, which introduces the background, research statement, literature reviews, and theoretical and conceptual frameworks,

II. *Anatomical and Functional Characteristics*, which describes anatomical and functional associations with cam-type femoroacetabular impingement,

III. *Determining Appropriate Modelling Characteristics*, which illustrates the technical protocols of modelling and characterizing the hip joint geometries and material properties,

IV. *Modelling of Clinically Relevant Scenarios*, which examines adverse hip joint stresses during two loading situations,

V. *Closing*, which includes the points of discussion, limitations, recommendations, and concluding remarks.

The dissertation is comprised of seven original research articles. I was lead author for all seven articles and was fully involved with: 1) the conception and design of the studies, acquisition of the data, analysis and interpretation of the data; 2) drafting the articles and revising them critically for important scientific and intellectual content; and 3) final approval of the versions to be submitted. At the time of thesis submission, the seven articles were either published, accepted, or prepared for peer review in journals specializing in areas of clinical orthopaedics, biomechanics, engineering, and scientific research. Each of the seven articles, within this doctoral thesis, was formatted to the journal's and publisher's requirements.

Lastly, I have no conflicts of interest to report and certify that the research ethics of both institutions (University of Ottawa and The Ottawa Hospital) approved the investigation protocols (Appendix B – Ethics). All investigations were conducted in conformity with ethical research principles and informed consent for participation in the study was obtained.

Table of Contents

List of Figures

List of Tables

I Opening

1 Introduction

Statement | Rationale | Background

1.0 Statement

By 2020, almost one in five Canadians will suffer from osteoarthritis (OA) [22] – a debilitating and painful, degenerative joint condition. For many, the thought of OA not only means severe hip pain and reduced mobility, but also translates into work absenteeism, loss of income, decreased productivity, increased medication, and more time and money spent on rehabilitation treatments. This contributes, in part, to the 32,300 total hip replacements in Canada each year [53], and will resultantly incur an approximate annual economic burden of $405B, by the year 2020 [22].

Pathological deformities leading to mechanical hip joint failures constitute a large proportion of ongoing challenges in orthopaedics. Although the hip can remain functional, the deformity may lead to early anatomical and functional adaptations, resulting to progressive cartilage degradation. It has been theorized that a major contributing factor to the onset of early adult hip OA is attributed to an enlarged, aspherical femoral head deformity, which causes joint stiffness and pain at higher amplitudes of motion [3]. Characterized as cam femoroacetabular impingement (FAI), the prevalence of this pathomechanical failure process is present in approximately 25% of men and 5% of women [74], however, it was not until the last decade that a closer association was identified between cam FAI and hip degeneration [42, 43].

Based on a recent cost analysis in the US, by Kahlenberg and associates [58], FAI patients included in their cost study visited up to four health care providers, underwent more than three diagnostic imaging tests, and tried three different treatments, all prior to receiving a correct diagnosis of labral damage due to FAI. The duration between the initial onset of symptoms and diagnosis for the FAI patients lasted approximately 32 months, while incurring an average cost of $2,457 USD, per patient towards Medicare. With current literature on FAI focusing primarily on radiographic indications, surgical methods and success rates, patient follow-up data, and subsequent comprehensive literature reviews, very little research has been performed to examine the effects of the cam morphology and the pathomechanics of FAI.

With the ultimate goal to better understand the pathomechanisms of cam FAI, the purpose of this research will be to address the question at large: *what are the effects of cam FAI on mechanical hip joint loading?* This research proposes to:

- Examine the anatomical and functional characteristics associated with cam FAI symptoms

- Reconstruct a comprehensive subject-specific, computational hip joint model with the cam morphology
- Examine the contact stresses in the hip joint with the cam morphology, using finite element methods

1.1 Rationale

Femoroacetabular impingement (FAI) has received a great extent of clinical and biomechanical interest, with an exponentially increasing rate of scientific publications in recent years [74]. The concept of FAI remains elusive and sometimes wrongly associated with other hip morphologies [46, 83, 112], with the aetiology and prevalence of the cam morphology still unanswered [47, 112].

The morphology leading to mechanical FAI occurs when the anterosuperior aspect of the femoral head obstructs the acetabulum during large and combined motions in hip flexion and rotation [29, 100], as well as during squatting [26, 67, 69]. Patients with a more severe and larger cam deformity, as defined by higher alpha angles [13, 111], can be susceptible to anterosuperior cartilage and chondrolabral damage [13, 14]. Although the pathomechanism of FAI involves a complex spectrum of anatomical and functional parameters, the detection protocols to recognize the symptomatic morphology remains an ongoing challenge [42]. It is therefore imperative to increase the understanding of this hip disorder and its effect on daily activities.

Although patients have demonstrated different hip kinematics at a higher range of motion, such as during deep squatting [67, 69] resulting in higher hip joint stresses [86], it is still unclear why many individuals with a cam deformity do not exhibit any clinical signs [49, 91, 95], thus categorizing these individuals as asymptomatic [25, 47, 59, 107]. Moreover, the worry lies with the early adaptation of the subchondral bone, perhaps initiated earlier due to the presence of the cam deformity [93]. Knowing that both symptomatic and asymptomatic individuals with a similar cam deformity experience changes in subchondral bone density [103, 104], which may lead to eventual OA, it is imperative to delineate the differences of the asymptomatic group from the symptomatic patients and healthy individuals, in efforts to establish a better detection protocol and explain the risk of symptoms.

1.2 Background

1.2.1 History

The concept of FAI was initially introduced as a combination of various mechanical hip disorders and multi-factorial failure processes. A relationship was initially established between proximal femoral, "head-tilt" abnormalities with the onset of hip OA [83], where subsequently correlations were established between femoral head deformities following a slipped capital femoral epiphysis (SCFE). However, the early theories and relationships were not yet supported with clinical evidence. The "pistol grip" term was also used to describe the shape of the femoral head-neck, in comparison with a pistol handle, from anterior-posterior (AP) radiographs (Figure 1.1) [106]. The abnormal geometric configurations showed signs of early cartilage degeneration, but no direct correlations were evident between the deformity and end-stage OA. At this point, the observations were based on visual interpretations of radiographic evidence and no work was done to determine the attainable motions in a "pistol grip" joint [48, 106].

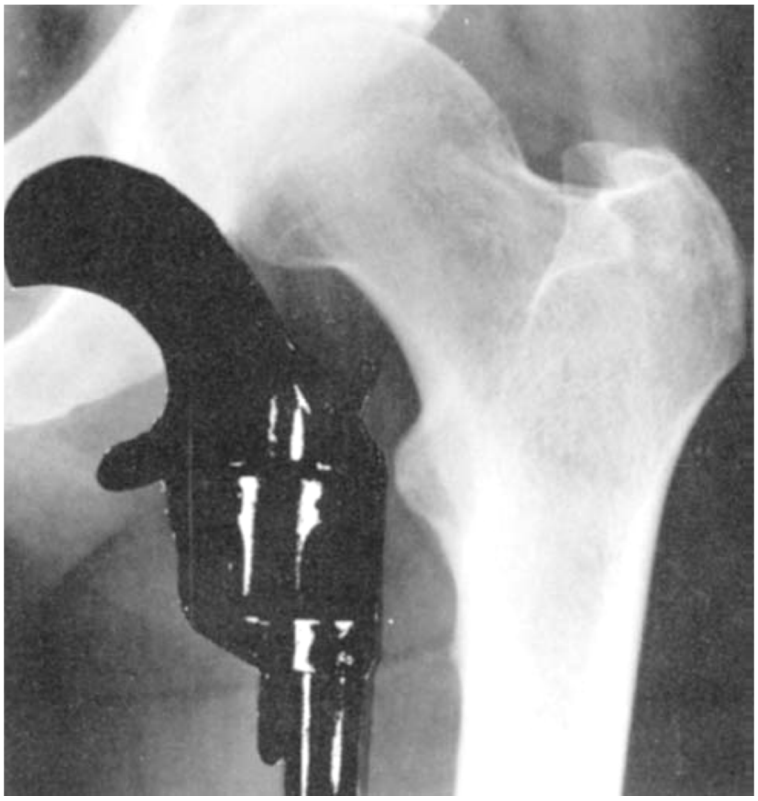

Figure 1.1. Stulberg and associates' (1975) anterior-posterior radiographic view of the "pistol grip" deformity, comparing an aspherical femoral head with a pistol handle. The aspherical abnormality was an early representation that characterised the deformity. Reproduced with permission of Springer (Ganz et al., 2008).

Subsequent works noted that impingement was experienced at high amplitudes of hip motions. Based on a combination of visual radiographic and preliminary physical examinations, general terms were used to describe the impingement, referring to the deformity as: “head tilt” or “post-slip”, epiphyseal displacement [43, 46, 75, 83], acetabular rim syndrome [65, 112], and cervico-acetabular impingement [112].

It was then introduced that anterior hip obstruction was due to peri-acetabular osteotomy [84], proposing that impingement was secondary to surgical repositioning of dysplastic acetabula. It was possible that the newly realigned bone structure overcompensated for the adjusted adverse conditions during the reparative phase of bone remodelling [51], subsequently causing an abnormal rate of bone turnover and forming a bony protrusion. Variable degrees of groin pain and limited hip motion were now observed in patients, explaining the ossification of the anterior rim. Dynamic hip flexion and internal rotation were noticed to be restricted as well. An additional follow-up study investigated the presence of protrusions after femoral neck fractures [35]. Similar consequences of secondary anterior FAI were observed. The focus was on the femoral head, where an oversized bony protrusion was formed at the site of the anterior fracture, bridging between the femoral head and neck. This bridge of the bump again could be explained by the reparative phase of bone remodelling during fracture healing. The intention of these combined studies, of reparative bone remodelling, was to explain the mechanisms that initiated FAI, proposing that a deformity was formed at the femoral neck or acetabular rim due to trauma or surgery.

The continuing research led Ganz and associates (2003) to recognize FAI as a pathomechanical disease process and a contributor to early adult hip pain and OA [43]. The intention of their research was to link FAI, as a hip deformity, with the pathogenesis of idiopathic OA. An emphasis was placed on distinguishing relative causes of OA, trying to distinguish if and which hip deformity would initiate secondary cartilage degeneration [42, 83]. To avoid confusion and to isolate various pathomechanical processes, a set of exclusions were established to neglect other morphological hip abnormalities (*e.g.*, Legg-Calvé-Perthes, avascular necrosis, SCFE, dysplasia). The exclusions were necessary to better characterize OA without extraneous aetiologies due to inflammation, trauma, or metabolic causes [42]. With more than 600 open surgical dislocations observed, Ganz and associates proposed that FAI was a mechanism for the development of early OA for most non-dysplastic hips [43]. It was suggested

that FAI was no longer just a resolute deformity of the hip joint, but rather a failure process initiated by a multitude of possible biological and mechanical mechanisms that would eventually provoke the onset of OA. This notion of FAI causing OA focused more on dynamic motion as opposed to directional axial loading of the hip. The theory of axial hip overload to provoke OA was disputed, further justifying that the development of OA in young adults, with normal hip configurations, cannot be correctly justified with solely concentric and eccentric overload. The studies thus far were unable to discuss mechanisms that initiate FAI or justify the etiology of the deformity, but provided significant groundwork for clinical and radiographic assessments to distinguish FAI types.

Recently, FAI has been deemed a pathomechanical process by which a human hip can fail [30, 74] rather than a disease, with emerging clinical evidence and ongoing biomechanical studies continuing to support that FAI provokes hip OA [14, 43, 71, 75]. Active adults with groin pain may now be successfully treated with early detection [29, 43, 52, 70, 74]. From the systematic review of literature on FAI, a great extent of past research focused on recognizing the correct pathology and deformity leading to OA (Figure 1.2), leading to subsequent treatment techniques and devising surgical solutions for FAI. Although there were recent efforts to discuss the mechanisms that initiate the failure process, there is still a gap in the literature that does not delineate FAI with the progression of OA. Although many studies noted that the cam deformity is predominantly situated at the anterosuperior femoral head, subsequently leading to end-stage cartilage damage, very few of these studies could confirm the exact location and progression of damage [11, 13-15, 27].

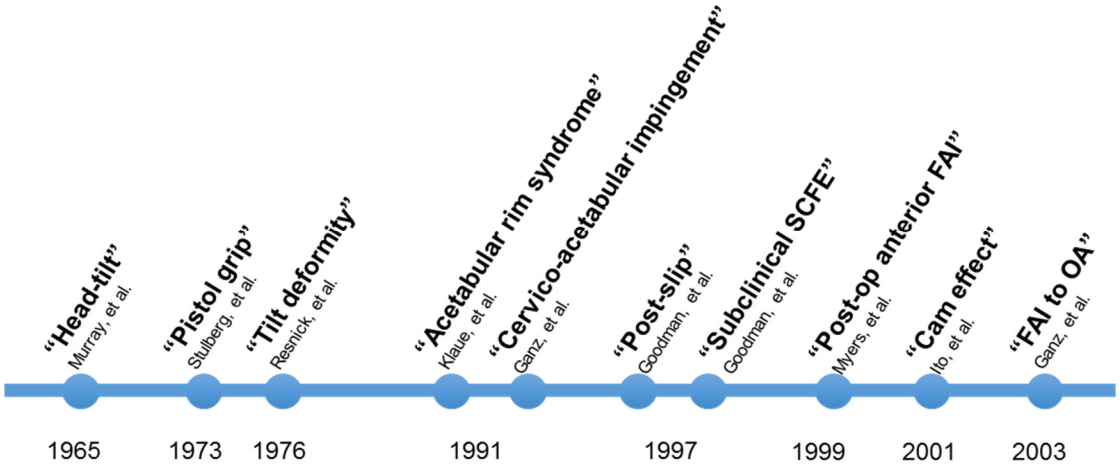

Figure 1.2. Timeline of terminology from previous studies leading up to the association of FAI to OA.

1.2.2 Cam vs. Pincer

The deformities that cause FAI can be distinguished as either cam or pincer [43]. In comparison with a normal femoral head (Figure 1.3.A), the structural cam-type morphology is characterized by an enlarged, aspherical femoral head, where an oversized junction leads to an insufficient femoral head-neck offset and limits clearance between the head-neck and labrum (Figure 1.3.B). The pincer-type morphology is characterized by an ossified labrum and over-coverage of the femoral head (Figure 1.3.C). A combination of both types is often found in patients, with one type likely leading to the other (Figure 1.3.D) [14].

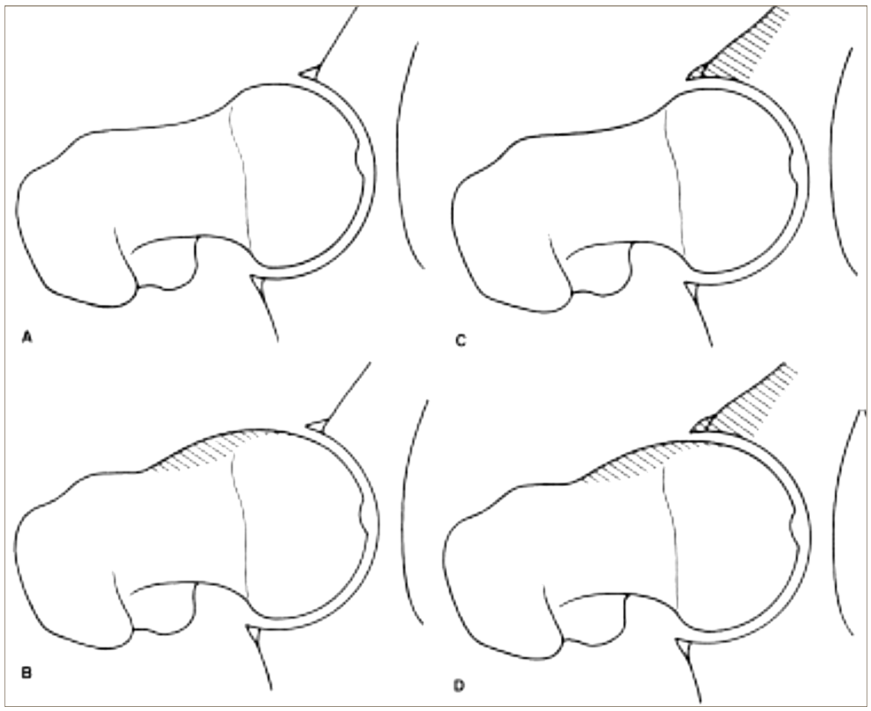

Figure 1.3. Comparison between a: **A**) healthy, normal hip; **B**) cam FAI; **C**) pincer FAI; and **D**) mixed FAI. Reproduced with permission of Wolters Kluwer Health, Inc (Lavigne et al., 2004).

The cam-type deformity is due to a decreased head-neck offset with an aspherical contour of the femoral head-neck junction [43, 62, 112], giving it a pronounced anterolateral bump and retroverted femoral head [54, 100]. The curvature is larger than average around the head-neck junction, resulting in a bony triangular shaped extension and articular cartilage onto the anterosuperior femoral neck [29]. The impingement is caused by a jamming of the abnormally shaped femoral head with increasing amplitudes of motions – most noticeably, the osteochondral

lesion impacts the acetabular rim with flexion, internal rotation [1, 2, 17, 29, 61, 89, 100], and with squatting motions [26, 67, 68, 86].

1.2.3 Cam Morphology

The typical measure to quantify the size and severity of the cam-type deformity uses the alpha angle, to visually measure the asphericity of the dysmorphic bump and quantify the head-to-neck relationship on imaging data [87]. The alpha angle is formed by the line parallel to the longitudinal femoral neck axis and the femoral head-neck offset, where the femoral head is no longer spherical (Figure 1.4).

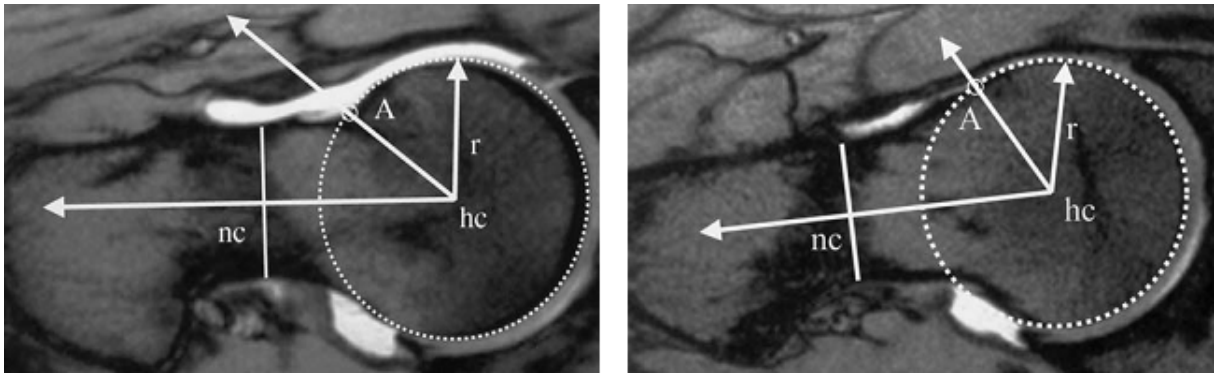

Figure 1.4. Oblique-axial view measuring the alpha angle of a healthy, normal femur (left) and a cam-type deformity (right). The circle with radius (r) is centered on the head center (hc), with an axis through the neck center (nc) and another axis through the point of asphericity (A), forming the alpha angle. Reproduced with permission of Elsevier (Nötzli et al., 2002).

Nötzli and associates (2002) established that a cam deformity was indicated by an alpha greater than 55°, in the oblique-axial plane [62, 87, 88]; while some other studies were more conservative, using an angle of 50° [13, 112] or 50.5 [9, 47, 64] in their cohort. Individuals with a higher alpha angle, thus more severe deformity, had prevalent labral and cartilage lesions at the anterosuperior acetabular cartilage; which was confirmed with open surgical dislocations [13, 14], radiographic evidence [14, 112], as well as subchondral bone mineral density analyses [104]. There was no mention yet as to how the presence or size of a cam deformity, using the alpha angle, was representative of symptoms. Up until this point, it was assumed that a large cam deformity would likely lead to symptoms. There was also no mention that the alpha angle was gender-specific.

The modification of the imaging views, to observe the alpha angle in multiple radial views around the clock-face of the femoral head and acetabulum, improved the assessment of the cam deformity. Recognizing that the cam deformity was statistically prevalent at the anterosuperior femoral head [94, 107], leading to degeneration of the anterosuperior acetabular cartilage [13, 14], a higher alpha angle value greater than 60° in the radial 1:30 plane was established as a threshold and predictor of hip pain [47, 64, 107] (Figure 1.5).

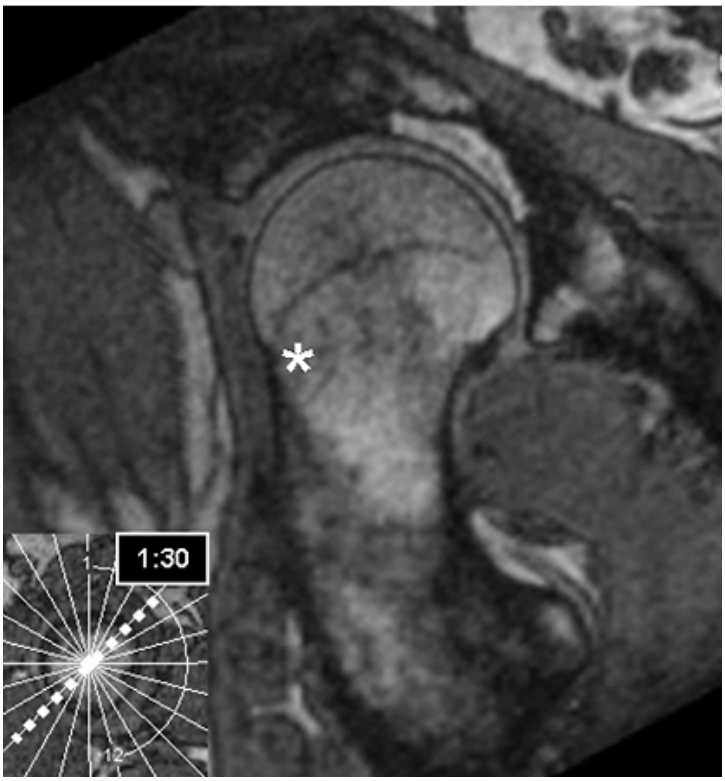

Figure 1.5. Radial 1:30 view indicating the large cam deformity in the anterosuperior region. Reproduced with permission of Wolters Kluwer Health, Inc (Hack et al., 2010).

However, it was often argued that the alpha angle cannot adequately quantify the severity of FAI [9, 66, 80, 82, 88, 107]. Moreover, radiologists may sometimes measure from planar imaging, without any high level of accuracy or precision, potentially leading to misinterpretations [88]. This further suggested that both views, axial and radial, must be considered and perhaps in conjunction with three-dimensional (3D) models, to provide clinicians with another perspective to confirm a deformity [13, 94].

Typically, a cam deformity is indicated by an alpha angle greater than 50.5° or 60° in the oblique-axial or radial plane, respectively [11, 87, 88, 94]. Although several studies

demonstrated that the severity of the cam deformity (thus, elevated alpha angles) were associated with hip pain and joint degeneration [11, 64, 70], there has been no significant correlation between the deformity and the severity of symptoms. Moreover, other common radiographic measures and anatomical features of the femoral head-neck and acetabulum have been mentioned as potential factors for symptomatic FAI [8, 16, 59, 95], although it remains unclear as to which combination of anatomical parameters can predict which patients are at-risk of developing symptoms.

1.2.4 Symptoms

It is believed that hip trauma [43, 100], significant athletic activity [2, 90], and contact sports [71, 84], before or during skeletal maturation, can contribute to the risk of developing a cam deformity. Though the mechanisms that initiate FAI are elusive and considered to be multi-factorial, it is evident that each morphology type (cam or pincer) has its own respective root causes, precursors, and associated hip disorders; moreover, each having its own respective group of associated demographics.

Cam FAI is statistically more common with young athletic males, whereas pincer FAI is more common with middle-aged and older females [59, 62, 72, 85, 112]. This distinction justifies the inclusion of male-dominant, athletic participant groups, in several previous studies of cam FAI [2, 3, 57, 61, 63, 69]. Nepple and associates recently found sex-dependent patterns in symptomatic patients [85], confirming that women have milder morphologies, whereas men have a higher activity level leading to larger morphologies, extensive intra-articular diseases, and combined-type morphologies.

FAI is rarely painful in its early stages, thus can go unrecognized for several years during its preliminary asymptomatic settling-in phase [36, 55, 57, 105]. Early diagnosis and treatment of FAI is important to alleviate severe hip pain, irreparable cartilage damage, and OA. The difficulty sometimes with early diagnosis is that cam and pincer FAI appear to look normal during early stages of development [71], where there is an evident lack of focus in implementing additional diagnostic tools to assess the severity of the morphology leading to FAI.

Although diagnostic imaging (*e.g.*, x-ray, CT, MRI) is the standard practice to confirm the presence of any hip deformity, it may be very difficult to determine if an individual will show any symptoms or indicate signs of FAI, especially if dynamic hip motions are not performed.

Primary symptom of hip impingement are indicated by groin and thigh stiffness and the inability to flex the hip beyond a right angle [28, 71]. Further physical examinations are assessed with internal-external rotations and hip flexion-extensions, to observe the difficulties in achieving a full range of motion (ROM) and to confirm impingment, with reasonable reliability [96]. During preliminary phases of the cam morphology, pain may be exacerbated by excessive cyclic loads applied on the hip, such as extensive walking, deep flexion, and strenuous activities. Hip and groin discomfort would frequently present itself during or after prolonged flexed positions (*e.g.*, running, jumping, sitting or squatting) [28].

In addition to imaging and physical examinations, previous motion analyses observed that symptomatic patients demonstrate different dynamic hip motions, such as level-walking [63] and squatting [69], in comparison with a healthy, control population. Cam FAI had an adverse effect on the dynamic squat motion, limiting squat depth and reducing pelvic ROM [69], and had slightly lower peaks in abduction. Constrained abduction could be justified by the restricting soft tissues in the hip joint with cam FAI. It was suggested that the squat motion could be incorporated as a possible diagnostic tool [67, 69], to notice any impediment in motion and detect symptoms at an earlier stage. However, the dynamic squat motion should be performed correctly, according to Lamontagne and associates (2009, 2011), as an additional diagnostic physical examination tool (with feet shoulder-width apart, toes point anteriorly, squatting to the lowest possible depth [67, 69]) and refraining from a shallow squat (Figure 1.6) [7].

As mentioned before, the cam morphology leads to acetabular cartilage damage predominantly at the anterosuperior region [11, 13-15, 27, 104]. Beck and associates (2005) observed 26 surgically dislocated hips and noted that the greatest depth of the cartilage lesions were located at anterosuperior quadrant [14]. Similarly, Beaulé and associates (2005) observed 23 hips and noted cartilage lesions combined with labral tears, also located at the anterosuperior clock-face, at the time of surgery [13]. In addition, Beaulé and associates (2012) reported severe acetabular cartilage damage (Type 3 and 4, chondral delamination [15]) at the anterosuperior region and further correlated the cartilage damage with elevated alpha angles [11]; whereas Clohisy and associates (2013) observed slightly higher articular cartilage abnormalities at the superolateral region, rather than at the anterior periphery [27].

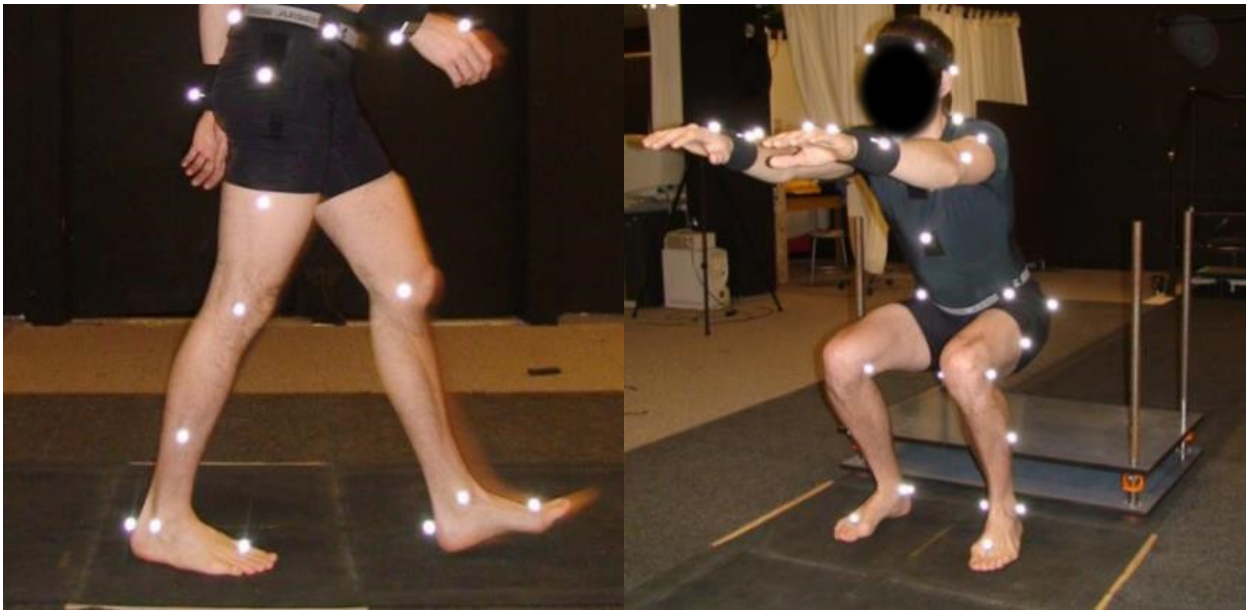

Figure 1.6. A) Level-walking [63] and **B**) maximal squat depth trials [69], comparing symptomatic cam FAI patients with healthy, control participants. Reproduced with permission of Elsevier (Kennedy et al., 2009) and Springer (Lamontagne et al., 2009).

From motion analyses and 3D kinematics and kinetics data, net hip joint forces and moments can be calculated from inverse dynamics. These forces and moments represent intersegmental reaction loads, though the approach excludes individual muscle contributions, co-contractions, and other soft tissue loading (*i.e.*, net passive moments). Nevertheless, the approach is still commonly used to estimate net joint moments and forces. To better understand the effect of cam FAI on the internal mechanical loading, hip contact forces are required, and necessitate the determination of muscle and soft tissue loading contributions. Although in vivo contact force measurements are possible with instrumented prostheses [20, 21, 32, 50], their invasiveness raises numerous technical and ethical concerns. The data received from the instrumented prostheses contributed to numerous studies and publications, towards the better understanding of joint contact loading, and leading to a renowned online database. However, these studies were often limited by sample size and population, as most of the patients implanted with instrumented prostheses represented a specific age group and disease process (*i.e.*, older population with severe arthritis, in contrast with a younger, athletic FAI population).

Alternatively, several studies implemented in vitro methods using cadaveric hip joints and uniaxial mechanical testers, providing indications of hip joint contact pressures [4, 10, 33, 41, 101]. Many of these studies were restricted by the loading calibration of the tensile tester and

pressure sensors, as well as the ROM simulating the activity of daily living. Moreover, with an excised joint capsule and ignoring muscles contributions and external forces, functional and physiological contributions were neglected. Though hip motions and reaction forces can be quantified using biomechanics testing, the principal stress and strain components within the hip joint were still not apparent. The use of finite element methods provides an attractive approach, since it avoids invasive in vivo experimentations.

The computational musculoskeletal models approach appears to be the most appropriate method to estimate joint loadings in efforts to include muscle contributions [23, 34, 79]. The musculoskeletal model can implement a forward dynamics approach to estimate muscle forces, from muscular activities measured by electromyography (EMG) [24, 79, 99], showing a good sensitivity to the subject-specific muscle activation [73]. In conjunction with an EMG-driven musculoskeletal model, to determine the individual muscle and hip contact forces, a finite element (FE) model can assess the mechanical stimuli in bone and soft tissues as necessary to investigate the abnormal bone distribution in the hip with FAI. The inclusion of muscle and contact forces obtained from the EMG-driven musculoskeletal model may yield a more complete and accurate simulation with respect to the FE analyses currently available in the literature

1.2.5 Hip Joint Modelling

Subject-specific reconstruction is often avoided due to the time consuming efforts and complexities of geometric variables. Many studies of hip joint biomechanics have resorted to analyses of simplified 2D planar [97, 115] or idealized to a ball-and-socket models, which were deemed by some researchers as appropriate for preliminary approximations [44]. However, knowing that the femoral head conforms to a conchoid shape rather than a perfect sphere [81], it would be important to incorporate subject-specific contour data of the femoral head to accurately estimate the cartilage stresses and contact areas.

Thanks to CT-based navigation for preoperative planning, 3D FE models can now be reconstructed using imaging data to follow a subject-specific approach [45]. Since the segmentation process is time consuming and tedious, many studies implemented semi-automated segmentation methods to extract objects of interests from CT and MRI data [40, 60, 78]. The clarity and the sensitivity of the images tend to vary from scan to scan, therefore, it is often best to perform manual segmentation.

The selection of the material properties for FE modelling and simulations often depends on the physiological application and mechanical assembly of the models. Nonlinear effects of soft tissues can be approximated with hyperelastic [5] or poroelastic material properties [39, 102]. As for the bone geometries, some studies opted to apply an elastic modulus based on an empirical formula derived from the apparent density of bone [18, 92, 108-110]. In this case, knowing that bone is an anisotropic material, the material properties would differ in various planes and directions. Since, bone is macroscopically composed of compact and trabecular bone, there would be the need to consider dissimilar material properties with different elastic and shear moduli. However, for a quasi-static condition with a low frequency of loading, a linear elastic model would be deemed appropriate to model the bone structures. Therefore, many studies opted for two separate, linear elastic, isotropic entities to represent the cortical shell and the internal trabecular structure (Table 1.1) [6, 26, 77, 97, 98, 109]. Anderson and associates (2005, 2008) further justified that the trabecular structure, while contributing very little stiffness, occupied copious amounts of computational memory, and did not provide much function within their simulation; thus, they suggested to only model a cortical shell for their study [4, 5].

Table 1.1. Selected summary of elastic moduli and Poisson's ratios values for assembling finite element models of the cortical and trabecular bone structure of the hip joint

Cortical Bone		Trabecular Bone		References
Elastic Modulus	Poisson's Ratio	Elastic Modulus	Poisson's Ratio	
17 GPa	0.29	Not used	Not used	Anderson, et al., 2008 [4]
20 GPa	Not disclosed	100 MPa	Not disclosed	Chegini, et al., 2009 [26]
17 GPa	0.3	100 to 400 MPa	0.3	Rudman, et al., 2006 [97]
Not disclosed	Not disclosed	120 MPa	0.3	Russell, et al., 2006 [98]
17 GPa	0.28 to 0.3	0.6 to 1 GPa	0.3	Wei, et al., 2005 [115]

Moreover, other studies considered orthotropic properties to define the hip joint as a solid model (Table 1.2) [31, 86, 113]. The use of orthotropic properties accounts for both cortical and trabecular structures, thus eliminating the need to segment an additional trabecular component and alleviate overuse of finite elements and computational memory. Additional details on mechanical properties and stress analyses are included in (Appendix C – Mechanical Properties).

Table 1.2. Mechanical properties of linear elastic orthotropic bone used for femur and pelvis [31]

Elastic Modulus (GPa)	$E_x = 11.6$	$E_y = 12.2$	$E_z = 19.9$
Shear Modulus (GPa)	$G_{xy} = 4.0$	$G_{yz} = 5.0$	$G_{xz} = 5.4$
Poisson Ratio	$\nu_{xy} = 0.42$	$\nu_{yz} = 0.23$	$\nu_{xz} = 0.23$

In most cases, FE simulations of the hip considered mainly bone models and the articulation components [4-6, 26, 86, 97, 98], and overlooked the role of muscle tissues. As an improvement to the subject-specific material characteristics, FE hip joint models can be constructed from segmented bone and soft tissue geometries obtained from subject-specific CT and MRI data, using image segmentation software. It will be imperative to examine soft tissues landmarks around the hip joint. The inclusion of the labrum in hip joint modelling will also be crucial to understand the nature of the seal on pathological hip deformities [37-39]. The labrum can be reconstructed around the periphery of the acetabulum, creating a seal around the femoral head. To ensure that the articulation components from MRI will be in accordance with the CT based bone models, the bone landmarks in each set of imaging data must be registered [76, 114].

The early FE simulations contributed substantially to the understanding and direction of hip joint modelling and simulations. However, they also revealed numerous areas that needed improvements. In addition, to further the understanding of subject-specific hip joint stresses, the loading should be specific and integrated with the associated hip joint model (*i.e.*, subject-specific joint loading should not be approximated from instrumented prostheses data, if possible).

1.3 References

1. Agricola R, Heijboer MP, Bierma-Zeinstra SM, Verhaar JA, Weinans H, Waarsing JH. Cam impingement causes osteoarthritis of the hip: a nationwide prospective cohort study (CHECK). *Ann Rheum Dis*. 2012;72:918-923.
2. Agricola R, Heijboer MP, Ginai AZ, Roels P, Zadpoor AA, Verhaar JA, Weinans H, Waarsing JH. A Cam Deformity Is Gradually Acquired During Skeletal Maturation in Adolescent and Young Male Soccer Players: A Prospective Study With Minimum 2-Year Follow-up. *Am J Sports Med*. 2014;
3. Allen D, Beaule PE, Ramadan O, Doucette S. Prevalence of associated deformities and hip pain in patients with cam-type femoroacetabular impingement. *J Bone Joint Surg Br*. 2009;91:589-594.
4. Anderson AE, Ellis BJ, Maas SA, Peters CL, Weiss JA. Validation of finite element predictions of cartilage contact pressure in the human hip joint. *J Biomech Eng*. 2008;130:051008.
5. Anderson AE, Ellis BJ, Maas SA, Weiss JA. Effects of idealized joint geometry on finite element predictions of cartilage contact stresses in the hip. *J Biomech*. 2010;43:1351-1357.
6. Arbabi E, Chegini S, Boulic R, Tannast M, Ferguson SJ, Thalmann D. Penetration depth method--novel real-time strategy for evaluating femoroacetabular impingement. *J Orthop Res*. 2010;28:880-886.
7. Ayeni O, Chu R, Hetaimish B, Nur L, Simunovic N, Farrokhyar F, Bedi A, Bhandari M. A painful squat test provides limited diagnostic utility in CAM-type femoroacetabular impingement. *Knee Surg Sports Traumatol Arthrosc*. 2013;
8. Bardakos NV, Villar RN. Predictors of progression of osteoarthritis in femoroacetabular impingement: a radiological study with a minimum of ten years follow-up. *J Bone Joint Surg Br*. 2009;91:162-169.
9. Barton C, Salineros MJ, Rakhra KS, Beaule PE. Validity of the alpha angle measurement on plain radiographs in the evaluation of cam-type femoroacetabular impingement. *Clin Orthop Relat Res*. 2011;469:464-469.
10. Basso T, Klaksvik J, Syversen U, Foss OA. Biomechanical femoral neck fracture experiments--a narrative review. *Injury*. 2012;43:1633-1639.
11. Beaulé P, Hynes K, Parker G, Kemp K. Can the Alpha Angle Assessment of Cam Impingement Predict Acetabular Cartilage Delamination? *Clin Orthop Rel Res*. 2012;470:3361-3367.
12. Beaule PE. Femoroacetabular impingement: current status of diagnosis and treatment: editorial comment. *Clin Orthop Relat Res*. 2009;467:603-604.
13. Beaulé PE, Zaragoza E, Motamedi K, Copelan N, Dorey FJ. Three-dimensional computed tomography of the hip in the assessment of femoroacetabular impingement. *J Orthop Res*. 2005;23:1286-1292.
14. Beck M, Kalhor M, Leunig M, Ganz R. Hip morphology influences the pattern of damage to the acetabular cartilage: femoroacetabular impingement as a cause of early osteoarthritis of the hip. *J Bone Joint Surg Br*. 2005;87:1012-1018.
15. Beck M, Leunig M, Parvizi J, Boutier V, Wyss D, Ganz R. Anterior femoroacetabular impingement: part II. Midterm results of surgical treatment. *Clin Orthop Relat Res*. 2004;67-73.
16. Bedi A, Dolan M, Leunig M, Kelly BT. Static and Dynamic Mechanical Causes of Hip Pain. *Arthroscopy*. 2011;27:235-251.
17. Bedi A, Thompson M, Uliana C, Magennis E, Kelly BT. Assessment of range of motion and contact zones with commonly performed physical exam manoeuvers for femoroacetabular impingement (FAI): what do these tests mean? *Hip Int*. 2013;23 Suppl 9:S27-34.
18. Behrens BA, Nolte I, Wefstaedt P, Stukenborg-Colsman C, Bouguecha A. Numerical investigations on the strain-adaptive bone remodelling in the periprosthetic femur: influence of the boundary conditions. *Biomed Eng Online*. 2009;8:7.
19. Bergmann G, Deuretzbacher G, Heller M, Graichen F, Rohlmann A, Strauss J, Duda GN. Hip contact forces and gait patterns from routine activities. *J Biomech*. 2001;34:859-871.

20. Bergmann G, Graichen F, Rohlmann A. Hip joint loading during walking and running, measured in two patients. *J Biomech*. 1993;26:969-990.

21. Bergmann G, Graichen F, Rohlmann A, Bender A, Heinlein B, Duda GN, Heller MO, Morlock MM. Realistic loads for testing hip implants. 2010;20:65-75.

22. Bombardier C, Hawker G, Mosher D, *The Impact of Arthritis in Canada: Today and Over the Next 30 Years*, 2011, Arthritis Alliance of Canada.

23. Buchanan TS, Lloyd DG, Manal K, Besier TF. Estimation of muscle forces and joint moments using a forward-inverse dynamics model. *Med Sci Sports Exerc*. 2005;37:1911-1916.

24. Buchanan TS, Lloyd DG, Manal K, Besier TF. Neuromusculoskeletal modeling: estimation of muscle forces and joint moments and movements from measurements of neural command. *J Appl Biomech*. 2004;20:367-395.

25. Chakraverty JK, Sullivan C, Gan C, Narayanaswamy S, Kamath S. Cam and pincer femoroacetabular impingement: CT findings of features resembling femoroacetabular impingement in a young population without symptoms. *AJR Am J Roentgenol*. 2013;200:389-395.

26. Chegini S, Beck M, Ferguson SJ. The effects of impingement and dysplasia on stress distributions in the hip joint during sitting and walking: a finite element analysis. *J Orthop Res*. 2009;27:195-201.

27. Clohisy JC, Baca G, Beaule PE, Kim YJ, Larson CM, Millis MB, Podeszwa DA, Schoenecker PL, Sierra RJ, Sink EL, Sucato DJ, Trousdale RT, Zaltz I. Descriptive epidemiology of femoroacetabular impingement: a North American cohort of patients undergoing surgery. *Am J Sports Med*. 2013;41:1348-1356.

28. Clohisy JC, Knaus ER, Hunt DM, Lesher JM, Harris-Hayes M, Prather H. Clinical presentation of patients with symptomatic anterior hip impingement. *Clin Orthop Relat Res*. 2009;467:638-644.

29. Clohisy JC, McClure JT. Treatment of anterior femoroacetabular impingement with combined hip arthroscopy and limited anterior decompression. *Iowa Orthop J*. 2005;25:164-171.

30. Clohisy JC, St John LC, Schutz AL. Surgical treatment of femoroacetabular impingement: a systematic review of the literature. *Clin Orthop Relat Res*. 2010;468:555-564.

31. Couteau B, Hobatho MC, Darmana R, Brignola JC, Arlaud JY. Finite element modelling of the vibrational behaviour of the human femur using CT-based individualized geometrical and material properties. *J Biomech*. 1998;31:383-386.

32. Davy DT, Kotzar GM, Brown RH, Heiple KG, Goldberg VM, Heiple KG, Jr., Berilla J, Burstein AH. Telemetric force measurements across the hip after total arthroplasty. *J Bone Joint Surg Am*. 1988;70:45-50.

33. Day WH, Swanson SA, Freeman MA. Contact pressures in the loaded human cadaver hip. *J Bone Joint Surg Br*. 1975;57:302-313.

34. Delp SL, Anderson FC, Arnold AS, Loan P, Habib A, John CT, Guendelman E, Thelen DG. OpenSim: open-source software to create and analyze dynamic simulations of movement. *IEEE Trans Biomed Eng*. 2007;54:1940-1950.

35. Eijer H, Myers SR, Ganz R. Anterior femoroacetabular impingement after femoral neck fractures. *J Orthop Trauma*. 2001;15:475-481.

36. Ergen FB, Vudali S, Sanverdi E, Dolgun A, Aydingoz U. CT assessment of asymptomatic hip joints for the background of femoroacetabular impingement morphology. *Diagn Interv Radiol*. 2013;

37. Ferguson SJ, Bryant JT, Ganz R, Ito K. The acetabular labrum seal: a poroelastic finite element model. *Clin Biomech (Bristol, Avon)*. 2000;15:463-468.

38. Ferguson SJ, Bryant JT, Ganz R, Ito K. An in vitro investigation of the acetabular labral seal in hip joint mechanics. *J Biomech*. 2003;36:171-178.

39. Ferguson SJ, Bryant JT, Ganz R, Ito K. The influence of the acetabular labrum on hip joint cartilage consolidation: a poroelastic finite element model. *J Biomech*. 2000;33:953-960.

40. Fornaro J, Székely G, Harders M, *Semi-automatic Segmentation of Fractured Pelvic Bones for Surgical Planning*, in *Biomedical Simulation*, F. Bello and S. Cotin, Editors. 2010, Springer Berlin Heidelberg. p. 82-89.

41. Fu M, Xiang S, Zhang Z, Huang G, Liu J, Duan X, Yang Z, Wu P, Liao W. The biomechanical differences of rotational acetabular osteotomy, Chiari osteotomy and shelf procedure in developmental dysplasia of hip. *BMC Musculoskelet Disord*. 2014;15:47.

42. Ganz R, Leunig M, Leunig-Ganz K, Harris WH. The etiology of osteoarthritis of the hip: an integrated mechanical concept. *Clin Orthop Relat Res*. 2008;466:264-272.

43. Ganz R, Parvizi J, Beck M, Leunig M, Nötzli H, Siebenrock KA. Femoroacetabular Impingement: A Cause for Osteoarthritis of the Hip. *Clin Orthop Rel Res*. 2003;417:112-120.

44. Genda E, Iwasaki N, Li G, MacWilliams BA, Barrance PJ, Chao EY. Normal hip joint contact pressure distribution in single-leg standing--effect of gender and anatomic parameters. *J Biomech*. 2001;34:895-905.

45. Gilles B, Christophe FK, Magnenat-Thalmann N, Becker CD, Duc SR, Menetrey J, Hoffmeyer P. MRI-based assessment of hip joint translations. *J Biomech*. 2009;42:1201-1205.

46. Goodman DA, Feighan JE, Smith AD, Latimer B, Buly RL, Cooperman DR. Subclinical slipped capital femoral epiphysis. Relationship to osteoarthrosis of the hip. *J Bone Joint Surg Am*. 1997;79:1489-1497.

47. Hack K, Di Primio G, Rakhra K, Beaule PE. Prevalence of cam-type femoroacetabular impingement morphology in asymptomatic volunteers. *J Bone Joint Surg Am*. 2010;92:2436-2444.

48. Harris WH. Etiology of osteoarthritis of the hip. *Clin Orthop Relat Res*. 1986;20-33.

49. Hartofilakidis G, Bardakos NV, Babis GC, Georgiades G. An examination of the association between different morphotypes of femoroacetabular impingement in asymptomatic subjects and the development of osteoarthritis of the hip. *J Bone Joint Surg Br*. 2011;93:580-586.

50. Heller MO, Bergmann G, Deuretzbacher G, Durselen L, Pohl M, Claes L, Haas NP, Duda GN. Musculo-skeletal loading conditions at the hip during walking and stair climbing. *J Biomech*. 2001;34:883-893.

51. Henriksen K, Neutzsky-Wulff AV, Bonewald LF, Karsdal MA. Local communication on and within bone controls bone remodeling. *Bone*. 2009;44:1026-1033.

52. Ilizaliturri VM, Jr., Orozco-Rodriguez L, Acosta-Rodriguez E, Camacho-Galindo J. Arthroscopic treatment of cam-type femoroacetabular impingement: preliminary report at 2 years minimum follow-up. *J Arthroplasty*. 2008;23:226-234.

53. Information CIfH, *Hip and Knee Replacements in Canada: Canadian Joint Replacement Registry 2014 Annual Report*, 2014: Ottawa, Ontario.

54. Ito K, Minka MA, 2nd, Leunig M, Werlen S, Ganz R. Femoroacetabular impingement and the cam-effect. A MRI-based quantitative anatomical study of the femoral head-neck offset. *J Bone Joint Surg Br*. 2001;83:171-176.

55. Jaberi FM, Parvizi J. Hip pain in young adults: femoroacetabular impingement. *J Arthroplasty*. 2007;22:37-42.

56. Jorge JP, Simoes FM, Pires EB, Rego PA, Tavares DG, Lopes DS, Gaspar A. Finite element simulations of a hip joint with femoroacetabular impingement. *Comput Methods Biomech Biomed Engin*. 2014;17:1275-1284.

57. Jung KA, Restrepo C, Hellman M, AbdelSalam H, Morrison W, Parvizi J. The prevalence of cam-type femoroacetabular deformity in asymptomatic adults. *J Bone Joint Surg Br*. 2011;93:1303-1307.

58. Kahlenberg CA, Han B, Patel RM, Deshmane PP, Terry MA. Time and Cost of Diagnosis for Symptomatic Femoroacetabular Impingement. 2014;2:

59. Kang AC, Gooding AJ, Coates MH, Goh TD, Armour P, Rietveld J. Computed tomography assessment of hip joints in asymptomatic individuals in relation to femoroacetabular impingement. *Am J Sports Med*. 2010;38:1160-1165.

60. Kang Y, Engelke K, Kalender WA. A new accurate and precise 3-D segmentation method for skeletal structures in volumetric CT data. *IEEE Trans Med Imaging*. 2003;22:586-598.

61. Kapron AL, Anderson AE, Aoki SK, Phillips LG, Petron DJ, Toth R, Peters CL. Radiographic prevalence of femoroacetabular impingement in collegiate football players: AAOS Exhibit Selection. *J Bone Joint Surg Am*. 2011;93:1-10.

62. Kassarjian A, Brisson M, Palmer WE. Femoroacetabular impingement. *Eur J Radiol*. 2007;63:29-35.

63. Kennedy MJ, Lamontagne M, Beaule PE. Femoroacetabular impingement alters hip and pelvic biomechanics during gait Walking biomechanics of FAI. *Gait Posture*. 2009;30:41-44.

64. Khanna V, Caragianis A, Diprimio G, Rakhra K, Beaule PE. Incidence of hip pain in a prospective cohort of asymptomatic volunteers: is the cam deformity a risk factor for hip pain? *Am J Sports Med*. 2014;42:793-797.

65. Klaue K, Durnin CW, Ganz R. The acetabular rim syndrome. A clinical presentation of dysplasia of the hip. *J Bone Joint Surg Br*. 1991;73:423-429.

66. Konan S, Rayan F, Haddad FS. Is the frog lateral plain radiograph a reliable predictor of the alpha angle in femoroacetabular impingement? *J Bone Joint Surg Br*. 2010;92:47-50.

67. Lamontagne M, Brisson N, Kennedy MJ, Beaule PE. Preoperative and postoperative lower-extremity joint and pelvic kinematics during maximal squatting of patients with cam femoro-acetabular impingement. *J Bone Joint Surg Am*. 2011;93 Suppl 2:40-45.

68. Lamontagne M, Brisson N, Kennedy MJ, Beaulé PE. Preoperative and Postoperative Lower-Extremity Joint and Pelvic Kinematics During Maximal Squatting of Patients with Cam Femoro-Acetabular Impingement. *J Bone Joint Surg*. 2011;93:40-45.

69. Lamontagne M, Kennedy MJ, Beaule PE. The effect of cam FAI on hip and pelvic motion during maximum squat. *Clin Orthop Relat Res*. 2009;467:645-650.

70. Larson CM, Giveans MR. Arthroscopic management of femoroacetabular impingement: early outcomes measures. *Arthroscopy*. 2008;24:540-546.

71. Laude F, Boyer T, Nogier A. Anterior femoroacetabular impingement. *Joint Bone Spine*. 2007;74:127-132.

72. Lavigne M, Parvizi J, Beck M, Siebenrock KA, Ganz R, Leunig M. Anterior femoroacetabular impingement: part I. Techniques of joint preserving surgery. *Clin Orthop Relat Res*. 2004;61-66.

73. Lenaerts G, Bartels W, Gelaude F, Mulier M, Spaepen A, Van der Perre G, Jonkers I. Subject-specific hip geometry and hip joint centre location affects calculated contact forces at the hip during gait. *J Biomech*. 2009;42:1246-1251.

74. Leunig M, Beaule PE, Ganz R. The concept of femoroacetabular impingement: current status and future perspectives. *Clin Orthop Relat Res*. 2009;467:616-622.

75. Leunig M, Ganz R. [Femoroacetabular impingement. A common cause of hip complaints leading to arthrosis]. *Unfallchirurg*. 2005;108:9-10, 12-17.

76. Li X, Yankeelov TE, Peterson TE, Gore JC, Dawant BM. Automatic nonrigid registration of whole body CT mice images. *Med Phys*. 2008;35:1507-1520.

77. Liechti EF, Ferguson SJ, Tannast M. Protrusio acetabuli: Joint loading with severe pincer impingement and its theoretical implications for surgical therapy. *J Orthop Res*. 2014;

78. Liu H, Zhao J, Dai N, Qian H, Tang Y. Improve accuracy for automatic acetabulum segmentation in CT images. *Biomed Mater Eng*. 2014;24:3159-3177.

79. Lloyd DG, Besier TF. An EMG-driven musculoskeletal model to estimate muscle forces and knee joint moments in vivo. *J Biomech*. 2003;36:765-776.

80. Lohan DG, Seeger LL, Motamedi K, Hame S, Sayre J. Cam-type femoral-acetabular impingement: is the alpha angle the best MR arthrography has to offer? *Skeletal Radiol*. 2009;38:855-862.

81. Menschik F. The hip joint as a conchoid shape. *J Biomech*. 1997;30:971-973.

82. Meyer DC, Beck M, Ellis T, Ganz R, Leunig M. Comparison of six radiographic projections to assess femoral head/neck asphericity. *Clin Orthop Relat Res*. 2006;445:181-185.

83. Murray RO. The aetiology of primary osteoarthritis of the hip. *Br J Radiol*. 1965;38:810-824.

84. Myers SR, Eijer H, Ganz R. Anterior femoroacetabular impingement after periacetabular osteotomy. *Clin Orthop Relat Res*. 1999;93-99.

85. Nepple JJ, Riggs CN, Ross JR, Clohisy JC. Clinical presentation and disease characteristics of femoroacetabular impingement are sex-dependent. *J Bone Joint Surg Am*. 2014;96:1683-1689.

86. Ng KCG, Rouhi G, Lamontagne M, Beaulé PE. Finite Element Analysis Examining the Effects of Cam FAI on Hip Joint Mechanical Loading Using Subject-Specific Geometries During Standing and Maximum Squat. *HSS J*. 2012;8:206-212.

87. Nötzli HP, Wyss TF, Stoecklin CH, Schmid MR, Treiber K, Hodler J. The contour of the femoral head-neck junction as a predictor for the risk of anterior impingement. *J Bone Joint Surg Br*. 2002;84-B:556-560.

88. Nouh MR, Schweitzer ME, Rybak L, Cohen J. Femoroacetabular impingement: can the alpha angle be estimated? *AJR Am J Roentgenol*. 2008;190:1260-1262.

89. Nussbaumer S, Leunig M, Glatthorn JF, Stauffacher S, Gerber H, Maffiuletti NA. Validity and test-retest reliability of manual goniometers for measuring passive hip range of motion in femoroacetabular impingement patients. *BMC Musculoskelet Disord*. 2010;11:194.

90. Philippon M, Schenker M, Briggs K, Kuppersmith D. Femoroacetabular impingement in 45 professional athletes: associated pathologies and return to sport following arthroscopic decompression. *Knee Surg Sports Traumatol Arthrosc*. 2007;15:908-914.

91. Pollard TC, Villar RN, Norton MR, Fern ED, Williams MR, Simpson DJ, Murray DW, Carr AJ. Femoroacetabular impingement and classification of the cam deformity: the reference interval in normal hips. *Acta Orthop*. 2010;81:134-141.

92. Radcliffe IA, Taylor M. Investigation into the affect of cementing techniques on load transfer in the resurfaced femoral head: a multi-femur finite element analysis. *Clin Biomech (Bristol, Avon)*. 2007;22:422-430.

93. Radin EL, Paul IL, Tolkoff MJ. Subchondral bone changes in patients with early degenerative joint disease. *Arthritis Rheum*. 1970;13:400-405.

94. Rakhra KS, Sheikh AM, Allen D, Beaule PE. Comparison of MRI alpha angle measurement planes in femoroacetabular impingement. *Clin Orthop Relat Res*. 2009;467:660-665.

95. Ranawat A, Schulz B, Baumbach S, Meftah M, Ganz R, Leunig M. Radiographic Predictors of Hip Pain in Femoroacetabular Impingement. *HSS J*. 2011;7:115-119.

96. Ratzlaff C, Simatovic J, Wong H, Li L, Ezzat A, Langford D, Esdaile JM, Kennedy C, Embley P, Caves D, Hopkins T, Cibere J. Reliability of hip examination tests for femoroacetabular impingement. *Arthritis Care Res (Hoboken)*. 2013;65:1690-1696.

97. Rudman KE, Aspden RM, Meakin JR. Compression or tension? The stress distribution in the proximal femur. *Biomed Eng Online*. 2006;5:12.

98. Russell ME, Shivanna KH, Grosland NM, Pedersen DR. Cartilage contact pressure elevations in dysplastic hips: a chronic overload model. *J Orthop Surg Res*. 2006;1:6.

99. Sartori M, Reggiani M, Lloyd DG, Pagello E. A neuromusculoskeletal model of the human lower limb: towards EMG-driven actuation of multiple joints in powered orthoses. *IEEE Int Conf Rehabil Robot*. 2011;2011:5975441.

100. Siebenrock KA, Wahab KH, Werlen S, Kalhor M, Leunig M, Ganz R. Abnormal extension of the femoral head epiphysis as a cause of cam impingement. *Clin Orthop Relat Res*. 2004;54-60.

101. Sparks DR, Beason DP, Etheridge BS, Alonso JE, Eberhardt AW. Contact pressures in the flexed hip joint during lateral trochanteric loading. *J Orthop Res*. 2005;23:359-366.

102. Speirs AD, Beaule PE, Ferguson SJ, Frei H. Stress distribution and consolidation in cartilage constituents is influenced by cyclic loading and osteoarthritic degeneration. *J Biomech*. 2014;47:2348-2353.

103. Speirs AD, Beaule PE, Rakhra KS, Schweitzer ME, Frei H. Bone density is higher in cam-type femoroacetabular impingement deformities compared to normal subchondral bone. *Osteoarthritis Cartilage*. 2013;21:1068-1073.

104. Speirs AD, Beaule PE, Rakhra KS, Schweitzer ME, Frei H. Increased acetabular subchondral bone density is associated with cam-type femoroacetabular impingement. *Osteoarthritis Cartilage*. 2013;21:551-558.

105. Standaert CJ, Manner PA, Herring SA. Expert opinion and controversies in musculoskeletal and sports medicine: femoroacetabular impingement. *Arch Phys Med Rehabil*. 2008;89:890-893.

106. Stulberg S, Cordell L, Harris WH, Ramsey P, MacEwen G. *Unrecognized childhood disease: A major cause of idiopathic osteoarthritis of the hip.* in *Third Open Scientific Meeting of The Hip Society*. 1975. St. Louis, MO.

107. Sutter R, Dietrich TJ, Zingg PO, Pfirrmann CWA. How Useful Is the Alpha Angle for Discriminating between Symptomatic Patients with Cam-type Femoroacetabular Impingement and Asymptomatic Volunteer*Radiology*. 2012;264:514-521.

108. Taddei F, Cristofolini L, Martelli S, Gill HS, Viceconti M. Subject-specific finite element models of long bones: An in vitro evaluation of the overall accuracy. *J Biomech*. 2006;39:2457-2467.

109. Taddei F, Martelli S, Reggiani B, Cristofolini L, Viceconti M. Finite-element modeling of bones from CT data: sensitivity to geometry and material uncertainties. *IEEE Trans Biomed Eng*. 2006;53:2194-2200.

110. Taddei F, Schileo E, Helgason B, Cristofolini L, Viceconti M. The material mapping strategy influences the accuracy of CT-based finite element models of bones: an evaluation against experimental measurements. *Med Eng Phys*. 2007;29:973-979.

111. Tannast M, Mistry S, Steppacher SD, Reichenbach S, Langlotz F, Siebenrock KA, Zheng G. Radiographic analysis of femoroacetabular impingement with Hip2Norm-reliable and validated. *J Orthop Res*. 2008;26:1199-1205.

112. Tannast M, Siebenrock KA, Anderson SE. Femoroacetabular Impingement: Radiographic Diagnosis—What the Radiologist Should Know. *AJR Am J Roentgenol*. 2007;188:1540-1552.

113. Taylor WR, Roland E, Ploeg H, Hertig D, Klabunde R, Warner MD, Hobatho MC, Rakotomanana L, Clift SE. Determination of orthotropic bone elastic constants using FEA and modal analysis. *J Biomech*. 2002;35:767-773.

114. Tomazevic D, Likar B, Slivnik T, Pernus F. 3-D/2-D registration of CT and MR to X-ray images. *IEEE Trans Med Imaging*. 2003;22:1407-1416.

115. Wei HJ, Liang HC, Lee MH, Huang YC, Chang Y, Sung HW. Construction of varying porous structures in acellular bovine pericardia as a tissue-engineering extracellular matrix. *Biomaterials*. 2005;26:1905-1913.

2 Hip Joint Stresses due to Cam-Type Femoroacetabular Impingement: A Systematic Review of Finite Element Simulations

K. C. Geoffrey Ng [1] | Mario Lamontagne [2,1] | Michel R. Labrosse [1] | Paul E. Beaulé [3]

[1] Department of Mechanical Engineering | University of Ottawa | Ottawa, Ontario, Canada

[2] School of Human Kinetics | University of Ottawa | Ottawa, Ontario, Canada

[3] Division of Orthopaedic Surgery | University of Ottawa | Ottawa, Ontario, Canada

Contents of this chapter published as an article in *PLoS ONE* | 26 January 2016

Ng KCG, Lamontagne M, Labrosse MR, Beaulé PE, Hip Joint Stresses due to Cam Type Femoroacetabular Impingement: A Systematic Review of Finite Element Simulations. *PLoS ONE*, 2016;11. DOI: 10.1371/journal.pone.0147813.

2.0 Abstract

Background: The cam deformity causes the anterosuperior femoral head to obstruct with the acetabulum, resulting in femoroacetabular impingement (FAI) and elevated risks of early osteoarthritis. Several finite element models have simulated adverse loading conditions due to cam FAI, to better understand the relationship between mechanical stresses and cartilage degeneration. Our purpose was to conduct a systematic review and examine the previous finite element models and simulations that examined hip joint stresses due to cam FAI.

Methods: The systematic review was conducted to identify those finite element studies of cam-type FAI. The review conformed to the Preferred Reporting Items for Systematic Reviews and Meta-Analyses guidelines and studies that reported hip joint contact pressures or stresses were included in the quantitative synthesis.

Results: Nine articles studied FAI morphologies using finite element methods and were included in the qualitative synthesis. Four articles specifically examined contact pressures and stresses due to cam FAI and were included in the quantitative synthesis. The studies demonstrated that cam FAI resulted in substantially elevated contact pressures (median = 10.4 MPa, range = 8.5 – 12.2 MPa) and von Mises stresses (median 15.5 MPa, range = 15.0 – 16.0 MPa) at the acetabular cartilage; and elevated maximum shear stress on the bone (median = 15.2 MPa, range = 14.3 – 16.0 MPa), in comparison with control hips, during large amplitudes of hip motions. Many studies implemented or adapted idealized, ball-and-cup, parametric models to predict stresses, along with homogeneous bone material properties and in vivo instrumented prostheses loading data.

Conclusion: The formulation of a robust subject-specific FE model, to delineate the pathomechanisms of FAI, remains an ongoing challenge. The available literature provides clear insight into the estimated stresses due to the cam deformity and provides an assessment of its risks leading to early joint degeneration.

2.1 Introduction

The morphologies leading to mechanical femoroacetabular impingement (FAI) can be distinguished as either cam (enlarged femoral head deformity), pincer (acetabular over-coverage), or a combination of both [27, 48]. The cam-type deformity is characterized by a decreased head-neck offset [27, 42, 77], giving it a pronounced anterolateral bump with lack of concavity at the femoral head-neck junction [35, 69] (Figure 2.1). It has been attributed to adverse hip trauma and loading [27, 63, 69], significant athletic activity [2, 59, 63], and contact sports [47, 55], prior to skeletal maturation. Individuals with a larger cam deformity, as defined by higher alpha angles [58], ultimately leads to a greater risk of the anterosuperior femoral head obstructing with the acetabulum during combined motions of hip flexion, rotations [1, 2, 17, 41, 44, 46, 69], and squatting [17, 44, 45, 56, 57], resulting in early adult cartilage degeneration [1, 10, 27, 71].

FAI is rarely painful in its early stages, thus can go unrecognized for several years during its preliminary asymptomatic settling-in phase [22, 36, 38, 72]. Early diagnosis and treatment of FAI is important to alleviate the risk of severe hip pain, irreversible cartilage damage, and osteoarthritis (OA). The difficulty with early diagnosis is that the deformities appear to look normal during its early stages of development [47], when there is an evident lack of focus in implementing additional visualization or diagnostic tools to assess the severity of the deformity.

Although diagnostic imaging (*e.g.*, x-ray, computed tomography (CT), magnetic resonance imaging (MRI) is the standard practice to confirm the presence of any hip deformity, it may be very difficult to determine if an individual will show any symptoms or indicate FAI, especially if dynamic hip motions are not performed. From previous motion analyses, symptomatic patients demonstrated constrained hip motions, such as during level walking [15, 43, 67] and squatting [45, 46]. Additional studies that involved finite element (FE) modelling and analysis examined resultant hip joint stresses due to cam FAI, providing a better picture of the pathomechanism. Many in silico simulations shared similar FE methods, however, posed various research questions that resulted in different observations and dependent variables. Moreover, while several studies implemented different mechanical stress analyses, it was unclear which were more applicable to assess adverse loading conditions in the hip joint due to cam FAI. In efforts to examine the effects of cam-type FAI on mechanical hip joint loading and to better understand the causal relationship between mechanical stimulus and cartilage degeneration, our purpose in this systematic review was to examine previous studies involving finite element

analysis (FEA) that simulated hip joint loading due to cam-type FAI and determined hip joint stresses.

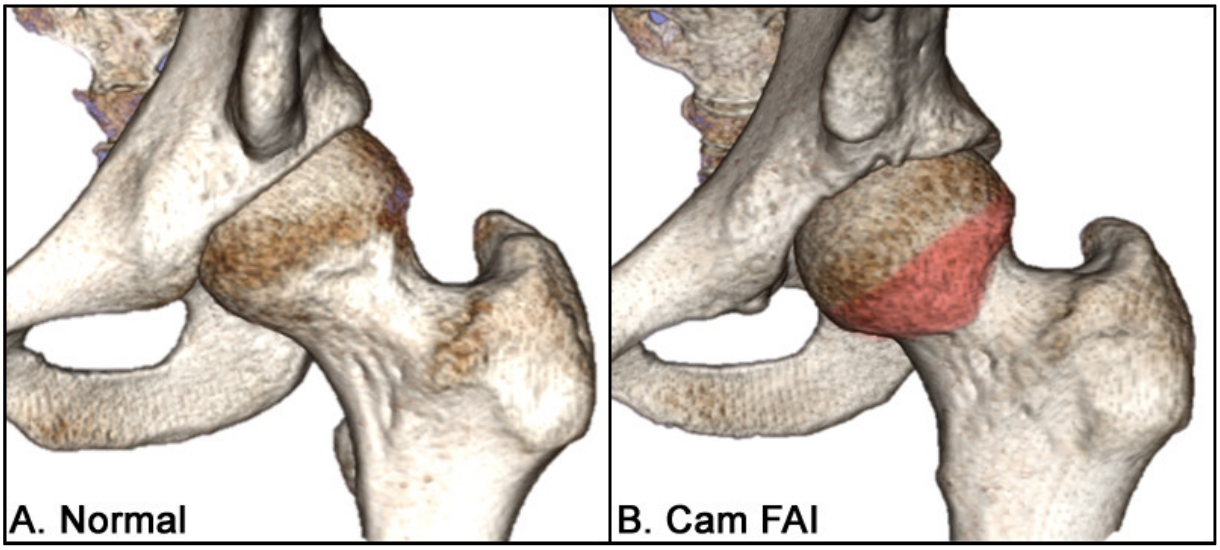

Figure 2.1. Comparison between a normal and a cam FAI hip. Three-dimensional models representing a healthy, normal left hip joint (**A**) and a left hip joint with severe cam-type femoroacetabular impingement (**B**), with the cam deformity highlighted in red.

2.2 Methods

The systematic review conformed to the Preferred Reporting Items for Systematic Reviews and Meta-Analyses (PRISMA) guidelines (2.7 Appendix – PRISMA Checklist). The protocol started with a literature search, from three electronic databases: PubMed, Web of Science (Thomas Reuters), and Cochrane Library. The protocol subsequently consisted of a screening process, to further justify the pertinence and eligibility, and was completed on February 28, 2015.

2.2.1 Identification

A general search was conducted in each of the three online databases using the terms "femoroacetabular impingement", "femoro-acetabular impingement", and "hip impingement", with any of the terms to appear as a keyword or within a field of the article. Among the articles, the earliest was defined by Myers and associates (1999) [55], thus the time period for the literature search was limited from 1999 to 2015. This preliminary search resulted in 2559 combined articles from the three databases.

2.2.2 Screening and Eligibility

The articles were imported into a citation management program (EndNote X4, Thomas Reuters, Philadelphia, PA, USA) where duplicates were removed. Among the remaining articles, a second search used the term "finite element" and further narrowed down the pertinent literature (n = 17). The abstracts of the remaining articles were then reviewed for eligibility and any study that did not examine a cam or pincer morphology was excluded. The included articles were reviewed and a qualitative synthesis compared each study's methodology. A quantitative meta-analysis was conducted on the studies that specifically examined hip joint stresses due to cam FAI. Measurable dependent variable and stress parameters were thoroughly examined in each of the eligible articles, looking specifically for "von Mises stress" (or "maximum distortion energy"), "maximum shear stress" (or "Tresca stress"), or "contact pressure". Studies that reported results with a common dependent variable were grouped together for the meta-analysis.

2.3 Results

A total of 9 articles, in which a cam (8) or pincer (1) hip deformity was simulated using FEA, were deemed eligible and included in the qualitative synthesis. From those, a total of 4 articles examined hip joint contact pressures or stresses due to cam FAI (Figure 2.2).

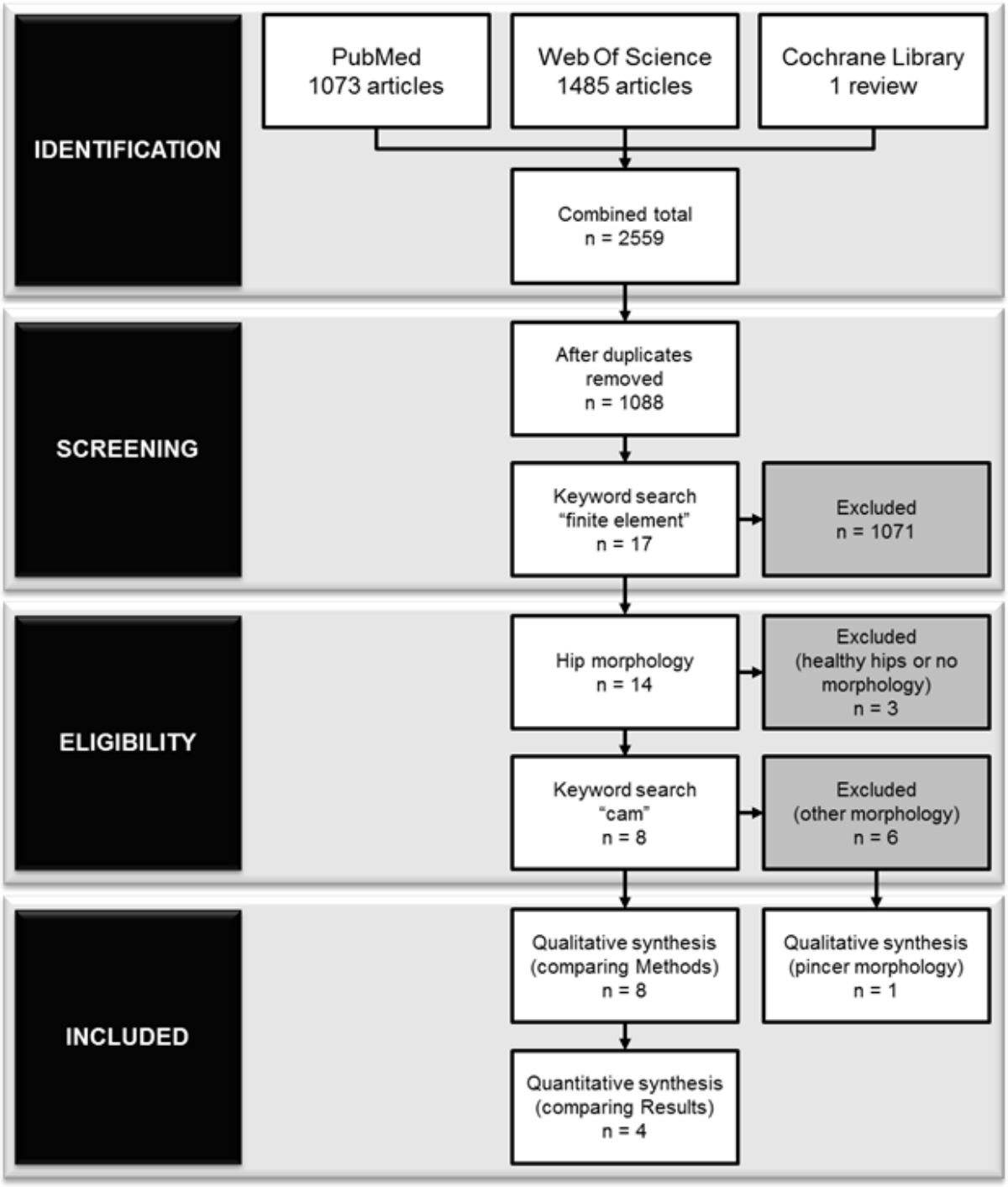

Figure 2.2. Flowchart of selection criteria. According to the PRISMA guidelines, the number of articles started with a total of 2559 combined articles from 3 databases (PubMed, Web of Science, and Cochrane Library). From those, a total of 9 and 4 articles were included in the qualitative and quantitative syntheses, respectively.

2.3.1 Preliminary Parametric Models

The first documented simulation that examined cam FAI was performed by Chegini and associates, focusing on impingement and dysplasia during sitting and walking [17]. The simulations comprised of a spherical, ball-and-cup FE model that was parameterized to various alpha and lateral center-edge (CE) angles, according to the severity of cam FAI (higher alpha angle), pincer FAI (higher CE angle), or dysplasia (lower CE angle). The advantage with using an idealized, parametric model was that the deformities were easily defined and simulated at every 10-degree increments for alpha and center-edge angles (alpha angle = 40 to 80°; CE angle = 0 to 40°). The study took a single patient and considered two loading scenarios – walking and stand-to-sit. Hip contact loads were taken from in vivo instrumented prostheses data and applied through the femoral head [12]. No specifications were given on patient details and dimensions of the final model. Peak contact pressures and von Mises stresses were found in the acetabular cartilage for both activities. During walking, no adverse stresses were noticed with increasing alpha angles. This justified that peak stresses would be more prominent at higher dynamic motions (*i.e.*, higher stresses during squatting motions, as opposed to walking). For the stand-to-sit activity, higher alpha and CE angles resulted in higher contact pressures and stresses.

Chegini and associates' study only considered the oblique-axial plane when varying alpha angles and did not consider radial planes. Moreover, the cam and pincer deformities were limited to an alpha angle and CE angle of 80° and 40°, respectively, thus a more severe cam or pincer deformity was not observed. The cam-only deformity cases showed peak contact pressures that varied from 3.67 to 12.84 MPa (alpha angle = 60 to 80°, CE angle = 20 to 30°); and von Mises stresses from 9.7 to 27.2 MPa (alpha angle = 60 to 80°, CE angle = 20 to 30°), situated at the anterosuperior cartilage. Their mixed impingement cases demonstrated slightly higher peak contact pressures from 10.52 to 16.51 MPa (alpha angle = 60 to 80°, CE angle = 40°); and much higher von Mises stresses from 30 to 37 MPa (alpha angle = 60 to 80°, CE angle = 40°), situated at the anterosuperior cartilage and labrum. It was uncertain if the acetabulum or innominate bone structure was included. The magnitudes of the von Mises stresses for the cam FAI models were provided, however, it was not explicitly reported for the control models. Only cartilage stresses and contact pressures were reported and no results pertaining to the acetabulum, pelvis, or femoral head were featured.

As a follow-up to Chegini and associates' study, Arbabi and associates further examined penetration depths in the acetabular cartilage and labrum, indicating very high curvilinear and radial penetration due to the idealized geometries [6]. However, no specific information about the resultant von Mises stresses was provided. Although an idealized model was implemented, Chegini and associates contributed an exploratory study in the early phases of FAI research, which emerged as a preliminary benchmark.

2.3.2 Subject-Specific Bone Models

The next set of simulations involving FEA attempted to improve the subject-specificity of the models. In an earlier work by Ng and associates, two patients with severe cam FAI were matched with two healthy control participants [57]. Each participant's geometric model was segmented from subject-specific CT data and supplemented with subject-specific, intersegmental hip joint reaction forces. The manually segmented models provided a more realistic representation of the cam deformity, demonstrating the adverse loading conditions in the hip joint during standing and squatting. Elevated stresses were located on the anterosuperior bone surface, beneath the acetabular cartilage, during squatting for patients with severe cam FAI (15.2 ± 1.8 MPa), in comparison with healthy control participants (4.5 ± 0.1 MPa). This study provided a modelling perspective of cam FAI and integrated more subject-specific data to further understand the pathomechanism with mechanical stimuli corresponding to the known areas of acetabular cartilage damage. With elevated stresses on the bone surface (as opposed to direct loading on the cartilage), it emphasized the need to further understand the morphology and determine if joint degeneration may be due to the indirect changes in the subchondral bone. Although the inclusion of a labrum in FEA remains elusive [5], it would be beneficial in future studies to understand the residual physiological effect of the labral seal for this pathological hip condition [23-25]. In addition, the hip joint reaction forces provided valuable approximations of net forces and moments, but were still underestimations of in vivo contact forces. Future initiatives to include individual muscles and hip contact forces would better represent the physiological reactions and resultant hip contact stresses.

In contrast, Jorge and associates developed their subject-specific bone models from radial MRI, while cartilage and labrum were approximated using computer-aided design software [37]. Only one FAI patient model was developed (male, age = 27 years, alpha angle = 98°), matched

with one healthy control model (female, age = 50 years, alpha angle = 48°). All soft tissues were considered linear elastic and isotropic, and the bones were assumed rigid. A compression load was applied to the femur on the acetabular cavity as well as flexural movements and internal rotations. Loading data from in vivo instrumented prostheses database were used in the simulations, using an arbitrary weight not specific to either participant. Jorge and associates also found an elevated peak contact pressure and von Mises stress in the anterosuperior cartilage (11.6 and 14.4 MPa, respectively) and labrum (16.4 and 14.7 MPa, respectively), during hip flexion for their FAI model, however, observed a substantially higher peak contact pressure (20.6 MPa) and von Mises stress (28.2 MPa) during partial and full internal rotation, respectively. The von Mises stress magnitudes for the control model was not explicitly reported. However, their study was limited by the sample size and poor matching criteria – one young male, with a severe cam deformity, matched with one healthy older female. This single comparison exhibited substantial differences, but may not have explained the differences or variations among the FAI and the control populations.

2.3.3 Effects of Surgery

Alternatively, a few studies recently implemented FE models to examine the effect of surgical osteochondroplasty, specifically looking at the influence of resection depths with fracture loading and risks due to adverse loading [3, 64]. Alonso-Rasagado and associates developed a single FE hip model from CT data of a typical cam-type hip to predict stresses in the femoral head-neck junction after open surgical resection [3]. Based on this single hip model, bone resections were parameterized and performed virtually to incremental resection depths, instead of incorporating real post-operative CT data and hip joint loadings. No information was provided about the single femur model (*e.g.*, sex, age, other morphologies). It was concluded that higher amplitudes of hip motion (*e.g.*, knee bend and stairs descent) yielded the highest stresses when resection depth was beyond 10 mm. However, the authors used in vivo instrumented prostheses data (taken from an older population) which led them to reduce the elastic moduli of the bone models. This lacked a level of patient-specificity to represent the correct amount of bone resection for a younger population with cam FAI, although still suggesting a relative limit for resection depth.

Rothenfluh and associates used a general 3D femur model taken from a public anatomy database to simulate resection geometry on fracture risks [64]. Using in vivo data from instrumented prostheses data for stumbling and walking, they concluded that a resection should be limited to 20% depth and 35% length of the femoral neck. The group acknowledged that large inter-patient variations in bone quality, stature, and anatomy can occur; and, as a consequence, suggested that subject-specific models would greatly improve fracture risk predictions.

Liechti and associates expanded the early parametric hip models by Chegini and associates [17], to further examine pincer FAI and influences of contemporary surgical interventions on stress distributions in protrusio hips [51]. Material properties and pre-processing conditions were similar to the previous simulations [6. 17]. Hip joint loading data were again taken from in vivo instrumented prostheses data, for walking and stand-to-sit motions, and applied to several parameterized hip models (*e.g.*, normal, dysplasia, protrusio) and surgical intervention methods (*e.g.*, rim trimming and acetabular reorientation). No other models or components were considered, other than the cartilage and labrum components. The protrusio hip resulted in elevated contact pressures in the medial acetabular cartilage (1.62 MPa, 24% higher than their normal hip) and substantially higher von Mises stresses in the medial aspect of the posteroinferior acetabulum (54% higher than their normal hip). Acetabular reorientation decreased peak contact pressures, while additional rim trimming substantially reduced peak stresses. The authors noted that subject-specificity was not considered or addressed, as their models represented averaged geometries based on empirical, morphological data and not representative of a "larger spectrum of anatomy" [51].

2.3.4 Cartilage Behaviours

A more recent FE study by Hellwig and associates adapted Chegini and associates' parametric hip model [17] to examine cartilage stresses due to cam FAI [33]. Only two conditions were parameterized that compared a hip with cam FAI (alpha angle = 74°) and a healthy control hip (alpha angle = 40°). The cartilage component was modelled as a poroelastic, orthotropic material to characterize biphasic properties. Similar to the previous parametric studies [6, 17, 51], the activities of walking and stand-to-sit were simulated. As result, peak contact pressures for the normal hip were located in the superior cartilage during walking (2.87 MPa) and in the posteromedial cartilage during stand-to-sit (3.58 MPa). Peak pore pressure was noticeably

different between the control model (0.42 MPa, in the posterior cartilage) and the FAI model (3.76 MPa, in the anterosuperior cartilage). No other bone component was considered in the analysis. The study implemented in vivo contact loads from the instrumented prostheses database [12], neglecting the subject-specificity of hip joint loading due to cam FAI. The study was also limited by a low sample size – one FAI condition matched with one control. Moreover, the authors noted that their 3D geometries were simplified and optimized for convergence, which may overlook the subject-specificity of inter-individual anatomical characteristics and material properties [33].

2.3.5 Development of the Cam Deformity

A recent study by Roels and associates investigated mechanical factors leading to the development of a cam-type deformity [63]. A single FE model of the proximal femur was reconstructed from CT data (age = 12 years, left leg), parameterized with 3 different growth plate shapes, and simulated under 4 activities (normal walking, internal rotation, external rotation, hip flexion) using loading data from in vivo instrumented prostheses data. They implemented an osteogenic index to look at changes to the epiphyseal plate and followed up with their previous findings on young athletes undergoing skeletal maturation [2]. As a result, Roels and associates observed larger epiphyseal extensions during external rotation and hip flexion, with elevated osteogenic indexes localized where the cam deformity would likely develop. Unlike the previous models of cam FAI, they modelled the growth plate with a constant elastic modulus and considered heterogeneous bone material properties for the femur, taken from CT data, to better represent the varying densities.

In contrast with the other FE studies, Roels and associates' intention was not to examine hip joint stresses, but rather to look at the development of the cam deformity and its association with various activities and loading parameters. Thus, their study and modelling parameters were reviewed and included in the qualitative synthesis to thoroughly examine pre-processing FE methods; however, since their study posed a different research question, their results were not included in the quantitative synthesis

2.3.6 Meta-Analysis

Table 2.1 lists the previous FE studies in literature that examined FAI – summarizing the study details, participant details, loading details, and results. Among the screened studies that had comparable quantifiable results, the most common dependent variable was an acetabular cartilage contact pressure or stress parameter during an activity that required larger amplitudes of hip motions (stand-to-sit, maximum squat depth, or deep hip flexion). Two studies reported peak contact pressures and peak von Mises stresses in the acetabular cartilage due to cam FAI, indicating a median contact pressure of 10.4 MPa (range = 8.5 – 12.2 MPa) and median von Mises stress of 15.5 MPa (range = 15.0 – 16.0 MPa) [17, 37], while two studies reported maximum shear stresses, indicating a much lower median of 3.10 MPa (range = 2.84 – 3.35 MPa) [33, 57]. Only one of the studies examined stresses in the bone underneath the acetabular cartilage and indicated maximum shear stresses of 15.2 MPa (range = 14.3 – 16.0 MPa) [57] and one study indicated a peak pore pressure of 4.10 MPa [33]. A comparison of all reported peak stresses for each study's FAI and control groups can be seen in Figure 2.3.

Table 2.1. Previous studies on cam FAI that implemented finite element methods, summarizing the study detail, modelling and simulation methods, and results of the cam FAI group.

Study Details			**Participant Details**		**Loading Details**		**Results**	
Scope	**Author (year)**	**Purpose**	**Sample Size**	**Model**	**Activities**	**Methods**	**Peak Stress Magnitude**	**Peak Stress Location**
Stresses due to cam deformity	Chegini, et al. [17] (2009)	Contact pressure and stress in cam and pincer FAI, dysplasia	n = 1 (25 conditions, parameterized for alpha and center-edge angles)	Spherical, ball-and-cup model; uniform cortical shell; with linear-elastic, isotropic bone and cartilage	Walking and stand-to-sit	Percentage of bodyweight load, from in vivo instrumented prostheses data	Contact pressures from 3.67 to 12.84 MPa and von Mises stresses from 9.70 to 27.20 MPa, during stand-to-sit	Anterosuperior cartilage and labrum, during stand-to-sit
	Ng, et al. [57] (2012)	Stresses on cartilage and bone layer due to cam FAI	n = 4 (2 cam males; 29, 44 years; alpha angle = 74, 84°; matched with 2 control males; 36, 54 years; alpha angle = 41, 45°)	Subject-specific hip joint geometry, from CT data; variable cartilage thickness; with orthotropic bone and isotropic cartilage	Standing and squatting	Subject-specific intersegmental reaction forces from inverse dynamics	Maximum shear stress in cartilage from 3.3 to 3.9 MPa and in bone from 13.4 to 16.9 MPa, during squatting	Anterosuperior quadrant of acetabulum, during squatting
	Jorge, et al. [37] (2014)	Contact pressure and stress on cartilage due to cam FAI	n = 2 (1 cam male, 27 years, alpha angle = 98°; matched with 1 control female, 48 years, alpha angle = 48°)	Subject-specific geometry, from MRI; no information on bone model or materials; linear-elastic, isotropic soft tissues	Joint compression with full flexion and internal rotation	Percentage of bodyweight load, from in vivo instrumented prostheses data	Contact pressures from 11.6 to 16.4 MPa and von Mises stresses from 14.4 to 14.7 MPa, during flexion	Anterosuperior cartilage and labrum, during flexion
	Hellwig, et al. [33] (2015)	Cartilage behaviour due to cam FAI	n = 2 (1 cam, alpha angle = 74°; matched with 1 control, alpha angle = 40°)	Spherical, ball-and-cup model; uniform cortical shell; linear elastic, isotropic bone with poroelastic, orthotropic cartilage	Walking and stand-to-sit	Percentage of bodyweight load, from in vivo instrumented prostheses data	Contact pressure of 4.09 MPa and Tresca stress of 2.59 MPa, during stand-to-sit	Posteromedial cartilage, during stand-to-sit
Penetration Depth	Arbabi, et al. [6] (2010)	Penetration depth and stresses in labrum	n = 1 (25 conditions, parameterized for alpha and center-edge angles)	Spherical, ball-and-cup model; uniform cortical shell; with linear elastic, isotropic bone and cartilage	Stand-to-sit	Percentage of bodyweight load, from in vivo instrumented prostheses data	High curvilinear and very high radial penetration; no details on peak stress magnitude	Anterolateral labrum
Development of cam deformity	Roels, et al. [63] (2014)	Loading on epiphyseal growth plate	n = 1 (male, 12 years; parameterized for flat and convex growth plate shapes)	Subject-specific femur geometry, from CT data; with subject-specific bone material properties, based on empirical formula	Walking, internal rotation, external rotation, deep flexion	Percentage of bodyweight load, from in vivo instrumented prostheses data	Osteogenic index of 0.7 MPa, during external rotation; noticeable increase in osteogenic index, during external rotation and flexion	Superolateral side of growth plate, during external rotation
Effects of surgery	Alonso-Rasagado, et al. [3] (2012)	Stresses on femoral head-neck after cam resection	n = 1 (6 conditions, parameterized for various resection depths)	Subject-specific femur geometry, from CT data; with elastic-plastic, isotropic bone	Single and double leg stance, walking, stairs descent, knee bend	Percentage of bodyweight load, from in vivo instrumented prostheses data	von Mises stresses of 16 to 17.5 MPa, at resection depth > 10 mm, during knee bend	Superolateral femoral neck, with resection depth > 10 mm, during knee bend
	Rothenfluh, et al. [64] (2012)	Fracture loads after cam resection	n = 1 (3 conditions, parameterized for various resection depths)	Subject-specific femur geometry, from anatomy database; with linear elastic, isotropic bone	Stumbling, fast walking, normal walking	Percentage of bodyweight load, from in vivo instrumented prostheses data	Critical fracture load = 4150 N, at 30% resection (28 mm length, 39 mm width	Location of fracture at inferomedial femoral neck
Stresses due to pincer deformity	Liechti, et al. [51] (2014)	Stresses due to pincer FAI	n = 1 (6 conditions, parameterized center-edge angles for various acetabular shapes)	Spherical, ball-and-cup model; uniform cortical shell; with linear elastic, isotropic bone and cartilage	Walking and stand-to-sit	Percentage of bodyweight load, from in vivo instrumented prostheses data	Contact pressure of 1.62 MPa, for protrusio hip during stand-to-sit	Posteromedial cartilage (5.1 mm from medial margin, with respect to acetabular arc), for protrusio hip during stand-to-sit

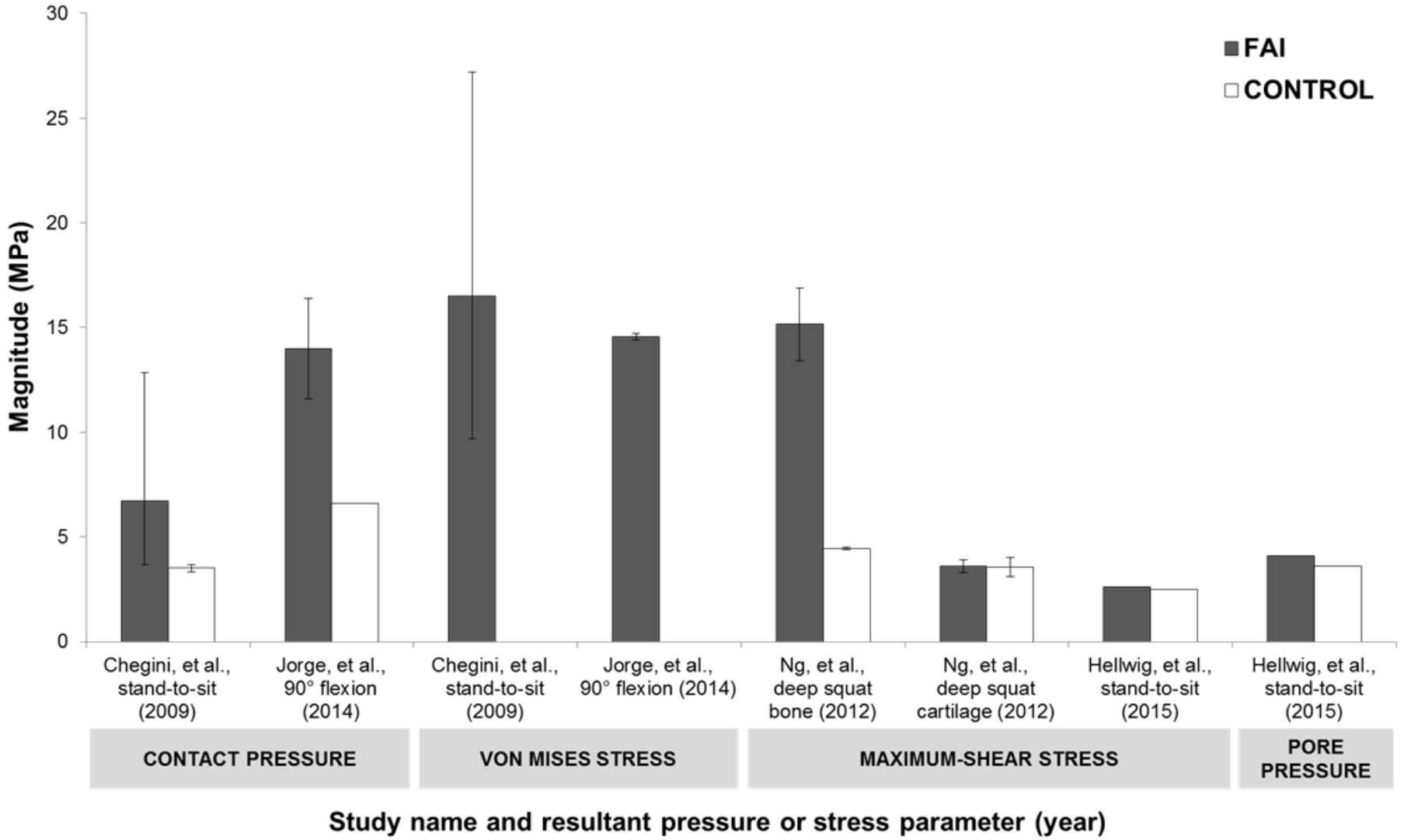

Figure 2.3. Summary of previous studies' peak hip joint contact pressures and stresses. Peak contact pressure or stress on the acetabular cartilage or bone, during a deep hip flexion task for each study's cam FAI (grey) and control group (white), reporting the averaged peak magnitude and maximum and minimum range. (The von Mises stresses for the control groups were not explicitly reported in Chegini, et al. 2009 and Jorge, et al. 2014, therefore, were intentionally omitted.)

2.4 Discussion

2.4.1 Model Predictions

The previous generation of in silico FE studies provided clear objectives in examining contact pressures and stresses due to cam FAI, with each study's parameters justifying their initial research questions. The simulations provided a concrete understanding of pathological joint loading and showed that the cam morphology led to substantially elevated stresses in the acetabulum at a higher range of hip motion. The different studies implemented various methods to characterize hip joint contact mechanics, using different parameters to measure contact stresses, thus making a direct comparison of dependent variables slightly more difficult. The extracted data indicated that contact pressure and von Mises stress were higher in the acetabular cartilage [17, 37], in comparison with maximum shear stress and pore pressure [33, 57], in cam FAI models.

As with any in silico study, there are many limitations associated with FE methods and its resultant predictions. As noted by Viceconti and associates, sensitivity and validity are still ongoing challenges to be addressed in FEA, especially when the study involves complex multicomponent, musculoskeletal systems [79]. They further outlined that simulations should implement a well-defined and assessed model with correctly identified and verified input parameters, in efforts to ensure accurate and representative predictions. Many of the previous FE studies of cam FAI featured convergence analyses to address concerns of meshing sensitivities, but their conclusions were still cautious. The FE predictions were often validated against case controlled hip joint simulations, involving other similar FE hip models, or validated against previous clinical observations.

A comparison with clinical observations can partially justify the validity of predictive models. As many of the FE simulations demonstrated, the cam morphology can lead to acetabular cartilage damage predominantly in the anterosuperior region [8-10, 18, 71]. Beck and associates observed 26 surgically dislocated hips and noted that the greatest depth of the cartilage lesions were located in the anterosuperior quadrant [10]. Similarly, Beaulé and associates observed 23 hips and noted cartilage lesions combined with labral tears, also located in the anterosuperior clock-face, at the time of surgery [9]. In addition, another study by Beaulé and associates reported severe acetabular cartilage damage in the anterosuperior region and further

correlated the cartilage damage with elevated alpha angles [8]; whereas Clohisy and associates observed slightly higher articular cartilage abnormalities in the superolateral region, rather than the anterior periphery [18].

2.4.2 Hip Joint Modelling

Comprehensive, subject-specific reconstructions were often avoided, perhaps due to the time-consuming efforts and complexities of imaging, geometric, and loading parameters, which ultimately resulted in lower inter-subject variability [79]. In most cases, FE simulations of the hip considered mainly bone models and the articulation components [4-6, 17, 57, 65, 66]. As a future improvement to the subject-specific material characteristics, FE hip joint models may be constructed from segmented bone and soft tissue geometries obtained from subject-specific CT and MRI data, using image segmentation software. It will be imperative to examine soft tissues landmarks around the hip joint. The inclusion of the labrum in hip joint modelling will also be crucial to understand the nature of the seal in pathological hip deformities [23-25]. The labrum can be reconstructed around the periphery of the acetabulum, creating a seal around the femoral head. To ensure that the articulation components as obtained from MRI are in accordance with the CT based bone models, the bone landmarks in each set of imaging data must be registered [50, 78].

Many studies of hip joint biomechanics have been simplified into 2D planar [65, 80] or idealized into a ball-and-socket analyses, which was deemed by some researchers as appropriate for preliminary approximations [28]. Knowing that the femoral head conforms to a conchoid shape rather than a perfect sphere [54], it would now be important to incorporate subject-specific contour data of the femoral head to accurately estimate the cartilage stresses and contact areas. Similar to the approach of CT-based navigation for preoperative planning, 3D FE models are now reconstructed using imaging data following a subject-specific approach [29]. Since the segmentation process is time-consuming, many studies implemented semi-automated segmentation methods to extract objects of interests from CT and MRI data [26, 40, 52]. The clarity and the sensitivity of the images tend to vary from scan to scan, often requiring more manual segmentation methods to ensure a higher level of confidence.

The selection of the material properties for FE modelling and simulations often depends on the physiological application and mechanical assembly of the models. Nonlinear effects of

soft tissues can be approximated with hyperelastic [5] or poroelastic material properties [25, 70] to estimate responses. As for the bone geometries, some studies opted to apply an elastic modulus based on an empirical formula derived from the apparent density of bone [11, 61, 75, 76]. A common limitation that all the previous FE studies on cam FAI had was that bone was modelled as a homogeneous material. It was argued in many studies that linear elastic models would be sufficient for quasi-static loading frequencies, and therefore two separate, linear elastic isotropic entities to represent the cortical shell and internal trabecular structure were often implemented [6, 17, 51, 65, 66, 75]. However, knowing that bone is heterogeneous, the material properties would react differently in various locations. At minimum, since bone is macroscopically composed of cortical and trabecular bone with varying bone densities, there is a need to consider varying elastic moduli throughout its composition according to Hounsfield units from quantitative CT data.

In Anderson and associates' FEA of the subject-specific hip joint (2008), bone was modelled as a hyperelastic, isotropic material (with tetrahedral elements), whereas cartilage was modelled as a neo-Hookean material (using brick elements) [4]. As a follow-up study, Anderson and associates (2010) used the same biomechanical approach to examine different modelling parameters – altering the femur's and cartilage's material models to examine their effects on stress predictions [5]. Their models neglected the trabecular bone component, arguing that a cortical shell was sufficient to demonstrate joint reactions [4, 5]. For the purpose of predicting the mechanical stimuli and areas of bone formation in a subject-specific fashion, it may not be sensible to disregard the trabecular bone component when simulating FAI, as it provides inherent stability and the foundation of the bone remodelling matrix.

Anderson and associates' latter study was meant as a comparative study to delineate the possible outcomes from various methods. Their parametric models demonstrated that spherical and conchoidal femoral head models, together with a smooth cartilage, distributed the stresses more evenly and underestimated stresses, in comparison with a subject-specific geometry. Furthermore, a constant cartilage thickness approach would be less realistic for pathologic hip deformities. It was not suggested which of their parametric hip models was the most correct; instead, it was described what should be the expectation in terms of stress patterns given specific input parameters. This further confirms that idealized models cannot adequately assess stress predictions and reiterates the need for subject-specific geometric models. In addition, Harris and

associates reconstructed statistical shape models of hips with and without the cam deformity, from subject-specific CT data [30]. Although their intention was not FEA modelling, the statistical shape models compared the cam morphology with control femurs, emphasizing the need for subject-specific geometries. There was a noticeable difference between the two groups at the anterolateral head-neck junction, corresponding with the locations of cam deformity.

2.4.3 Motion and Loading with Cam FAI

To further the understanding of subject-specific hip joint stresses, the joint loading should be specific and integrated with the associated hip joint model (*i.e.*, subject-specific joint loading should not be approximated from instrumented prostheses data, if possible). Motion analysis can evaluate 3D kinematics and kinetics, during various activities of daily living. Since the structure and range of hip motion is vital to locomotion, standing upright, and performing many daily activities, it is important to determine how a deformity potentially impacts hip biomechanics. In a level-walking study by Kennedy and associates [43], it was found that walking biomechanics of cam FAI demonstrated marginal kinetic differences, when compared with a control group, but showed constrained abduction in the frontal plane. In contrast, Hunt and associates found lower hip extension, adduction, and internal rotation during the stance phase [34]. Lamontagne and associates further showed significant differences in pelvic motion between cam FAI and control subjects for a deep squat motion, where participants performed a maximum dynamic squat [46]. Their cam FAI group was unable to squat as low (41.5 ± 12.5%, as a percentage of leg height) compared with the control group (32.3 ± 6.8%, $p = 0.037$), suggesting that the maximal squat depth may be feasible as a diagnostic test [46]. This further motivates FE studies of cam FAI to involve larger amplitudes of hip motions.

In a follow-up study, post-operative patients (8 to 32 months after open surgical dislocation) were able to squat significantly lower (33.2 ± 10.3%), compared with their pre-operative performance (36.9 ± 12.0%, $p = 0.027$) [44]. However, these patients were unable to return to their pre-operative walking performance [15]. Contrarily, Rylander and associates found significant improvements in level-walking, confirming positive improvements for post-operative patients [67].

From 3D kinematics and kinetics data, net hip joint forces and moments can be calculated from inverse dynamics. These forces and moments represent intersegmental reaction loads, but

the approach excludes individual muscle contributions, co-contractions, and other soft tissue loading (*i.e.*, net passive moments). Nevertheless, the approach is still commonly used to estimate net joint moments and forces. To better understand the effect of cam FAI on the internal mechanical loading, hip contact forces are required and necessitate muscle and soft tissue loading contributions. In vivo contact force measurements are possible with instrumented prostheses [13, 14, 19, 32]. The data received from instrumented prostheses contributed to numerous studies and publications, towards the better understanding of joint contact loading, and leading to a renowned online database. These studies were often limited by sample size and population, as most of the patients implanted with instrumented prostheses represented a specific age group and disease process (*i.e.*, older population with severe arthritis, in contrast with a younger, athletic FAI population). Overall, this invasive method raises numerous technical and ethical concerns.

The approach followed by computational musculoskeletal models appears to be more general and versatile to estimate joint loadings, in efforts to include muscle contributions [20, 53]. The EMG-driven musculoskeletal models can implement a forward dynamics analysis to estimate muscle forces, from muscular activities [16, 53, 68], showing a better sensitivity to the subject-specific muscle activation [49]. The inclusion of muscle and contact forces obtained from such models may yield more complete and accurate loading conditions for FE analyses compared to what is currently available in the literature. To our knowledge, no FE study has implemented subject-specific muscle and hip joint contact forces, to examine resultant contact stresses.

2.4.4 Asymptomatic Population

There has been growing interest to understand why many individuals with the cam deformity do not develop early symptoms of FAI [31, 60, 62]. Asymptomatic individuals are characterized by a cam-type deformity; however, do not demonstrate FAI (*i.e.*, individuals with the cam deformity but do not demonstrate any impingement, clinical signs, symptoms, or pain). Although several studies examined the asymptomatic population, measuring additional anatomical parameters from radiographic [7, 31, 62], CT [22, 39, 56], or MRI [21, 73, 74] data; there are currently no FE studies that indicate hip joint stresses in the asymptomatic population. The health risk with the asymptomatic cam deformity is that it can remain undetected even though it predisposes to

early joint degeneration. Ultimately, a closer examination of additional anatomical parameters, hip motion, joint loading and stresses, and correlation with resultant bone mineral density, might shed some light into possible clinical associations, and could greatly contribute to the to the understanding of the pathomechanisms at play in cam FAI.

2.5 Conclusion

There is an evident trend to implement FEA toward the study of cam-type FAI. It was apparent that the previous FE studies were limited by incorrectly matched groups, which also indicated the rigorous and time-consuming efforts required to manually segment imaging data. Several of the previous studies implemented or adapted idealized, ball-and-cup, parametric models to predict hip joint stresses, in addition to homogeneous material properties and in vivo instrumented prostheses loading data. Although simplified for convergence, the parametric models in combination with in vivo hip contact loads measured from an older population may not be adequate to satisfy broader subject-specificity requirements. One of the biggest gaps in literature, and one of the ongoing challenges, is the formulation of a robust subject-specific FE model – one that will consider subject-specific parameters, hip joint loading, geometric models – that can predict the adverse loading conditions in the symptomatic and asymptomatic populations, ultimately delineating the pathomechanisms of FAI. This systematic review highlighted three main areas for development, which were not addressed in previous studies:

1. There was no consideration for anatomical parameters associated with FAI symptoms and very little emphasis on subject-specific hip joint geometries (where several studies implemented idealized, ball-and-cup parametric models)
2. There was no consideration for subject-specific bone material properties
3. There was no consideration for subject-specific hip joint loading parameters

Moving forward, although there is strong suggestion from clinical observations that the presence of cam FAI presents a substantial risk of developing early hip OA, there are still large gaps in literature that cannot yet support such causality or account for different paths between the symptomatic and asymptomatic populations in the face of apparently similar mechanical effects due to the deformity. The data to accurately model, simulate, and understand the morphologies associated with FAI are still growing. Furthermore, very few studies incorporated subject-specific models to simulate biomechanical loading scenarios with the intention to address FAI.

To better understand the pathomechanisms of cam FAI, one will have to answer the question: *what are the effects of cam FAI on mechanical hip joint loading*? Currently, although the results are not quite robust yet to reflect actual in vivo loading, as there is still room for improvement in terms of hip joint modelling, the available literature provides some insight into the estimated stresses due to the cam morphology; in turn this stress estimation may provide an assessment of the risk of early joint degeneration.

2.6 References

1. Agricola R, Heijboer MP, Bierma-Zeinstra SM, Verhaar JA, Weinans H, Waarsing JH. Cam impingement causes osteoarthritis of the hip: a nationwide prospective cohort study (CHECK). *Ann Rheum Dis*. 2012;72:918-923.
2. Agricola R, Heijboer MP, Ginai AZ, Roels P, Zadpoor AA, Verhaar JA, Weinans H, Waarsing JH. A Cam Deformity Is Gradually Acquired During Skeletal Maturation in Adolescent and Young Male Soccer Players: A Prospective Study With Minimum 2-Year Follow-up. *Am J Sports Med*. 2014;
3. Alonso-Rasgado T, Jimenez-Cruz D, Bailey CG, Mandal P, Board T. Changes in the stress in the femoral head neck junction after osteochondroplasty for hip impingement: A finite element study. *J Orthop Res*. 2012;30:1999-2006.
4. Anderson AE, Ellis BJ, Maas SA, Peters CL, Weiss JA. Validation of finite element predictions of cartilage contact pressure in the human hip joint. *J Biomech Eng*. 2008;130:051008.
5. Anderson AE, Ellis BJ, Maas SA, Weiss JA. Effects of idealized joint geometry on finite element predictions of cartilage contact stresses in the hip. *J Biomech*. 2010;43:1351-1357.
6. Arbabi E, Chegini S, Boulic R, Tannast M, Ferguson SJ, Thalmann D. Penetration depth method--novel real-time strategy for evaluating femoroacetabular impingement. *J Orthop Res*. 2010;28:880-886.
7. Bardakos NV, Villar RN. Predictors of progression of osteoarthritis in femoroacetabular impingement: a radiological study with a minimum of ten years follow-up. *J Bone Joint Surg Br*. 2009;91:162-169.
8. Beaulé P, Hynes K, Parker G, Kemp K. Can the Alpha Angle Assessment of Cam Impingement Predict Acetabular Cartilage Delamination? *Clin Orthop Rel Res*. 2012;470:3361-3367.
9. Beaulé PE, Zaragoza E, Motamedi K, Copelan N, Dorey FJ. Three-dimensional computed tomography of the hip in the assessment of femoroacetabular impingement. *J Orthop Res*. 2005;23:1286-1292.
10. Beck M, Kalhor M, Leunig M, Ganz R. Hip morphology influences the pattern of damage to the acetabular cartilage: femoroacetabular impingement as a cause of early osteoarthritis of the hip. *J Bone Joint Surg Br*. 2005;87:1012-1018.
11. Behrens BA, Nolte I, Wefstaedt P, Stukenborg-Colsman C, Bouguecha A. Numerical investigations on the strain-adaptive bone remodelling in the periprosthetic femur: influence of the boundary conditions. *Biomed Eng Online*. 2009;8:7.
12. Bergmann G, Deuretzbacher G, Heller M, Graichen F, Rohlmann A, Strauss J, Duda GN. Hip contact forces and gait patterns from routine activities. *J Biomech*. 2001;34:859-871.
13. Bergmann G, Graichen F, Rohlmann A. Hip joint loading during walking and running, measured in two patients. *J Biomech*. 1993;26:969-990.
14. Bergmann G, Graichen F, Rohlmann A, Bender A, Heinlein B, Duda GN, Heller MO, Morlock MM. Realistic loads for testing hip implants. 2010;20:65-75.
15. Brisson N, Lamontagne M, Kennedy MJ, Beaulé PE. The effects of cam femoroacetabular impingement corrective surgery on lower-extremity gait biomechanics. *Gait Posture*. 2013;37:258-263.
16. Buchanan TS, Lloyd DG, Manal K, Besier TF. Neuromusculoskeletal modeling: estimation of muscle forces and joint moments and movements from measurements of neural command. *J Appl Biomech*. 2004;20:367-395.
17. Chegini S, Beck M, Ferguson SJ. The effects of impingement and dysplasia on stress distributions in the hip joint during sitting and walking: a finite element analysis. *J Orthop Res*. 2009;27:195-201.
18. Clohisy JC, Baca G, Beaulé PE, Kim YJ, Larson CM, Millis MB, Podeszwa DA, Schoenecker PL, Sierra RJ, Sink EL, Sucato DJ, Trousdale RT, Zaltz I. Descriptive epidemiology of femoroacetabular impingement: a North American cohort of patients undergoing surgery. *Am J Sports Med*. 2013;41:1348-1356.
19. Davy DT, Kotzar GM, Brown RH, Heiple KG, Goldberg VM, Heiple KG, Jr., Berilla J, Burstein AH. Telemetric force measurements across the hip after total arthroplasty. *J Bone Joint Surg Am*. 1988;70:45-50.

20. Delp SL, Anderson FC, Arnold AS, Loan P, Habib A, John CT, Guendelman E, Thelen DG. OpenSim: open-source software to create and analyze dynamic simulations of movement. *IEEE Trans Biomed Eng*. 2007;54:1940-1950.

21. Ejnisman L, Philippon M, Lertwanich P, Pennock A, Herzog M, Briggs K, Ho C. Relationship Between Femoral Anteversion and Findings in Hips With Femoroacetabular Impingement. *Orthopedics*. 2013;36:e293-300.

22. Ergen FB, Vudali S, Sanverdi E, Dolgun A, Aydingoz U. CT assessment of asymptomatic hip joints for the background of femoroacetabular impingement morphology. *Diagn Interv Radiol*. 2013;

23. Ferguson SJ, Bryant JT, Ganz R, Ito K. The acetabular labrum seal: a poroelastic finite element model. *Clin Biomech (Bristol, Avon)*. 2000;15:463-468.

24. Ferguson SJ, Bryant JT, Ganz R, Ito K. An in vitro investigation of the acetabular labral seal in hip joint mechanics. *J Biomech*. 2003;36:171-178.

25. Ferguson SJ, Bryant JT, Ganz R, Ito K. The influence of the acetabular labrum on hip joint cartilage consolidation: a poroelastic finite element model. *J Biomech*. 2000;33:953-960.

26. Fornaro J, Székely G, Harders M, *Semi-automatic Segmentation of Fractured Pelvic Bones for Surgical Planning*, in *Biomedical Simulation*, F. Bello and S. Cotin, Editors. 2010, Springer Berlin Heidelberg. p. 82-89.

27. Ganz R, Parvizi J, Beck M, Leunig M, Nötzli H, Siebenrock KA. Femoroacetabular Impingement: A Cause for Osteoarthritis of the Hip. *Clin Orthop Rel Res*. 2003;417:112-120.

28. Genda E, Iwasaki N, Li G, MacWilliams BA, Barrance PJ, Chao EY. Normal hip joint contact pressure distribution in single-leg standing--effect of gender and anatomic parameters. *J Biomech*. 2001;34:895-905.

29. Gilles B, Christophe FK, Magnenat-Thalmann N, Becker CD, Duc SR, Menetrey J, Hoffmeyer P. MRI-based assessment of hip joint translations. *J Biomech*. 2009;42:1201-1205.

30. Harris MD, Datar M, Whitaker RT, Jurrus ER, Peters CL, Anderson AE. Statistical shape modeling of cam femoroacetabular impingement. *J Orthop Res*. 2013;31:1620-1626.

31. Hartofilakidis G, Bardakos NV, Babis GC, Georgiades G. An examination of the association between different morphotypes of femoroacetabular impingement in asymptomatic subjects and the development of osteoarthritis of the hip. *J Bone Joint Surg Br*. 2011;93:580-586.

32. Heller MO, Bergmann G, Deuretzbacher G, Durselen L, Pohl M, Claes L, Haas NP, Duda GN. Musculo-skeletal loading conditions at the hip during walking and stair climbing. *J Biomech*. 2001;34:883-893.

33. Hellwig FL, Tong J, Hussell JG. Hip joint degeneration due to cam impingement: a finite element analysis. *Comput Methods Biomech Biomed Engin*. 2015;1-8.

34. Hunt MA, Guenther JR, Gilbart MK. Kinematic and kinetic differences during walking in patients with and without symptomatic femoroacetabular impingement. *Clin Biomech (Bristol, Avon)*. 2013;28:519-523.

35. Ito K, Minka MA, 2nd, Leunig M, Werlen S, Ganz R. Femoroacetabular impingement and the cam-effect. A MRI-based quantitative anatomical study of the femoral head-neck offset. *J Bone Joint Surg Br*. 2001;83:171-176.

36. Jaberi FM, Parvizi J. Hip pain in young adults: femoroacetabular impingement. *J Arthroplasty*. 2007;22:37-42.

37. Jorge JP, Simoes FM, Pires EB, Rego PA, Tavares DG, Lopes DS, Gaspar A. Finite element simulations of a hip joint with femoroacetabular impingement. *Comput Methods Biomech Biomed Engin*. 2014;17:1275-1284.

38. Jung KA, Restrepo C, Hellman M, AbdelSalam H, Morrison W, Parvizi J. The prevalence of cam-type femoroacetabular deformity in asymptomatic adults. *J Bone Joint Surg Br*. 2011;93:1303-1307.

39. Kang AC, Gooding AJ, Coates MH, Goh TD, Armour P, Rietveld J. Computed tomography assessment of hip joints in asymptomatic individuals in relation to femoroacetabular impingement. *Am J Sports Med*. 2010;38:1160-1165.

40. Kang Y, Engelke K, Kalender WA. A new accurate and precise 3-D segmentation method for skeletal structures in volumetric CT data. *IEEE Trans Med Imaging*. 2003;22:586-598.

41. Kapron AL, Anderson AE, Aoki SK, Phillips LG, Petron DJ, Toth R, Peters CL. Radiographic prevalence of femoroacetabular impingement in collegiate football players: AAOS Exhibit Selection. *J Bone Joint Surg Am*. 2011;93:e111(111-110).

42. Kassarjian A, Brisson M, Palmer WE. Femoroacetabular impingement. *Eur J Radiol*. 2007;63:29-35.

43. Kennedy MJ, Lamontagne M, Beaulé PE. Femoroacetabular impingement alters hip and pelvic biomechanics during gait Walking biomechanics of FAI. *Gait Posture*. 2009;30:41-44.

44. Lamontagne M, Brisson N, Kennedy MJ, Beaulé PE. Preoperative and postoperative lower-extremity joint and pelvic kinematics during maximal squatting of patients with cam femoro-acetabular impingement. *J Bone Joint Surg Am*. 2011;93 Suppl 2:40-45.

45. Lamontagne M, Brisson N, Kennedy MJ, Beaulé PE. Preoperative and Postoperative Lower-Extremity Joint and Pelvic Kinematics During Maximal Squatting of Patients with Cam Femoro-Acetabular Impingement. *J Bone Joint Surg*. 2011;93:40-45.

46. Lamontagne M, Kennedy MJ, Beaulé PE. The effect of cam FAI on hip and pelvic motion during maximum squat. *Clin Orthop Relat Res*. 2009;467:645-650.

47. Laude F, Boyer T, Nogier A. Anterior femoroacetabular impingement. *Joint Bone Spine*. 2007;74:127-132.

48. Lavigne M, Parvizi J, Beck M, Siebenrock KA, Ganz R, Leunig M. Anterior femoroacetabular impingement: part I. Techniques of joint preserving surgery. *Clin Orthop Relat Res*. 2004;61-66.

49. Lenaerts G, Bartels W, Gelaude F, Mulier M, Spaepen A, Van der Perre G, Jonkers I. Subject-specific hip geometry and hip joint centre location affects calculated contact forces at the hip during gait. *J Biomech*. 2009;42:1246-1251.

50. Li X, Yankeelov TE, Peterson TE, Gore JC, Dawant BM. Automatic nonrigid registration of whole body CT mice images. *Med Phys*. 2008;35:1507-1520.

51. Liechti EF, Ferguson SJ, Tannast M. Protrusio acetabuli: Joint loading with severe pincer impingement and its theoretical implications for surgical therapy. *J Orthop Res*. 2014;

52. Liu H, Zhao J, Dai N, Qian H, Tang Y. Improve accuracy for automatic acetabulum segmentation in CT images. *Biomed Mater Eng*. 2014;24:3159-3177.

53. Lloyd DG, Besier TF. An EMG-driven musculoskeletal model to estimate muscle forces and knee joint moments in vivo. *J Biomech*. 2003;36:765-776.

54. Menschik F. The hip joint as a conchoid shape. *J Biomech*. 1997;30:971-973.

55. Myers SR, Eijer H, Ganz R. Anterior femoroacetabular impingement after periacetabular osteotomy. *Clin Orthop Relat Res*. 1999;93-99.

56. Ng KCG, Lamontagne M, Adamczyk AP, Rakhra KS, Beaulé PE. Patient-specific anatomical and functional parameters provide new insights into the pathomechanism of cam FAI. *Clin Orthop Relat Res*. 2015;473:1289-1296.

57. Ng KCG, Rouhi G, Lamontagne M, Beaulé PE. Finite Element Analysis Examining the Effects of Cam FAI on Hip Joint Mechanical Loading Using Subject-Specific Geometries During Standing and Maximum Squat. *HSS J*. 2012;8:206-212.

58. Nötzli HP, Wyss TF, Stoecklin CH, Schmid MR, Treiber K, Hodler J. The contour of the femoral head-neck junction as a predictor for the risk of anterior impingement. *J Bone Joint Surg Br*. 2002;84:556-560.

59. Philippon M, Schenker M, Briggs K, Kuppersmith D. Femoroacetabular impingement in 45 professional athletes: associated pathologies and return to sport following arthroscopic decompression. *Knee Surg Sports Traumatol Arthrosc*. 2007;15:908-914.

60. Pollard TC, Villar RN, Norton MR, Fern ED, Williams MR, Simpson DJ, Murray DW, Carr AJ. Femoroacetabular impingement and classification of the cam deformity: the reference interval in normal hips. *Acta Orthop*. 2010;81:134-141.

61. Radcliffe IA, Taylor M. Investigation into the affect of cementing techniques on load transfer in the resurfaced femoral head: a multi-femur finite element analysis. *Clin Biomech (Bristol, Avon)*. 2007;22:422-430.

62. Ranawat A, Schulz B, Baumbach S, Meftah M, Ganz R, Leunig M. Radiographic Predictors of Hip Pain in Femoroacetabular Impingement. *HSS J*. 2011;7:115-119.

63. Roels P, Agricola R, Oei E, Weinans H, Campoli G, Zadpoor AA. Mechanical factors explain development of cam-type deformity. *Osteoarthritis Cartilage*. 2014;

64. Rothenfluh E, Zingg P, Dora C, Snedeker JG, Favre P. Influence of resection geometry on fracture risk in the treatment of femoroacetabular impingement: a finite element study. *Am J Sports Med*. 2012;40:2002-2008.

65. Rudman KE, Aspden RM, Meakin JR. Compression or tension? The stress distribution in the proximal femur. *Biomed Eng Online*. 2006;5:12.

66. Russell ME, Shivanna KH, Grosland NM, Pedersen DR. Cartilage contact pressure elevations in dysplastic hips: a chronic overload model. *J Orthop Surg Res*. 2006;1:6.

67. Rylander JH, Shu B, Andriacchi TP, Safran MR. Preoperative and postoperative sagittal plane hip kinematics in patients with femoroacetabular impingement during level walking. *Am J Sports Med*. 2011;39 Suppl:36S-42S.

68. Sartori M, Reggiani M, Lloyd DG, Pagello E. A neuromusculoskeletal model of the human lower limb: towards EMG-driven actuation of multiple joints in powered orthoses. *IEEE Int Conf Rehabil Robot*. 2011;2011:5975441.

69. Siebenrock KA, Wahab KH, Werlen S, Kalhor M, Leunig M, Ganz R. Abnormal extension of the femoral head epiphysis as a cause of cam impingement. *Clin Orthop Relat Res*. 2004;54-60.

70. Speirs AD, Beaulé PE, Ferguson SJ, Frei H. Stress distribution and consolidation in cartilage constituents is influenced by cyclic loading and osteoarthritic degeneration. *J Biomech*. 2014;47:2348-2353.

71. Speirs AD, Beaulé PE, Rakhra KS, Schweitzer ME, Frei H. Increased acetabular subchondral bone density is associated with cam-type femoroacetabular impingement. *Osteoarthritis Cartilage*. 2013;21:551-558.

72. Standaert CJ, Manner PA, Herring SA. Expert opinion and controversies in musculoskeletal and sports medicine: femoroacetabular impingement. *Arch Phys Med Rehabil*. 2008;89:890-893.

73. Sutter R, Dietrich TJ, Zingg PO, Pfirrmann CW. Femoral antetorsion: comparing asymptomatic volunteers and patients with femoroacetabular impingement. *Radiology*. 2012;263:475-483.

74. Sutter R, Dietrich TJ, Zingg PO, Pfirrmann CWA. How Useful Is the Alpha Angle for Discriminating between Symptomatic Patients with Cam-type Femoroacetabular Impingement and Asymptomatic Volunteers? *Radiology*. 2012;264:514-521.

75. Taddei F, Martelli S, Reggiani B, Cristofolini L, Viceconti M. Finite-element modeling of bones from CT data: sensitivity to geometry and material uncertainties. *IEEE Trans Biomed Eng*. 2006;53:2194-2200.

76. Taddei F, Schileo E, Helgason B, Cristofolini L, Viceconti M. The material mapping strategy influences the accuracy of CT-based finite element models of bones: an evaluation against experimental measurements. *Med Eng Phys*. 2007;29:973-979.

77. Tannast M, Siebenrock KA, Anderson SE. Femoroacetabular Impingement: Radiographic Diagnosis—What the Radiologist Should Know. *Am J Roentgenol*. 2007;188:1540-1552.

78. Tomazevic D, Likar B, Slivnik T, Pernus F. 3-D/2-D registration of CT and MR to X-ray images. *IEEE Trans Med Imaging*. 2003;22:1407-1416.

79. Viceconti M, Olsen S, Nolte LP, Burton K. Extracting clinically relevant data from finite element simulations. *Clin Biomech (Bristol, Avon)*. 2005;20:451-454.

80. Wei HJ, Liang HC, Lee MH, Huang YC, Chang Y, Sung HW. Construction of varying porous structures in acellular bovine pericardia as a tissue-engineering extracellular matrix. *Biomaterials*. 2005;26:1905-1913.

2.7 Appendix – PRISMA Checklist

PRISMA 2009 Checklist

Section/topic	#	Checklist item	Reported on page #
TITLE			
Title	1	Identify the report as a systematic review, meta-analysis, or both.	1, Title
ABSTRACT			
Structured summary	2	Provide a structured summary including, as applicable: background; objectives; data sources; study eligibility criteria, participants, and interventions; study appraisal and synthesis methods; results; limitations; conclusions and implications of key findings; systematic review registration number.	2, Abstract
INTRODUCTION			
Rationale	3	Describe the rationale for the review in the context of what is already known.	3, Introduction
Objectives	4	Provide an explicit statement of questions being addressed with reference to participants, interventions, comparisons, outcomes, and study design (PICOS).	4, Introduction
METHODS			
Protocol and registration	5	Indicate if a review protocol exists, if and where it can be accessed (e.g., Web address), and, if available, provide registration information including registration number.	N/A
Eligibility criteria	6	Specify study characteristics (e.g., PICOS, length of follow-up) and report characteristics (e.g., years considered, language, publication status) used as criteria for eligibility, giving rationale.	4-5, Methods
Information sources	7	Describe all information sources (e.g., databases with dates of coverage, contact with study authors to identify additional studies) in the search and date last searched.	4-5, Methods
Search	8	Present full electronic search strategy for at least one database, including any limits used, such that it could be repeated.	4, Methods
Study selection	9	State the process for selecting studies (i.e., screening, eligibility, included in systematic review, and, if applicable, included in the meta-analysis).	4-5, Methods
Data collection process	10	Describe method of data extraction from reports (e.g., piloted forms, independently, in duplicate) and any processes for obtaining and confirming data from investigators.	5, Methods
Data items	11	List and define all variables for which data were sought (e.g., PICOS, funding sources) and any assumptions and simplifications made.	5, Methods
Risk of bias in individual studies	12	Describe methods used for assessing risk of bias of individual studies (including specification of whether this was done at the study or outcome level), and how this information is to be used in any data synthesis.	5, Methods
Summary measures	13	State the principal summary measures (e.g., risk ratio, difference in means).	5, Methods
Synthesis of results	14	Describe the methods of handling data and combining results of studies, if done, including measures of consistency (e.g., I^2) for each meta-analysis.	N/A

PRISMA 2009 Checklist

Section/topic	#	Checklist item	Reported on page #
Risk of bias across studies	15	Specify any assessment of risk of bias that may affect the cumulative evidence (e.g., publication bias, selective reporting within studies).	N/A
Additional analyses	16	Describe methods of additional analyses (e.g., sensitivity or subgroup analyses, meta-regression), if done, indicating which were pre-specified.	N/A
RESULTS			
Study selection	17	Give numbers of studies screened, assessed for eligibility, and included in the review, with reasons for exclusions at each stage, ideally with a flow diagram.	5, Results; Figure 1
Study characteristics	18	For each study, present characteristics for which data were extracted (e.g., study size, PICOS, follow-up period) and provide the citations.	6-12, Results; Table 1
Risk of bias within studies	19	Present data on risk of bias of each study and, if available, any outcome level assessment (see item 12).	6-12, Results
Results of individual studies	20	For all outcomes considered (benefits or harms), present, for each study: (a) simple summary data for each intervention group (b) effect estimates and confidence intervals, ideally with a forest plot.	6-12; Results
Synthesis of results	21	Present results of each meta-analysis done, including confidence intervals and measures of consistency.	12 Results; Figure 2
Risk of bias across studies	22	Present results of any assessment of risk of bias across studies (see Item 15).	N/A
Additional analysis	23	Give results of additional analyses, if done (e.g., sensitivity or subgroup analyses, meta-regression [see Item 16]).	N/A
DISCUSSION			
Summary of evidence	24	Summarize the main findings including the strength of evidence for each main outcome; consider their relevance to key groups (e.g., healthcare providers, users, and policy makers).	13-19, Discussion
Limitations	25	Discuss limitations at study and outcome level (e.g., risk of bias), and at review-level (e.g., incomplete retrieval of identified research, reporting bias).	13-19, Discussion
Conclusions	26	Provide a general interpretation of the results in the context of other evidence, and implications for future research.	19-20, Conclusion
FUNDING			
Funding	27	Describe sources of funding for the systematic review and other support (e.g., supply of data); role of funders for the systematic review.	Online

From: Moher D, Liberati A, Tetzlaff J, Altman DG, The PRISMA Group (2009). Preferred Reporting Items for Systematic Reviews and Meta-Analyses: The PRISMA Statement. PLoS Med 6(6): e1000097. doi:10.1371/journal.pmed1000097

For more information, visit: www.prisma-statement.org.

3 Study Design

Theoretical Framework | Conceptual Framework

3.0 Gaps in Literature

From the systematic review on hip joint stresses due to cam FAI (Chapter 2), it was apparent that many of the previous finite element models simulated adverse loading conditions, in efforts to better understand the relationship between mechanical stresses and risks of cartilage degeneration. However, the systematic review highlighted three main areas for development, because they were not addressed in previous finite element studies:

1. Consideration of anatomical parameters associated with FAI symptoms and emphasis on subject-specific hip joint geometries
2. Consideration of subject-specific bone material properties
3. Consideration of subject-specific hip joint loading parameters

Several of the previous finite element studies parameterized idealized, ball-and-cup, parametric models to predict stresses; in addition to implementing homogeneous material properties and in vivo instrumented prostheses loading data. The formulation of a robust subject-specific model was partially considered in the past, but remains an ongoing challenge. To adequately contribute to the understanding of hip joint loading due to cam FAI and the associated risks of joint degeneration, it would be imperative to bridge these gaps in the literature.

3.1 Theoretical Framework

Although there is strong clinical evidence that cam FAI presents a substantial risk for early hip osteoarthritis, there are still large gaps in the literature, such that causality has not been established and it is still unknown why certain individuals with the cam deformity experience clinical signs and symptoms early on, while others remain asymptomatic with the morphology. Furthermore, as mentioned in Chapter 2, very few studies have attempted to incorporate subject-specific models to simulate biomechanical loading scenarios with the intention to address FAI.

3.1.1 Participant Cohort

It has long been reported that the cam deformity leading to mechanical FAI is predominantly associated with male individuals [2, 3, 20, 21, 29, 33, 34]. Although the cam morphology can appear in females as well, there may be etiological reasons for the deformity to either be more asymptomatic in female population or more symptomatic in the male population. The disparity

observed between males and females may potentially be explained by: congenital deformity [20, 21], different levels of mineralization during skeletal maturation [23], subclinical slipped capital femoral epiphysis (SCFE) [4, 16, 22, 51], or repetitive load bearing activities [1-3, 50]. In terms of study design, it may be feasible to investigate a male-only cohort to compare functional anatomy and its effects towards symptoms.

The association of FAI with symptoms has been long studied, to try and better elucidate the pathomechanisms leading to cartilage degeneration. Often, symptoms may be demonstrated as a clinical sign and expressed in terms of pain. There may be a link between an individual's functional anatomy with their functional range of motion, which could help associate those who are at risk of developing symptoms. A clinically defined symptomatic group may represent those in the population who have a cam deformity and experience clinical signs and symptoms; whereas a clinically defined asymptomatic group may represent a population with a cam morphology, but which does not experience the resulting clinical signs and symptoms. The primary intention of a combined cohort (consisting of symptomatic, asymptomatic, control individuals) should be to enable a longitudinal study of pathomechanical progression – from a healthy, non-pathological hip, to the development of an asymptomatic cam morphology, and to the progression of symptoms due to a symptomatic cam deformity. The secondary intention of a combined cohort is to structure a cross-sectional study to examine differences between each subgroup.

3.1.2 Functional Anatomy Associated with Symptoms

As mentioned earlier (Chapter 1.2.4 – Symptoms), it has been long observed that the cam deformity and its related pathoanatomical parameters result in early symptoms and joint degeneration [20, 26, 27, 54]. Subclinical femoral head deformities may be a reason that leads to the development of the cam deformity, in addition to overload of the physeal plate during skeletal maturation. Symptomatic individuals with the cam deformity typically indicate anatomical features on clinical imaging data (*e.g.*, large alpha angle and reduced anterior femoral head-neck offset).

Interestingly, many individuals with a cam deformity do not experience mechanical impingement, remaining asymptomatic for much of their life. This provides a theoretical framework per which a cam deformity, alone, does not lead to pain and clinical symptoms. It has

been reported that several common radiographic measures of the femoral head, femoral neck, and acetabulum have been associated with symptoms of FAI, but it remains unclear as to which combination of parameters can stratify patients at risk of developing clinical signs. It was hypothesized that FAI symptoms may be associated with additional anatomical parameters that can exacerbate mechanical impingement in patients at risk of developing symptoms. The consideration of additional anatomical parameters (Table 3.1) could establish a more clinically relevant cohort for comparative analyses of resultant hip joint stresses. As a first step, the goal is to closely examine the potential cause-and-effects of certain anatomical differences, which can result in various hip joint loading and stresses.

Table 3.1. Anatomical parameter corresponding with anatomical hip joint features associated with symptoms

Anatomical Feature	Anatomical Parameter (units)	References
Cam Deformity	Axial alpha angle (°)	Nötzli, et al. 2002 [43] Nouh, et al. 2008 [44] Sutter, et al. 2012 [55]
	Radial alpha angle (°)	Rakhra, et al. [46] Sutter, et al. [55]
	Femoral head-neck offset (mm)	Ito, et al. 2001 [27] Kang, et al. 2010 [28] Chakraverty, et al. 2013 [13]
Neck Angle	Femoral neck-shaft angle (°)	Hartofilakidis, et al. 2011 [25] Ranawat, et al. 2011 [47]
	Medial proximal femoral angle (°)	Bardakos, et al. 2009 [7] Banerjee, et al. 2011 [6] Monazzam, et al. 2013 [40]
Version	Femoral torsion (°)	Bedi, et al. 2011 [11] Ejnisman, et al. 2013 [18]
	Acetabular version (°)	Reynolds, et al. 1999 [48] Dandachil, et al. 2009 [15] Chakraverty, et al. 2013 [13]
Pincer Deformity	Lateral centre-edge angle (°)	Kang, et al. 2010 [28] Kutty, et al. 2012 [30]

In addition to stratifying anatomical differences between symptomatic, asymptomatic, and control individuals, it may be further warranted to examine individuals with bilateral cam deformities. In these particular individuals with bilateral deformities, symptoms usually persist in one hip while the contralateral hip remains unaffected and asymptomatic. There may be further anatomical differences between the affected symptomatic side and the unaffected asymptomatic side, that can help explain the risks of early pain.

3.1.3 Motions Associated with Symptoms

As mentioned earlier (Chapter 1.2.4 – Symptoms), FAI has been known to reduce both passive and dynamic hip range of motion. In the clinical setting, a physical examination can be used to assess an individuals' passive hip range of motion (flexion-extension, internal-external rotations, abduction-adduction), in efforts to observe limits of motion (impingement signs) and note any indications of pain (clinical signs). Level walking has been one of the most of studied motions, when comparing pathological conditions, among others. It would be feasible to examine the resultant hip joint stresses due to level walking conditions, comparing the instance of peak hip joint loading between symptomatic, asymptomatic, and control participants. In addition, since cam FAI demonstrated adverse effects on the dynamic squat motion (limiting squat depth, reducing pelvic range of motion and abduction [31, 32]), it would be feasbile to compare a standardized, common squat depth among symptomatic, asymptomatic, and control participants. Since many individuals with symptomatic FAI are unable to accomplish a deep squat (due to the restricted squat motion), a common squat depth ensures that all participant are compared at a standard depth, near a deep squat (*e.g.*, 50% of leg height, resulting in 90° of hip flexion and an approximate of 90° of knee flexion).

3.1.4 Subchondral Bone

It has been observed that both symptomatic and asymptomatic individuals with cam deformities undergo similar levels of acetabular subchondral bone remodelling [52] (Figure 3.1). A stiffer subchondral bone could lead to a lower compliance for the articulating cartilage, which in turn could result in elevated stresses and early cartilage degeneration.

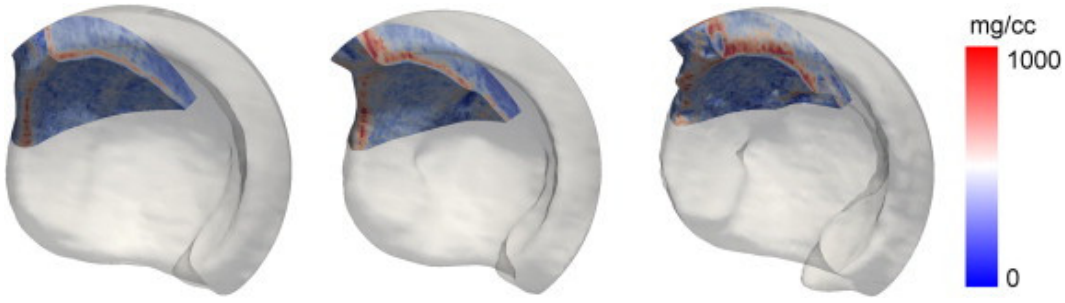

Figure 3.1. Bone density in the anterosuperior quadrant of a control (left), asymptomatic (middle), and symptomatic (right) participant. The asymptomatic participant exhibited denser subchondral bone near the rim, while the symptomatic participant exhibited a larger region or denser subchondral bone. Reproduced with permission of Elsevier (Speirs et al., 2013).

However, knowing that the cam deformity causes stiffer acetabular subchondral bone, in symptomatic and asymptomatic individuals alike, does not justify why some individuals with the morphology experience clinical signs and symptoms while others do not. Since cam FAI is a pathological hip condition, that may be specific to symptomatic and asymptomatic populations, it would be feasible to implement finite element models that considered subject-specific bone material properties, to adequately represent the symptomatic group (with larger regions of denser subchondral bone), asymptomatic group (with regions of denser subchondral bone), and control group (with well distributed subchondral bone densities). Since a CT scanner is calibrated to measurable Hounsfield Unit (HU) scale, there is a need to include a reference object (of known density and attenuation properties) during imaging. In efforts to quantify bone density from subject-specific imaging data, a calibration phantom (Model 3, Mindways Software, Austin, TX, USA) can be included at the time of imaging (Figure 3.2).

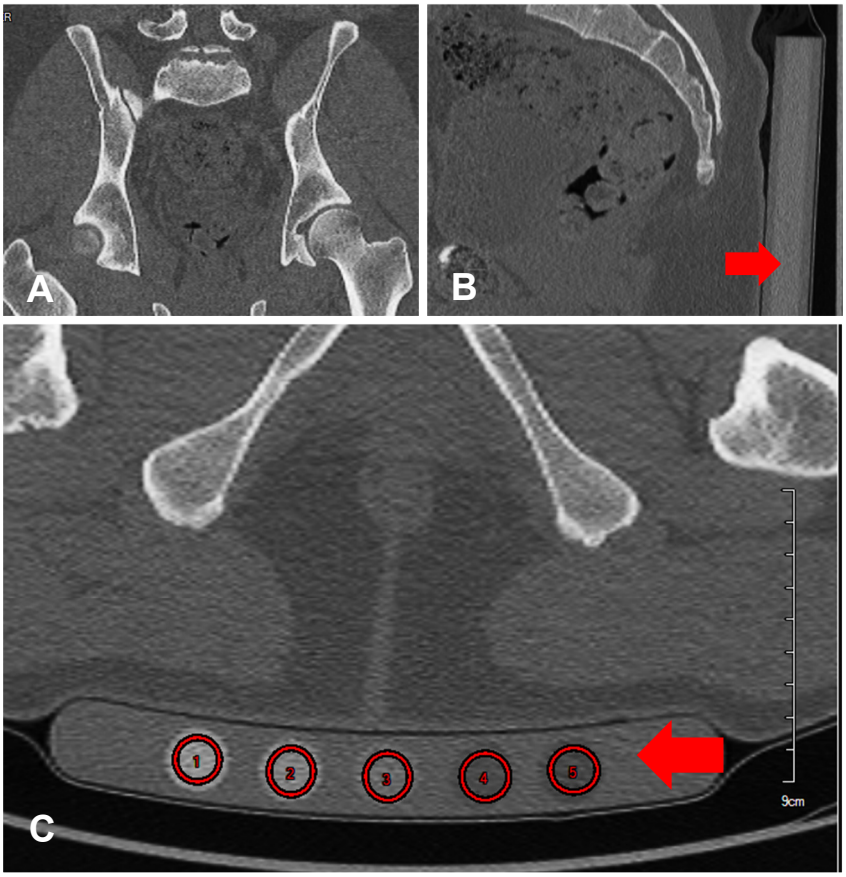

Figure 3.2. CT images of a supine participant in the: **A**) frontal, **B**) sagittal, and **C**) transverse views; indicating the flat calibration phantom placed beneath the participant (as indicated by the red arrow). The calibration phantom contained five material rods (numbered 1 to 5), with known densities, used to correct the CT calibration settings.

The calibration phantom contained five cylindrical materials, with known densities, and was encased in a flat plastic base. By measuring the pixel value of each of the five materials, and knowing their actual effective densities (in K_2HPO_4 – dipotassium monohydrogen phosphate), proper calibration of the CT images can be achieved, to determine bone mineral density. Reconstructing finite element models with subject-specific bone densities is expected to provide a more accurate representation of the pathological group.

3.2 Conceptual Framework

With the goal to better understand the pathomechanisms of cam FAI, the purpose of this research was to address the question at large: *what are the effects of cam FAI on mechanical hip joint loading*? Implementing a participant cohort (comparing symptomatic, asymptomatic, control groups), this research program was broken down into three areas of study:

1. **Anatomical and Functional Characteristics**: which examined additional anatomical and functional characteristics, that could be associated with the symptoms due to the cam morphology
2. **Determining Appropriate Modelling Characteristics:** which reconstructed subject-specific, computational hip joint models, representative of each group (symptomatic, asymptomatic, control)
3. **Modelling of Clinically Relevant Scenarios:** which examined hip joint contact stresses (in the cartilage, labrum, subchondral bone) using the finite element methods and hip joint contact loading

3.2.1 Anatomical and Functional Characteristics

Since many individuals with cam deformities may not experience mechanical impingement or pain symptoms, it is hypothesized that FAI symptoms may be related to other anatomical parameters that can exacerbate mechanical impingement in patients at risk of developing symptoms. The purpose of this study was to examine other anatomical and functional parameters that were associated with symptoms resulting from the cam deformity. In this study section, the questions were:

1. Which of the anatomical and functional squat parameters best classify symptomatic, asymptomatic, and control individuals with their respective subgroups and identify patients at risk of developing symptoms?
2. What are the differences in the additional anatomical parameters, between the affected and unaffected hips, in patients with bilateral cam deformities who demonstrate unilateral FAI symptoms?

Each participant's anatomical and functional parameters were measured from CT imaging (Figure 3.3) and motion data, respectively. The common anatomical parameters, associated with symptoms of cam FAI, included: the cam morphology parameters (axial and radial alpha angles, femoral head-neck offset), neck angle parameters (femoral neck-shaft and medial proximal femoral angles), version angle (femoral torsion and acetabular version), and acetabular overcoverage (lateral centre-edge angle). From a dynamic squat motion, two common parameters were collected for comparison: sagittal pelvic range of motion (from anterior to posterior pelvic tilt) and maximal squat depth (with respect to leg height).

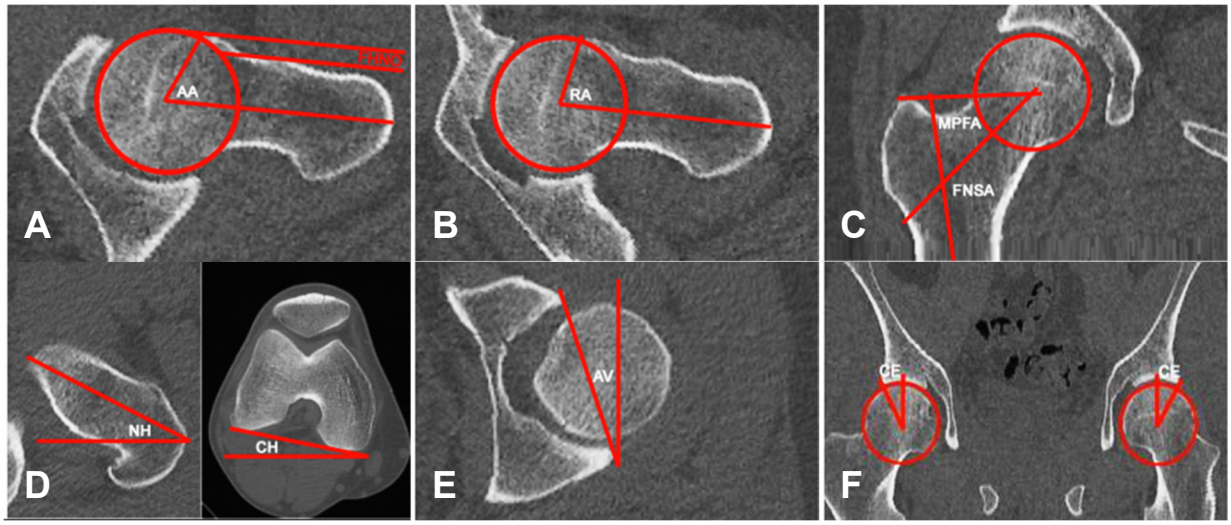

Figure 3.3. Anatomical CT parameters measuring the: **A**) axial alpha angle (AA) and femoral head-neck offset (FHNO); **B**) radial alpha angle (RA); **C**) femoral neck-shaft angle (FNSA) and medial proximal femoral angle (MPFA); **D**) neck and condyle horizontal (NH and CH) for femoral torsion; **E**) acetabular version (AV); and **F**) lateral centre-edge angle (CE).

A stepwise discriminant function analysis (DFA) can be implemented to identify which of the anatomical and functional squat kinematics parameters are most suitable to classify an affected hip with their respective subgroup. Like a hierarchical linear regression, where multiple

parameters describe the level of variance, the DFA further predicts how subjects are classified based on the most suitable parameters. Moreover, the outputs from the DFA can provide two predictive equations, based on standardized canonical discriminant function coefficients. These coefficients will only consider the best anatomical or functional parameters that can significantly classify groups. Thus, by inputting a future participant's anatomical or squat information into the predictive equations, the resultant functions will provide a visual indication of classification based on their proximity to a group centroid. Sample sizes were adequate because the smallest group size (either in the symptomatic, asymptomatic, or control group) exceeded the number of total parameters ($n > k$). The minimum F values for entry and removal were 3.00 and 2.71, respectively. Although, the alpha angles and clinical signs were determinants for *a priori* classification, the DFA assumed that each of the anatomical CT and squat parameters were treated as an independent variable for grouping. Symptomatic patients who had bilateral cam deformities (high alpha angles in both hips), but demonstrated only unilateral symptoms, were further considered to look at anatomical differences between their affected (symptomatic) and contralateral, unaffected (asymptomatic) hips. A paired sample t-test further compared differences in anatomical parameters and physical examination measurements, between each symptomatic patient's affected and unaffected hips ($CI = 95\%$). All statistical analyses were performed using statistics software (SPSS Statistics Version 21, IBM Corporation, Armonk, NY, USA).

To better predict which individuals with a cam deformity can be at risk of developing hip symptoms, subject-specific functional parameters as well as additional anatomical parameters were used to discriminate individuals with and without symptoms. In addition to providing predictive algorithms, the outputs from the DFA classified the participant cohort into appropriate respective subgroups – in efforts to establish an accurate baseline for group comparison for modelling and simulation (Study 2 and Study 3). Also, the comparison of the affected and unaffected hips in symptomatic patients with bilateral deformities may provide valuable insight as to which parameters will significantly predict early symptoms. Table 3.2 summarizes the implementation framework of Study 1, examining the anatomical and functional characteristics (needed for Study 2 and Study 3).

Table 3.2. Implementation framework summarizing the subcomponent studies towards the understanding of anatomical and functional characteristics associated with symptoms

	Study 1	
	A) Group classification	B) Affected vs. unaffected hip in symptomatic patients
Groups	Symptomatic Asymptomatic Control	Symptomatic – with bilateral cam deformities
Data	Anatomical parameters Functional squat parameters	Anatomical parameters Clinical physical examinations
Methods	Discriminant function analysis	Paired sample t-test
Results	Group classification Association of parameter(s) with symptoms	Anatomical parameter(s) leading to onset of symptoms

3.2.2 Determining Appropriate Modelling Characteristics

To validate the segmentation process and evaluate potential measurement differences between CT images and 3D models, anatomical parameters associated with symptoms (from Study 1) were examined and compared using two diagnostic measurement methods: A) planar 2D CT images and B) segmented 3D models. Moreover, with several different material modelling parameters, it was unclear how resultant contact mechanics would compare in terms of stress characteristics, under similar geometric assumptions and loading conditions. Therefore, an evaluation of the conventional bone and soft tissue material properties was necessary to compare existing standards. This study section focused on two questions:

1. Are there differences in anatomical parameters, measured from CT images and from segmented 3D models?
2. Can the hip joint be better elucidated by including subject-specific bone densities and various soft tissue properties?

This study section involved extensive computational work and image segmentation. Hip joint models were segmented from a participant's CT and MRI data, using image segmentation software (3D-Doctor 4.0, Able Software Corp., Lexington, MA, USA). A threshold-density base method was first implemented, by identifying the Hounsfield unit applicable to bone. This resulted in outlines around the contour of the pelvic and femoral bones, per CT slice. On the CT slices with the femoral head and acetabulum, many of the contours combined the pelvic and

femoral bones as one single object. Therefore, manual segmentation was required to further separate the two objects (pelvis and femur). A final step segmentation step was taken to remove any of the geometric artefacts. A set of CT data were segmented by two observers, each repeating the segmentation two weeks after the first. Using a Boolean operation in computer-aided software (SolidWorks, Dassault Systèmes, Concord, MA, USA), each observer's first segmented model was subtracted from one another, to confirm inter-observer reliability. Each observer's repeated segmentation was also compared to their first model, using Boolean subtraction, to ascertain intra-observer reliability. Comparisons were confirmed near-perfect, with marginal volume differences (difference < 8%).

As the segmented models may contain surface irregularities, each component was then resurfaced using computer-aided design software (SolidWorks, Dassault Systèmes, Concord, MA, USA), to reduce geometric artefacts (Figure 3.4). Not only did the resurfacing procedure provide a smoother model, but it also reduced the number of elements generated and computation time (for Study 3) [42]. To confirm that the smoothed models were representative of the segmented data, the Boolean subtraction operator was used to compare the volume differences (between the original, segmented file and the final, resurfaced geometry). Comparisons were confirmed near-perfect, with marginal volume differences (difference < 10%). Observed differences were not located near the articulating surfaces (femoral head and acetabulum).

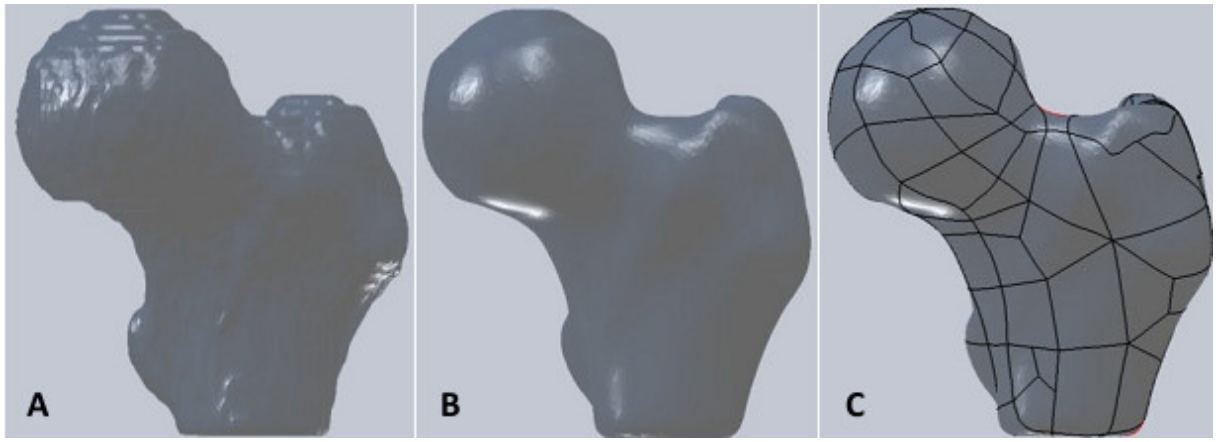

Figure 3.4. The resurfacing procedure for each component from: **A**) original, segmented geometry with geometric artefacts, to **B**) smoothed geometry, with minimal geometric artefacts, to **C**) final resurfaced model.

To segment the cartilage and labrum, each participant's MRI data were registered and fused with their CT data. Using the segmentation software, both imaging sets were centered at control points, where the deepest width of the acetabulum and the femoral head centre were used as primary registration landmarks. First, the hip joint centre (femoral head centre) was located on both CT and MRI data and matched according to the position in their modality's Cartesian coordinate system. Second, the MRI data were transformed onto the landmarks of the anterior and posterior acetabular notches of the CT slice. With several control points, a least square method generated an optimal mathematical transformation to map the MRI to the new coordinate system.

After the soft tissue models were segmented, if there were any marginal discrepancies between the bone model (segmented from CT) and the soft tissue models (segmented from MRI), the bone models would take precedence. A Boolean subtraction operation was implemented, to remove part the of the soft tissue layer, if there was any of the bone model overlapping it.

To further confirm the accuracy of the resurfacing and modelling procedure and to validate the hip joint geometries, all anatomical parameters were re-measured (Figure 3.5), using the computer-aided design software, and compared to the original CT measurements (from Study 1). As anatomical characteristics are clinically pertinent to diagnose FAI and predict symptoms associated with morphologies, it would be imperative to examine to what extent anatomical characteristics from segmented models would be representative of the original CT data. The segmented models were blinded and reassigned filenames, to eliminate measurement bias. Intermethod reliability was assessed between measurements from both planar, CT data and from segmented, 3D models.

Next, a comparison of conventional material modelling properties was needed to understand the variability and resultant stresses from hip joint simulations. Using a baseline model for comparison, large-scale geometries and hip joint loading conditions were standardized, while parameterizing hard and soft tissue material properties. As mentioned in the previous chapter, the selection of material properties for the bone and soft tissues (cartilage and labrum) of the hip joint was restricted to common linear-elastic, isotropic materials. Moreover, bone material properties were implemented as homogeneous, regardless of any hip pathologies; thus, neglecting the subject-specific density-elasticity relationship.

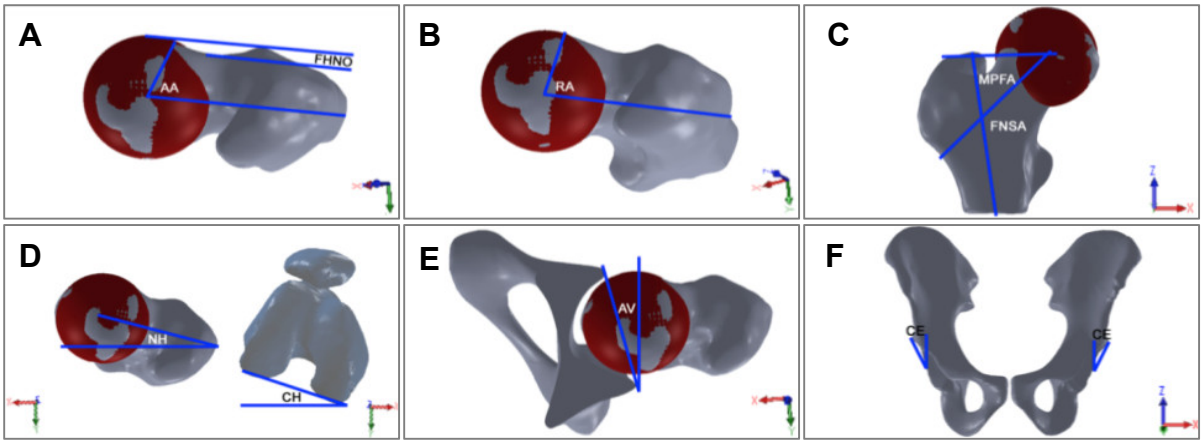

Figure 3.5. Anatomical parameters, measured from the 3D segmented models, measuring the: **A**) axial alpha angle (AA) and femoral head-neck offset (FHNO); **B**) radial alpha angle (RA); **C**) femoral neck-shaft angle (FNSA) and medial proximal femoral angle (MPFA); **D**) neck and condyle horizontal (NH and CH) for femoral torsion; **E**) acetabular version (AV); and **F**) lateral centre-edge angle (CE).

To obtain subject-specific bone material properties for each model, the calibration phantom was scanned with the participant and indicated on CT data. The five materials (reference rods) within the plastic base were identified and a region of interest was circled within each of the five rods, through the middle of the plastic base in the transverse plane (Figure 3.6). Each of the reference rod had a reference area of approximately 285 mm^2 and was provided with validated densities in water and K_2HPO_4 scales. From a participant's CT data, the region of interest acquired an average HU from the CT slice, per the imaging setting (Table 3.3). A region of interest greater than 50% of the reference rod's area would be sufficient to obtain the HU.

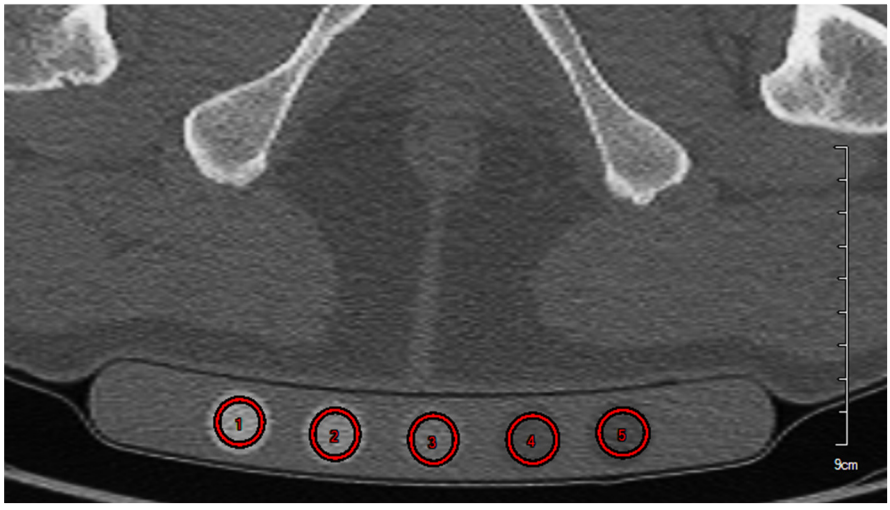

Figure 3.6. The calibration phantom encased five reference rods, seen at mid-base in the transverse plane. The rods provided reference scales in water and K_2HPO_4 densities and the Hounsfield Units were measured from the CT slice.

Table 3.3. Composition of solid reference materials measured in water density, effective density, and Hounsfield Units (from a participant's CT data) for each reference rod of the calibration phantom

Reference rod	Water density (mg/cc)	K_2HPO_4 density (mg/cc)	Read Hounsfield Unit (HU)
A	1012.2	-51.8	-57.963
B	1057.0	-53.4	-19.142
C	1103.6	58.9	189.609
D	1119.5	157.0	355.253
E	923.2	375.8	459.134

Although this measurement of the HUs provided a generalized relationship scaled to the effective K_2HPO_4 density, the relationship was not linearly correlated, thus the density-elasticity relationship was not linearly scaled from the CT imaging setting (Figure 3.7).

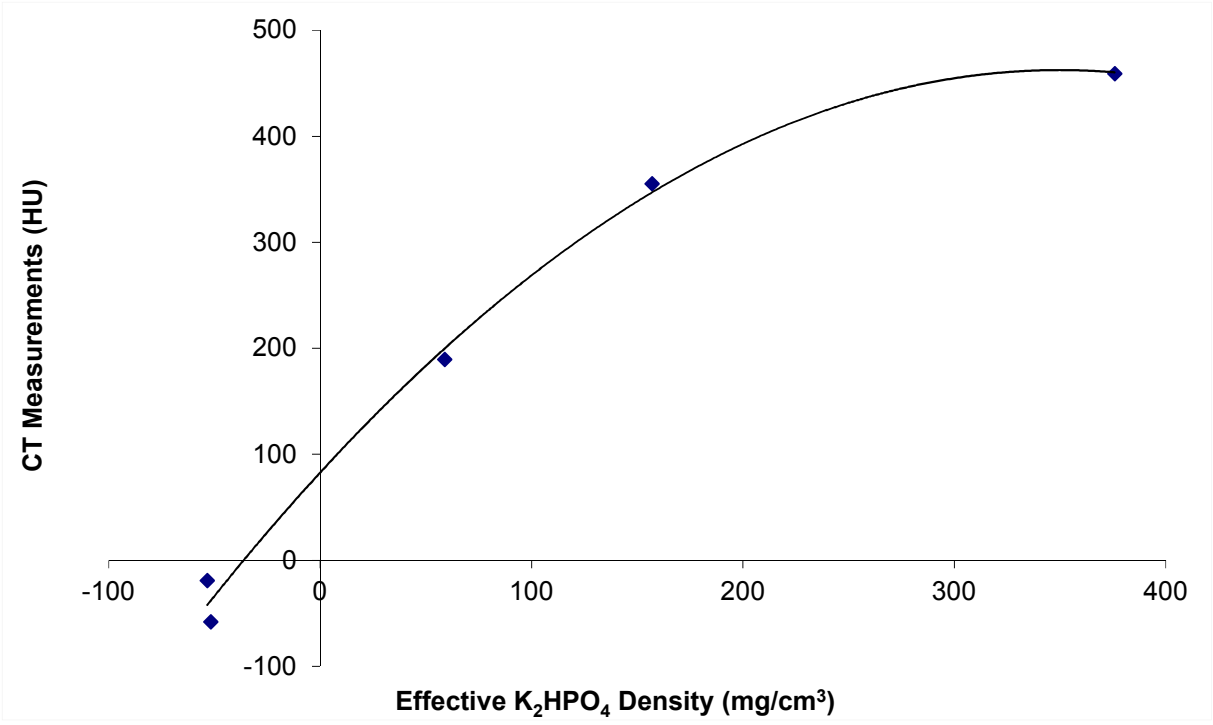

Figure 3.7. Relationship of the effective K_2HPO_4 density (from known density) with the measured Hounsfield Unit (from the CT slice).

To correct the measurements from CT data, the reading in HU were converted to intensity values, by considering the physical effects of air (~ -1000 HU). This converted value was then subtracted from the known scaled water densities (Table 3.4). The correction resulted in a linear relationship for each participant's CT calibration (Figure 3.8), that associated the measured

intensity value (measured from the CT image) with the known effective density of each reference rod (scaled to K_2HPO_4 density).

Table 3.4. Composition of solid reference materials' water density, effective density, measured Hounsfield Units (from a participant's CT data), and converted intensity values for each reference rod of the calibration phantom

Reference rod	Water density (mg/cc)	K_2HPO_4 density (mg/cc)	Read Hounsfield Unit (HU)	Read intensity value	Read intensity value – water (HU)
A	1012.2	-51.8	-57.963	942.037	-70.163
B	1057.0	-53.4	-19.142	980.858	-76.142
C	1103.6	58.9	189.609	1189.609	86.009
D	1119.5	157.0	355.253	1355.253	235.753
E	923.2	375.8	459.134	1459.134	535.934

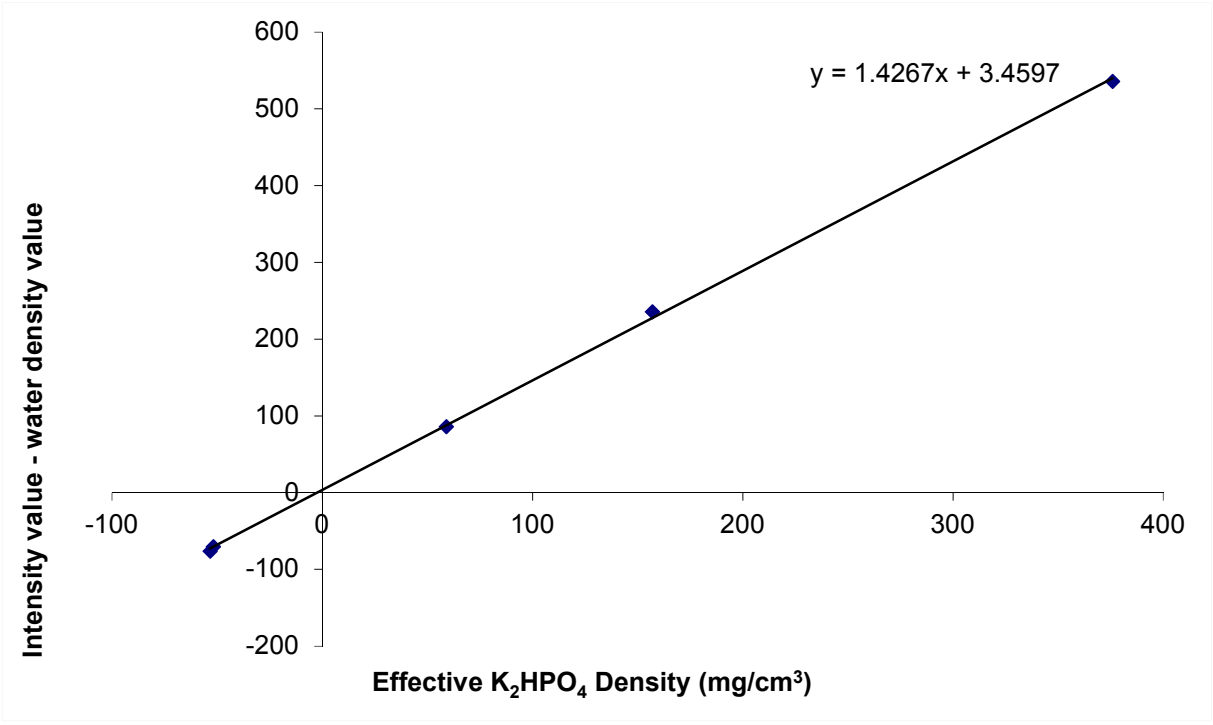

Figure 3.8. A participant's corrected linear relationship of the effective K_2HPO_4 density (from known density) with the corrected Hounsfield Unit (from the CT slice), accounting for water density subtracted from the intensity value. (The equation, slope, intercept from the CT densitometric calibration are applicable to this participant only.)

The regression provided the slope and intercept of the CT correction factors needed to scale each participant's density-elasticity relationships. The slope and intercept were used for the densitometric calibration equation:

$$\rho = slope \quad \rho_{CT} + intercept \qquad \text{Equation 3.1}$$

Each participant's CT densitometric calibration varied, as CT imaging varied from scan to scan, thus this correction factor was performed for each participant. To obtain hip joint models with heterogeneous material properties that varied with subject-specific bone densities, a bone density mapping program (Bonemat v3.1, Istituto Ortopedico Rizzoli, Bologna, Italy) was used to assign subject-specific elastic moduli to individual elements. Two density-elasticity relationships were used to relate the bone density to elastic modulus:

$$E = 6.950\rho^{1.49} \qquad [41] \qquad \text{Equation 3.2}$$

$$E = 3.790\rho^{3} \qquad [12] \qquad \text{Equation 3.3}$$

The coefficients were determined from previous studies and derived from empirical data [49]. Equation 3.2 was used as the primary density-elasticity power law, while Equation 3.3 was used if a second interval of elasticity assignment was needed to account for discontinuities. The resultant bone models had heterogeneous, isotropic material properties that were representative of the cortical and trabecular elastic moduli (Figure 3.9).

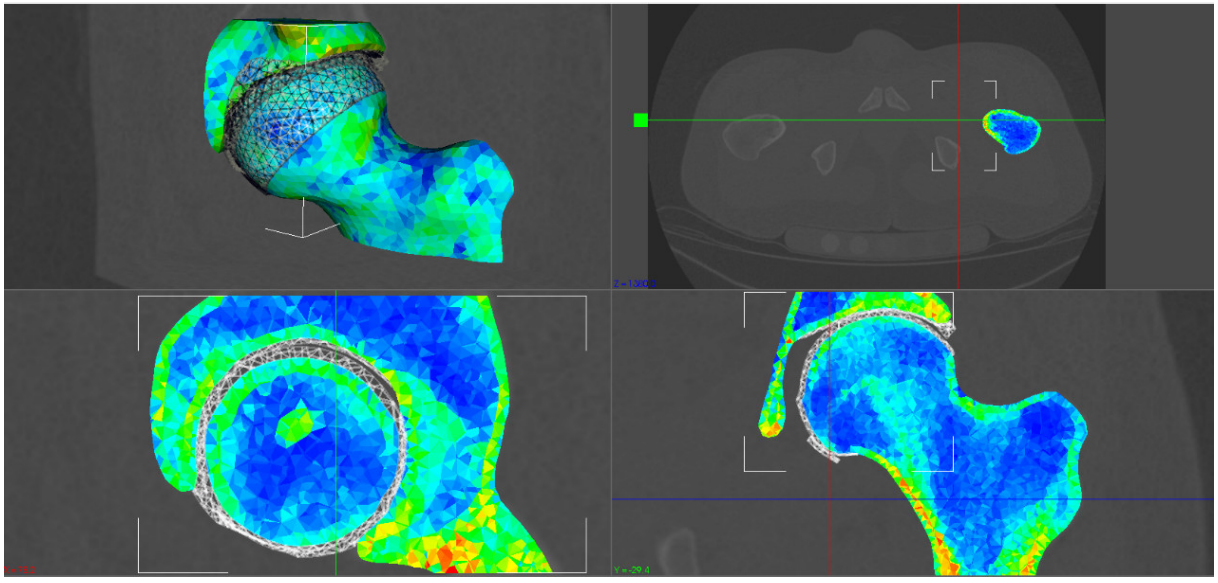

Figure 3.9. Assembly of a pelvis and proximal femur (along with the wireframes of the cartilage and labrum models) in Bonemat, indicating the distribution of the subject-specific heterogeneous bone material properties.

With the ultimate goal of understanding the pathomechanisms of cam FAI, the collective sub-studies were expected to contribute to the modelling of cam FAI, by integrating more subject-specific data to investigate stresses corresponding to the articulating cartilage and subchondral

bone. The reliability analysis would confirm the appropriateness of the segmentation and modelling process, as well as which selection of material properties would be adequate for further modelling and simulation. If the reliability coefficients were near-identical, for the crucial anatomical parameters and subject-specific representations of hip geometry, this would demonstrate that the 3D models can be further implemented for finite element simulations. Table 3.5 summarizes the implementation framework of Study 2, examining the development (from Study 1) and implementation (for Study 3) of subject-specific hip joint models.

Table 3.5. Implementation framework summarizing the subcomponent studies towards the understanding of subject-specific modelling characteristics

	Study 2	
	A) Evaluation of 3D models	B) Comparison of material properties
Groups (from Study 1A)	Symptomatic Asymptomatic Control	Control (parameterized to various conditions)
Data	Anatomical parameters from CT data Anatomical parameters from segmented, 3D models	Modelling parameters Material properties Joint loading for level walking
Methods	Bland-Altman reliability Intraclass correlation coefficient	Comparative analysis of stress magnitude and distributions
Results	Sensitivity study of modelling and measurements Comparative analysis of anatomical measurements	Sensitivity study of material modelling and relative measurements Comparative analysis of resultant stress measurements

3.2.3 Modelling of Clinically Relevant Scenarios

The pathomechanism of the cam-type deformity has been intensely investigated to better understand anatomical and functional parameters associated with symptomatology. Previous studies tried to delineate the pathomechanism and loading nature of cam FAI using finite element methods involving idealized geometries, loading inputs from inverse dynamics, or reaction loads from instrumented hip prostheses. However, muscle activity needed for joint stability was typically ignored in inverse dynamics, although it can potentially contribute up to 70% towards total hip contact forces [35, 53]. Since in vivo measurements are invasive, musculoskeletal modelling has been considered as an ethical alternative to estimate hip contact forces [19]. These

analyses are critical as recent work showed that elevated mechanical stresses in the subchondral bone may represent the dominant pathomechanism in cam-type FAI.

The purpose of this study was to examine hip joint stresses in individuals with an asymptomatic cam deformity, incorporating subject-specific hip joint contact forces and geometries. Using two activities of daily living, it was hypothesized that the asymptomatic group would demonstrate different loading patterns during level-walking and squat, in comparison with the symptomatic and control groups. It was hypothesized that the symptomatic group would demonstrate the highest stress increase, between the level walking and maximal squat loads. In this study section, two questions were to be addressed:

1. Do peak stresses of asymptomatic individuals resemble the symptomatic or healthy control population, during level walking?
2. Are the peak stresses of symptomatic, asymptomatic, and healthy control individuals situated on the acetabular cartilage, labrum, or subchondral bone during squatting?

In addition to the above research questions, it was important to also examine if other anatomical parameters influenced the peak stress magnitudes and distributions in each of the symptomatic, asymptomatic, and control participants.

Each participant's hip joint assembly was imported into finite element software (ANSYS 12.1, ANSYS Inc., Canonsburg, PA, USA), for static structural analysis. The material properties and modelling parameters were established from Study 2 and were implemented towards these models. Contact between the femoral and acetabular cartilage was modelled with friction. Each cartilage model was bonded, as contact elements, to the target elements of the acetabulum and femoral head, respectively. The trabecular bones were bonded and restrained within the cortical shell model. Moreover, the labrum was bonded to the periphery of the acetabular cartilage and adjacent cortical bone. The contact mechanics, between the articulating surfaces, were defined using an augmented Lagrange method (KEYOPT(2) = 0), which implemented an iterative series of penalty methods to impose contact compatibility.

The hip joint assembly was meshed using SOLID187 (10-node, tetrahedral) elements, adequate for complex 3D assemblies and assignment of subject-specific elastic moduli (Study 2). A patch independent scoping method was implemented along with a global minimum element size to capture the curvatures of the models. Although the solving process could take longer, this potentially eliminates the need to seek an extensive mesh convergence. Still, to ensure mesh

sensitivity and convergence, a refinement step was defined for the acetabular cartilage, labrum, and subchondral bone to automatically refine the mesh at locations with a tighter radius of curvature.

Fixed boundary conditions were enforced at the pubis symphysis and iliac crest, from the anterior to the posterior superior iliac spines, while the femur was free to translate in the direction of load. A quasi-static loading scenario, using the highest resultant hip joint forces during level walking, was simulated and a standardized squat depth may be better for comparison among different individuals. For each simulation, the femur model was oriented with respect to the pelvis model, using the kinematics data during the loading condition, applying the hip contact forces at the femoral head, in the pelvic reference frame.

The bone and soft tissues models were segmented from CT and MRI data, respectively, of the supinated participants. The neutral standing position referred to the orientation of the hip joint in the supine imaging position. After reorienting the femur with respect to the hip joint kinematics, if the femoral and acetabular layers overlapped, the assembly of the femur and femoral cartilage were marginally displaced laterally, only until the cartilage layers no longer overlapped. This was verified for all participant models, during the walking and squatting positions, but was performed only if it was deemed necessary (*i.e.*, material overlap).

Maximum shear stresses were examined in each participant's acetabular cartilage, labrum, and subchondral bone [5, 34, 36, 45]. The acetabular cartilage, labrum, and subchondral bone were examined in four quadrants: anterior, superior, posterior, and inferior; where the acetabular cartilage and subchondral bone were further divided into lateral and medial subsections (Figure 3.10). The peak stresses were examined in each of these components, determining the subsection where the peak magnitudes were located.

Although the maximum shear stress analysis is another conventional failure criterion for ductile materials, it is less conservative in comparison with von Mises criterion. Moreover, since cartilage is mostly under shear stress, it may be more suitable to examine adverse hip loading conditions by considering principal stresses and resultant maximum shear stresses. As described in Radin and associates' work (1991), maximum shear stresses could indicate risks of adverse loading conditions leading to cartilage failure and across the cartilage-bone interface [45].

For each individual simulation, a mesh convergence analysis was performed to ensure adequate solution. Convergence was deemed adequate when the changes in maximum shear

stress magnitudes were less than 5% after mesh refinement. In addition, similarity between averaged and unaveraged nodal stresses was verified. Results were compared with previous in silico analyses on cam FAI and hip joint loading. Significantly high stresses on the cartilage and labrum, indicative of cartilage degeneration, were compared with previous open surgical dislocations [9, 10] and intraoperative joint preservations [8]. Elevated stresses on the bone layer were compared with recent findings, by Speirs and associates [52], on acetabular subchondral bone density, representative of the symptomatic, asymptomatic, and control populations.

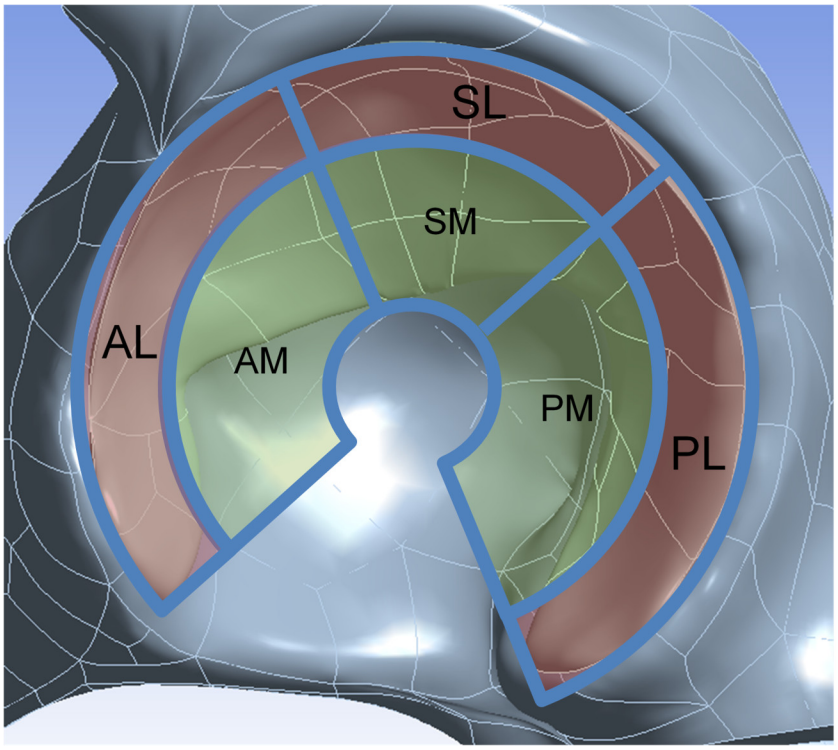

Figure 3.10. Sagittal view of the left acetabulum indicating the anterior (A), superior (S), and posterior (P) regions; and in the lateral (L) and medial (M) sections.

Each participant was asked to perform level-walking trials and maximal squat-depth trials, at a self-selected pace, in a motion capture environment. Although the symptomatic participants were aware of their cam deformity and scheduled for surgery prior to motion analysis, the asymptomatic and control participants were not informed if they had a cam deformity until after the completion of the protocol and motion analysis. In efforts to minimize skin artefacts and locate hip joint centers, surface electrodes were placed onto each participant's pelvic landmarks prior to CT imaging, at the left and right anterior superior iliac spines (ASIS) and posterior superior iliac spines (PSIS). After CT imaging was completed, the surface electrodes were

replaced with retro-reflective surface markers used for motion capture. Thus, the surface electrodes represented the reference locations of each pelvic retro-reflective marker, with respect to the hip joint center. Three-dimensional kinematics were recorded using a ten-camera motion capture system (MX-13, Vicon, Oxford, UK) with retro-reflective markers attached onto each participant's anatomical landmarks according to a modified Plug-in-Gait model (University of Ottawa Motion Analysis Model [38]). The model included additional medial knee and ankle markers, to better identify frontal planes and joint centres; as well as iliac crest and greater trochanter markers, to better identify the pelvis and femur segments, respectively.

Participants were first asked to perform five level walking trials, walking at a self-selected pace. Ground reaction forces of each participant's affected leg, during single-stance, were captured using two stationary force plates (FP4060-08, Bertec, Columbus, OH, USA). Participants were then instructed to perform five maximal dynamic squats, squatting to the lowest possible depth at a controlled, self-selected pace. The squat activity involves multiple planes of motion and is as considered a demanding activity to repeat. Furthermore, the squat activity subjects the hip to a flexed position, potentially forcing the hip to impinge. It has been observed that this potential impingement, during a deep squat, can act as a diagnostic tool, to differentiate symptomatic FAI from healthy, control individuals [32]. Moreover, there is the possibility that a limited squat depth or range of motion may be a result of an apprehension due to pain. Each foot was placed shoulder-width apart on a force plate, directed anteriorly, with toes and heels in full contact with the ground during the entire squat cycle. Five squat depths were averaged as a percentage with respect to leg height, where ground level represented a leg height of 0%. The trajectories were filtered (Woltring, MSE = 15 mm^2) using motion analysis software (Nexus 1.8, Vicon, Oxford, UK) and ground reaction forces were filtered (zero-lag, 4^{th} order Butterworth, cut-off 6Hz) using numerical computations software (MATLAB R2014a, MathWorks, Nantick, MA, USA).

Coinciding with another doctoral research work [37], muscle and hip contact forces were estimated using a musculoskeletal modelling program (OpenSim 3.1, SimTK, USA). Adapting an earlier model [24], the full-body representation was comprised of 12 segments, 29 degrees of freedom, and 92 musculotendon actuators. The hip was modelled as a ball-and-socket joint with 3 degrees of freedom, whereas the knee was modeled as a custom joint with 1 degree of freedom, and the ankle was modeled as a revolute joint with 1 degree of freedom. Muscle forces were

computed using a static optimization approach with a quadratic cost function [14, 39]. Resultant 3D hip contact forces were calculated and expressed in the pelvic reference system [56].

For each participant's walking activity, the instant with the highest resultant loading was identified (Figure 3.11). During level walking, the loading response and terminal stance phases were observed to distinguish which would have higher resultant forces. During maximal squat depth, although participants were requested to reach their maximal squat depth (Figure 3.12), it is the standard deep squat (at 90° hip flexion, near 90° knee flexion) that was analyzed and compared among the participants. This was because some participants may not have been able to achieve a deep squat (< 50% leg height).

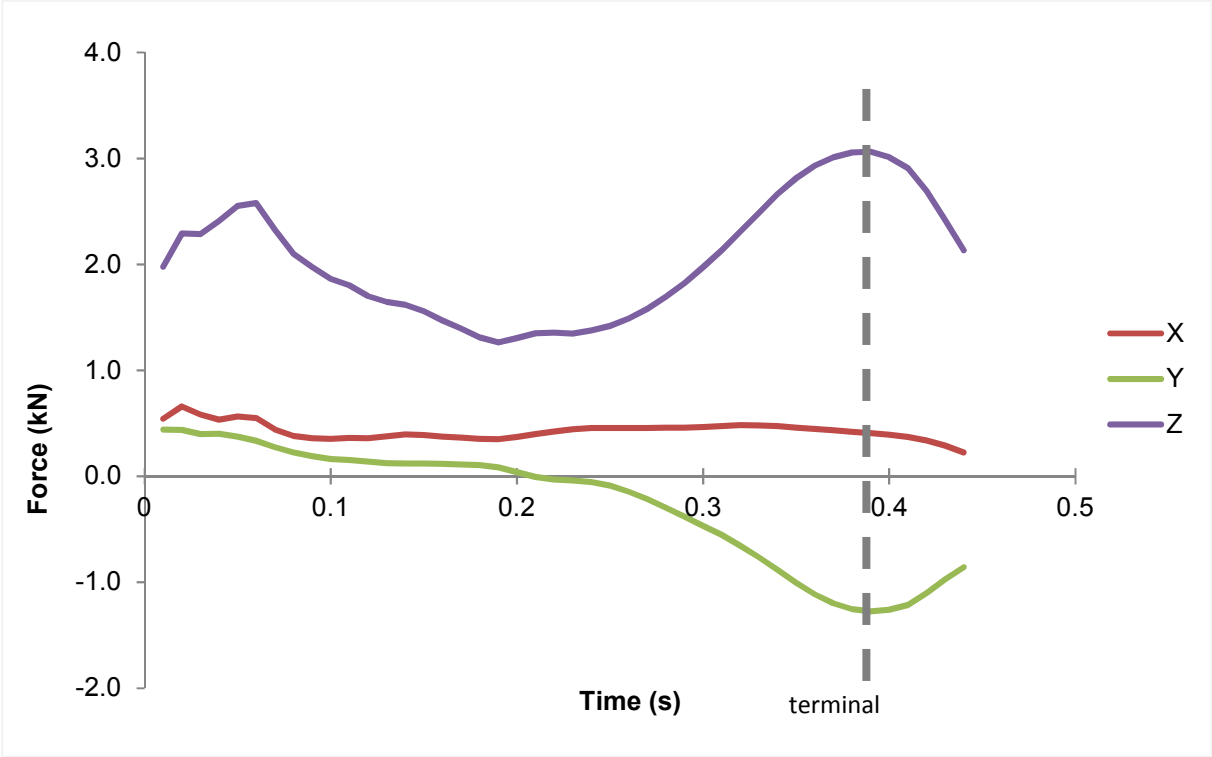

Figure 3.11. Hip contact force for single-leg stance a participant during level-walking, showing the resultant load vectors in the X (+medial, -lateral), Y (+posterior, -anterior), and Z (+superior, -inferior). The highest load was experienced at terminal stance (dashed grey line), during the single-stance phase.

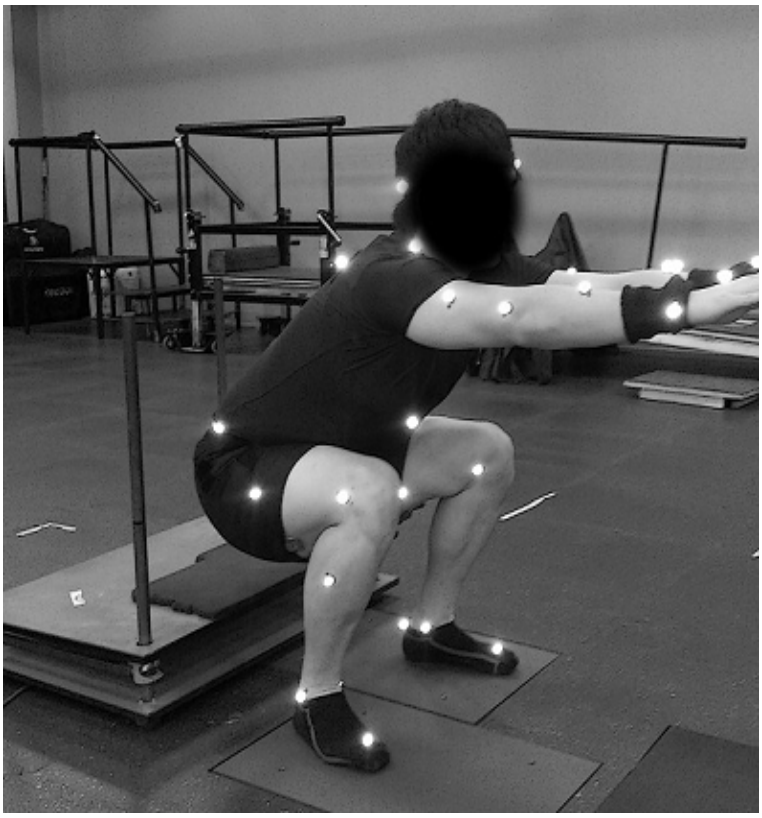

Figure 3.12. Squat depth analysis, showing a participant performing maximal dynamic squats, capturing the lowest depth of the squat and pelvic range of motion. Reproduced with permission University of Ottawa (Dwyer, 2014).

It is still unclear why certain individuals with a cam deformity go on to develop degenerative changes while others will remain asymptomatic for most of their adult life. Gaining a better understanding of hip joint stresses in asymptomatic individuals with a cam deformity can also provide critical insights into who is at risk of arthritic changes. It remains unknown what level of stress leads to those changes and if there would be any pathomechanical differences among individuals. In efforts to address differences in the FAI population, subject-specific hip joint loading and models can be incorporated to decipher if stresses due to an asymptomatic deformity share similarities with symptomatic or healthy cases. Table 3.6 summarizes the implementation framework of Study 3, incorporating participant groups classified by significant parameters (Study 1) and subject-specific hip joint models (Study 2).

Table 3.6. Implementation framework summarizing the subcomponent studies towards the understanding of finite element simulations of clinically relevant scenarios

	Study 3	
	A) Loading during level walking	B) Loading during squat
Groups (from Study 1A)	Symptomatic Asymptomatic Control	Symptomatic Asymptomatic Control
Data	Joint loading for level walking Hip joint model (established from Study 2B)	Joint loading for squatting Hip joint model (established from Study 2B)
Methods	Finite element analysis Discretized for highest instance of load during level walking	Finite element analysis Discretized to compare common squat depth among participants
Results	Peak stress on cartilage, labrum, subchondral bone during level walking	Peak stress on cartilage, labrum, subchondral bone during squatting

3.2.4 Summary of Study Framework

Implementing a participant cohort (comparing symptomatic, asymptomatic, and control groups), this research program was broken down into three studies (Figure 3.13). First, Study 1 determined anatomical and functional parameters that were associated with each participant group (symptomatic, asymptomatic, control). This section established which parameters were the most significant discriminants and, more importantly, which participants from each group were to be selected for further examinations of hip joint stresses (for Study 3). Second, Study 2 evaluated the hip joint models, reconstructing subject-specific geometries representative of each group (from Study 1). This section confirmed that the large-scale anatomical parameters of the segmented models were representative of the participants' CT data and further established which material properties and modelling parameters were to be implemented for further examinations of hip joint stresses (for Study 3). Third, Study 3 examined walking and squatting conditions, comparing selected symptomatic, asymptomatic, and control participants (dependent on Study 1) and incorporated the modelling parameters (dependent on Study 2). This section examined resultant hip joint stresses each participant group, to determine if there were potential pathoanatomical influences towards adverse loading conditions.

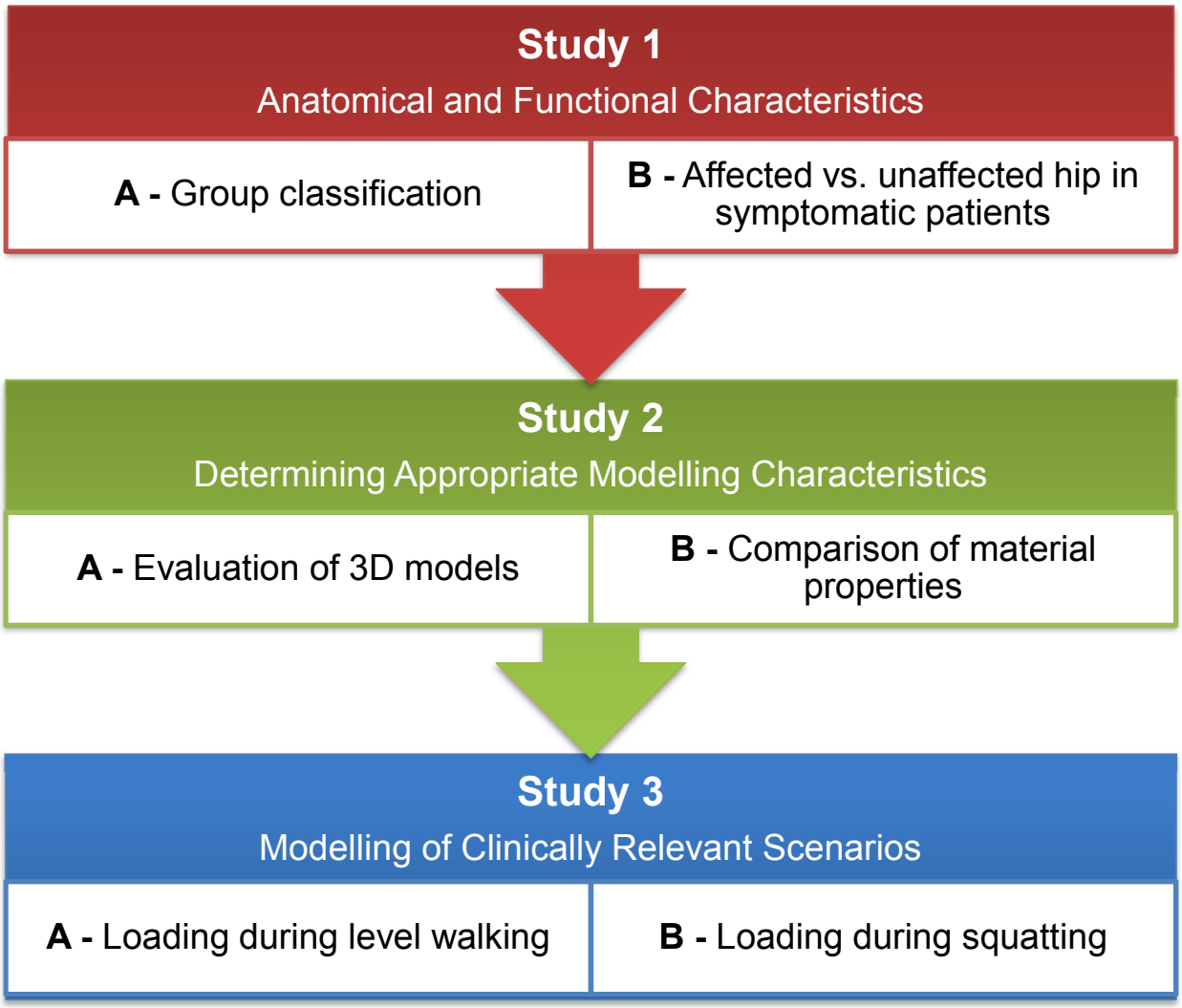

Figure 3.13. Conceptual framework summarizing the individual studies (1, 2, 3) and components (A, B) that will contribute to and address the question: *what are the effects of cam FAI on mechanical hip joint loading***?**

3.3 References

1. Agricola R, Heijboer MP, Bierma-Zeinstra SM, Verhaar JA, Weinans H, Waarsing JH. Cam impingement causes osteoarthritis of the hip: a nationwide prospective cohort study (CHECK). *Ann Rheum Dis*. 2012;72:918-923.
2. Agricola R, Heijboer MP, Ginai AZ, Roels P, Zadpoor AA, Verhaar JA, Weinans H, Waarsing JH. A Cam Deformity Is Gradually Acquired During Skeletal Maturation in Adolescent and Young Male Soccer Players: A Prospective Study With Minimum 2-Year Follow-up. *Am J Sports Med*. 2014;
3. Agricola R, Waarsing JH, Thomas GE, Carr AJ, Reijman M, Bierma-Zeinstra SM, Glyn-Jones S, Weinans H, Arden NK. Cam impingement: defining the presence of a cam deformity by the alpha angle: data from the CHECK cohort and Chingford cohort. *Osteoarthritis Cartilage*. 2014;22:218-225.
4. Albers CE, Steppacher SD, Haefeli PC, Werlen S, Hanke MS, Siebenrock KA, Tannast M. Twelve percent of hips with a primary cam deformity exhibit a slip-like morphology resembling sequelae of slipped capital femoral epiphysis. *Clin Orthop Relat Res*. 2015;473:1212-1223.
5. Ateshian GA, Henak CR, Weiss JA. Toward patient-specific articular contact mechanics. *J Biomech*. 2015;48:779-786.
6. Banerjee P, Mclean CR. Femoroacetabular impingement: a review of diagnosis and management. 2011;4:23-32.
7. Bardakos NV, Villar RN. Predictors of progression of osteoarthritis in femoroacetabular impingement: a radiological study with a minimum of ten years follow-up. *J Bone Joint Surg Br*. 2009;91:162-169.
8. Beaulé P, Hynes K, Parker G, Kemp K. Can the Alpha Angle Assessment of Cam Impingement Predict Acetabular Cartilage Delamination? *Clin Orthop Rel Res*. 2012;470:3361-3367.
9. Beaulé PE, Zaragoza E, Motamedi K, Copelan N, Dorey FJ. Three-dimensional computed tomography of the hip in the assessment of femoroacetabular impingement. *J Orthop Res*. 2005;23:1286-1292.
10. Beck M, Kalhor M, Leunig M, Ganz R. Hip morphology influences the pattern of damage to the acetabular cartilage: femoroacetabular impingement as a cause of early osteoarthritis of the hip. *J Bone Joint Surg Br*. 2005;87:1012-1018.
11. Bedi A, Dolan M, Leunig M, Kelly BT. Static and Dynamic Mechanical Causes of Hip Pain. *Arthroscopy*. 2011;27:235-251.
12. Carter DR, Hayes WC. The compressive behavior of bone as a two-phase porous structure. *J Bone Joint Surg Am*. 1977;59:954-962.
13. Chakraverty JK, Sullivan C, Gan C, Narayanaswamy S, Kamath S. Cam and pincer femoroacetabular impingement: CT findings of features resembling femoroacetabular impingement in a young population without symptoms. *AJR Am J Roentgenol*. 2013;200:389-395.
14. Crowninshield RD, Brand RA. A physiologically based criterion of muscle force prediction in locomotion. *J Biomech*. 1981;14:793-801.
15. Dandachli W, Islam SU, Liu M, Richards R, Hall-Craggs M, Witt J. Three-dimensional CT analysis to determine acetabular retroversion and the implications for the management of femoro-acetabular impingement. *J Bone Joint Surg Br*. 2009;91:1031-1036.
16. Dodds MK, McCormack D, Mulhall KJ. Femoroacetabular impingement after slipped capital femoral epiphysis: does slip severity predict clinical symptoms? *J Pediatr Orthop*. 2009;29:535-539.
17. Dwyer KD, *The Effect of Femoroacetabular Deformity on Lower-Limb Joint Biomechanics during Daily Functional Tasks*, in *School of Human Kinetics*2014, University of Ottawa: Ottawa. p. 109.
18. Ejnisman L, Philippon M, Lertwanich P, Pennock A, Herzog M, Briggs K, Ho C. Relationship Between Femoral Anteversion and Findings in Hips With Femoroacetabular Impingement. *Orthopedics*. 2013;36:293-300.

19. Erdemir A, McLean S, Herzog W, van den Bogert AJ. Model-based estimation of muscle forces exerted during movements. *Clin Biomech (Bristol, Avon)*. 2007;22:131-154.

20. Ganz R, Leunig M, Leunig-Ganz K, Harris WH. The etiology of osteoarthritis of the hip: an integrated mechanical concept. *Clin Orthop Relat Res*. 2008;466:264-272.

21. Ganz R, Parvizi J, Beck M, Leunig M, Nötzli H, Siebenrock KA. Femoroacetabular Impingement: A Cause for Osteoarthritis of the Hip. *Clin Orthop Rel Res*. 2003;417:112-120.

22. Goodman DA, Feighan JE, Smith AD, Latimer B, Buly RL, Cooperman DR. Subclinical slipped capital femoral epiphysis. Relationship to osteoarthrosis of the hip. *J Bone Joint Surg Am*. 1997;79:1489-1497.

23. Haider I, Speirs A, Alnabelseya A, Beaule PE, Frei H. Femoral subchondral bone properties of patients with cam-type femoroacetabular impingement. *Osteoarthritis Cartilage*. 2016;24:1000-1006.

24. Hamner SR, Seth A, Delp SL. Muscle contributions to propulsion and support during running. *J Biomech*. 2010;43:2709-2716.

25. Hartofilakidis G, Bardakos NV, Babis GC, Georgiades G. An examination of the association between different morphotypes of femoroacetabular impingement in asymptomatic subjects and the development of osteoarthritis of the hip. *J Bone Joint Surg Br*. 2011;93:580-586.

26. Ito K, Leunig M, Ganz R. Histopathologic features of the acetabular labrum in femoroacetabular impingement. *Clin Orthop Relat Res*. 2004;262-271.

27. Ito K, Minka MA, 2nd, Leunig M, Werlen S, Ganz R. Femoroacetabular impingement and the cam-effect. A MRI-based quantitative anatomical study of the femoral head-neck offset. *J Bone Joint Surg Br*. 2001;83:171-176.

28. Kang AC, Gooding AJ, Coates MH, Goh TD, Armour P, Rietveld J. Computed tomography assessment of hip joints in asymptomatic individuals in relation to femoroacetabular impingement. *Am J Sports Med*. 2010;38:1160-1165.

29. Kapron AL, Anderson AE, Aoki SK, Phillips LG, Petron DJ, Toth R, Peters CL. Radiographic prevalence of femoroacetabular impingement in collegiate football players: AAOS Exhibit Selection. *J Bone Joint Surg Am*. 2011;93:1-10.

30. Kutty S, Schneider P, Faris P, Kiefer G, Frizzell B, Park R, Powell J. Reliability and predictability of the centre-edge angle in the assessment of pincer femoroacetabular impingement. 2012;36:505-510.

31. Lamontagne M, Brisson N, Kennedy MJ, Beaule PE. Preoperative and postoperative lower-extremity joint and pelvic kinematics during maximal squatting of patients with cam femoro-acetabular impingement. *J Bone Joint Surg Am*. 2011;93 Suppl 2:40-45.

32. Lamontagne M, Kennedy MJ, Beaule PE. The effect of cam FAI on hip and pelvic motion during maximum squat. *Clin Orthop Relat Res*. 2009;467:645-650.

33. Lavigne M, Parvizi J, Beck M, Siebenrock KA, Ganz R, Leunig M. Anterior femoroacetabular impingement: part I. Techniques of joint preserving surgery. *Clin Orthop Relat Res*. 2004;61-66.

34. Leunig M, Beaule PE, Ganz R. The concept of femoroacetabular impingement: current status and future perspectives. *Clin Orthop Relat Res*. 2009;467:616-622.

35. Lu TW, O'Connor JJ, Taylor SJ, Walker PS. Validation of a lower limb model with in vivo femoral forces telemetered from two subjects. *J Biomech*. 1998;31:63-69.

36. Macirowski T, Tepic S, Mann RW. Cartilage stresses in the human hip joint. *J Biomech Eng*. 1994;116:10-18.

37. Mantovani G, *Hip Joint Contact Load and Muscle Force in Femoroacetabular Impingement Population*, 2016, University of Ottawa: Ottawa. p. 182.

38. Mantovani G, Lamontagne M. How Different Marker Sets Affect Joint Angles in Inverse Kinematics Framework. *J Biomech Eng*. 2017;139:1-7.

39. Modenese L, Phillips AM. Prediction of hip contact forces and muscle activations during walking at different speeds. *Multibody Syst Dyn*. 2012;28:157-168.

40. Monazzam S, Bomar JD, Agashe M, Hosalkar HS. Does femoral rotation influence anteroposterior alpha angle, lateral center-edge angle, and medial proximal femoral angle? A pilot study. *Clin Orthop Relat Res*. 2013;471:1639-1645.

41. Morgan EF, Bayraktar HH, Keaveny TM. Trabecular bone modulus-density relationships depend on anatomic site. *J Biomech*. 2003;36:897-904.

42. Ng KCG, Rouhi G, Lamontagne M, Beaule PE. Finite Element Analysis Examining the Effects of Cam FAI on Hip Joint Mechanical Loading Using Subject-Specific Geometries During Standing and Maximum Squat. *HSS J*. 2012;8:206-212.

43. Nötzli HP, Wyss TF, Stoecklin CH, Schmid MR, Treiber K, Hodler J. The contour of the femoral head-neck junction as a predictor for the risk of anterior impingement. *J Bone Joint Surg Br*. 2002;84-B:556-560.

44. Nouh MR, Schweitzer ME, Rybak L, Cohen J. Femoroacetabular impingement: can the alpha angle be estimated? *AJR Am J Roentgenol*. 2008;190:1260-1262.

45. Radin EL, Burr DB, Caterson B, Fyhrie D, Brown TD, Boyd RD. Mechanical determinants of osteoarthrosis. *Semin Arthritis Rheum*. 1991;21:12-21.

46. Rakhra KS, Sheikh AM, Allen D, Beaule PE. Comparison of MRI alpha angle measurement planes in femoroacetabular impingement. *Clin Orthop Relat Res*. 2009;467:660-665.

47. Ranawat A, Schulz B, Baumbach S, Meftah M, Ganz R, Leunig M. Radiographic Predictors of Hip Pain in Femoroacetabular Impingement. *HSS J*. 2011;7:115-119.

48. Reynolds D, Lucas J, Klaue K. Retroversion of the acetabulum. A cause of hip pain. *J Bone Joint Surg Br*. 1999;81:281-288.

49. Schileo E, Taddei F, Malandrino A, Cristofolini L, Viceconti M. Subject-specific finite element models can accurately predict strain levels in long bones. *J Biomech*. 2007;40:2982-2989.

50. Siebenrock KA, Ferner F, Noble PC, Santore RF, Werlen S, Mamisch TC. The cam-type deformity of the proximal femur arises in childhood in response to vigorous sporting activity. *Clin Orthop Relat Res*. 2011;469:3229-3240.

51. Siebenrock KA, Wahab KH, Werlen S, Kalhor M, Leunig M, Ganz R. Abnormal extension of the femoral head epiphysis as a cause of cam impingement. *Clin Orthop Relat Res*. 2004;54-60.

52. Speirs AD, Beaule PE, Rakhra KS, Schweitzer ME, Frei H. Increased acetabular subchondral bone density is associated with cam-type femoroacetabular impingement. *Osteoarthritis Cartilage*. 2013;21:551-558.

53. Steele KM, Seth A, Hicks JL, Schwartz MS, Delp SL. Muscle contributions to support and progression during single-limb stance in crouch gait. *J Biomech*. 2010;43:2099-2105.

54. Stulberg S, Cordell L, Harris WH, Ramsey P, MacEwen G. *Unrecognized childhood disease: A major cause of idiopathic osteoarthritis of the hip.* in *Third Open Scientific Meeting of The Hip Society*. 1975. St. Louis, MO.

55. Sutter R, Dietrich TJ, Zingg PO, Pfirrmann CWA. How Useful Is the Alpha Angle for Discriminating between Symptomatic Patients with Cam-type Femoroacetabular Impingement and Asymptomatic Volunteers? *Radiology*. 2012;264:514-521.

56. Wu G, Siegler S, Allard P, Kirtley C, Leardini A, Rosenbaum D, Whittle M, D'Lima DD, Cristofolini L, Witte H, Schmid O, Stokes I. ISB recommendation on definitions of joint coordinate system of various joints for the reporting of human joint motion--part I: ankle, hip, and spine. International Society of Biomechanics. *J Biomech*. 2002;35:543-548.

II Anatomical and Functional Characteristics

4 Patient-Specific Anatomical and Functional Parameters Provide New Insights into the Pathomechanism of Cam FAI

K. C. Geoffrey Ng [1] | Mario Lamontagne [2,1] | Andrew P. Adamczyk [3] | Kawan S. Rakhra [4] | Paul E. Beaulé [5]

[1] Department of Mechanical Engineering | University of Ottawa | Ottawa, Ontario, Canada

[2] School of Human Kinetics | University of Ottawa | Ottawa, Ontario, Canada

[3] Faculty of Medicine | University of Ottawa | Ottawa, Ontario, Canada

[4] Department of Diagnostic Radiology | University of Ottawa | Ontario, Canada

[5] Division of Orthopaedic Surgery | University of Ottawa | Ottawa, Ontario, Canada

Contents of this chapter published as an article in *Clinical Orthopaedics and Related Research*® | 22 July 2014

Ng KCG, Lamontagne M, Adamczyk AP, Rakhra KS, Beaulé PE. Patient-specific anatomical and functional parameters provide new insights into the pathomechanism of cam FAI. *Clin Orthop Relat Res*. 2015;473:1289-1296. DOI: 10.1007/s11999-014-3797-1.

4.0 Abstract

Background: Femoroacetabular impingement (FAI) represents a constellation of anatomic and clinical features, but definitive diagnosis is often difficult. The high prevalence of cam deformity of the femoral head in the asymptomatic population as well as clinical factors leading to the onset of symptoms raises questions as to what other factors increase the risk of cartilage damage and hip pain.

Questions/Purposes: The purpose was to identify any differences in anatomical parameters and squat kinematics among symptomatic, asymptomatic, and control individuals and if these parameters can determine individuals at risk of developing symptoms of cam FAI.

Methods: Forty-three participants (n = 43) were recruited and divided into three groups: symptomatic (12), asymptomatic (17), and control (14). Symptomatic participants presented a cam deformity (identified by an elevated alpha angle on CT images), pain symptoms, clinical signs, and were scheduled for surgery. The other recruited volunteers were blinded and unaware whether they had a cam deformity. After the CT data were assessed for an elevated alpha angle, participants with a cam deformity but who did not demonstrate any clinical signs or symptoms were considered asymptomatic, whereas participants without a cam deformity and without clinical signs or symptoms were considered healthy control subjects. For each participant, anatomical CT parameters (axial alpha angle, radial alpha angle, femoral head-neck offset, femoral neck-shaft angle, medial proximal femoral angle, femoral torsion, acetabular version) were evaluated. Functional squat parameters (maximal squat depth, pelvic range of motion) were determined using a motion capture system. A stepwise discriminant function analysis was used to determine which of the parameters were most suitable to classify each participant with their respective subgroup.

Results: The symptomatic group showed elevated alpha angles and lower femoral neck-shaft angles, whereas the asymptomatic group showed elevated alpha angles in comparison with the control group. The best discriminating parameters to determine symptoms were radial alpha angle, femoral neck-shaft angle, and pelvic range of motion ($p < 0.001$).

Conclusions: In the presence of a cam deformity, indications of a decreased femoral neck-shaft angle and reduced pelvic range of motion can identify those at risk of symptomatic FAI.

Level of Evidence: Level III, diagnostic study.

4.1 Introduction

Cam-type femoroacetabular impingement (FAI), characterized by an enlarged, aspherical deformity of the femoral head and neck, is recognized as a pathomechanical disease process of the hip and a possible cause for early adult osteoarthritis [1, 16, 23]. This mechanical impingement is typically observed at the limit of ROM [31, 32] when the aspherical femoral head comes into contact with lateral aspects of the anterosuperior labrum and acetabulum. In the presence of a larger cam deformity, it further reduces the clearance between the femoral head-neck junction and the labrum, therefore imposing an obstruction and inducing elevated stresses [35].

Defining who is at risk of impingement and cartilage damage has been mainly based on the size and location of the cam deformity, which has been traditionally quantified by the alpha angle on multiplane imaging [3, 7, 36, 37, 39, 43, 45]. Several authors have shown that the severity of the cam deformity (that is, a higher alpha angle) is associated with an increased risk of hip pain and joint degeneration [7, 28, 33]. Typically, a cam deformity is indicated by an alpha angle greater than 50.5° and 60° in the oblique-axial and radial plane, respectively [7, 36, 37, 39]. However, the accuracy and sensitivity of the alpha angle in determining the risk of developing symptomatic FAI is inconsistent [6, 30, 34, 37, 43]. Moreover, other common radiographic measures of the femoral head and neck and acetabulum have been associated with symptomatic FAI [5, 10, 26, 40], but it remains unclear as to which combination of parameters plays a role in identifying patients at risk of developing symptoms. Although patients have demonstrated higher hip stresses [35] and different hip kinematics at higher ROMs such as during maximal squatting [31, 32], it is still unclear why many individuals with cam deformity do not exhibit any clinical signs [22, 38, 40].

Many individuals with cam deformities may not experience mechanical impingement or pain symptoms, thus qualifying them as asymptomatic individuals [11, 18, 26, 43]. Therefore, we postulated that FAI symptoms may be related to other anatomical parameters that can exacerbate mechanical impingement in patients at risk of developing symptoms.

The purpose of this study was to examine other anatomical features of the hip that could be associated with symptoms resulting from the cam deformity. In this study, we addressed two research questions: (1) Can additional anatomical parameters, in addition to the conventional alpha angles, and functional squat parameters determine differences among symptomatic,

asymptomatic, and control individuals? (2) Which of the anatomical and functional squat parameters best classify symptomatic, asymptomatic, and control individuals with their respective subgroups and identify patients at risk of developing symptoms?

4.2 Patients and Methods

Initially, 50 male volunteers were recruited in a 2-year period through the hospital's Division of Orthopaedic Surgery. The participants were classified based on indications of a cam deformity on CT scans, clinical impingement signs, and plans to undergo hip surgery. Symptomatic participants with the deformity, who presented themselves with hip pain and clinical signs of impingement, were recruited from the orthopaedic surgeon's clinical practice once scheduled for surgery. Additional participants volunteered for the study and were blinded and unaware whether they had a cam deformity. Pelvic and knee CT data were acquired from each participant using either a Toshiba Acquilion (Toshiba Medical Systems Corporation, Otawara, Japan) or a GE Discover CT750 (GE Healthcare, Mississauga, Ontario, Canada) and observed for a cam deformity, as indicated by an elevated alpha angle, by a musculoskeletal radiologist (KSR). After the CT data were assessed, participants with a cam deformity but who did not demonstrate any clinical signs or symptoms were considered asymptomatic. Participants without a cam deformity and without any clinical signs or symptoms were considered as healthy control subjects. Participants with any neurological or musculoskeletal disorders, degenerative diseases, previous major lower limb injuries, or a body mass index greater than 30 kg/m^2 were excluded.

This a priori classification resulted in 15 symptomatic, 19 asymptomatic, and 16 control participants. All participants completed pain questionnaires to ascertain their Hip Disability and Osteoarthritis Outcome Score and WOMAC. Participants signed and provided informed consent before the study. The university and hospital research institute ethics boards approved this study and all investigations were conducted ethically in conformity with research principles.

To remove bias from a priori classifications, CT data were then blinded and randomly assigned new file names. Both left and right hips were measured for multiple anatomical CT measures, which included axial alpha angle, radial alpha angle, femoral head-neck offset, femoral neck-shaft angle, medial proximal femoral angle, femoral torsion, and acetabular version using Onis 2.4 (DigitalCore, Tokyo, Japan). To confirm the reliability of the measurements, two observers (KCGN, APA) evaluated the anatomical CT parameters, each performing two readings.

Both observers received training and instructions from a musculoskeletal radiologist (KSR). Each observer's second reading was performed 2 weeks after the completion of the first.

The axial alpha angle was measured on the oblique-axial plane of the longitudinal femoral neck axis, observing for the cam deformity in the anterior aspect of the femoral head [36]. With the vertex centered at the femoral head, the angle measured the femoral neck axis to the head-neck junction (Figure 4.1.A). Anterior femoral head-neck offset was also observed on the oblique-axial plane [11, 26], measuring the offset distance between the two tangents of the anterior femoral head and neck (Figure 4.1.A). The radial alpha angle was obtained through a 1:30 clock face rotation about the longitudinal femoral neck axis [39, 43], observing the anterosuperior quadrant (Figure 4.1.B). An axial alpha angle greater than 50.5° or radial alpha angle greater than 60° was considered as cam deformity [6, 43].

The femoral neck-shaft angle, from the frontal plane, was formed between the femoral neck and shaft axes (Figure 4.1.C) [22, 40]. Similarly, the medial proximal femoral angle was measured between the femoral shaft axis and the line joining the center of the femoral head to the superior greater trochanter (Figure 4.1.D) [5]. Femoral torsion was determined as the difference between the femoral neck horizontal and condyle horizontal angles, each taking the angle with respect to the transverse plane's horizontal plane (Figure 4.1.E-F) [10, 15]. Acetabular version was measured on the transverse plane coincident with the left and right femoral head centers [11, 12, 41]. This angle was formed by the line connecting the anterior and posterior acetabular notches and the perpendicular axis to the posterior acetabular notch (Figure 4.1.G). Detailed measurement protocols for each anatomical parameter were provided to the observers before the readings (Supplemental materials are available with the online version of CORR®, 4.6 Appendix – CT Measures Protocol).

Three-dimensional (3-D) hip kinematics were collected from each participant's maximal squat depth motion using 10 Vicon MX-13 cameras (Vicon, Los Angeles, CA, USA) and retroreflective skin markers placed on anatomical landmarks using a modified Helen-Hayes marker set [13, 25]. Participants were instructed to perform five maximal dynamic squats, squatting to the lowest possible depth at a controlled, self-selected pace. Feet were placed shoulder-width apart, directed anteriorly, with toes and heels in full contact with the ground during the entire squat cycle [31, 32]. Five squat depths were averaged as a percentage with

respect to leg height, where ground level represented a leg height of 0%. Total sagittal pelvic ROM was calculated from peak pelvic angles during descent, maximal squat, and ascent phases.

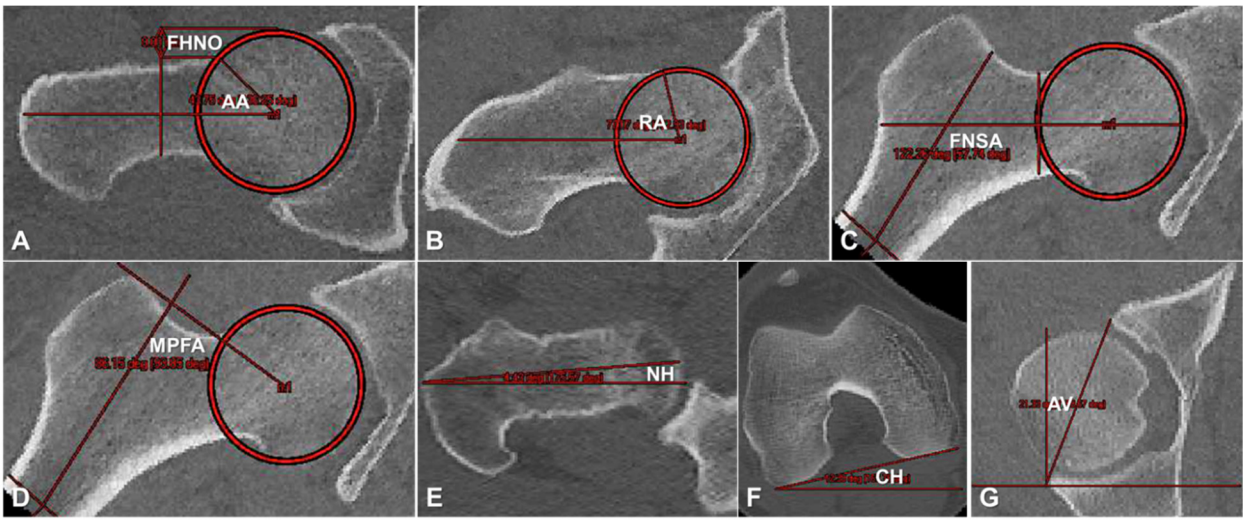

Figure 4.1. Anatomical CT parameters measure the: **A**) axial alpha angle (AA) and femoral head-neck offset (FHNO); **B**) radial alpha angle (RA); **C**) femoral neck-shaft angle (FNSA); **D**) medial proximal femoral angle (MPFA); **E**) neck (NH) and **F**) condyle horizontals (CH) for femoral torsion; and **G**) acetabular version (AV).

The resultant CT measurements were then unblinded and matched with the squat results. For each of the symptomatic, asymptomatic, or control participants, the affected side was defined by the side with symptoms, higher alpha angle, or smaller alpha angle, respectively. Five participants (three symptomatic, one asymptomatic, one control) were excluded as a result of their inability to perform an adequate deep squat (< 70% of leg height). A gray zone range for the alpha angles was defined to account for potential reading errors (axial = 50.5° ± 3°; radial = 60° ± 3°). Two participants (one asymptomatic, one control) were excluded as a result of their alpha angles being within this gray zone. This resulted in a final sample size of 43 participants (n = 43), with 12 symptomatic, 17 asymptomatic, and 14 control participants.

For each anatomical CT measure, intra- and interrater reliability was quantified using the intraclass correlation coefficient (ICC) using two-way mixed models. Intrarater considered single measures whereas interrater considered average measures, both seeking absolute agreement [19, 42]. The intra- and interrater anatomical observations were in strong to near-perfect agreement ($0.847 \leq ICC_{Obs1} \leq 0.987$; $0.867 \leq ICC_{Obs2} \leq 0.967$; $0.703 \leq ICC_{Obs1\text{-}2} \leq 0.886$; Table 4.1). To examine if there were differences among each of the anatomical and functional parameters among the groups, a one-way between-groups analysis of variance was used ($\alpha = 0.05$). A

stepwise discriminant function analysis (DFA) was implemented to identify which of the anatomical and squat kinematics parameters were most suitable to classify each participant's affected hip with their respective subgroup. Similar to a hierarchical linear regression, where multiple parameters describe the level of variance, the DFA further predicts how subjects are classified based on the most suitable parameters. Sample sizes were deemed adequate because the smallest group size (12) exceeded the number of total parameters (9) [44]. The DFA assumed that each of the anatomical CT and squat parameters was treated as an independent variable for grouping. Statistical analysis was performed using SPSS Statistics Version 21 (IBM Corporation, Armonk, NY, USA).

Table 4.1. Intraclass correlation coefficient indicating the intra- and interrater reliability for each measured anatomical CT parameter

Anatomical parameter	Intrarater 1	Intrarater 2	Interrater 1-2
Axial alpha angle	0.957	0.948	0.881
Radial alpha angle	0.972	0.929	0.865
Femoral neck-shaft angle	0.847	0.867	0.854
Medial proximal femoral angle	0.969	0.904	0.783
Femoral head-neck offset	0.927	0.903	0.758
Femoral torsion	0.987	0.916	0.703
Acetabular version	0.968	0.967	0.886

4.3 Results

Other than the alpha angles and femoral head-neck offset, characteristic parameters of the cam deformity, the asymptomatic group demonstrated similar anatomical and squat parameters as the control group (Table 4.2). Both symptomatic and asymptomatic groups demonstrated higher axial alpha angles (56 ± 8° and 57 ± 8°, respectively), radial alpha angles (67 ± 6° and 71 ± 6°, respectively), and lower femoral head-neck offsets (6 ± 2 mm and 7 ± 2 mm, respectively) in comparison with the control group (axial = 43 ± 3°, $\eta^2 = 0.517$, $p < 0.001$; radial = 52 ± 4°, $\eta^2 = 0.705$, $p < 0.001$; offset = 9 ± 1 mm, $\eta^2 = 0.440$, $p < 0.001$). Femoral neck-shaft angles were higher for the asymptomatic and control groups (127 ± 3° and 128 ± 2°, respectively) in comparison with the symptomatic group (123 ± 2°, $\eta^2 = 0.496$, $p < 0.001$). The symptomatic group showed prominent femoral antetorsion ($\eta^2 = 0.164$, $p = 0.039$) in comparison with the control group, but did not show any differences in medial proximal femoral angle or acetabular

version. Moreover, the symptomatic group had a substantially reduced squat depth (44 ± 10%) and pelvic ROM (11 ± 4°) in comparison with the asymptomatic (39 ± 9%; 15 ± 7°) and control groups (37 ± 8%; 15 ± 7°).

Table 4.2. Descriptive anatomical CT parameters, squat depth parameters, and pain scores associated with the symptomatic, asymptomatic, and control groups (reporting mean ± SD)

Group descriptive	Symptomatic	Asymptomatic	Control	Total
Number of participants	12	17	14	43
Age (years)	38 ± 9	31 ± 5	32 ± 6	33 ± 7
Body mass index (kg/m^2)	26 ± 3	25 ± 2	26 ± 3	26 ± 3
Anatomical parameter				
Axial alpha angle (°)	56 ± 8*	57 ± 8*	43 ± 3	52 ± 9
Radial alpha angle (°)	67 ± 6*	71 ± 6*	52 ± 4	64 ± 10
Femoral head-neck offset (mm)	6 ± 2*	7 ± 2*	9 ± 1	7 ± 2
Femoral neck-shaft angle (°)	123 ± 2*,†	127 ± 3	128 ± 2	126 ± 3
Medial proximal femoral angle (°)	80 ± 4	83 ± 4	82 ± 4	82 ± 4
Femoral torsion (°)	14 ± 9*	13 ± 8	6 ± 7	11 ± 8
Acetabular version (°)	22 ± 5	18 ± 4	19 ± 6	19 ± 5
Maximal squat depth parameter				
Depth (percent leg height)	44 ± 10	39 ± 9	37 ± 8	40 ± 9
Pelvic ROM (°)	11 ± 4	15 ± 7	15 ± 7	14 ± 6
Pain questionnaire				
HOOS – pain	64 ± 21*,†	99 ± 5	99 ± 4	88 ± 20
WOMAC – pain	71 ± 21*,†	100 ± 1	99 ± 3	91 ± 18

* Significant difference ($p < 0.05$) compared with control group
† Significant difference ($p < 0.05$) compared with asymptomatic group

The best parameters to classify the participants and to determine symptoms were radial alpha angle, femoral neck-shaft angle, and pelvic ROM. The three-step DFA included radial alpha angle in the first step (Wilk's $\lambda_1 = 0.295$, $p < 0.001$), femoral neck-shaft angle in the second (Wilk's $\lambda_2 = 0.157$, $p < 0.001$), then pelvic ROM in the third (Wilk's $\lambda_3 = 0.135$, $p < 0.001$). The resultant two predictive equations based on the standardized canonical discriminant function coefficients were:

$$\text{Function 1} = (0.962 \bullet zRA) - (0.156 \bullet zFNSA) - (0.050 \bullet zROM) \quad [1]$$

$$\text{Function 2} = (0.325 \bullet zRA) + (0.973 \bullet zFNSA) + (0.517 \bullet zROM) \quad [2]$$

where *zRA*, *zFNSA*, and *zROM* represent the standardized normal scores of their respective measures. Inputting an additional participant's radial alpha angle, femoral neck-shaft angle, and pelvic ROM z-values into the predictive equations (equations [1] and [2]), the resultant functions would provide a visual indication of classification based on their proximity to a group centroid (Figure 4.2). It was determined that 95% (41 of 43) of the original group was classified correctly. A participant, initially classified as asymptomatic, was reclassified closer to the symptomatic group based on the stepwise parameters. This asymptomatic participant had an elevated radial alpha angle and decreased femoral neck-shaft angle (122°), similar to characteristic mean values of the symptomatic group. Another symptomatic participant was predicted to be significantly closer to the asymptomatic group with a radial alpha angle and femoral neck-shaft angle (125°) closer to the mean values of the asymptomatic group (Figure 4.2).

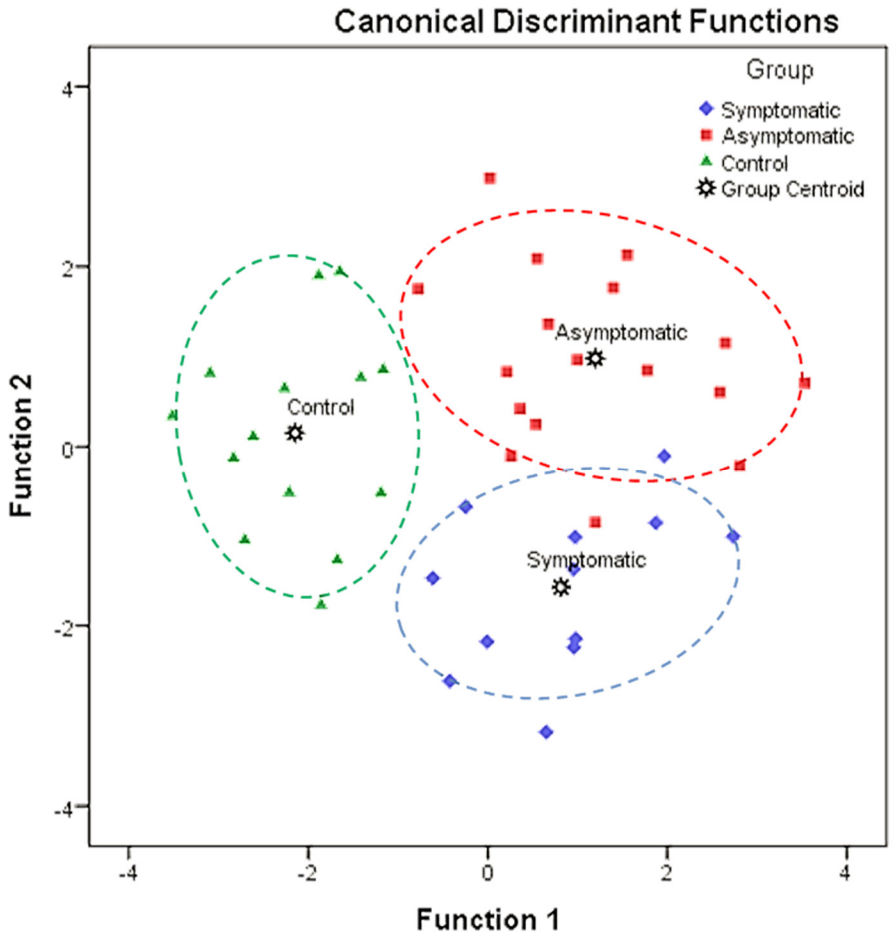

Figure 4.2. Discriminant function analysis with canonical discriminant functions classifies symptomatic (diamond), asymptomatic (square), and control (triangle) individuals based on the radial alpha angle, femoral neck-shaft angle, and pelvic ROM. Group envelopes (ellipses, CI = 95%) are centered on the group centroids (star markers)

4.4 Discussion

Recent publications have highlighted the prevalence of the cam deformity in the normal population based on the alpha angle [17, 18, 24]. However, we do not know what factors increase the likelihood that a patient with cam FAI morphology will become symptomatic. To better predict which individuals with a cam deformity who are at risk of developing hip symptoms, we used subject-specific motion analysis as well as additional anatomical parameters in discriminating individuals with and without symptoms. We found that radial alpha angle, femoral neck-shaft angle, and pelvic ROM predicted FAI symptoms.

One of the limitations was the number of CT parameters considered. Because the focus was on cam-type FAI, we selected common recurring parameters of the proximal femur, as opposed to the acetabulum, postulated to describe characteristics of FAI. To fully understand the relationship among joint structures, clinical signs, and the role of acetabular orientation on joint kinematics, an extensive study of the morphological parameters associated with the acetabulum (*e.g.*, lateral center-edge angle and retroversion index) may be needed in the future along with a 3-D shape analysis of the cam deformity [20, 21]. Because the cam morphology is statistically more prevalent in males [2, 9, 27], our sample population consisted of only male participants. The inclusion of females could introduce variances in anatomical structure and squat kinematics. Nonetheless, studies comparing sex in regards to anatomical parameters and motion analysis should be addressed in the future. The differences in age may also have been a limitation, because cartilage and labral damage not only depends on the size of the deformity, but can also increase with age. Although our symptomatic group was slightly older, age differences were not significant and there were a few older symptomatic participants who performed deeper squats and wider pelvic motions. It may have been possible that pelvic ROM was limited by pain. During the maximal dynamic squat, participants were asked if they experienced any discomfort or pain during the motion and none of the patients stated that pain limited their squat capacity. In addition, none of the patients had evidence of osteoarthritis on radiographs. Having said that, we cannot fully account for other possible causes of limited squat such as apprehension by the participant to avoid pain. It is possible that the pace of the squat motion can affect the loading dynamics of the cam deformity onto the articulating surfaces. A subject-specific finite element model, incorporating the viscoelastic characteristics of the cartilage, could be considered in the future to better address the loading dynamics of the hip. The other limitation is the use of pain to

help classify the different groups. Because there are multiple sources of pain in and around the hip, we cannot make conclusions as to the risk of eventual hip arthritis. Use of quantitative cartilage MRI may provide further insight into the biomechanical parameters associated with FAI in patients with the cam morphology [4, 8].

We found that the symptomatic group had a substantially smaller femoral neck-shaft angle with angles approaching coxa vara; others have suggested that this can predispose to labral-chondral damage in patients with a cam deformity [10, 14, 45]. In addition, Bedi and associates [10] recognized that shortening of the varus neck resulted in intraarticular and extra-articular mechanical impingement. Hartofilakidis and associates [22] reported a femoral neck-shaft angle for their symptomatic group (119°), which corresponded closely with our findings. Ranawat and associates [40] reported a much higher symptomatic femoral neck-shaft angle (132°) but was still lower than their respective contralateral asymptomatic side. A decrease in femoral neck-shaft angle, although small, could explain symptoms of unilateral FAI [40]. The medial proximal femoral angle for our symptomatic group was not substantially lower than our asymptomatic or control group but was similar to previous findings for progressive osteoarthritis [5]. The medial proximal femoral angle measures between the femoral head-to-neck from the greater trochanter as opposed to the neck-to-shaft angle. The correct CT slice may not have been selected to locate our superior greater trochanter, thus underestimating its implication toward understanding the onset of osteoarthritis. The symptomatic group's femoral torsion corresponded with previous findings, indicating an increased risk for labral damage [15]. However, results for acetabular version were inconclusive because several asymptomatic and control participants demonstrated retroversion but did not show any clinical signs or symptoms. This contradicts previous findings for acetabular version associated with symptoms [12, 26, 29, 41] and may not yet be adequate to explain differences between symptomatic and asymptomatic individuals.

The stepwise DFA indicated that radial alpha angle, femoral neck-shaft angle, and pelvic ROM were the best classifiers. Including other parameters in the stepwise DFA would not have substantially improved the predictive power of the model. Alternatively, all parameters could have been included in the DFA to obtain predictive functions dependent on all anatomical and squat parameters. However, this would not have predicted which parameters were the most suitable for classification and, thus, would not have established characteristics most potentially associated with symptoms. Interestingly, the radial alpha angle was more predictive than the

axial alpha angle [43], reiterating that it should be the preferred alpha angle to observe for the increased severity of the cam deformity [6, 7, 39, 43]. The femoral neck-shaft angle was considered as a second discriminating parameter to distinguish symptomatic from asymptomatic individuals, because it was substantially different among the two groups. Although medial proximal femoral angle and femoral torsion for the symptomatic group were slightly lower, compared with asymptomatic, the difference was not large enough for the analysis to consider them as discriminating parameters. Pelvic ROM was used as the final parameter to further distinguish symptomatic from asymptomatic individuals. The symptomatic group could not squat as low and had a reduced pelvic ROM in comparison with the other groups, reiterating the implementation of a maximal squat motion as a functional diagnostic test in determining individuals at risk of developing hip symptoms. The inclusion of femoral neck-shaft angle reveals that there is an association between the neck orientation with a severe cam deformity and dynamic hip motion, which improves previous understandings of the pathoanatomy [10, 14, 46]. Ultimately, for mechanical impingement to occur as a result of the cam morphology, symptoms could persist attributable to a combination of several anatomical factors. Limited squat depth is reflective of decreased pelvic mobility, putting the hip further at risk of developing pain.

From the canonical discriminant plot, for the symptomatic participants to move closer to the asymptomatic ellipse, their femoral neck-shaft angle would have to increase. Ultimately, for symptomatic and asymptomatic participants to move closer to the control ellipse, their cam deformity parameters would have to decrease. It should be noted that the resultant canonical discriminant equations and plots were applicable to this specific cohort of 43 males. As a long-term comparative analysis, a larger multicentre study could be considered, to examine if a discriminant function analysis would predict similar group memberships using a combination of similar or additional anatomical parameters.

Our findings confirm the complex nature of impingement as well as other anatomical parameters that play important roles in the onset of hip symptomatology. Consequently, providing the clinicians with additional and more specific anatomical measurements (*e.g.*, radial alpha angle, femoral neck-shaft angle, pelvic ROM) can identify who is at greater risk of coming to surgical intervention as well as developing screening programs for the cam morphology at risk of FAI.

4.5 References

1. Agricola R, Heijboer MP, Bierma-Zeinstra SM, Verhaar JA, Weinans H, Waarsing JH. Cam impingement causes osteoarthritis of the hip: a nationwide prospective cohort study (CHECK). *Ann Rheum Dis*. 2012;72:918-923.
2. Allen D, Beaulé PE, Ramadan O, Doucette S. Prevalence of associated deformities and hip pain in patients with cam-type femoroacetabular impingement. *J Bone Joint Surg Br*. 2009;91:589-594.
3. Anderson LA, Peters CL, Park BB, Stoddard GJ, Erickson JA, Crim JR. Acetabular cartilage delamination in femoroacetabular impingement. Risk factors and magnetic resonance imaging diagnosis. *J Bone Joint Surg Am*. 2009;91:305-313.
4. Apprich S, Mamisch TC, Welsch GH, Bonel H, Siebenrock KA, Kim YJ, Trattnig S, Dudda M. Evaluation of articular cartilage in patients with femoroacetabular impingement (FAI) using T2* mapping at different time points at 3.0 Tesla MRI: a feasibility study. *Skeletal Radiol*. 2012;41:987-995.
5. Bardakos NV, Villar RN. Predictors of progression of osteoarthritis in femoroacetabular impingement: a radiological study with a minimum of ten years follow-up. *J Bone Joint Surg Br*. 2009;91:162-169.
6. Barton C, Salineros MJ, Rakhra KS, Beaulé PE. Validity of the alpha angle measurement on plain radiographs in the evaluation of cam-type femoroacetabular impingement. *Clin Orthop Relat Res*. 2011;469:464-469.
7. Beaulé P, Hynes K, Parker G, Kemp K. Can the alpha angle assessment of cam impingement predict acetabular cartilage delamination? *Clin Orthop Relat Res*. 2012;470:3361-3367.
8. Beaulé PE, Kim YJ, Rakhra KS, Stelzeneder D, Brown TD. New frontiers in cartilage imaging of the hip. *Instr Course Lect*. 2012;61:253-262.
9. Beck M, Kalhor M, Leunig M, Ganz R. Hip morphology influences the pattern of damage to the acetabular cartilage: femoroacetabular impingement as a cause of early osteoarthritis of the hip. *J Bone Joint Surg Br*. 2005;87:1012-1018.
10. Bedi A, Dolan M, Leunig M, Kelly BT. Static and dynamic mechanical causes of hip pain. *Arthroscopy*. 2011;27:235-251.
11. Chakraverty JK, Sullivan C, Gan C, Narayanaswamy S, Kamath S. Cam and pincer femoroacetabular impingement: CT findings of features resembling femoroacetabular impingement in a young population without symptoms. *AJR Am J Roentgenol*. 2013;200:389-395.
12. Dandachli W, Islam SU, Liu M, Richards R, Hall-Craggs M, Witt J. Three-dimensional CT analysis to determine acetabular retroversion and the implications for the management of femoro-acetabular impingement. *J Bone Joint Surg Br*. 2009;91:1031-1036.
13. Davis RB, Ounpuu S, Tyburski D, Gage JR. A gait analysis data collection and reduction technique. *Hum Mov Sci*. 1991;10:575-587.
14. Doherty M, Courtney P, Doherty S, Jenkins W, Maciewicz RA, Muir K, Zhang W. Nonspherical femoral head shape (pistol grip deformity), neck shaft angle, and risk of hip osteoarthritis: a case-control study. *Arthritis Rheum*. 2008;58:3172-3182.
15. Ejnisman L, Philippon M, Lertwanich P, Pennock A, Herzog M, Briggs K, Ho C. Relationship between femoral anteversion and findings in hips with femoroacetabular impingement. *Orthopedics*. 2013;36:293-300.
16. Ganz R, Parvizi J, Beck M, Leunig M, Nötzli H, Siebenrock KA. Femoroacetabular impingement: a cause for osteoarthritis of the hip. *Clin Orthop Relat Res*. 2003;417:112-120.
17. Gosvig KK, Jacobsen S, Palm H, Sonne-Holm S, Magnusson E. A new radiological index for assessing asphericity of the femoral head in cam impingement. *J Bone Joint Surg Br*. 2007;89:1309-1316.
18. Hack K, Di Primio G, Rakhra K, Beaulé PE. Prevalence of cam-type femoroacetabular impingement morphology in asymptomatic volunteers. *J Bone Joint Surg Am*. 2010;92:2436-2444.
19. Hallgren KA. Computing inter-rater reliability for observational data: an overview and tutorial. *Tutor Quant Methods Psychol*. 2012;8:23-34.

20. Harris MD, Datar M, Whitaker RT, Jurrus ER, Peters CL, Anderson AE. Statistical shape modeling of cam femoroacetabular impingement. *J Orthop Res*. 2013;31:1620-1626.

21. Harris MD, Reese SP, Peters CL, Weiss JA, Anderson AE. Three-dimensional quantification of femoral head shape in controls and patients with cam-type femoroacetabular impingement. *Ann Biomed Eng*. 2013;41:1162-1171.

22. Hartofilakidis G, Bardakos NV, Babis GC, Georgiades G. An examination of the association between different morphotypes of femoroacetabular impingement in asymptomatic subjects and the development of osteoarthritis of the hip. *J Bone Joint Surg Br*. 2011;93:580-586.

23. Ito K, Leunig M, Ganz R. Histopathologic features of the acetabular labrum in femoroacetabular impingement. *Clin Orthop Relat Res*. 2004;429:262-271.

24. Jung KA, Restrepo C, Hellman M, AbdelSalam H, Morrison W, Parvizi J. The prevalence of cam-type femoroacetabular deformity in asymptomatic adults. *J Bone Joint Surg Br*. 2011;93:1303-1307.

25. Kadaba MP, Ramakrishnan HK, Wootten ME. Measurement of lower extremity kinematics during level walking. *J Orthop Res*. 1990;8:383-392.

26. Kang AC, Gooding AJ, Coates MH, Goh TD, Armour P, Rietveld J. Computed tomography assessment of hip joints in asymptomatic individuals in relation to femoroacetabular impingement. *Am J Sports Med*. 2010;38:1160-1165.

27. Kassarjian A, Brisson M, Palmer WE. Femoroacetabular impingement. *Eur J Radiol*. 2007;63:29-35.

28. Khanna V, Cariagani A, Rakhra K, Di Primio G, Beaulé PE. Incidence of hip pain in a prospective cohort of asymptomatic volunteers: is the cam deformity a risk factor for hip pain? *Am J Sports Med*. 2014;42:793-797.

29. Kim WY, Hutchinson CE, Andrew JG, Allen PD. The relationship between acetabular retroversion and osteoarthritis of the hip. *J Bone Joint Surg Br*. 2006;88:727-729.

30. Konan S, Rayan F, Haddad FS. Is the frog lateral plain radiograph a reliable predictor of the alpha angle in femoroacetabular impingement? *J Bone Joint Surg Br*. 2010;92:47-50.

31. Lamontagne M, Brisson N, Kennedy MJ, Beaulé PE. Preoperative and postoperative lower-extremity joint and pelvic kinematics during maximal squatting of patients with cam femoro-acetabular impingement. *J Bone Joint Surg Am*. 2011;93(Suppl 2):40-45.

32. Lamontagne M, Kennedy MJ, Beaulé PE. The effect of cam FAI on hip and pelvic motion during maximum squat. *Clin Orthop Relat Res*. 2009;467:645-650.

33. Larson CM, Giveans MR. Arthroscopic management of femoroacetabular impingement: early outcomes measures. *Arthroscopy*. 2008;24:540-546.

34. Lohan DG, Seeger LL, Motamedi K, Hame S, Sayre J. Cam-type femoral-acetabular impingement: is the alpha angle the best MR arthrography has to offer? *Skeletal Radiol*. 2009;38:855-862.

35. Ng KCG, Rouhi G, Lamontagne M, Beaulé PE. Finite element analysis examining the effects of cam FAI on hip joint mechanical loading using subject-specific geometries during standing and maximum squat. *HSS J*. 2012;8:206-212.

36. Nötzli HP, Wyss TF, Stoecklin CH, Schmid MR, Treiber K, Hodler J. The contour of the femoral head-neck junction as a predictor for the risk of anterior impingement. *J Bone Joint Surg Br*. 2002;84:556-560.

37. Nouh MR, Schweitzer ME, Rybak L, Cohen J. Femoroacetabular impingement: can the alpha angle be estimated? *AJR Am J Roentgenol*. 2008;190:1260-1262.

38. Pollard TC, Villar RN, Norton MR, Fern ED, Williams MR, Simpson DJ, Murray DW, Carr AJ. Femoroacetabular impingement and classification of the cam deformity: the reference interval in normal hips. *Acta Orthop*. 2010;81:134-141.

39. Rakhra KS, Sheikh AM, Allen D, Beaulé PE. Comparison of MRI alpha angle measurement planes in femoroacetabular impingement. *Clin Orthop Relat Res*. 2009;467:660-665.

40. Ranawat A, Schulz B, Baumbach S, Meftah M, Ganz R, Leunig M. Radiographic predictors of hip pain in femoroacetabular impingement. *HSS J*. 2011;7:115-119.

41. Reynolds D, Lucas J, Klaue K. Retroversion of the acetabulum. A cause of hip pain. *J Bone Joint Surg Br*. 1999;81:281-288.

42. Shrout PE, Fleiss JL. Intraclass correlations: uses in assessing rater reliability. *Psychol Bull*. 1979;86:420-428.

43. Sutter R, Dietrich TJ, Zingg PO, Pfirrmann CWA. How useful is the alpha angle for discriminating between symptomatic patients with cam-type femoroacetabular impingement and asymptomatic volunteers? *Radiology*. 2012;264:514-521.

44. Tabachnick BG, Fidell LS. *Using Multivariate Statistics*. 5th ed. Boston, MA, USA: Pearson Education, Inc; 2007.

45. Tannast M, Siebenrock KA, Anderson SE. Femoroacetabular impingement: radiographic diagnosis—what the radiologist should know. *AJR Am J Roentgenol*. 2007;188:1540-1552.

46. Tibor LM, Leunig M. The pathoanatomy and arthroscopic management of femoroacetabular impingement. *Bone Joint Res*. 2012;1:245-257.

4.6 Appendix – CT Measures Protocol

Radiographic CT Measures Protocol for Cam FAI

Participants

- Patients and participants first classified according to presence of cam deformity, symptoms, clinical signs
- Cam deformity defined by an elevated alpha angle in the oblique-axial or radial plane
  - Symptomatic femoroacetabular impingement (sFAI) – cam deformity, clinical signs
  - Asymptomatic femoroacetabular deformity (aFAD) – cam deformity, no clinical signs
  - Control (CON) – no cam deformity, no clinical signs

GROUP	ALPHA ANGLE (axial > 50.5° or radial > 60°)	CLINICAL SIGNS AND SYMPTOMS	NUMBER
sFAI	Yes	Yes	15
aFAD	Yes	No	19
CON	No	No	16
		TOTAL	50

Measures

- Subject-specific CT data are blinded, randomized, then evaluated
  - Blinded – CTs and filenames are renamed to "HJC XX" (where "XX" denotes a two-digit number); patient information removed from filenames to eliminate identification
  - Randomized – CTs are reassigned random number for "XX" and then randomly reordered
  - Evaluated – perform all measurements of the left hip, then right hip, for each patient in the reordered list
- Observations are recorded in a spreadsheet, that will indicate "HJC XX" and the parameters to be measured for the left and right hip
- Complete all measures for all patients within a two-day period
- Reading sequence for "HJC XX" will be randomized and reordered for second evaluation
- Second intra-rater evaluation, to start two weeks after completion of first evaluation, on a new spreadsheet (previous intra-rater evaluations are not to be seen)
- Previous inter-rater evaluations are not to be discussed, to eliminate bias

Parameters

1. Alpha Angle – Axial 3:00 (AA)

- Axial plane found from cross-sectional view through centroid of femoral head and longitudinal femoral neck axis
- Trace a circle around contour of femoral head, with centroid centred in the frontal, sagittal, and transverse planes
- Using the axial view, find the narrowest part (width) of the femoral neck and draw a line (Line A) through its cross section
- Draw a second line (Line B) through centre of the femoral neck (longitudinally) perpendicular to previous line
- Draw best-fit circle, following the outer edge of the femoral head (compact bone)
- Draw line (Line C) from centre of circle to the edge of the circle, where the femoral head exceeds the circle (head neck junction)
- Alpha angle is the angle between the line B and C

Classification: cam deformity defined by axial alpha angle > 50.5°

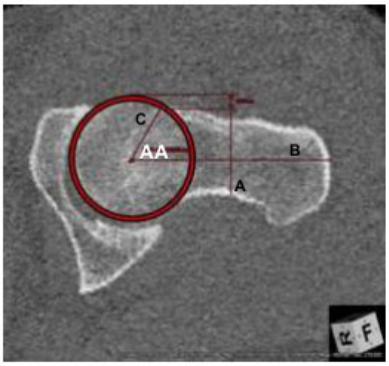

2. Alpha Angle – Radial 1:30 (RA)

- Radial plane found from 45° rotation along the narrowest mid-sectional axis of the femoral neck, exposing the anterosuperior quadrant (1:30) of the femoral head
- Trace a circle around contour of femoral head, with centroid centred in the frontal, sagittal, and transverse planes
- Using the axial view, find the narrowest part (width) of the femoral neck and draw a line (Line A) through its cross section
- Draw a second line (Line B) through the centre of the femoral neck (longitudinally) perpendicular to previous line
- Then, draw best-fit circle, following the outer edge of the femoral head (compact bone)
- Draw line (Line C) from centre of circle to the edge of the circle, where the femoral head exceeds the circle (head neck junction)
- Alpha angle is the angle between the line B and C

Classification: cam deformity defined by radial alpha angle > 60°

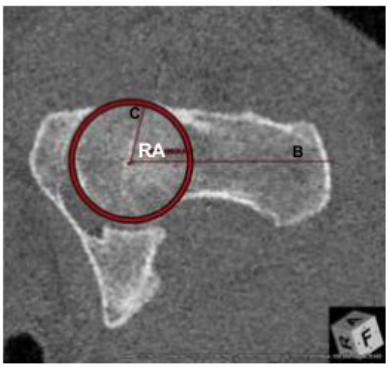

3. Femoral Neck-Shaft Angle (FNSA)

- Axial plane found from cross-sectional view through centroid of femoral head and longitudinal femoral neck axis
- From the frontal plane, trace a circle around and centred at femoral head
- Make sure that the slice used exposes the widest/thickest portion of the femoral diaphysis
- Draw a line going through both the centre of the femoral neck and femoral head (Line A)
- Draw a second line (Line B) beginning at the edge of the piriformis fossa all the way down through the centre of the femur
- Femoral neck-shaft angle is angle between lines A and B

Classification: normal neck-shaft, defined by angle between 124-136°; coxa vara, defined as ≤ 120°

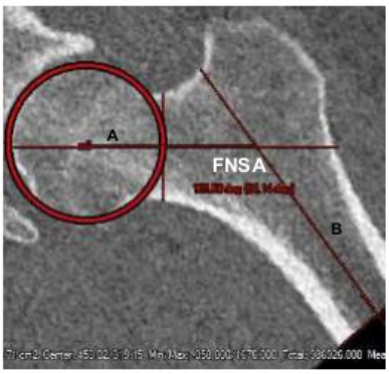

4. Medial Proximal Femoral Angle (MPFA)

- Trace a circle around contour of femoral head, with head centroid centred in the frontal, sagittal, and transverse planes
- From the frontal view, ensure that the slice exposes the widest/thickest portion of the femoral diaphysis
- Draw a line (Line A) from the centre of the femoral head to the superior tip of the greater trochanter
- Draw a second line (Line B) beginning at the edge of the piriformis fossa all the way down through the centre of the femur
- Medial proximal femoral angle is angle between lines A and B

Classification: normal MPFA is between 84-89°

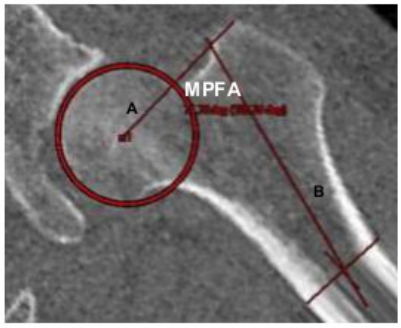

5. Femoral Head-Neck Offset (FHNO)

- Trace a circle around contour of femoral head, with head centroid centred in the frontal, sagittal, and transverse planes
- Using the axial view, find the narrowest part (width) of the femoral neck and draw a line (Line A) through its cross section
- Draw a line (Line B) through the centre of the femoral neck longitudinally and perpendicular to line A
- Draw a line (Line C) perpendicular to line A and parallel to line B, lining it up with the edge of the compact bone of the neck itself (anterior wall of femoral neck)
- Draw another line (Line D) parallel to line C, lining it up with the outer edge of the circle drawn around the femoral head.
- Femoral head-neck offset is the thickness of the femoral head that lies anterior to the line passing the anterior wall of the femoral neck, between line C and D

Classification: decreased femoral head-neck offset defined as < 8mm

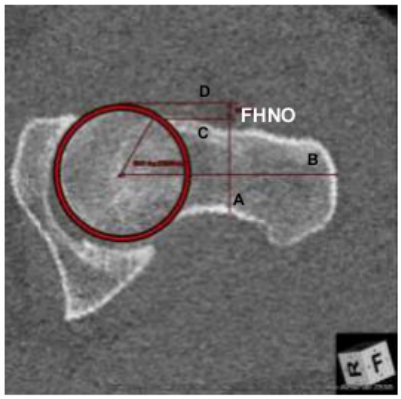

6. Femoral Version (FV)

Neck Horizontal

- From the transverse plane, take the slice with the thickest cross section of femoral neck making sure that the lesser trochanter is not visible in the slice selected
- Draw the first line (Line A) through both the centre of the femoral head and longitudinally along the femoral neck axis
- The second line (Line B) is a straight horizontal line with respect to the image plane that intersects with line A
- Neck-horizontal angle is the angle between line A and B

Condyle Horizontal

- From the transverse plane, take the slice about the knee with both epicondyles in view
- Draw the first line (Line C) tangential to the most posterior convexity of both epicondyles (can also use femoral condyles as reference point) and the second line (Line D) in the horizontal plane that intersects with line C
- Condyle-horizontal angle is the angle between line C and D

- Femoral version (absolute anteversion or retroversion) obtained by subtracting the condyle-horizontal from the femoral neck-horizontal
- If femoral epicondyles are internally rotated on the images, the angle is negative, therefore must be added to the angle of anteversion
- If the femoral epicondyles are externally rotated on the images the angle of rotation must be subtracted to the angle of anteversion
- Knees rotated inward when increased femoral anteversion and compensatory external tibial torsion
- Rotated outward when decreased femoral anteversion and compensatory internal tibial torsion

Classification: femoral retroversion can be defined as < 15°; anteversion ≥ 15°

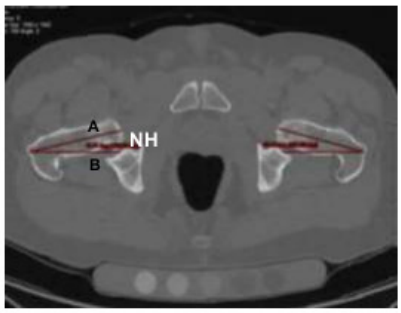

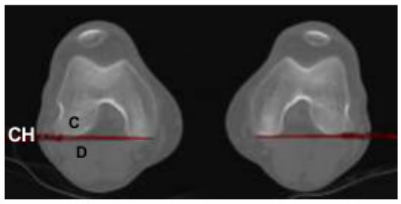

7. Acetabular Version (AV)

- Correct for pelvic tilt, by aligning all left-right and anterior-posterior superior iliac spines on the transverse plane
- From the transverse plane, locate the slice where the acetabular cup is the deepest – where the medial wall of the acetabulum is most medial
- Draw a line (Line A) horizontally across both posterior edges of the acetabulum
- Draw a second line (Line B) perpendicularly to line A, crossing at the posterior edge of the acetabulum.
- Draw a third line (Line C) tangentially from the anterior to posterior margins of the acetabulum
- Acetabular version is the angle between line B and C

Classification: acetabular retroversion defined by an angle < 15°; normal acetabular version is between 15-20°

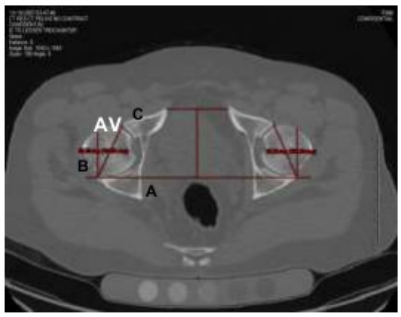

5 Differences in Anatomical Parameters between the Affected and Unaffected Hip in Patients with Bilateral Cam-Type Deformities

K. C. Geoffrey Ng [1] | Mario Lamontagne [2,1] | Paul E. Beaulé [3]

[1] Department of Mechanical Engineering | University of Ottawa | Ottawa, Ontario, Canada

[2] School of Human Kinetics | University of Ottawa | Ottawa, Ontario, Canada

[3] Division of Orthopaedic Surgery | University of Ottawa | Ottawa, Ontario, Canada

Contents of this chapter published as an article in *Clinical Biomechanics* | March 2016

Ng KCG, Lamontagne M, Beaulé PE. Differences in anatomical parameters between the affected and unaffected hip in patients with bilateral cam-type deformities. *Clin Biomech*. 2016;33:13-19. DOI: 10.1016/j.clinbiomech.2016.01.007

5.0 Abstract

Background: It is still unclear why many individuals with bilateral cam deformities demonstrate only unilateral symptoms of femoroacetabular impingement, thus symptoms may be attributed to additional anatomical parameters. The purpose was to examine patients with bilateral cam deformities, with unilateral symptoms, and compare anatomical hip joint parameters between their affected (symptomatic) hip and their contralateral, unaffected (asymptomatic) hip.
Methods: Twenty participants (n = 20) with unilateral symptoms, but bilateral cam deformities, underwent CT imaging to measure their affected and unaffected hip's: axial and radial alpha angles, femoral head-neck offset, femoral neck-shaft angle, medial proximal femoral angle, femoral torsion, acetabular version, center-edge angle; and a physical examination (hip flexion, straight-leg raise, internal rotation, external rotation) to ascertain clinical signs.
Findings: The affected hips demonstrated limited motions during physical examination, compared with unaffected hips (effect size $d = 0.550$ to 0.955). The affected hips had significantly lower femoral neck-shaft angles (125° ± 3) and lower medial proximal femoral angles (79° ± 4), compared with the unaffected hips (127° ± 3, $p = 0.001$, $d = 0.922$; and 81° ± 4, $p = 0.011$, $d = 0.632$; respectively). There were no differences in cam deformity parameters (axial and radial alpha angles, femoral head-neck offset), femoral torsion, acetabular version, and center-edge angle, between affected and unaffected hips.
Interpretation: A decreased femoral neck-shaft angle or medial proximal femoral angle can be implemented as a diagnostic predictor, to determine which hip may be at a greater risk of developing early symptoms.
Level of Evidence: Level III, diagnostic study.

5.1 Introduction

The cam deformity is recognized as a predominant morphology of the proximal femur that causes femoroacetabular impingement (FAI) [7, 8, 20, 31, 45]. Characterized by a combined aspherical femoral head and reduced offset, the cam deformity induces impingement between the proximal femur and the hip socket, resulting in clinical symptoms of labral damage, groin pain, and reduced pelvic and hip motions [3, 13, 26, 30]. The abnormal joint contact loading can result in elevated hip joint stresses [14, 37] and a greater risk of developing early osteoarthritis [1, 6-8, 20].

There has been emerging interest to understand why many individuals with cam deformities do not develop early FAI symptoms (*i.e.*, asymptomatic individuals with the cam deformity but do not demonstrate impingement, clinical signs, symptoms, or pain) [2, 22, 23, 42]. The presence of a large cam deformity, indicated by elevated alpha angles, may not be sufficient to characterize FAI symptoms [5, 27, 34, 36, 47], especially when the pathomechanical threat of the asymptomatic cam deformity can remain undetected, but can still onset early subchondral bone adaptation and joint degeneration [35, 46]. In addition to the conventional alpha angles, recent studies examined FAI populations and measured additional anatomical parameters from radiographic [4, 23, 42], computed tomography (CT) [18, 25, 36], and magnetic resonance imaging (MRI) data [17, 47], to associate various femoral and pelvic structural parameters with the onset of symptoms.

Knowing that many individuals in the FAI population may have bilateral cam deformities [3], it is still unclear why symptoms are often experienced only in one hip, while their other contralateral hip remains unaffected. The prevalence of bilateral cam deformities in the same individual provides a unique opportunity to better delineate pathomechanisms leading to FAI and to possibly further predict the progression of symptoms that will require physical therapy or surgical intervention [3, 12, 24, 28, 35]. The purpose of this study was to examine patients with bilateral cam-type deformities, who demonstrate unilateral FAI symptoms, and determine if there are differences in anatomical hip joint parameters between their affected (symptomatic) and their contralateral, unaffected (asymptomatic) hips.

5.2 Methods

This diagnostic study (Level of Evidence III – STROBE Guidelines) involved anatomical parameters and physical examinations associated with cam-type FAI symptoms. An observational, case-control study was performed for a symptomatic group, where each participant's affected (case) and unaffected (control) hips' anatomical parameters were blinded and measured.

5.2.1 Participants

Twenty-two participants (n = 22; m = 19, f = 3) were initially recruited from the senior orthopaedic surgeon's clinical practice (PEB), during a two-year recruitment period at The Ottawa Hospital. All participants presented themselves with primary unilateral hip pain, clinical signs, and symptoms. Pelvic and knee CT images were acquired from each participant, using a clinical CT scanner (Acquilion, Toshiba Medical Systems Corporation, Otawara, Japan; or Discovery CT750, GE Healthcare, Mississauga, Ontario, Canada) and confirmed by a musculoskeletal radiologist (KSR) to have a cam deformity on their affected (symptomatic) hip, with elevated axial or radial alpha angles [5, 22, 27, 41, 47]. Any participant with neurological or musculoskeletal disorders, degenerative diseases, or any previous major lower limb injuries or surgeries was excluded. Participants were excluded if they indicated pain in their contralateral, unaffected (asymptomatic) hip or other areas of their lower limbs. Two participants did not show a cam deformity on their contralateral, unaffected (asymptomatic) hip, thus were excluded for unilateral-only deformities. A total of twenty patients (n = 20; m = 17, f = 3) indicated elevated alpha angles for both affected and unaffected hips, confirming bilateral cam deformities (Table 5.1). Each participant completed pain questionnaires – Hip Disability and Osteoarthritis Outcome Score (HOOS) and Western Ontario and McMaster Universities Arthritis Index (WOMAC) – to ascertain their level of symptoms. Participants signed and provided informed consent prior to the study. The university and hospital research institute ethics boards approved this study, to ensure that all investigations are to be conducted ethically in conformity with research principles.

Table 5.1. Participant demographics, pain questionnaires, and bilateral cam deformity observations, reporting mean and (SD)

n = 20 (m : f)	Age (years)	BMI (kg/m^2)	HOOS Pain (%)	WOMAC Pain (%)	Axial Alpha Angle > 50.5° or Radial Alpha Angle > 60°	
					Affected Hip	Unaffected Hip
17 : 3	36 (8)	26 (5)	64 (21)	71 (21)	Yes	Yes

HOOS = Hip Disability and Osteoarthritis Outcome Score
WOMAC = Western Ontario and McMaster Universities Arthritis Index

5.2.2 Anatomical Parameters

To remove bias, each participant's CT data were blinded and randomly assigned new filenames. Using an image reading software (Onis 2.4, DigitalCore, Tokyo, Japan), both left and right hips were measured for multiple anatomical CT parameters, which included: axial alpha angle, radial alpha angle, femoral head-neck offset, femoral neck-shaft angle, medial proximal femoral angle, femoral torsion, acetabular version, and lateral centre-edge angle; all corresponding with common anatomical features of the hip joint that may distinguish symptoms [9, 25, 36, 42].

Prior to measuring the alpha angles and neck angles, the slice of the femoral head center was located on the oblique-axial, frontal, and sagittal planes. Using the femoral head center as the point of rotation, the frontal plane was corrected to display the widest femoral neck and shaft regions. A circle was traced around the femoral head on each of the three planes, where the longitudinal femoral neck axis was determined as the line from the femoral head center through the narrowest part of the femoral neck, on the oblique-axial and corrected frontal planes. The longitudinal femoral shaft axis was defined as the line from the piriformis fossa through the midpoint of diaphysis on the corrected frontal plane.

The axial alpha angle was measured on the oblique-axial plane of the longitudinal femoral neck axis, observing for an aspherical anterior femoral head [38, 39]. With the vertex centered at the femoral head, the angle was formed from the femoral neck axis to the head-neck junction (Figure 5.1.A). Anterior femoral head-neck offset was also observed on the oblique-axial plane [13, 25], measuring the offset distance between the two tangents of the anterior femoral head and neck (Figure 5.1.A). The radial alpha angle was obtained by a 1:30 clock-face rotation about the longitudinal femoral neck axis, observing for an anterosuperior asphericity [41,

47] (Figure 5.1.B). An axial alpha angle, greater than 50.5°, or radial 1:30 alpha angle, greater than 60°, was considered as cam deformity [22, 27].

The femoral neck-shaft angle was measured on the frontal plane [23, 42] (Figure 5.1.C), between the femoral neck and shaft axes, with values below 120° deemed as coxa vara and above 135° as coxa valga. Similarly, the medial proximal femoral angle was measured between the femoral shaft axis and the line joining the center of the femoral head to the superior greater trochanter [4] (Figure 5.1.C).

Femoral torsion was measured as the difference between the femoral neck horizontal and condyle horizontal angles [9, 17], each taking the angle with respect to the transverse view's horizontal plane (Figure 5.1.D). Acetabular version was determined on the transverse plane coincident with the left and right femoral head centers [13, 16, 44]. This angle was constructed by the line connecting the anterior and posterior acetabular notches and the perpendicular axis to the posterior acetabular notch (Figure 5.1.E). A femoral torsion or acetabular version angle less than 15° was considered as retrotorsion or retroversion, respectively.

To measure the lateral center-edge angle, pelvic tilt and obliquity was first corrected by lining up the ischial tuberosities on the frontal plane. The angle was formed by the superior-inferior axis, perpendicular to the ischial tuberosity, and the line from the femoral head center extending to the lateral edge of the acetabular rim [25, 29] (Figure 5.1.F). An angle greater than 39° was considered as over-coverage [29, 48].

To confirm the reliability of the anatomical measurements, two observers evaluated each participant's CT data, with each observer performing two readings. Both observers received training and instructions from the senior-level musculoskeletal radiologist (KSR), and performed the second reading two weeks after their first.

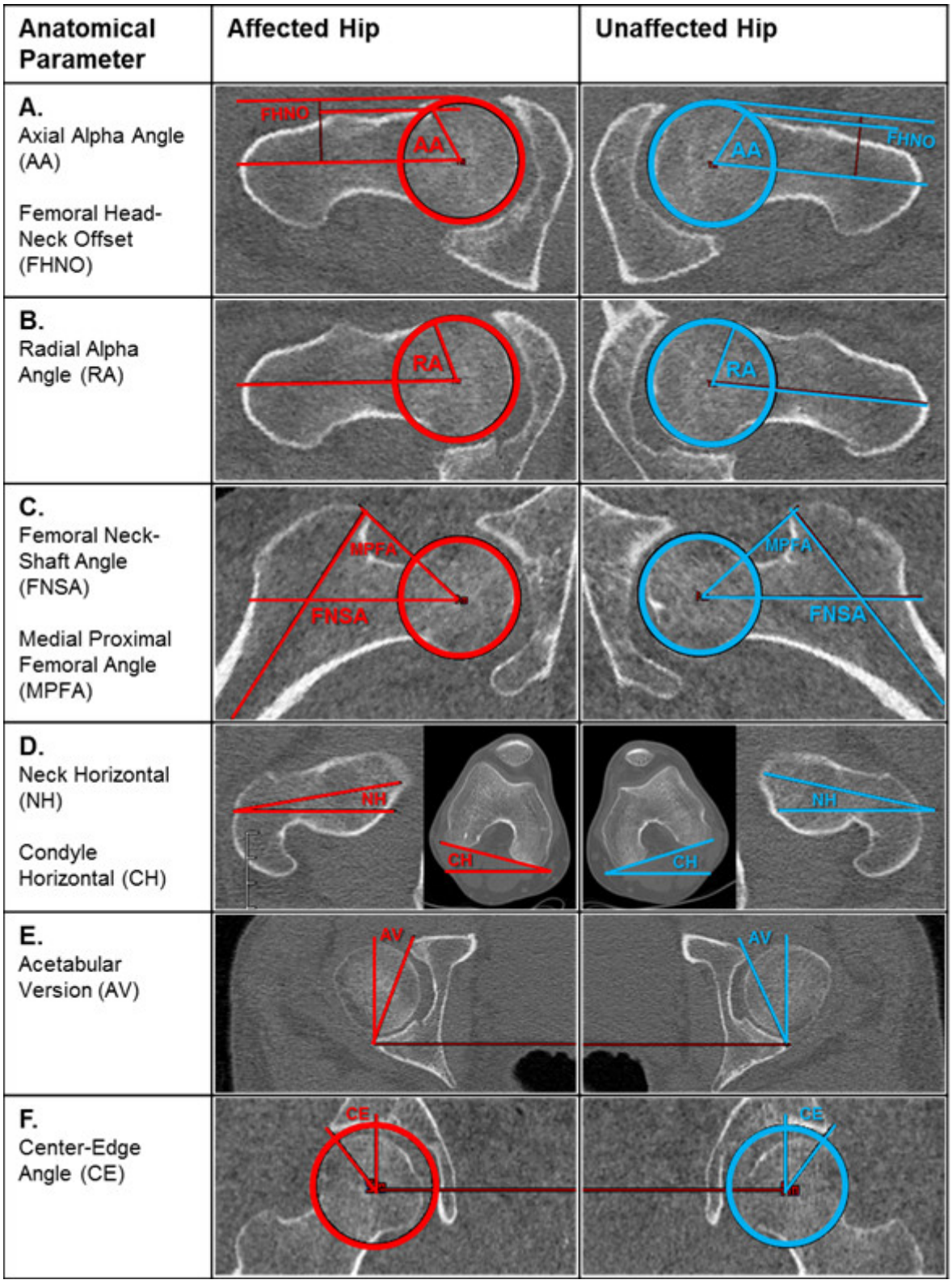

Figure 5.1. Anatomical CT parameters comparing participant's affected and unaffected hips, measuring: **A**) axial alpha angle (AA) and femoral head-neck offset (FHNO); **B**) radial alpha angle (RA); **C**) femoral neck-shaft angle (FNSA) and medial proximal femoral angle (MPFA); **D**) neck horizontal (NH) and condyle horizontal (CH) for femoral torsion; **E**) acetabular version (AV); and **F**) center-edge angle (CE).

5.2.3 Physical Examinations

To ascertain differences in clinical symptoms between the affected and unaffected sides, each participant underwent a series of physical examinations for both hips, performing: hip flexion (with knee flexion permitted), straight-leg raise, internal rotation, and external rotation, all in a supine position (Figure 5.2); and measured using a goniometer (Zimmer Mfg Co., Warsaw, IN, USA).

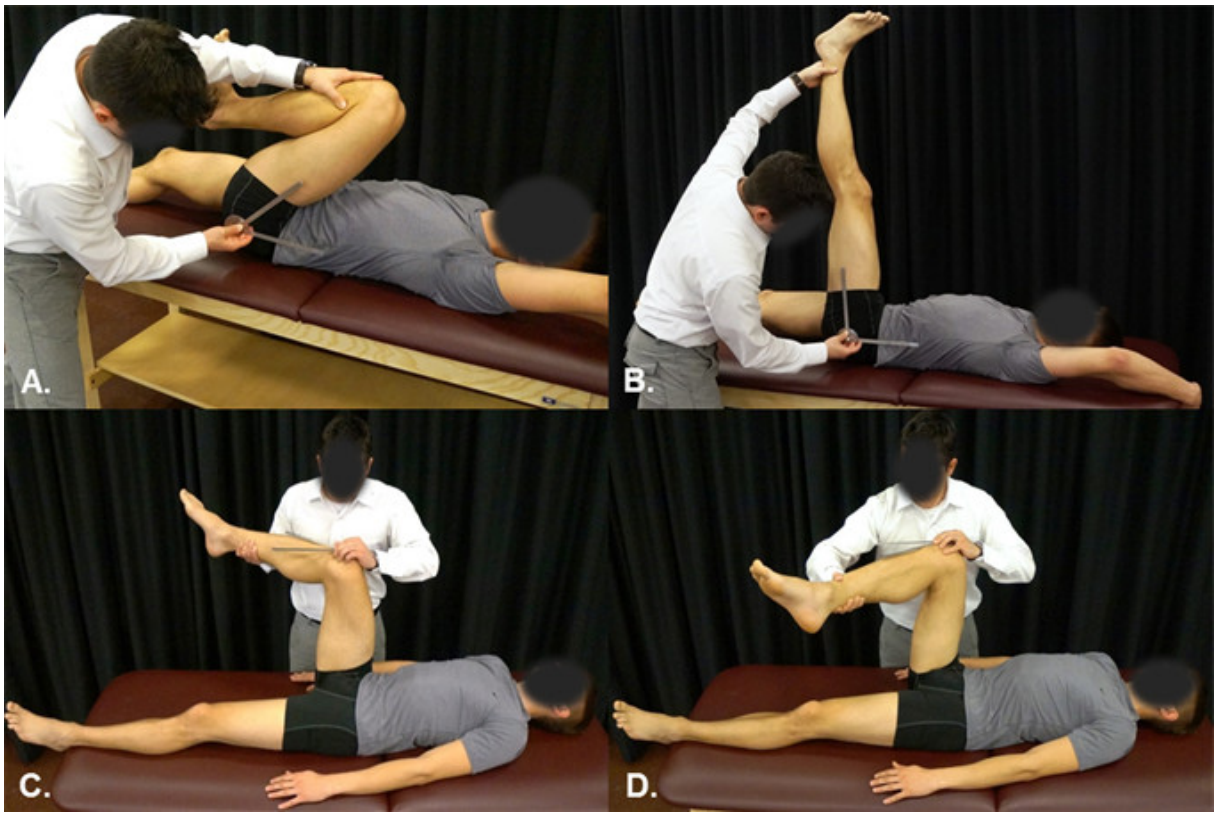

Figure 5.2. Physical examination measuring each participant's affected and unaffected hip's: **A**) flexion, **B**) straight-leg raise, **C**) internal rotation, and **D**) external rotation.

5.2.4 Reliability and Statistical Analysis

Intra-observer reproducibility and inter-observer reliability were quantified using the concordance correlation coefficient (ρ_c) [33], appropriate to assess linear agreements between continuous variables within a smaller sample size [32, 33]. The ρ_c was considered either as poor (< 0.20), weak (0.20 to 0.39), moderate (0.40 to 0.59), strong (0.60 to 0.79), or near-perfect (> 0.80). The resultant CT measurements were unblinded and matched with the physical

examination results. A paired sample t-test was computed to compare differences in anatomical parameters and physical examinations, between each participant's affected and unaffected hips (CI = 95%). Effect size was determined using Cohen's d, considering the mean differences and pooled variance, to indicate small (d = 0.2), medium (d = 0.5), and large (d = 0.8) effects and various levels of practical significance [15]. Statistical analyses were performed using statistics software (SPSS Statistics v.23, IBM Corporation, Armonk, NY, USA).

5.3 Results

Intra-observer reproducibility and inter-observer reliability for the anatomical observations were in near-perfect agreements, for all parameters (ρ_c > 0.81). The affected side confirmed clinical signs and demonstrated significantly reduced hip flexion, straight-leg raise, internal and external rotations, in comparison with the unaffected hip (P < 0.05; Table 5.2). The effect sizes further demonstrated moderate to high levels of practical significance, for each of the physical examinations (d = 0.550 to 0.955).

Table 5.2. Summary of physical examinations and anatomical parameters of the paired affected and unaffected hips, reporting mean and (SD)

Physical Examination (units)	Affected Hip	Unaffected Hip	*t*-value	*p*-value	Cohen's *d* Effect Size
Hip Flexion (°)	123 (14)	130 (20)	-2.20	0.047 *	0.588 †
Straight-Leg Raise (°)	90 (16)	97 (16)	-2.33	0.032 *	0.550 †
Internal Rotation (°)	31 (15)	38 (12)	-2.20	0.045 *	0.567 †
External Rotation (°)	33 (21)	42 (19)	-3.94	0.001 **	0.955 ‡
Anatomical Parameters (units)	**Affected Hip**	**Unaffected Hip**	***t*-value**	***p*-value**	**Cohen's *d* Effect Size**
Axial Alpha Angle (°)	55 (7)	54 (5)	0.76	0.456	0.169
Radial Alpha Angle (°)	63 (6)	63 (4)	0.27	0.787	0.061
Femoral Head-Neck Offset (mm)	6 (2)	6 (2)	-0.50	0.621	0.113
Femoral Neck-Shaft Angle (°)	125 (3)	128 (3)	-4.12	0.001 **	0.922 ‡
Medial Proximal Femoral Angle (°)	79 (4)	81 (4)	-2.83	0.011 *	0.632 †
Femoral Torsion (°)	14 (6)	15 (8)	-0.19	0.854	0.042
Acetabular Version (°)	24 (4)	24 (4)	0.50	0.616	0.113
Center-Edge Angle (°)	32 (4)	32 (6)	0.51	0.617	0.114

* significant difference (p < 0.05)
** significant difference (p < 0.01)
† medium effect size (d > 0.5)
‡ large effect size (d > 0.8)

There were no differences in axial and radial alpha angles, femoral head-neck offset, femoral torsion, acetabular version, and center-edge angle, between affected and unaffected hips (Table 5.2). Marginal femoral retrotorsion was observed between the affected (mean 14° (SD 6)) and unaffected hips (mean 15° (SD 8)), whereas acetabular versions and center-edge angles were considered normal and similar between affected and unaffected hips. Eleven participants had slightly higher axial alpha angles on their unaffected side, while eight of those participants had higher radial alpha angles on their unaffected side as well (Figure 5.3).

There were significant differences in femoral neck-shaft angle, between the affected (mean 125° (SD 3)) and unaffected hips (mean 127° (SD 3); $t(19) = -4.12$, $P = 0.001$, $d = 0.922$); and medial proximal femoral angle, between the affected (mean 79° (SD 4)) and unaffected hips (mean 81° (SD 4); $t(19) = -2.83$, $P = 0.011$, $d = 0.632$); suggesting that the affected side had much lower neck angles, in comparison with the unaffected side (Figure 5.4). The medium-to-large effect sizes of the medial proximal femoral angle and femoral neck-shaft angle further suggested moderate to very high levels of practical significance.

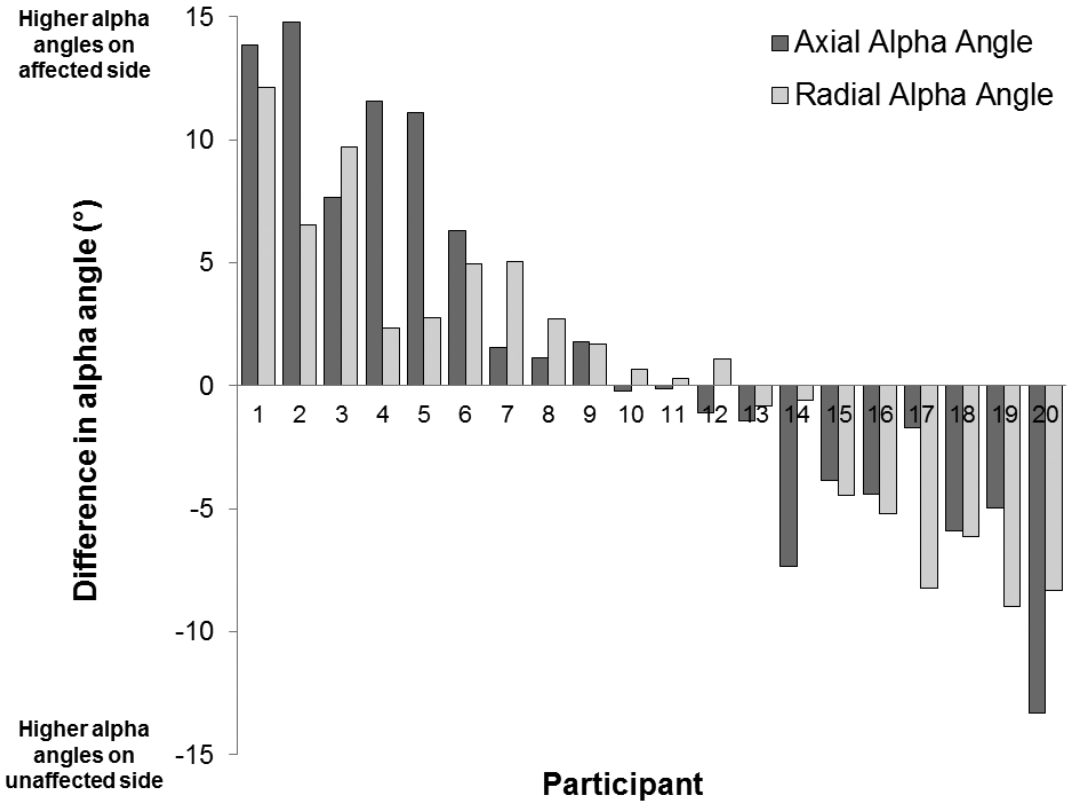

Figure 5.3. Difference in axial and radial alpha angles, indicating the number of participants with larger cam deformities (elevated alpha angles) on their affected (positive values) and on their unaffected sides (negative values).

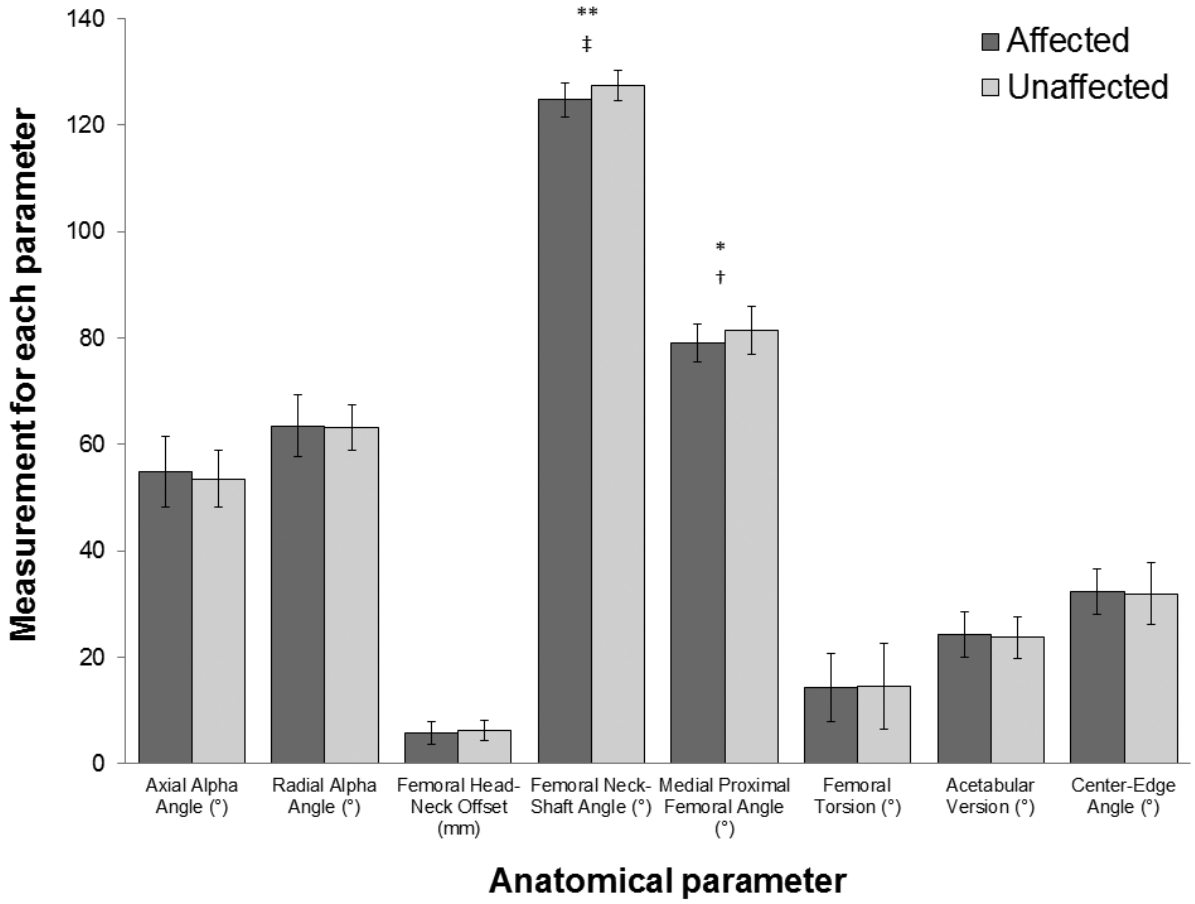

Figure 5.4. Resultant anatomical parameter measurements of the affected and unaffected hips, comparing the: axial alpha angle, radial alpha angle, femoral head-neck offset, femoral neck-shaft angle, medial proximal femoral angle, femoral torsion, acetabular version, and center-edge angle (* significant difference, $p < 0.05$; ** significant difference, $p < 0.01$; † medium effect size, $d > 0.5$; ‡ large effect size, $d > 0.8$).

5.4 Discussion

Although the clinical diagnosis of cam-type FAI is relatively well-established, our understanding of the pathomechanisms leading to cartilage degeneration is still evolving. While the alpha angle has been conventionally used to quantify the cam deformity, how to characterize associated biomechanical abnormalities leading to symptoms and degeneration remain to be determined. In efforts to predict the likelihood of symptoms and examine primary anatomical indictors of FAI, we compared the symptomatic and the contralateral, asymptomatic hips in individuals with bilateral cam deformities. To our knowledge, no study incorporated a patient cohort with bilateral cam deformities to specifically compare differences in anatomical parameters and clinical physical examinations, between the affected and unaffected sides. In our study, the affected sides were confirmed to be symptomatic (and the unaffected sides were confirmed to be asymptomatic) with history and physical examination.

The affected sides demonstrated restricted motions, during physical examinations. The straight leg raise test can indicate a lumbar spine pathology or sciatic nerve irritation, if pain is experienced at 30 to 70° (Lasègue's sign). However, during the consultation with the senior orthopaedic surgeon (PEB) and musculoskeletal radiologist (KSR), none of the participants had any underlying herniated or degenerative disc disease. Moreover, all participants straight leg raises exceeded 70° (for both affected and unaffected hips) and demonstrated that their limits were not affected by lumbar pain.

Prior to measuring the anatomical parameters from CT data, efforts were made to correct for pelvic obliquity and reorient slices to display the widest regions of the femoral head, neck, and shaft (which cannot be done in planar x-rays). Also, two observers performed the readings, each performing two observations seeking absolute agreement, to ensure that the measurements were accurate, precise, and with no bias. As expected, there were no differences in cam deformity parameters (axial and radial alpha angles, femoral head-neck offset) between the bilateral hips, since participants showed an aspherical head and reduced anterior offset. Interestingly, several participants (40%) had higher alpha angles on their unaffected hips, reiterating that a cam deformity, alone, cannot explain symptomatology and does not necessarily lead to FAI [5, 11, 27, 34, 36, 47]. In addition, there were no differences in femoral torsion, acetabular version, or center-edge angle, between affected and unaffected hips. This further suggests that pelvic orientation and version is symmetric in the FAI population. A slight femoral

retrotorsion was noticed, however, it is unclear which hip would lead to early symptoms due to symmetry. A combination of femoral and acetabular versions can still play a predominant role in limiting internal hip rotation and dynamic motions [9, 11, 19]. The femoral neck angles (femoral neck-shaft angle and medial proximal femoral angle) were significant parameters that distinguished the affected from the unaffected side [4, 36, 42]. Therefore, the medium-to-large effect sizes of the femoral neck-shaft angle and the medial proximal femoral angle demonstrate that both measures can potentially predict which hip will experience early symptoms, in individuals with bilateral cam deformities. Although our measurable differences in femoral neck angles between the affected and unaffected sides were small, the statistical and practical differences demonstrate important clinical implications.

In previous studies, Allen and associates (2009) observed an incidence of 77.8% (88/113 cases) of bilateral patients from their patient cohort, which was substantially higher than Klingenstein and associates' (2013) incidence of 20.4% (132/646 cases). The latter study further compared unilateral and bilateral FAI and examined if there were possible radiographic measures that could be associated with symptoms leading surgery. However, they were unable to find a predictive parameter, as to which side would require initial surgical treatment, attributing general surgical risks to sex, age, alpha angles, and acetabular anteversion [28]. A limitation of these studies is the use of "hip pain" as a surrogate to determine clinical significance, whereas asymptomatic individuals with a cam deformity have demonstrated that cartilage degeneration can occur prior to the onset of symptoms [40]. Moreover, McGuffin and associates (2015) recently showed no differences in proteoglycan depletion between symptomatic and asymptomatic hips, in individuals with bilateral cam deformities, indicating that there is still an increased risk of cartilage degeneration, regardless of hip pain.

An earlier study, by Bardakos and Villar (2009), investigated the effects of radiographic parameters on the progression of osteoarthritis, where there was a clear difference in medial proximal femoral angle between hips that indicated osteoarthritis (mean 81°) and normal hips that did not (mean 87°; $P = 0.004$). Hartofilakidis and associates (2011) also reported a decreased femoral neck-shaft angle for symptomatic hips (mean 119°). Ranawat and associates (2011) wanted to further correlate radiographic findings with hip pain, where it was observed that symptomatic hips had lower femoral neck-shaft angles, greater distances between the ilioischial line to the fossa, and greater distances from cross-over to the superolateral acetabulum, in

comparison with the contralateral, asymptomatic hip. However, there was no mention if their cohorts had an asymptomatic cam deformity on the contralateral side. More recently, a study on anatomical parameters implemented a discriminant function analysis and determined that radial alpha angle and femoral neck-shaft angle, along with pelvic range of motion, were significant predictors to distinguish symptomatic patients from asymptomatic individuals with cam deformities ($P < 0.001$) [36].

From the aforementioned studies, there was substantial insight as to how the orientation of the femoral axes influences clinical signs. Redmond and associates (2015) reported an association between decreased femoral neck-shaft angles and larger labral tears for their female population, using a multiple linear regression ($P = 0.0044$). Coxa vara combined with a cam deformity can potentially predispose to mechanical impingement and increase the risk of labral tears [21, 43, 49], resulting in early pain and clinical signs. Furthermore, a varus structure seats the femoral head further into the acetabulum and, thus, alters the abductor moment and brings the cam deformity closer to the anterosuperior labrum. This relatively higher greater trochanter results in a shortened abductor muscle and lengthened moment arm which, in turn, causes muscle imbalance and instability. This may provoke adverse contact loading to stabilize the pelvis, further justifying differences in clinical signs and as to why the asymptomatic hip does not experience early pain symptoms. Moreover, long-term effect of muscle imbalance may also play a role in bone geometry changes [10]. Further research will examine the functional outcomes of asymptomatic participants, to observe how different natural histories and the role of soft tissues (*i.e.*, capsular ligaments, muscles) will influence the progression of symptoms. In efforts to delay surgery and also preserve the inherent stability of the hip joint, physical examinations and anatomical parameters (femoral neck angles and cam deformity parameters) should be observed early, prior to the onset of symptoms. With the decreased neck angle in mind, other treatment options such as physiotherapy, abductor muscle training and recruitment strategies should be considered.

One of the limitations in our study was that our cohort consisted of a male-dominant population, as the cam deformity is statistically more prevalent in men. An additional study to examine sex-differences can provide more insights as to if the pathomechanics is specific to sex. Although it was determined that a sample size of 20 was adequate (to achieve a power of 0.95 and required large effect size of 0.8, using t-tests for matched pairs), a larger sample size would

further increase the predictive power of the anatomical parameters. Also, additional anatomical parameters could be considered (*e.g.*, pelvic orientation, retroversion index, acetabular crossover location) to further compare symmetry between the affected and unaffected sides. The ongoing study will examine asymmetry and the effect of leg dominance during joint loading – if compensatory load is applied onto the contralateral hip due to neuromuscular compensation.

In conclusion, in efforts to better predict early clinical signs and symptoms in patients with bilateral cam deformities, a decreased femoral neck shaft angle or medial proximal femoral angle can be implemented as a diagnostic predictor.

5.5 References

1. Agricola R, Heijboer MP, Bierma-Zeinstra SM, Verhaar JA, Weinans H, Waarsing JH. Cam impingement causes osteoarthritis of the hip: a nationwide prospective cohort study (CHECK). Ann Rheum Dis. 2012;72:918-923.
2. Agricola R, Heijboer MP, Ginai AZ, Roels P, Zadpoor AA, Verhaar JA, Weinans H, Waarsing JH. A Cam Deformity Is Gradually Acquired During Skeletal Maturation in Adolescent and Young Male Soccer Players: A Prospective Study With Minimum 2-Year Follow-up. Am J Sports Med. 2014;
3. Allen D, Beaulé PE, Ramadan O, Doucette S. Prevalence of associated deformities and hip pain in patients with cam-type femoroacetabular impingement. J Bone Joint Surg Br. 2009;91:589-594.
4. Bardakos NV, Villar RN. Predictors of progression of osteoarthritis in femoroacetabular impingement: a radiological study with a minimum of ten years follow-up. J Bone Joint Surg Br. 2009;91:162-169.
5. Barton C, Salineros MJ, Rakhra KS, Beaulé PE. Validity of the alpha angle measurement on plain radiographs in the evaluation of cam-type femoroacetabular impingement. Clin Orthop Relat Res. 2011;469:464-469.
6. Beaulé P, Hynes K, Parker G, Kemp K. Can the Alpha Angle Assessment of Cam Impingement Predict Acetabular Cartilage Delamination? Clin Orthop Rel Res. 2012;470:3361-3367.
7. Beaulé PE, Zaragoza E, Motamedi K, Copelan N, Dorey FJ. Three-dimensional computed tomography of the hip in the assessment of femoroacetabular impingement. J Orthop Res. 2005;23:1286-1292.
8. Beck M, Kalhor M, Leunig M, Ganz R. Hip morphology influences the pattern of damage to the acetabular cartilage: femoroacetabular impingement as a cause of early osteoarthritis of the hip. J Bone Joint Surg Br. 2005;87:1012-1018.
9. Bedi A, Dolan M, Leunig M, Kelly BT. Static and Dynamic Mechanical Causes of Hip Pain. Arthroscopy. 2011;27:235-251.
10. Bitsakos C, Kerner J, Fisher I, Amis AA. The effect of muscle loading on the simulation of bone remodelling in the proximal femur. J Biomech. 2005;38:133-139.
11. Bouma HW, Hogervorst T, Audenaert E, Krekel P, van Kampen PM. Can combining femoral and acetabular morphology parameters improve the characterization of femoroacetabular impingement? Clin Orthop Relat Res. 2015;473:1396-1403.
12. Casartelli NC, Bizzini M, Maffiuletti NA, Lepers R, Leunig M. Rehabilitation and return to sport after bilateral open surgery for femoroacetabular impingement in a professional ice hockey player: A case report. Phys Ther Sport. 2014.
13. Chakraverty JK, Sullivan C, Gan C, Narayanaswamy S, Kamath S. Cam and pincer femoroacetabular impingement: CT findings of features resembling femoroacetabular impingement in a young population without symptoms. AJR Am J Roentgenol. 2013;200:389-395.
14. Chegini S, Beck M, Ferguson SJ. The effects of impingement and dysplasia on stress distributions in the hip joint during sitting and walking: a finite element analysis. J Orthop Res. 2009;27:195-201.
15. Cohen J. Statistical Power Analysis for the Behavioural Sciences. 2nd ed. Hillsdale, NJ. Lawrence Erlbaum Associates. 1988.
16. Dandachli W, Islam SU, Liu M, Richards R, Hall-Craggs M, Witt J. Three-dimensional CT analysis to determine acetabular retroversion and the implications for the management of femoro-acetabular impingement. J Bone Joint Surg Br. 2009;91:1031-1036.
17. Ejnisman L, Philippon M, Lertwanich P, Pennock A, Herzog M, Briggs K, Ho C. Relationship Between Femoral Anteversion and Findings in Hips With Femoroacetabular Impingement. Orthopedics. 2013;36:e293-300.
18. Ergen FB, Vudali S, Sanverdi E, Dolgun A, Aydingoz U. CT assessment of asymptomatic hip joints for the background of femoroacetabular impingement morphology. Diagn Interv Radiol. 2013;

19. Fabricant PD, Fields KG, Taylor SA, Magennis E, Bedi A, Kelly BT. The effect of femoral and acetabular version on clinical outcomes after arthroscopic femoroacetabular impingement surgery. J Bone Joint Surg Am. 2015;97:537-543.

20. Ganz R, Parvizi J, Beck M, Leunig M, Nötzli H, Siebenrock KA. Femoroacetabular Impingement: A Cause for Osteoarthritis of the Hip. Clin Orthop Rel Res. 2003;417:112-120.

21. Guevara CJ, Pietrobon R, Carothers JT, Olson SA, Vail TP. Comprehensive morphologic evaluation of the hip in patients with symptomatic labral tear. Clin Orthop Relat Res. 2006;453:277-285.

22. Hack K, Di Primio G, Rakhra K, Beaulé PE. Prevalence of cam-type femoroacetabular impingement morphology in asymptomatic volunteers. J Bone Joint Surg Am. 2010;92:2436-2444.

23. Hartofilakidis G, Bardakos NV, Babis GC, Georgiades G. An examination of the association between different morphotypes of femoroacetabular impingement in asymptomatic subjects and the development of osteoarthritis of the hip. J Bone Joint Surg Br. 2011;93:580-586.

24. Haviv B, O'Donnell J. Arthroscopic treatment for symptomatic bilateral cam-type femoroacetabular impingement. Orthopedics. 2010;33:874.

25. Kang AC, Gooding AJ, Coates MH, Goh TD, Armour P, Rietveld J. Computed tomography assessment of hip joints in asymptomatic individuals in relation to femoroacetabular impingement. Am J Sports Med. 2010;38:1160-1165.

26. Kappe T, Kocak T, Reichel H, Fraitzl CR. Can femoroacetabular impingement and hip dysplasia be distinguished by clinical presentation and patient history? Knee Surg Sports Traumatol Arthrosc. 2012;20:387-392.

27. Khanna V, Caragianis A, Diprimio G, Rakhra K, Beaulé PE. Incidence of hip pain in a prospective cohort of asymptomatic volunteers: is the cam deformity a risk factor for hip pain? Am J Sports Med. 2014;42:793-797.

28. Klingenstein GG, Zbeda RM, Bedi A, Magennis E, Kelly BT. Prevalence and preoperative demographic and radiographic predictors of bilateral femoroacetabular impingement. Am J Sports Med. 2013;41:762-768.

29. Kutty S, Schneider P, Faris P, Kiefer G, Frizzell B, Park R, Powell J. Reliability and predictability of the centre-edge angle in the assessment of pincer femoroacetabular impingement. 2012;36:505-510.

30. Lamontagne M, Kennedy MJ, Beaulé PE. The effect of cam FAI on hip and pelvic motion during maximum squat. Clin Orthop Relat Res. 2009;467:645-650.

31. Leunig M, Beaulé PE, Ganz R. The concept of femoroacetabular impingement: current status and future perspectives. Clin Orthop Relat Res. 2009;467:616-622.

32. Li R, Chow M. Evaluation of reproducibility for paired functional data. 2005;93:81-101.

33. Lin LI. A concordance correlation coefficient to evaluate reproducibility. Biometrics. 1989;45:255-268.

34. Lohan DG, Seeger LL, Motamedi K, Hame S, Sayre J. Cam-type femoral-acetabular impingement: is the alpha angle the best MR arthrography has to offer? Skeletal Radiol. 2009;38:855-862.

35. McGuffin WS, Melkus G, Rakhra KS, Beaulé PE. Is the Contralateral Hip at Risk in Patients with Unilateral Symptomatic Cam Femoroacetabular Impingement? A Quantitative T1rho MRI Study. Osteoarthritis Cartilage. 2015;

36. Ng KCG, Lamontagne M, Adamczyk AP, Rakhra KS, Beaulé PE. Patient-specific anatomical and functional parameters provide new insights into the pathomechanism of cam FAI. Clin Orthop Relat Res. 2015;473:1289-1296.

37. Ng KCG, Rouhi G, Lamontagne M, Beaulé PE. Finite Element Analysis Examining the Effects of Cam FAI on Hip Joint Mechanical Loading Using Subject-Specific Geometries During Standing and Maximum Squat. HSS J. 2012;8:206-212.

38. Nötzli HP, Wyss TF, Stoecklin CH, Schmid MR, Treiber K, Hodler J. The contour of the femoral head-neck junction as a predictor for the risk of anterior impingement. J Bone Joint Surg Br. 2002;84:556-560.

39. Nouh MR, Schweitzer ME, Rybak L, Cohen J. Femoroacetabular impingement: can the alpha angle be estimated? AJR Am J Roentgenol. 2008;190:1260-1262.

40. Pollard TC, McNally EG, Wilson DC, Wilson DR, Madler B, Watson M, Gill HS, Carr AJ. Localized cartilage assessment with three-dimensional dGEMRIC in asymptomatic hips with normal morphology and cam deformity. J Bone Joint Surg Am. 2010;92:2557-2569.
41. Rakhra KS, Sheikh AM, Allen D, Beaulé PE. Comparison of MRI alpha angle measurement planes in femoroacetabular impingement. Clin Orthop Relat Res. 2009;467:660-665.
42. Ranawat A, Schulz B, Baumbach S, Meftah M, Ganz R, Leunig M. Radiographic Predictors of Hip Pain in Femoroacetabular Impingement. HSS J. 2011;7:115-119.
43. Redmond JM, Gupta A, Hammarstedt JE, Stake CE, Dunne KF, Domb BG. Labral injury: radiographic predictors at the time of hip arthroscopy. Arthroscopy. 2015;31:51-56.
44. Reynolds D, Lucas J, Klaue K. Retroversion of the acetabulum. A cause of hip pain. J Bone Joint Surg Br. 1999;81:281-288.
45. Siebenrock KA, Wahab KH, Werlen S, Kalhor M, Leunig M, Ganz R. Abnormal extension of the femoral head epiphysis as a cause of cam impingement. Clin Orthop Relat Res. 2004;54-60.
46. Speirs AD, Beaulé PE, Rakhra KS, Schweitzer ME, Frei H. Increased acetabular subchondral bone density is associated with cam-type femoroacetabular impingement. Osteoarthritis Cartilage. 2013;21:551-558.
47. Sutter R, Dietrich TJ, Zingg PO, Pfirrmann CWA. How Useful Is the Alpha Angle for Discriminating between Symptomatic Patients with Cam-type Femoroacetabular Impingement and Asymptomatic Volunteers? Radiology. 2012;264:514-521.
48. Tannast M, Siebenrock KA, Anderson SE. Femoroacetabular Impingement: Radiographic Diagnosis—What the Radiologist Should Know. Am J Roentgenol. 2007;188:1540-1552.
49. Tonnis D, Heinecke A. Acetabular and femoral anteversion: relationship with osteoarthritis of the hip. J Bone Joint Surg Am. 1999;81:1747-1770.

III Determining Appropriate Modelling Characteristics

6 Comparison of Anatomical Parameters of Cam FAI to Evaluate Hip Joint Models Segmented from CT Data

K. C. Geoffrey Ng [1] | Mario Lamontagne [2,1] | Michel R. Labrosse [1] | Paul E. Beaulé [3]

[1] Department of Mechanical Engineering | University of Ottawa | Ottawa, Ontario, Canada

[2] School of Human Kinetics | University of Ottawa | Ottawa, Ontario, Canada

[3] Division of Orthopaedic Surgery | University of Ottawa | Ottawa, Ontario, Canada

Contents of this chapter published as an article in *Computer Methods in Biomechanics and Biomedical Engineering: Imaging and Visualization* | August 2016

Ng KCG, Lamontagne M, Labrosse, MR, Beaulé PE. Comparison of Anatomical Parameters of Cam FAI to Evaluate Hip Joint Models Segmented from CT Data. *Comput Methods Biomech Eng Imaging Vis*. 2016; In Press. DOI: 10.1080/21681163.2016.1216805

6.0 Abstract

Subject-specific anatomical finite element models obtained from three-dimensional (3D) segmentation have the potential to provide great insights into the pathomechanisms of femoroacetabular impingement (FAI). Still, the accuracy of the geometries used to construct these models needs to be evaluated. To this aim, we segmented fifty-four (n = 54; age = 34 ± 7 years; BMI = 26 ± 4 kg/m^2) hip joint models from subject-specific computed tomography (CT) images, and measured multiple anatomical parameters (axial alpha angle, radial alpha angle, femoral head-neck offset, femoral neck-shaft angle, medial proximal femoral angle, femoral torsion, acetabular version, centre-edge angle) from both the multiplanar images and the 3D models, to assess the intraobserver, interobserver, and intermethod reliabilities. We implemented a method to ensure that anatomical characteristics from segmented models were representative of original CT data. Observations from both CT data and 3D models demonstrated strong to near-perfect intraobserver, interobserver, and intermethod agreements ($p < 0.01$). Bland-Altman plots indicated a slight discrepancy when assessing the asymptomatic FAI population, where planar CT images possibly did not capture the full depth of the cam deformity and underestimated geometric parameters. We indicated possible discrepancies to expect when segmenting hip joint models for clinical evaluation and finite element modelling, notably when observing femoral head-neck offset.

6.1 Introduction

Characterized by an aspherical femoral head or head-neck junction with a reduced offset, a cam deformity may induce femoroacetabular impingement (FAI) between the proximal femur and the hip socket during extreme limits of hip motion [25, 54]. This mechanical impingement results in higher joint stresses [18, 45, 55], putting the articulating cartilage at a greater risk of developing degenerative changes [1, 10, 25, 55]. Clinical symptoms associated with cam-type FAI typically include motion-induced pain, reduced hip flexion and sagittal range of motion [2, 36, 39].

As described by Nötzli and associates [46], the alpha angle was established to measure the size of the anterior and anterosuperior cam deformity on the axial and radial planes, respectively, from computed tomography (CT) and magnetic resonance imaging (MRI) data [9, 47, 51, 57, 58]. Despite the ongoing debate regarding the sensitivity of the alpha angle to detect cam FAI [9, 21, 22, 38, 47, 57], evaluations from conventional CT or MRI, that implement multiplanar imaging capacities to assess the cam deformity and anatomical hip joint parameters, have been used as a gold standard [15, 26, 29, 43, 51].

In addition to the cam deformity parameters, it has also been hypothesized that several other anatomical parameters, notably: femoral head-neck offset [17, 23, 35, 37, 49, 58], femoral neck-shaft angle [31, 52], medial proximal femoral angle [7, 42], femoral torsion [11, 15, 24], acetabular version [17, 19], and Wiberg's lateral center-edge angle [17]; may contribute to FAI symptomology [44].

In recent years, several finite element studies have examined hip joint stresses due to FAI; yet, many of these models implemented spherically-idealized femoral head and acetabular socket geometries, representing FAI by approximating only the alpha and centre-edge angles of the cam and pincer deformity, respectively [4, 18, 32]. Several other finite element simulations of FAI considered subject-specific geometries, by segmenting femur and pelvis models from imaging data [3, 33, 45, 53]. However, none of these studies validated their models by comparing multiple anatomical parameters of their segmented geometries with its associated imaging data. Still, anatomical parameters can sometimes be measured from reconstructed three-dimensional (3D) models, offering a more complete perspective of the cam deformity, potentially leading to more accurate diagnostics of cam FAI [5, 6, 8, 10, 16, 20, 28, 30, 43, 50]. In efforts to validate 3D subject-specific geometries of hip joints with cam FAI, the purpose of the present study was to compare the anatomical parameter measurements derived from 3D

segmented models with those directly obtained from CT data. Measurements from CT data were used as the reference gold standard to assess the cam deformity and anatomical parameters of the hip joint.

6.2 Methods

6.2.1 Patient Recruitment

Fifty-four participants (n = 54, male = 48, female = 6; age = 34 ± 7 years; BMI = 26 ± 4 kg/m^2) were retrospectively examined. Pelvic and knee CT data were acquired from each participant using either a Toshiba Acquilion (Toshiba Medical Systems, Markham, ON, Canada) or a GE Discovery CT750 (GE Healthcare, Mississauga, ON, Canada). The CT imaging protocol used a square 512×512 resolution, slice thickness of 0.625 mm, 120 kVp, and 200 mAs, with a resulting in-plane pixel spacing of 0.721–0.977 mm. A senior-level musculoskeletal radiologist first assessed the cam size, where a deformity was defined by an alpha angle greater than 50.5° or 60°, in the oblique-axial or radial 1:30 plane, respectively [9, 46, 47, 51]. Participants were first classified as either: 1) symptomatic, if they presented a cam deformity, clinical symptoms, and were scheduled for surgery; 2) asymptomatic, if they presented a cam deformity, but no clinical symptoms; or 3) control, if they did not present a cam deformity, symptoms, or lower-limb abnormalities. This resulted in fourteen 14 symptomatic, 22 asymptomatic, and 18 control participants (Table 6.1). Our protocol was approved by the university and hospital research institute ethics boards. All participants signed and provided informed consent prior to the study.

Table 6.1. Summary of participant demographics and initial clinical assessment of the axial and radial alpha angles

Group	Size (m:f)	Age (years)	BMI (kg/m^2)	Axial Alpha Angle (°)	Radial Alpha Angle (°)
Symptomatic	14 (13:1)	39 ± 8	27 ± 5	56 ± 8	65 ± 8
Asymptomatic	22 (19:3)	31 ± 6	25 ± 2	58 ± 9	68 ± 8
Control	18 (16:2)	34 ± 6	26 ± 3	42 ± 5	50 ± 3
Total	54 (48:6)	34 ± 7	26 ± 4	52 ± 11	62 ± 11

6.2.2 Measurements from Planar CT Images and from Three-Dimensional Segmented Models

Each participant's CT data were blinded and randomly assigned new filenames, to dissociate participant information and remove bias. The 3D left and right hip and knee models were manually segmented from CT data, using 3D-Doctor 4.0 (Able Software Corp., Lexington, MA, USA), reconstructing from the superior iliac crest to the proximal femur and from the distal femur to the inferior tibial plateau (Figure 6.1). The segmented models were also blinded and reassigned filenames prior to any measurements. Each participant's CT data and segmented models were measured for multiple anatomical parameters associated with FAI symptoms, including: axial alpha angle, radial alpha angle, anterior femoral head-neck offset, femoral neck-shaft angle, medial proximal femoral angle, femoral torsion, acetabular version, and lateral center-edge angle. The anatomical parameters from the CT images were read and measured using Onis 2.4 (DigitalCore, Tokyo, Japan), whereas the segmented models were resurfaced, to remove geometric artefacts, and measured using SolidWorks (Dassault Systèmes, Concord, MA, USA).

Prior to measuring the axial and radial angles, femoral neck-shaft angle, and medial proximal femoral angle from CT data, the slice of the femoral head center was located on the oblique-axial, frontal, and sagittal planes. Using the femoral head center as the point of rotation, the frontal plane was corrected to display the widest regions of the femoral neck and shaft. A circle was traced around the femoral head on each of the three planes, observing for the anterior-posterior, medial-lateral, and superior-inferior bony prominences. The longitudinal femoral neck axis was determined as the line from the femoral head center through the narrowest part of the femoral neck, on the oblique-axial and corrected frontal planes. The longitudinal femoral shaft axis was defined as the line from the piriformis fossa through the midpoint of diaphysis on the corrected frontal plane.

Prior to measuring the 3D models, a geometric sphere with a defined centroid was constructed by fitting a circle onto the contour of the femoral head. The circle was fitted by first observing on the oblique-axial plane. From this section, the most anterior, posterior, and medial bony prominences formed three control points for an arc of the circle. The sphere was then reconstructed from the arc. This provided a geometric centroid and reference to evaluate incongruences if the cam deformity exceeded its contours. The longitudinal femoral neck axis

was determined as the line from the centroid of the sphere through the centroid of the narrowest part of the femoral neck. A cross-sectional view was selected along the femoral neck axis to observe the oblique-axial plane. The longitudinal femoral shaft axis was determined as the line connecting the piriformis fossa through the centroid of the femoral shaft, bisecting the distal midpoint of the diaphysis. As with conventional CT imaging, there were potential variances in femoral and pelvic rotations and torsions among each participant. We corrected pelvic obliquity, pelvic tilt, and also considered femoral neck and shaft alignments that were consistent for both CT data and segmented models.

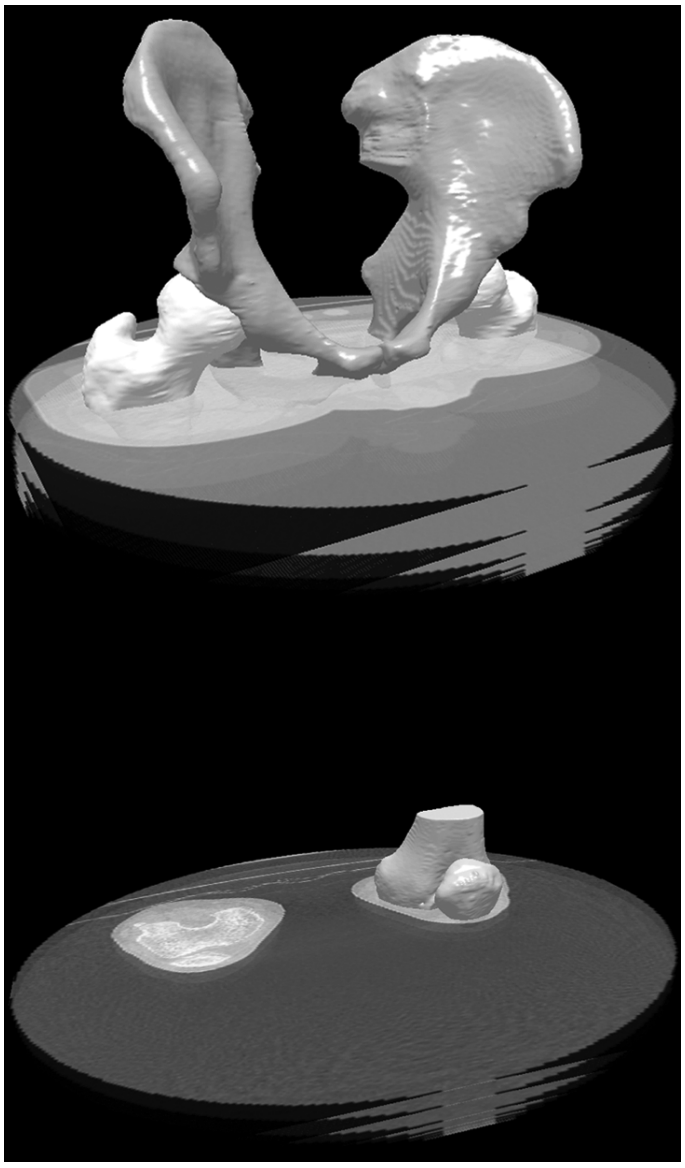

Figure 6.1. Three-dimensional models segmented from subject-specific CT data, considering the regions from the superior iliac crest to the femoral diaphysis and from the knee's inferior plateau to the posterior epicondyles.

6.2.3 Anatomical Parameters

6.2.3.1 Axial and Radial Alpha Angles

The axial alpha angle was measured on the oblique-axial plane of the longitudinal femoral neck axis, observing for an anterior asphericity. With the angle's vertex centered on the femoral head (on 2D images) and geometric centroid (on 3D models), the angle measured from the femoral neck axis to the point where the head was no longer contained within the circle or sphere [46] (Figure 6.2.A). The radial alpha angle was obtained by a 45-degree, 1:30 clock-face rotation about the longitudinal femoral neck axis, observing the cam deformity in the anterosuperior quadrant [51, 57] (Figure 6.2.B). An angle greater than 50.5° or 60° on the oblique-axial or radial plane, respectively, was considered as a cam deformity [8, 57].

6.2.3.2 Femoral Head-Neck Offset

On the oblique-axial plane of the CT slice and segmented model (Figure 6.2.A), two tangents were traced along the anterior femoral head and anterior femoral neck, both parallel with the femoral neck axis. The distance between the tangents defined the offset between the head and neck [17, 35].

6.2.3.3 Femoral Neck-Shaft Angle and Medial Proximal Femoral Angle

The femoral neck-shaft angle was measured on the frontal plane, formed by the longitudinal femoral neck axis and the longitudinal femoral shaft axis (Figure 6.2.C) [31, 52]. Similarly, the MPFA was measured between the longitudinal femoral shaft axis and the line joining the center of the femoral head to the superior greater trochanter [7] (Figure 6.2.C).

6.2.3.4 Femoral Torsion and Acetabular Version

The femoral torsion was determined as the difference between the femoral neck and condyle horizontals on the transverse plane. The neck horizontal angle was determined from the proximal femur, as the angle between the longitudinal femoral neck axis and the horizontal plane. The condyle horizontal angle was determined from the distal femur, formed by the posterior epicondyles with respect to the horizontal plane [11, 24] (Figure 6.2.D).

Acetabular version was measured on the transverse plane coincident with the left and right femoral head centers [17, 19]. On the image slice with the deepest acetabular socket, the

version angle was formed by the connecting line between the anterior and posterior acetabular notch with the perpendicular axis to the posterior acetabular notch (Figure 6.2.E).

6.2.3.5 Lateral Center-Edge Angle

Pelvic tilt and obliquity was first corrected by lining up the ischial tuberosities on the frontal plane. The centre-edge angle was formed by the superior-inferior axis, perpendicular to the ischial tuberosity, and the line from the femoral head center extending to the lateral edge of the acetabular rim (Figure 6.2.F).

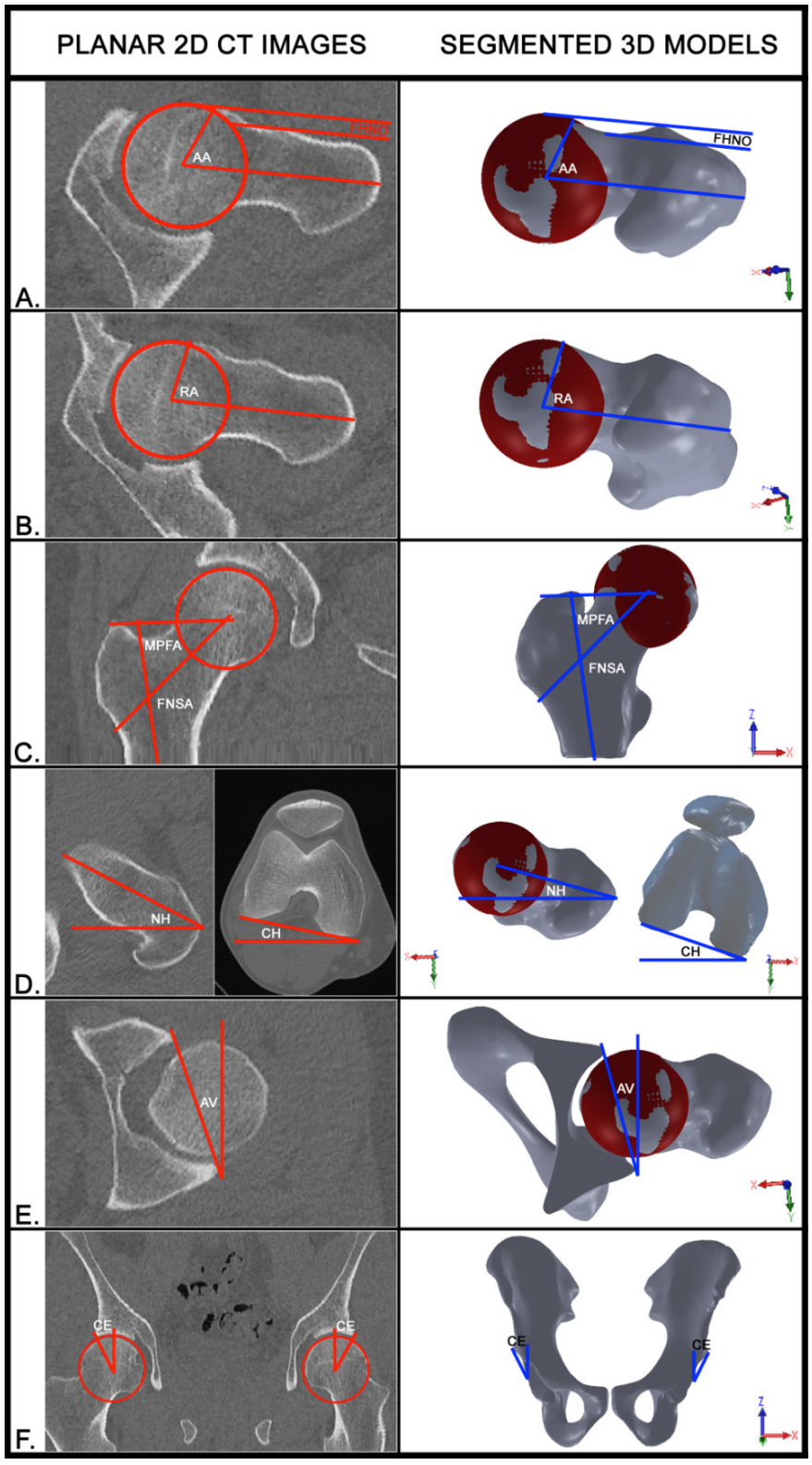

Figure 6.2. Comparison of each anatomical parameter measured from CT images and segmented models of: **A**) axial alpha angle (AA) and femoral head-neck offset (FHNO); **B**) radial alpha angle (RA); **C**) femoral neck-shaft angle (FNSA) and medial proximal femoral angle (MPFA); **D**) neck (NH) and condyle horizontals (CH) of femoral torsion; **E**) acetabular version (AV); and **F**) center-edge angle (CE).

6.2.4 Reliability and Statistical Analysis

To ensure that model segmentation was performed consistently, three models were initially segmented by two individuals, to confirm that both individuals' measurements were consistent. For these preliminary three models, measurement differences within one increment of the unit measure were considered acceptable. Once deemed adequate, all remaining models were manually segmented by one individual and three segmentations were repeated by the same individual, to ensure that the models were consistent. The three resegmented models were also verified to be within a unit measure, to be deemed adequate.

The resultant measurements from the CT images and segmented models were then unblinded and matched to analyze each participant's affected side. For the symptomatic group, each participant's affected hip was defined as the side with clinical signs. For the asymptomatic group, the affected hip was the side with the higher alpha angle. For the control group, the control-matching hip was the side with the smaller alpha angle. To assess the measurement reliability, the CT parameters were measured by two observers: Observer 1 performed the measurements twice, to examine intraobserver reliability, while Observer 2 performed the measurements once, to examine interobserver reliability with Observer 1. The segmented 3D models were also measured by two observers: Observer 1 performed the measurements twice, to examine intraobserver reliability and intermethod reliability with the CT measurements, while Observer 3 performed the measurements once, to examine interobserver reliability with Observer 1. The second sets of observations for Observer 1, from CT data and segmented models, were performed two weeks after the completion of the first. Statistical analysis was performed using SPSS Statistics v.23 (IBM Corporation, Armonk, NY, USA), where intra- and interobserver reliability was quantified using the intraclass correlation coefficient (*ICC*), using a two-way mixed model seeking absolute agreement. Intermethod reliability was also assessed using a two-way mixed *ICC* model, seeking consistency, and Bland-Altman scatter plots (CI = 95%). Intra- and interobserver and intermethod agreements were considered as either poor (< 0.2), weak (0.2 – 0.4), moderate (0.4 – 0.6), strong (0.6 – 0.8), or near-perfect (> 0.8) based on their *ICC*. A one-way, between groups analysis of variance was used to determine differences in mean intraobserver, interobserver, and intermethod observations ($\alpha = 0.05$).

6.3 Results

From CT images, the intraobserver reliability was in near-perfect agreement ($0.861 \leq ICC_{CT\ obs1} \leq 0.968$, $p < 0.01$), while the interobserver reliability was slightly lower, but still in strong to near-perfect agreement ($0.778 \leq ICC_{CT\ obs1\text{-}2} \leq 0.891$, $p < 0.01$). The lowest interobserver *ICC*s from CT images were for medial proximal femoral angle, centre-edge angle, and femoral head-neck offset (*ICC* = 0.778, 0.778, 0.789, respectively). From segmented 3D models, all intra- and interobserver reliabilities were in strong to near-perfect agreement ($0.774 \leq ICC_{MOD\ obs1} \leq 0.966$, $0.773 \leq ICC_{MOD\ obs1\text{-}3} \leq 0.983$, $p < 0.01$). The parameters from the segmented models with the lowest intra- and interobserver *ICC*s were femoral head-neck offset (0.774 and 0.798, respectively) and femoral torsion (0.773 and 0.778, respectively). The axial alpha angle, radial alpha angle, femoral neck-shaft angle, and acetabular version were measured consistently from CT images and 3D models, demonstrating near-perfect intra- and interobserver agreements (Table 6.2).

All intermethod measurements were also in strong to near-perfect agreement ($0.709 \leq ICC_{CT\text{-}MOD} \leq 0.924$, $p < 0.01$; Table 6.3). The femoral head-neck offset, femoral neck-shaft angle, centre-edge angle, and medial proximal femoral angle demonstrated the lowest intermethod reliabilities (*ICC* = 0.709, 0.731, 0.764, 0.776, respectively), while the other anatomical parameters were in near-perfect agreement. Although limits of intermethod agreement indicated slight variances, most noticeably for the axial alpha angle (*ICC* = 0.897, limits = -8.6 to 8.3°) and radial alpha angle (*ICC* = 0.874, limits = -10.4 to 8.7°), the mean differences for all parameters were centered on zero with very few comparisons found beyond the upper or lower limits (Figure 6.3). A few asymptomatic participants were observed to be outside the limits of agreement, most noticeably for radial alpha angle, femoral head-neck offset, femoral torsion, and acetabular version. The control participants were observed close to the mean differences, with very few participants exceeding the upper or lower limits. Comparing each of the three participant groups, there were no differences for each anatomical parameter measured from CT images and 3D models, ($p > 0.05$; Table 6.4).

Table 6.2. Summary of intraobserver and interobserver reliability for each anatomical parameter, measured from CT images and segmented models

Anatomical Parameter	CT Images		Segmented 3D Models	
	Observer 1 intraobserver *ICC* (mean ± SD)	Observer 1-2 interobserver *ICC* (mean ± SD)	Observer 1 intraobserver *ICC* (mean ± SD)	Observer 1-3 interobserver *ICC* (mean ± SD)
Axial alpha angle (°)	0.942 (52.1 ± 10.0°)	0.869 (51.8 ± 9.3°)	0.966 (52.0 ± 9.5°)	0.983 (52.4 ± 9.7°)
Radial alpha angle (°)	0.951 (61.5 ± 10.1°)	0.891 (63.4 ± 9.8°)	0.934 (62.2 ± 9.7°)	0.966 (62.9 ± 10.2°)
Femoral head-neck offset (mm)	0.923 (7.8 ± 2.0 mm)	0.789 (7.7 ± 2.5 mm)	0.774 (8.0 ± 2.1 mm)	0.773 (8.6 ± 2.0 mm)
Femoral neck-shaft angle (°)	0.861 (125.2 ± 3.8°)	0.856 (125.8 ± 3.9°)	0.957 (125.2 ± 3.5°)	0.978 (125.4 ± 3.5°)
Medial proximal femoral angle (°)	0.968 (80.7 ± 3.7°)	0.778 (81.7 ± 4.1°)	0.826 (81.9 ± 3.4°)	0.905 (81.8 ± 4.4°)
Femoral torsion (°)	0.883 (11.1 ± 10.3°)	0.874 (10.3 ± 10.3°)	0.798 (11.0 ± 9.0°)	0.778 (12.6 ± 7.5°)
Acetabular version (°)	0.900 (20.5 ± 5.2°)	0.840 (19.9 ± 5.2°)	0.855 (18.8 ± 5.2°)	0.922 (17.7 ± 5.5°)
Center-edge angle (°)	0.881 (33.3 ± 3.7°)	0.778 (33.7 ± 4.3°)	0.884 (33.8 ± 3.7°)	0.838 (34.0 ± 2.0°)

All intraclass correlation coefficients (*ICC*) significant to $p < 0.01$

Table 6.3. Summary of intermethod reliability for each anatomical parameter, comparing measurements from CT images and segmented models

Anatomical Parameter	Intermethod *ICC* (mean ± SD)		Mean difference (limits of agreement 95%)	
Axial alpha angle (°)	0.897	(51.9 ± 9.5°)	-0.15°	(-8.6 – 8.3°)
Radial alpha angle (°)	0.874	(61.7 ± 9.7°)	-0.86°	(-10.4 – 8.7°)
Femoral head-neck offset (mm)	0.709	(7.9 ± 2.1 mm)	-0.27 mm	(-3.5 – 2.9 mm)
Femoral neck-shaft angle (°)	0.731	(125.4 ± 3.6°)	0.29°	(-4.8 – 5.4°)
Medial proximal femoral angle (°)	0.776	(81.3 ± 3.5°)	-1.15°	(-5.8 – 3.5°)
Femoral torsion (°)	0.924	(10.9 ± 9.5°)	-0.20°	(-7.5 – 7.1°)
Acetabular version (°)	0.838	(19.8 ± 5.2°)	2.12°	(-3.6 – 7.9°)
Center-edge angle (°)	0.764	(51.9 ± 9.5°)	-0.76°	(-5.5 – 4.0°)

All intraclass correlation coefficients (*ICC*) significant to $p < 0.01$

Table 6.4. Summary of Observer 1's first reading of each anatomical parameter's mean and standard deviation, measured from CT images and segmented models

Anatomical Parameter	Symptomatic			Asymptomatic			Control		
	CT Images	3D Models	*p* value	CT Images	3D Models	*p* value	CT Images	3D Models	*p* value
Axial alpha angle (°)	55.6 ± 7.0	57.8 ± 6.2	0.395	57.6 ± 7.3	56.4 ± 7.9	0.596	41.9 ± 3.8	42.1 ± 4.2	0.849
Radial alpha angle (°)	64.6 ± 6.6	68.0 ± 5.4	0.146	68.1 ± 6.9	67.5 ± 7.2	0.775	50.5 ± 2.9	51.1 ± 3.4	0.543
Femoral head-neck offset (mm)	6.1 ± 1.7	7.1 ± 1.7	0.759	7.3 ± 1.9	6.9 ± 1.9	0.465	9.5 ± 1.4	10.0 ± 1.1	0.634
Femoral neck-shaft angle (°)	120.6 ± 1.4	120.8 ± 2.0	0.274	127.3 ± 2.6	126.7 ± 2.5	0.493	127.2 ± 2.3	126.9 ± 2.2	0.184
Medial proximal femoral angle (°)	79.2 ± 3.3	80.7 ± 3.9	0.127	81.5 ± 4.0	82.3 ± 3.8	0.487	80.9 ± 3.3	82.2 ± 2.3	0.238
Femoral torsion (°)	11.4 ± 12.0	11.7 ± 11.1	0.951	13.3 ± 7.5	12.5 ± 5.6	0.669	7.3 ± 10.5	8.7 ± 10.5	0.687
Acetabular version (°)	23.4 ± 5.3	21.2 ± 5.4	0.273	19.7 ± 3.8	17.5 ± 4.4	0.086	20.4 ± 5.9	18.5 ± 5.6	0.323
Center-edge angle (°)	33.7 ± 4.3	34.8 ± 3.9	0.487	32.1 ± 3.0	33.2 ± 3.7	0.228	33.4 ± 3.1	33.5 ± 3.6	0.945

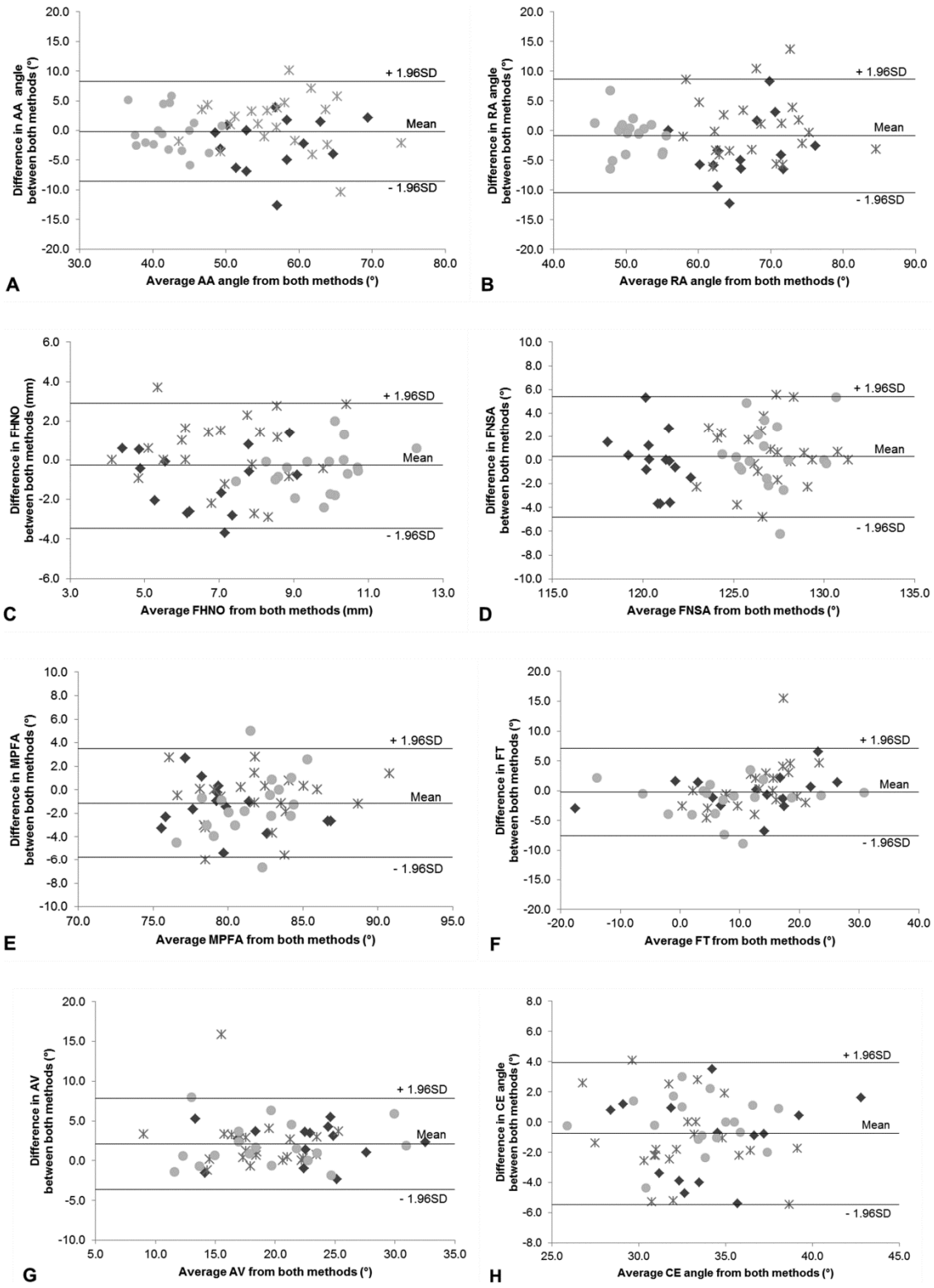

Figure 6.3. Bland-Altman scatter plots demonstrating intermethod agreements for the symptomatic (diamond), asymptomatic (star), and control (circle) participants, between the CT images and segmented models, for each parameter: **A**) axial alpha (AA) angle; **B**) radial alpha (RA) angle; **C**) femoral head-neck offset (FHNO); **D**) femoral neck-shaft angle (FNSA); **E**) medial proximal femoral angle (MPFA); **F**) femoral torsion (FT); **G**) acetabular version (AV); and **H**) center-edge (CE) angle.

6.4 Discussion

We measured diagnostic anatomical parameters, common for FAI morphologies. As anatomical characteristics are clinically pertinent to diagnose FAI and predict symptoms associated with morphologies, we examined to what extent the anatomical characteristics from the 3D segmented models were representative of the original CT data. While the clinical presentation and diagnosis of cam-type FAI is relatively well-established, our understanding of the pathomechanisms leading to cartilage degeneration is still evolving. Although the cam deformity has been well-described with the alpha angle, how to directly characterize biomechanical abnormalities leading to degeneration remains to be determined. While many studies focused on validating anatomical measurement methods from imaging protocols, using intra- and interobserver repeatability, few studies compared intermethod measurements to ascertain the geometric validity of segmented models. Moreover, no studies compared intermethod measurements in the context of clinical settings using three different participant groups (hip morphology involving symptomatic, asymptomatic, and control participants). Several of the recent finite element studies of FAI reconstructed idealized geometries to simulate hip joint stresses, using only alpha (cam deformity) and CE angles (pincer deformity) as geometric parameters, without considering any of the other subject-specific anatomical parameters as factors of mechanical impingement. Moreover, the FAI models that were reconstructed from subject-specific imaging data were not adequately validated against the original imaging data, thus it was unclear to what degree the segmented models were accurate representations of the subject-specific hip joint geometries.

Prior to completing all the segmentations and measurements, two individuals compared three preliminary segmentations and one individual resegmented three different models. Knowing that there is a level of subjectivity during the measurements, anatomical parameters of these preliminary models were measured and compared with one another. Any discrepancies with measurements and segmentations methods were discussed among the two individuals (where one unit of measure was deemed acceptable for clinical purposes). Our measurements demonstrated excellent reliability, when comparing the two methods, due to the lack of variability in patient positioning and imaging. Our intra- and interobserver reliabilities coincided with previous studies having achieved very similar, if not better, reliability coefficients for axial and radial alpha angles [5, 8, 16, 37, 49, 57], femoral head-neck offset [37, 49], femoral neck-shaft and medial proximal femoral angles [7, 11, 31, 41, 52], femoral torsion [15, 24], acetabular

version [19, 20], and centre-edge angle [16, 35, 37, 48]. However, many previous studies used various imaging views and methods, thus making it difficult to draw direct intermethod comparisons. Cadet and associates looked at intra- and interobserver reliabilities for planar radiographs and 3D CT models, for eight FAI patients, observing for only alpha angle, cam location, centre-edge angle, and crossover [16]. Their purpose was to examine whether measurements from 3D CT models would demonstrate higher intra- and interobserver reliabilities, in comparison with radiographic measurements. Their work suggested very little differences between both methods and that there were no advantages to the 3D models for their diagnostic purposes. However, their study was limited by a very small sample size (n = 8) with only four measured parameters. Cadet and associates further acknowledged that the segmentation process was time-consuming, but saw the potential for 3D models for surgical outcomes and preoperative planning. In contrast, our study examined additional anatomical FAI parameters for a larger sample size, examining intermethod discrepancies using Bland-Altman scatter plots. Interestingly, Nepple and associates suggested that the 45° Dunn view and frog-leg radiographs were adequate to approximate the cam deformity, in comparison with CT, but also acknowledged that multiplanar 3D imaging could be more advantageous for deformity characterization [43].

Although it took less time to measure parameters from planar images than from 3D models, the geometric centroid fitted on the femoral heads of the 3D models provided a higher level of certainty that the femoral neck and shaft axes were correctly represented, as they were determined based on volumetric properties of the models. This was different from 2D images, where measurements were recorded from subjectively traced geometric circles and axes, based on the images' contours.

Our 3D models were reoriented in SolidWorks to correct for pelvic incline. The models permitted us to visualize and measure a truly 3D deformity. Several studies reported that 3D measurements could be more accurate than 2D [10, 19, 22, 28, 30, 43, 50, 52], although this may be dependent on the parameter and application. Harris and associates emphasized that a statistical shape model could characterize the cam deformity [28]. The circle-fit implemented in our study served as a geometric, spherical centroid and reference point, similar to the conventional protocols established by Nötzli and associates [46], where a perfect circle was

traced around the femoral head on the oblique-axial plane. It may be useful to further examine whether or not the conchoidal-fit could better describe the severity of the cam deformity [30].

Although strongly correlated, our planar images possibly did not capture the full depth of the cam deformity or geometric structures, thus underestimating a few anatomical parameters. Due to characteristics of 2D images that display and project only one slice at a time, a lot of anatomical detail may be absent above or below the displayed slice, as evidenced by the femoral head-neck offset, femoral neck-shaft angle, and medial proximal femoral angle parameters. Our slight discrepancies could also be attributed to the different interobserver positioning of the longitudinal femoral neck or shaft axis on the plane of interest. This was perhaps more evident for the evaluation of the femoral head-neck offset, which could have resulted in different estimations of perpendicular offsets and not adequately capturing the depth of the cam deformity. A known recurring issue with 3D segmentation is the presence of geometric artefacts, generated from poor resolution and voxel sizing. The models were resurfaced in SolidWorks, which reduced geometric artefacts, but also produced a more smoothed representation of the model. The resurfacing procedure was performed to integrate a spline over the nodes, in efforts to reduce the number of jagged voxel edges that are typically produced from image segmentation.

We acknowledge that there are inherent limitations with segmentation and modelling that could greatly influence the outcome of finite element simulations. For our methods to measure the 3D anatomical parameters, we adhered to the 2D measurement methods as closely as possible (*i.e.*, circle-fitting to reconstruct a geometric centroid). The methods for 2D CT measurements are commonly practiced and, as we wanted to model large-scale anatomical parameters of the femoral head-neck and acetabulum, we implemented and compared anatomical measurements that were used in clinical practice.

According to our Bland-Altman plots, it was more difficult to assess the asymptomatic participants, making the limits of agreement slightly wider. With this discrepancy to characterize asymptomatic participants in mind, this further suggests the need to understand the risks and anatomical indicators of osteoarthritis to classify the asymptomatic population [27, 34, 44, 56, 57]. With the exception of the alpha angles, there were no other established anatomical thresholds to characterize asymptomatic individuals.

The comparison of intermethod clinical measurements raises many questions as to if and how methods can be confidently interchangeable [13, 14, 40]. The limits of agreement were

deemed reasonable, based on our clinical application [12], with mean differences centered on zero. Lee and associates considered that there should be no systematic bias; no significant mean differences between methods; and *ICC* should be at least 0.75 [40]. First, in our study, observer and systematic bias were removed as much as possible, with all data blinded and read multiple times, with multiple readers. Second, there were no statistical differences between intermethod means. Third, although only femoral head-neck offset and femoral neck-shaft angle did not meet the intermethod correlation criterion of 0.75, the parameters demonstrated very strong correlations. We noted a few underestimations to be expected with CT measurements, however, when doubt arises with the segmented models and in clinical practice, any measured hip joint parameter with an intermethod *ICC* near or below 0.75, should be repeated. If the intermethod *ICC* still falls below 0.75 after the repeated observation, the model could be re-segmented to ensure that the models are accurate geometric representations.

The importance of validating hip joint geometries cannot be overstated, especially when these models are used to study the natural history and pathomechanism. We demonstrated potential differences to be expected when performing subject-specific segmentation and modelling, with slight discrepancies noted from the Bland-Altman plots, and showed consistency to be implemented in clinical orthopaedics [12]. We implemented a method to help ensure that the anatomical characteristics from 3D segmented models were representative of the original CT data. The crucial anatomical parameters were near-identical, subject-specific representations of the hip joint geometry, demonstrating that the 3D models can be further implemented for computational analysis and finite element simulations.

6.5 References

1. Agricola R, Heijboer MP, Bierma-Zeinstra SM, Verhaar JA, Weinans H, Waarsing JH. Cam impingement causes osteoarthritis of the hip: a nationwide prospective cohort study (CHECK). *Ann Rheum Dis*. 2012;72:918-923.
2. Allen D, Beaulé PE, Ramadan O, Doucette S. Prevalence of associated deformities and hip pain in patients with cam-type femoroacetabular impingement. *J Bone Joint Surg Br*. 2009;91:589-594.
3. Alonso-Rasgado T, Jimenez-Cruz D, Bailey CG, Mandal P, Board T. Changes in the stress in the femoral head neck junction after osteochondroplasty for hip impingement: A finite element study. *J Orthop Res*. 2012;30:1999-2006.
4. Arbabi E, Chegini S, Boulic R, Tannast M, Ferguson SJ, Thalmann D. Penetration depth method--novel real-time strategy for evaluating femoroacetabular impingement. *J Orthop Res*. 2010;28:880-886.
5. Audenaert EA, Baelde N, Huysse W, Vigneron L, Pattyn C. Development of a three-dimensional detection method of cam deformities in femoroacetabular impingement. *Skeletal Radiol*. 2011;40:921-927.
6. Audenaert EA, Mahieu P, Pattyn C. Three-dimensional assessment of cam engagement in femoroacetabular impingement. *Arthroscopy*. 2011;27:167-171.
7. Bardakos NV, Villar RN. Predictors of progression of osteoarthritis in femoroacetabular impingement: a radiological study with a minimum of ten years follow-up. *J Bone Joint Surg Br*. 2009;91:162-169.
8. Barton C, Salineros MJ, Rakhra KS, Beaulé PE. Validity of the alpha angle measurement on plain radiographs in the evaluation of cam-type femoroacetabular impingement. *Clin Orthop Relat Res*. 2011;469:464-469.
9. Beaulé P, Hynes K, Parker G, Kemp K. Can the Alpha Angle Assessment of Cam Impingement Predict Acetabular Cartilage Delamination? *Clin Orthop Rel Res*. 2012;470:3361-3367.
10. Beaulé PE, Zaragoza E, Motamedi K, Copelan N, Dorey FJ. Three-dimensional computed tomography of the hip in the assessment of femoroacetabular impingement. *J Orthop Res*. 2005;23:1286-1292.
11. Bedi A, Dolan M, Leunig M, Kelly BT. Static and Dynamic Mechanical Causes of Hip Pain. *Arthroscopy*. 2011;27:235-251.
12. Bland JM, Altman DG. Applying the right statistics: analyses of measurement studies. *Ultrasound Obstet Gynecol*. 2003;22:85-93.
13. Bland JM, Altman DG. A note on the use of the intraclass correlation coefficient in the evaluation of agreement between two methods of measurement. *Comput Biol Med*. 1990;20:337-340.
14. Bland JM, Altman DG. Statistical methods for assessing agreement between two methods of clinical measurement. *Lancet*. 1986;1:307-310.
15. Botser IB, Ozoude GC, Martin DE, Siddiqi AJ, Kuppuswami S, Domb BG. Femoral anteversion in the hip: comparison of measurement by computed tomography, magnetic resonance imaging, and physical examination. *Arthroscopy*. 2012;28:619-627.
16. Cadet ER, Babatunde OM, Gorroochurn P, Chan AK, Stancato-Pasik A, Brown M, Johnson S, Kaiser PB, Gardner TR, Ayeni OR. Inter- and intra-observer agreement of femoroacetabular impingement (FAI) parameters comparing plain radiographs and advanced, 3D computed tomographic (CT)-generated hip models in a surgical patient cohort. *Knee Surg Sports Traumatol Arthrosc*. 2014;1-8.
17. Chakraverty JK, Sullivan C, Gan C, Narayanaswamy S, Kamath S. Cam and pincer femoroacetabular impingement: CT findings of features resembling femoroacetabular impingement in a young population without symptoms. *AJR Am J Roentgenol*. 2013;200:389-395.
18. Chegini S, Beck M, Ferguson SJ. The effects of impingement and dysplasia on stress distributions in the hip joint during sitting and walking: a finite element analysis. *J Orthop Res*. 2009;27:195-201.
19. Dandachli W, Islam SU, Liu M, Richards R, Hall-Craggs M, Witt J. Three-dimensional CT analysis to determine acetabular retroversion and the implications for the management of femoro-acetabular impingement. *J Bone Joint Surg Br*. 2009;91:1031-1036.

20. Dandachli W, Ul Islam S, Tippett R, Hall-Craggs MA, Witt JD. Analysis of acetabular version in the native hip: comparison between 2D axial CT and 3D CT measurements. *Skeletal Radiol*. 2011;40:877-883.

21. de Sa D, Urquhart N, Philippon M, Ye JE, Simunovic N, Ayeni OR. Alpha angle correction in femoroacetabular impingement. *Knee Surg Sports Traumatol Arthrosc*. 2014;22:812-821.

22. Dudda M, Albers C, Mamisch T, Werlen S, Beck M. Do Normal Radiographs Exclude Asphericity of the Femoral Head-Neck Junction? *Clin Orthop Relat Res*. 2009;467:651-659.

23. Eijer H, Leunig M, Mahomed N, Ganz R. Cross-table lateral radiographs for screening of anterior femoral head-neck offset in patients with femoro-acetabular impingement. 2001;11:37-41.

24. Ejnisman L, Philippon M, Lertwanich P, Pennock A, Herzog M, Briggs K, Ho C. Relationship Between Femoral Anteversion and Findings in Hips With Femoroacetabular Impingement. *Orthopedics*. 2013;36:e293-300.

25. Ganz R, Parvizi J, Beck M, Leunig M, Nötzli H, Siebenrock KA. Femoroacetabular Impingement: A Cause for Osteoarthritis of the Hip. *Clin Orthop Rel Res*. 2003;417:112-120.

26. Gupta AK, Abrams GD, Nho SJ. What's New in Femoroacetabular Impingement Surgery: Will We Be Better in 2023? *Sports Health*. 2014;6:162-170.

27. Hack K, Di Primio G, Rakhra K, Beaulé PE. Prevalence of cam-type femoroacetabular impingement morphology in asymptomatic volunteers. *J Bone Joint Surg Am*. 2010;92:2436-2444.

28. Harris MD, Datar M, Whitaker RT, Jurrus ER, Peters CL, Anderson AE. Statistical shape modeling of cam femoroacetabular impingement. *J Orthop Res*. 2013;31:1620-1626.

29. Harris MD, Kapron AL, Peters CL, Anderson AE. Correlations between the alpha angle and femoral head asphericity: Implications and recommendations for the diagnosis of cam femoroacetabular impingement. *Eur J Radiol*. 2014;83:788-796.

30. Harris MD, Reese SP, Peters CL, Weiss JA, Anderson AE. Three-dimensional quantification of femoral head shape in controls and patients with cam-type femoroacetabular impingement. *Ann Biomed Eng*. 2013;41:1162-1171.

31. Hartofilakidis G, Bardakos NV, Babis GC, Georgiades G. An examination of the association between different morphotypes of femoroacetabular impingement in asymptomatic subjects and the development of osteoarthritis of the hip. *J Bone Joint Surg Br*. 2011;93:580-586.

32. Hellwig FL, Tong J, Hussell JG. Hip joint degeneration due to cam impingement: a finite element analysis. *Comput Methods Biomech Biomed Engin*. 2016;19:41-48.

33. Jorge JP, Simoes FM, Pires EB, Rego PA, Tavares DG, Lopes DS, Gaspar A. Finite element simulations of a hip joint with femoroacetabular impingement. *Comput Methods Biomech Biomed Engin*. 2014;17:1275-1284.

34. Jung KA, Restrepo C, Hellman M, AbdelSalam H, Morrison W, Parvizi J. The prevalence of cam-type femoroacetabular deformity in asymptomatic adults. *J Bone Joint Surg Br*. 2011;93:1303-1307.

35. Kang AC, Gooding AJ, Coates MH, Goh TD, Armour P, Rietveld J. Computed tomography assessment of hip joints in asymptomatic individuals in relation to femoroacetabular impingement. *Am J Sports Med*. 2010;38:1160-1165.

36. Kappe T, Kocak T, Reichel H, Fraitzl CR. Can femoroacetabular impingement and hip dysplasia be distinguished by clinical presentation and patient history? *Knee Surg Sports Traumatol Arthrosc*. 2012;20:387-392.

37. Kapron AL, Anderson AE, Aoki SK, Phillips LG, Petron DJ, Toth R, Peters CL. Radiographic prevalence of femoroacetabular impingement in collegiate football players: AAOS Exhibit Selection. *J Bone Joint Surg Am*. 2011;93:1-10.

38. Konan S, Rayan F, Haddad FS. Is the frog lateral plain radiograph a reliable predictor of the alpha angle in femoroacetabular impingement? *J Bone Joint Surg Br*. 2010;92:47-50.

39. Lamontagne M, Kennedy MJ, Beaulé PE. The effect of cam FAI on hip and pelvic motion during maximum squat. *Clin Orthop Relat Res*. 2009;467:645-650.

40. Lee J, Koh D, Ong CN. Statistical evaluation of agreement between two methods for measuring a quantitative variable. *Comput Biol Med*. 1989;19:61-70.

41. Mast NH, Impellizzeri F, Keller S, Leunig M. Reliability and agreement of measures used in radiographic evaluation of the adult hip. *Clin Orthop Relat Res*. 2011;469:188-199.

42. Monazzam S, Bomar JD, Agashe M, Hosalkar HS. Does femoral rotation influence anteroposterior alpha angle, lateral center-edge angle, and medial proximal femoral angle? A pilot study. *Clin Orthop Relat Res*. 2013;471:1639-1645.

43. Nepple JJ, Martel JM, Kim YJ, Zaltz I, Clohisy JC. Do plain radiographs correlate with CT for imaging of cam-type femoroacetabular impingement? *Clin Orthop Relat Res*. 2012;470:3313-3320.

44. Ng KCG, Lamontagne M, Adamczyk AP, Rakhra KS, Beaulé PE. Patient-specific anatomical and functional parameters provide new insights into the pathomechanism of cam FAI. *Clin Orthop Relat Res*. 2015;473:1289-1296.

45. Ng KCG, Rouhi G, Lamontagne M, Beaulé PE. Finite Element Analysis Examining the Effects of Cam FAI on Hip Joint Mechanical Loading Using Subject-Specific Geometries During Standing and Maximum Squat. *HSS J*. 2012;8:206-212.

46. Nötzli HP, Wyss TF, Stoecklin CH, Schmid MR, Treiber K, Hodler J. The contour of the femoral head-neck junction as a predictor for the risk of anterior impingement. *J Bone Joint Surg Br*. 2002;84:556-560.

47. Nouh MR, Schweitzer ME, Rybak L, Cohen J. Femoroacetabular impingement: can the alpha angle be estimated? *AJR Am J Roentgenol*. 2008;190:1260-1262.

48. Pollard TC, Villar RN, Norton MR, Fern ED, Williams MR, Murray DW, Carr AJ. Genetic influences in the aetiology of femoroacetabular impingement: a sibling study. *J Bone Joint Surg Br*. 2010;92:209-216.

49. Pollard TC, Villar RN, Norton MR, Fern ED, Williams MR, Simpson DJ, Murray DW, Carr AJ. Femoroacetabular impingement and classification of the cam deformity: the reference interval in normal hips. *Acta Orthop*. 2010;81:134-141.

50. Preininger B, Schmorl K, von Roth P, Winkler T, Matziolis G, Perka C, Tohtz S. Femoral Offset (3D) in Patients without Osteoarthritis - Index Values from 200 Hip Joints. *Open Orthop J*. 2012;6:578-581.

51. Rakhra KS, Sheikh AM, Allen D, Beaulé PE. Comparison of MRI alpha angle measurement planes in femoroacetabular impingement. *Clin Orthop Relat Res*. 2009;467:660-665.

52. Ranawat A, Schulz B, Baumbach S, Meftah M, Ganz R, Leunig M. Radiographic Predictors of Hip Pain in Femoroacetabular Impingement. *HSS J*. 2011;7:115-119.

53. Roels P, Agricola R, Oei E, Weinans H, Campoli G, Zadpoor AA. Mechanical factors explain development of cam-type deformity. *Osteoarthritis Cartilage*. 2014;22:2074-2082.

54. Siebenrock KA, Wahab KH, Werlen S, Kalhor M, Leunig M, Ganz R. Abnormal extension of the femoral head epiphysis as a cause of cam impingement. *Clin Orthop Relat Res*. 2004;54-60.

55. Speirs AD, Beaulé PE, Rakhra KS, Schweitzer ME, Frei H. Bone density is higher in cam-type femoroacetabular impingement deformities compared to normal subchondral bone. *Osteoarthritis Cartilage*. 2013;21:1068-1073.

56. Speirs AD, Beaulé PE, Rakhra KS, Schweitzer ME, Frei H. Increased acetabular subchondral bone density is associated with cam-type femoroacetabular impingement. *Osteoarthritis Cartilage*. 2013;21:551-558.

57. Sutter R, Dietrich TJ, Zingg PO, Pfirrmann CWA. How Useful Is the Alpha Angle for Discriminating between Symptomatic Patients with Cam-type Femoroacetabular Impingement and Asymptomatic Volunteers? *Radiology*. 2012;264:514-521.

58. Tannast M, Siebenrock KA, Anderson SE. Femoroacetabular Impingement: Radiographic Diagnosis—What the Radiologist Should Know. *Am J Roentgenol*. 2007;188:1540-1552.

7 Comparison of Different Material Modelling Parameters on Hip Joint Stresses

K. C. Geoffrey Ng [1] | Mario Lamontagne [2,1] | Michel R. Labrosse [1] | Paul E. Beaulé [3]

[1] Department of Mechanical Engineering | University of Ottawa | Ottawa, Ontario, Canada

[2] School of Human Kinetics | University of Ottawa | Ottawa, Ontario, Canada

[3] Division of Orthopaedic Surgery | University of Ottawa | Ottawa, Ontario, Canada

Contents of this chapter prepared as a manuscript for submission | March 2017

Ng KCG, Lamontagne M, Labrosse, MR, Beaulé PE. Comparison of Different Material Modelling Parameters on Hip Joint Stresses. 2017; Pending Submission.

7.0 Abstract

Computational, finite element hip joint simulations can represent a patient demographic and help predict adverse loading conditions. It is unclear what combination of material properties should be implemented, when using similar geometric and loading assumptions, to examine hip joint stresses and elucidate risks of early joint degeneration. The purpose was to evaluate conventional material modelling properties, used for bone and cartilage models in finite element hip joint simulations, and compare their resultant peak maximum shear stress characteristics. Hip joint models (femur, pelvis, femoral and acetabular cartilages, labrum) were segmented from one male participant's CT and MRI data. Models were meshed and parameterized as either: 1) cortical with trabecular bone, 2) cortical without trabecular bone, or 3) heterogeneous, subject-specific bone; with either: A) linear-elastic, B) hyperelastic, or C) orthotropic soft tissues properties; for a total of nine hip joint assemblies. Subject-specific hip contact forces, during terminal stance, were determined from a musculoskeletal modelling program and applied to all models for simulation. The heterogeneous bone combined with hyperelastic soft tissues showed slightly higher absolute peak maximum shear stress at the anterolateral acetabular cartilage (5.8 MPa); whereas the cortical and trabecular bone assembly with orthotropic soft tissues showed the lowest peak stress (4.0 MPa). The heterogeneous, subject-specific bone density models also indicated moderate variability between soft tissues parameters (7.1 – 16.8%), but captured secondary stress concentrations. Although marginal differences, the heterogeneous bone density models may be more adequate to demonstrate inter-subject variability and represent specific pathologies.

7.1 Introduction

Early benchmark studies in hip joint contact mechanics implemented cadaveric specimens loaded into an instrumented testing apparatus [11, 25, 29, 45]. More recently, many studies focused on in silico methods to examine hip joint contact mechanics, having the advantages to reconstruct finite element hip joint models from subject-specific imaging data and parameterize different aspects of hip joint geometry, material properties, and loading parameters [3, 9, 49]. Many in silico hip joint studies report contact stresses as resultant dependent variables used for comparative analyses. Although biological implications of joint stresses are disputable [8], results from computational simulations can provide an assessment as to which geometric, material, or loading factors are associated with patient-specific demographics and risks of early joint degeneration [31, 44].

Early finite element hip joint simulations often included the femur, pelvis, articulating femoral and acetabular cartilages within the assembly, with more recent efforts accounting for the labrum as well [12, 13, 17, 18, 21], where material properties depended on the physiological application. Since bone is macroscopically composed of cortical and trabecular bones, several studies implemented conventional material properties to consider each bone as linear-elastic, isotropic materials with homogeneous elastic and shear moduli; as well as modelling cartilage and soft tissues as linear-elastic [10, 37, 38]. Anderson and associates (2008, 2010) further excluded the trabecular structures from simulations, justifying that they had very little influence on contact stresses and increased computation time. To account for variable bone densities in the femur and pelvis, many studies applied elastic moduli based on an empirical formula derived from apparent bone densities [6, 33, 42], to represent the stiffness of each individual finite element, resulting in more subject-specific, heterogeneous bone models. Nonlinear effects of soft tissues can also be approximated with hyperelastic properties, to estimate nonlinear, viscoelastic responses [3, 21]; or orthotropic properties, accounting for the different responses in each of the cylindrical directions [17].

With several different material modelling parameters, it is unclear how resultant contact mechanics would compare in terms of stress characteristics, under similar geometric assumptions and loading conditions. In efforts to understand the effects of material modelling parameters on hip joint morphology and simulations, the purpose was to evaluate various conventional material

modelling properties of the bone and cartilage, used in finite element hip joint loading simulations, and compare their resultant peak hip joint stress magnitudes and distributions.

7.2 Methods

7.2.1 Participant

One male participant, with no history of lower limb abnormalities, clinical signs, symptoms, or previous surgeries was recruited for this study (n = 1, age = 26 years, BMI = 23 kg/m^2). The participant underwent pelvic computed tomography (CT) and magnetic resonance imaging (MRI), to reconstruct bone and cartilage models, respectively; and walking kinematics and kinetics were recorded in a motion capture environment. Our protocol and analyses were approved by the university and hospital research institute ethics boards and the participant signed and provided informed consent prior to the study.

7.2.2 Imaging and Anatomical Parameters

Pelvic and knee CT data were acquired from the participant using a conventional scanner (Discovery CT750, GE Healthcare, Mississauga, ON, Canada); scanning in a supine position with a calibration phantom (Model 3, Mindways Software, Austin, TX, USA) placed under the lumbar vertebra for bone mineral densitometry. The CT data were captured (512×512 resolution, slice thickness of 0.625 mm, 120 kVp, 200 mAs, in-plane pixel spacing of 0.721 mm) and the hip joint anatomical parameters were first measured by a senior musculoskeletal radiologist (KSR) to determine which hip to model and analyze. Both hips showed no indications of acetabular overcoverage, dysplasia, crossover signs, femoral or acetabular retroversion; however, the left hip indicated smaller cam parameters (*i.e.*, lower axial and radial alpha angles compared with the right hip) and was selected for further modelling and analyses. The left hip underwent subsequent MRI (MAGNETOM Symphony, Siemens Healthcare GmbH, Erlangen, Germany), to determine the cartilage thickness and contour of the labrum, using a field strength of 1.5 T (384×384 resolution, slice thickness of 3 mm, in-plane pixel spacing of 0.469 mm).

7.2.3 Contact Forces

In efforts to minimize skin artefacts and locate hip joint centers, surface electrodes were placed onto the participant's pelvic landmarks prior to CT imaging, at the left and right anterior superior

iliac spines and posterior superior iliac spines. After CT imaging, the surface electrodes were replaced with retro-reflective surface markers used for motion capture. Therefore, the surface electrodes represented the reference locations of each pelvic retro-reflective marker, with respect to the hip joint center [27]. The participant performed level walking trials in our motion capture laboratory, where 3D kinematics were recorded using a ten-camera motion capture system (MX-13, Vicon, Oxford, UK) with retro-reflective markers attached onto each participant's anatomical landmarks according to a modified Plug-in-Gait model; and ground reaction forces were captured using two stationary force plates (FP4060-08, Bertec, Columbus, OH, USA). Hip contact forces were then estimated using a musculoskeletal modelling program (OpenSim 3.1, SimTK, USA), where resultant 3D hip contact forces were calculated and expressed in the pelvic reference system [26]. The loading response and terminal stance phases during walking were observed to distinguish which produced higher resultant forces. The instant with the highest resultant forces was simulated for the quasi-static loading condition, to compare differences in responses for each combination of material properties.

7.2.4 Segmentation and Modelling

The femur and pelvis were manually segmented from CT data, using image segmentation software (3D-Doctor 4.0, Able Software Corp., Lexington, MA, USA), reconstructing the bone contours from the superior iliac crest to the proximal femur. In addition, the contours of the trabecular bones were segmented. Each geometric model was resurfaced to reduce geometric artefacts, using computer-aided design software (SolidWorks, Dassault Systèmes, Concord, MA, USA). Anatomical hip joint parameters of the segmented models were measured to confirm the model's geometric accuracy with the associated CT data. Measurements were taken by two observers, each performing two observations, following an existing protocol to validate segmented hip joint models from its original CT data [30].

Using the segmentation software, the MRI data were centered on four control points of the target CT image, where the deepest width and depth of the acetabulum and the femoral head center were denoted as registration landmarks (Figure 7.1). The midpoint between the femoral and acetabular cartilage was determined as well, denoting the thickness of each cartilage. The peripheries of the femoral cartilage, acetabular cartilage, and labrum were manually segmented

and resurfaced. Each bone, cartilage, and labrum component was individually segmented, to be assigned unique material modelling properties.

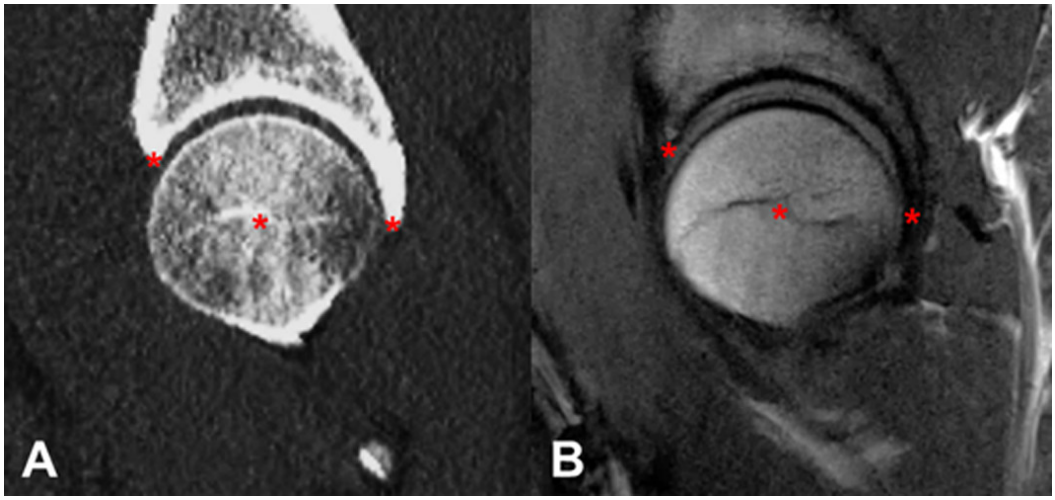

Figure 7.1. Sagittal view showing the image registration of a participant's left hip using CT (**A**) and MRI (**B**) data. The CT scan shows the dense tissues of the acetabulum and femoral head, while MRI shows the separation between the acetabular and femoral cartilage. The red asterisks denote registration landmarks and control points that were established at the deepest width and depth (not visible) of the acetabulum and the femoral head center.

7.2.5 Material Parameters and Pre-Processing

Each component was imported to finite element analysis software (ANSYS 12.1, ANSYS Inc., Canonsburg, PA, USA) and each model was meshed with SOLID187 elements – a ten-node tetrahedral element. Three bone (1-3; Figure 7.2) and three soft tissue (A-C) modelling parameters were considered and reconstructed (Table 7.1), for a total of nine pre-processed models:

1) **Cortical and trabecular bone assembly:** where both cortical and trabecular bone models were included and considered as two separate homogeneous, isotropic models in the each of the femur and pelvis components [10, 37, 38].
2) **Cortical shell model (trabecular bone removed):** where homogeneous trabecular components were neglected. A Boolean operation removed the trabecular components from the femur and pelvis, resulting in a homogeneous, isotropic cortical shell model with varying thickness [3].
3) **Heterogeneous bone model:** where material properties were based on subject-specific apparent density, using the calibration phantom and quantitative mapping. Properties were

determined using a density mapping script (Bonemat v3.1, Istituto Ortopedico Rizzoli, Bologna, Italy) resulting in a heterogeneous, isotropic bone model [39, 42]. Meshes were first imported into the bone density mapping software and a density-elasticity relationship assigned unique elastic moduli to individual elements of the entire model, based on the conversion from the densitometry calibration (ρ_{CT}) to the corrected apparent density (ρ_{ash}).

A) **Linear-elastic cartilage and labrum:** where both cartilage and labrum were modeled as linear-elastic and isotropic [10, 14].

B) **Hyperelastic cartilage and labrum:** where cartilage and labrum were modeled as Neo-Hookean, hyperelastic and incompressible models [21, 32].

C) **Orthotropic cartilage and labrum:** where linear-elastic, orthotropic properties were assigned to the femoral cartilage, acetabular cartilage, and labrum [5, 14, 17].

Biphasic formulations were not considered for soft tissue parameters. The hyperelastic soft tissues was configured to a mixed formulation with constant hydrostatic pressure (KEYOPT(6) = 1, hyperelasticity), with large deformations considered during simulation. Bone and soft tissue models started with a nominal element size of 3 and 2 mm, respectively, and then refined to ensure mesh sensitivity and convergence. Element sizes and counts were similar among modelling parameters, for each of the bone and soft tissue models, with the exception of the cortical shell assembly, which had a reduced total element count due to the excluded trabecular bone.

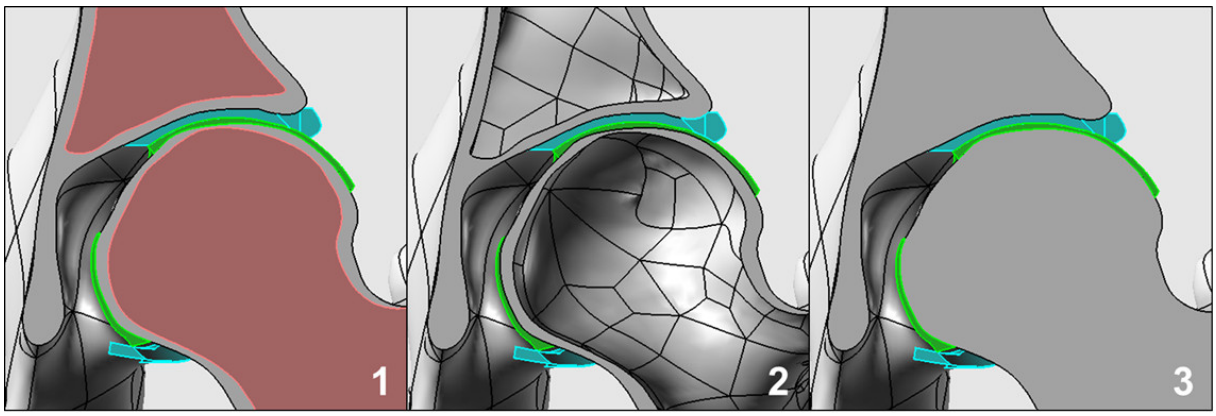

Figure 7.2. Section view of the left hip joint assembly in the frontal plane showing the bone (grey), acetabular cartilage and labrum (blue), and femoral cartilage (green) components in the: 1) cortical (grey) and trabecular (red) bone assembly; 2) cortical shell model, with the trabecular bones removed; and 3) heterogeneous model, that incorporated subject-specific bone density values throughout the entire bone.

Table 7.1. Summary of material properties for each bone and soft tissue modelling parameter

Modelling Parameter	Component	Material Properties	References
1) Cortical and trabecular bone assembly	Cortical bone	E_{cort} = 17 GPa ν_{cort} = 0.29	Chegini et al. 2009 Rudman et al. 2006 Russell et al. 2006
	Trabecular bone	E_{trab} = 100 MPa, ν_{trab} = 0.3	
2) Cortical shell model	Cortical bone	E_{cort} = 17 GPa, ν_{cort} = 0.29	Anderson et al. 2010
3) Heterogeneous bone model	Cortical and trabecular bone	$E = a + b\rho_{ash}^{c}$ based on empirical density-elasticity relationships	Carter and Hayes 1977 Morgan et al. 2003 Schileo et al. 2008 Taddei et al. 2007
A) Linear-elastic cartilage and labrum	Cartilage	$E_{cartilage}$ = 12 MPa, $\nu_{cartilage}$ = 0.45	Chegini et al. 2009 Ferguson et al. 2001
	Labrum	E_{labrum} = 20 MPa, ν_{labrum} = 0.4	
B) Hyperelastic cartilage and labrum	Cartilage and labrum	G = 13.6 MPa, K = 1.36 GPa, D_1 = 0	Henak et al. 2011 Park et al. 2004
C) Orthotropic cartilage and labrum	Femoral cartilage	E_1 = 1.18 MPa, $E_2 = E_3$ = 8.5 MPa; $\nu_{12} = \nu_{13}$ = 0.046, ν_{23} = 0.146; G = 2.5 MPa	Athanasiou et al. 1994 Ferguson et al. 2001 Hellwig et al. 2016
	Acetabular cartilage	E_1 = 1.23 MPa, $E_2 = E_3$ = 8.5 MPa; $\nu_{12} = \nu_{13}$ = 0.044, ν_{23} = 0.146; G = 2.5 MPa	
	Labrum	E_1 = 0.157 MPa, E_2 = 26, E_3 = 3 MPa; $\nu_{12} = \nu_{13}$ = 0.04, ν_{23} = 0.1; G = 1.5 MPa	

7.2.6 Finite Element Simulation

Boundary conditions were fixed at the sectioned proximal diaphysis, pubis symphysis, and iliac crest, from the anterior to the posterior superior iliac spines. Contact between femoral and acetabular cartilage was modelled with a coefficient of friction of 0.01 [43]. A quasi-static loading scenario, using the highest resultant hip joint forces during terminal stance, was discretized for comparison. The femur model was oriented with respect to the pelvis model, using the kinematics data during the loading condition, with the hip contact forces applied at the femoral head, in the pelvic reference frame. Peak maximum shear stresses were examined for each participant's acetabular cartilage and labrum, as it could indicate adverse loading leading to cartilage failure [34] and across the cartilage-bone interface [4]. A convergence analysis was performed to ensure that the refined mesh obtained an adequate solution, noting the relationship between the stress magnitude and the number of total elements (decrease in element size). Convergence was adequate if the change in stress magnitudes was less than 5%, with increasing

element refinement. Unaveraged stresses were also verified as well and compared with the averaged integration point results, to ensure that meshes were sufficiently refined.

7.3 Results

The anatomical parameters measured from the segmented models were similar to its associated CT data, confirming that the bone models were accurate geometric representations (Table 7.2). The cartilage and labrum geometries were identical for each simulated condition. The quasi-static loading condition was simulated for the terminal stance phase. After mesh refinement for each modelling parameter, the number of elements was substantially higher for the heterogeneous bone model (150,652 ± 160) and cortical and trabecular bone assembly (141,205 ± 112), compared to the cortical shell model (102,488 ± 93). For the nodal integration points, the unaveraged stresses were within 2% of the averaged stresses.

Table 7.2. Anatomical parameters measured from the original CT data and the segmented model

Anatomical Parameters	CT Data	Segmented Model
Axial 3:00 alpha angle (°)	45	46
Radial 1:30 alpha angle (°)	55	55
Femoral head-neck offset (mm)	9	8
Femoral neck-shaft angle (°)	130	129
Medial proximal femoral angle (°)	82	81
Femoral torsion (°)	4	5
Acetabular version (°)	17	19
Lateral center-edge angle (°)	31	30

The combination of heterogeneous bone with hyperelastic soft tissues had the highest absolute peak maximum shear stress (5.8 MPa; Figure 7.3), located in the anterolateral quadrant (Figure 7.4); while the cortical and trabecular bone assembly with orthotropic soft tissues had the lowest peak maximum shear stress (4.0 MPa; Figure 7.3), also in the anterolateral acetabulum (Figure 7.4). The cortical and trabecular bone assembly had the largest variability in peak maximum shear stresses (4.0 – 5.0 MPa) and largest percent differences, among soft tissue parameters (2.0 – 22.2%; Table 7.3). The heterogeneous, subject-specific bone density models showed moderate variability (4.9 – 5.8 MPa, 7.1 – 16.8%) and showed slightly higher peak stresses, with stress distributions indicating secondary stress concentrations. Although the

cortical shell model had lower variability (5.1 – 5.4 MPa, 2.0 to 7.7%), there were abrupt changes in stress distributions, for each of the soft tissue modelling parameters, and no evident secondary stress concentrations.

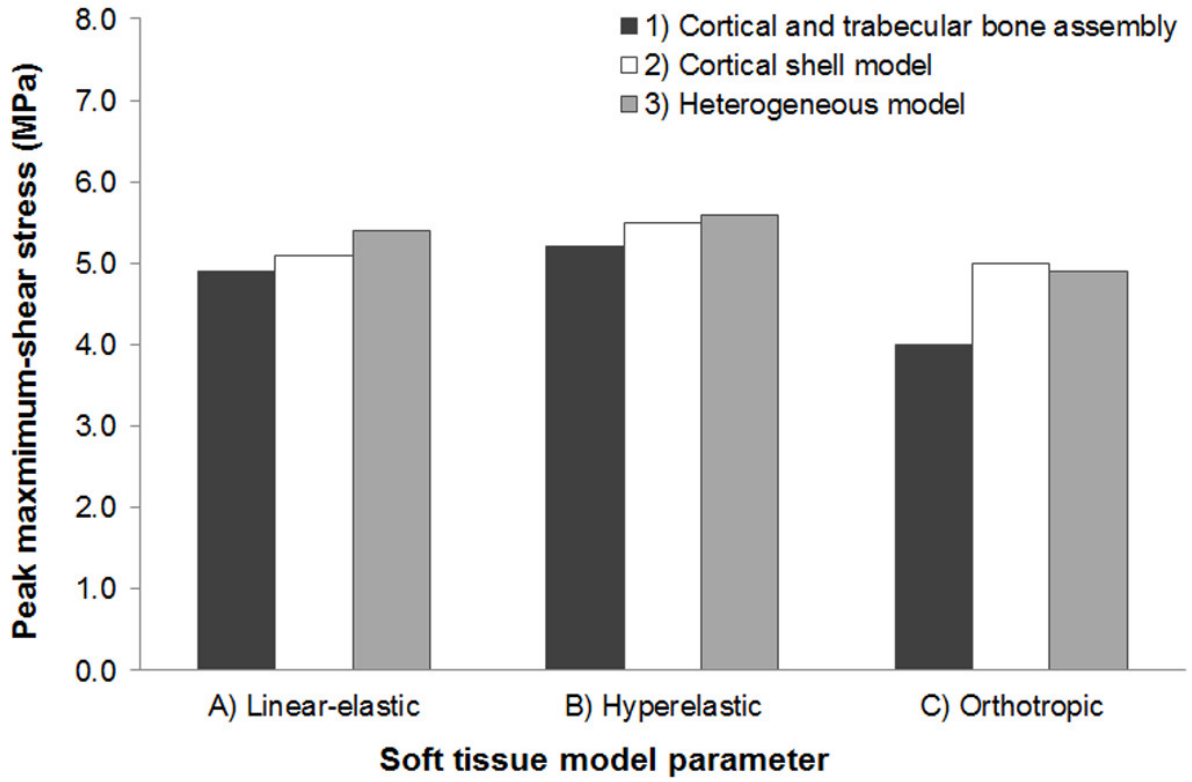

Figure 7.3. Peak maximum shear stress values for each combination of bone (1-3) and soft tissue (A-B) modelling parameter.

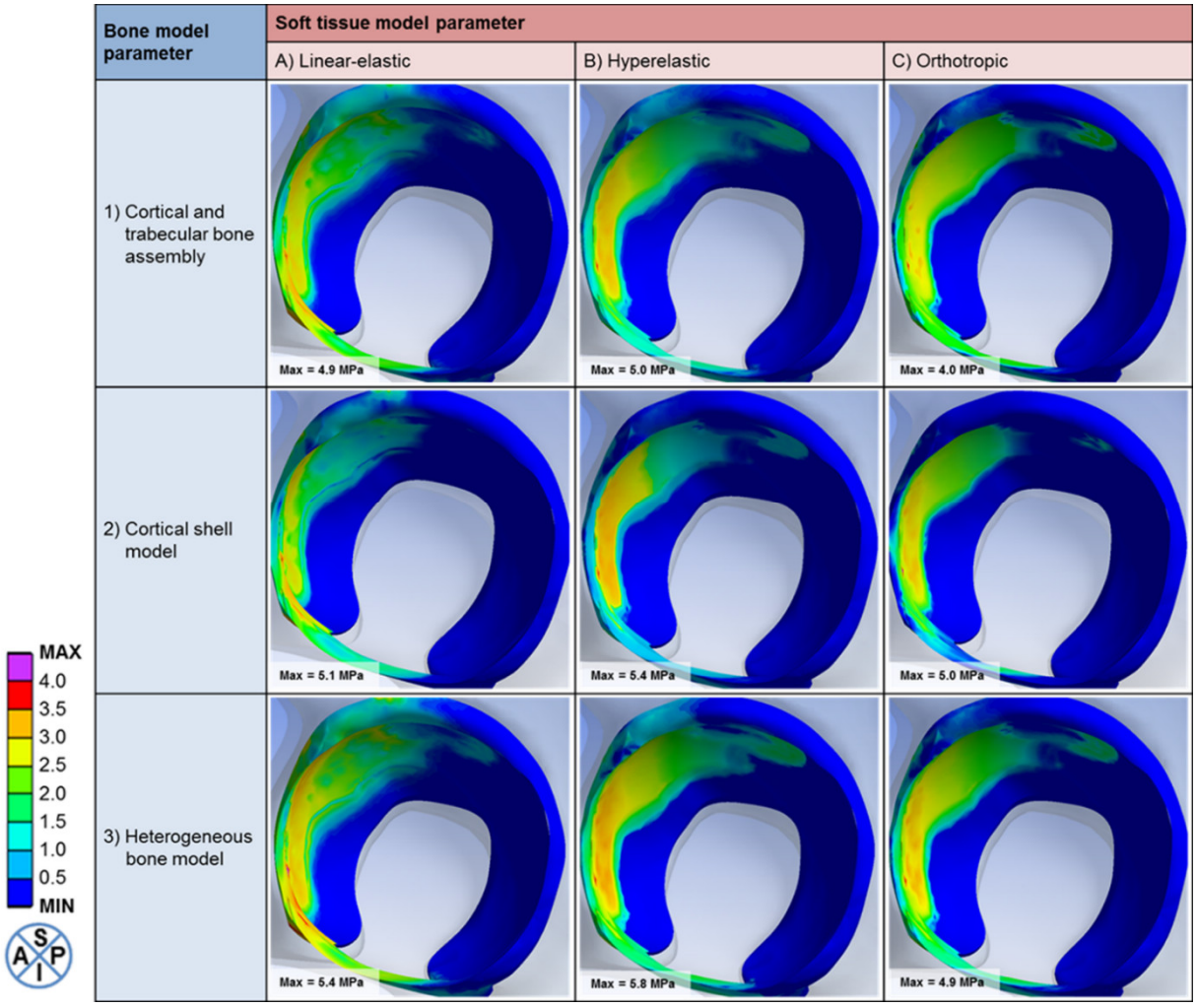

Figure 7.4. Sagittal view of a single participant's acetabular cartilage and labrum, showing the maximum shear stress distributions, for each bone (1-3) and soft tissue (A-C) modelling parameter. The reference locations are denoted by anterior (A), posterior (P), superior (S), and inferior (I). Peak stresses were localized in the anterolateral quadrant, with secondary stresses distributed in the anterosuperior quadrant and anterior labrum, dependent on the modelling parameters.

The linear-elastic soft tissues showed the lowest variability, between each of the bone modelling parameters, with stresses predominantly at the anteroinferior labrum, instead of the acetabular cartilage (4.9 – 5.4 MPa, 4.0 – 9.7%; Table 7.3). Although the hyperelastic models showed moderate variability (5.0 – 5.8 MPa, 7.7 – 14.8%), there was greatest amount of contact distribution, for each of the bone modelling parameters, with stresses concentrated at the anterolateral acetabulum; whereas changes in stress concentrations were most abrupt in the orthotropic soft tissues (4.0 – 4.9MPa, 2.0 – 20.2%).

Table 7.3. Comparison of percent differences between bone and soft tissue modelling parameters

Bone modelling parameter	**Percent difference between soft tissue modelling parameter**		
	A) Linear-elastic B) Hyperelastic	B) Hyperelastic C) Orthotropic	A) Linear-elastic C) Orthotropic
1) Cortical and trabecular bone assembly	2.0%	22.2%	20.2%
2) Cortical shell model	5.7%	7.7%	2.0%
3) Heterogeneous model	7.1%	16.8%	9.7%
Percent difference between bone modelling parameter	**Soft tissue modelling parameter**		
	A) Linear-elastic	B) Hyperelastic	C) Orthotropic
1) Cortical and trabecular bone assembly 2) Cortical shell model	4.0%	7.7%	22.2%
2) Cortical shell model 3) Heterogeneous model	5.7%	7.1%	2.0%
1) Cortical and trabecular bone assembly 3) Heterogeneous model	9.7%	14.8%	20.2%

7.4 Discussion

The intention of the study was to examine the influence of various bone and soft tissue material modelling parameters on hip joint stresses, while maintaining hip joint geometries and loading conditions consistent for all conditions. Although subject-specific reconstructions are sometimes avoided due to time consuming segmentations, it may be important to incorporate geometries that accurately reflect patient-specific demographics to predict contact stresses. We examined

differences in stress characteristics among each bone and soft tissues material modelling parameter, using the same subject-specific hip joint geometries and loading condition. The bone and soft tissue geometries were extracted from imaging data and, along with the mesh refinement parameters and boundary conditions, were consistent for all simulations. The joint loading condition was implemented as hip joint contact forces and was also consistent for all simulations. We accounted for differences in cartilage thickness in the models, knowing that femoral and acetabular cartilage are non-uniformly distributed and each have different thicknesses [23, 28].

We compared conventional soft tissues parameters and considered cartilage as a whole-body layer under quasi-static, non-cyclic loading parameters, where in many previous studies, simplified isotropic properties were often implemented [2, 3, 10, 37]. Various articular cartilage models in previous simulations also focused on biphasic [15, 17] or poroelastic, fibril-reinforced properties [12, 13, 40]. It may be interesting to further investigate stress consolidation due to fluid exudation and intermittent hydrostatic pressures in the future; however, may require a reduced axisymmetric hip joint model [12, 13, 40].

Our cortical and trabecular bone assembly implemented conventional principles to model linear-elastic, isotropic bone components [9, 10, 37, 38], but demonstrated the largest variability in peak maximum shear stresses, between each soft tissue parameter. The stress magnitudes were slightly lower than previous reports, as we reported peak maximum shear stresses, which tended to be consistently lower than contact pressures and von Mises stresses, reported in previous findings. The increased stresses at the anteroinferior labrum may be attributed to the linear response of the material property.

Our cortical shell and hyperelastic soft tissues model implemented the principles of Anderson and associates (2008, 2010), according to which the inclusion of the cortical bone, alone, should have been sufficient to predict adverse cartilage stresses. Similar to their study, we confirmed that including the trabecular bone did not show substantial differences in stress characteristics. Moreover, simulation time and mesh refinement were much shorter and simpler [2, 3]. Their studies used hexahedral elements for their cartilage geometry (~37,000 elements) and tetrahedral elements for their cortical shell mesh (~35,000 elements), which was far less than our element count (~ 103,600 elements). Similarly, we meshed our bones with tetrahedral elements, but decided to stay consistent with tetrahedral elements for soft tissue components. Although hexahedral elements are likely more stable and efficient for simplified femur models,

tetrahedral elements could produce a more accurate geometry [36]. Anderson and associates (2010) examined the effects of various bone and cartilage topologies and provided a well-defined benchmark for several subsequent in silico hip joint studies [1, 16, 18, 20-22]. Our peak maximum shear stresses were within range of Henak and associates' results [19], but again tended to be consistently lower than contact pressures [3]. Our cortical shell model was feasible to predict the absolute peak stress magnitude and location, compared with other bone modelling parameters, however, not sufficient to indicate secondary stress concentrations. For descriptive analyses involving several participant models, representative of specific demographics, it may be appropriate to implement this approach.

Our subject-specific bone density models showed slightly more distinct secondary stress concentrations that corresponded with areas of denser bone. With varying bone density, the stress differences demonstrated a level of sensitivity that the heterogeneous bone density model could capture, in comparison with the other two homogeneous structures. This approach may be more adequate for a cross-sectional analysis, comparing subject-specific hip joint stresses or pathological groups. We retrospectively examined the bone density distribution of the heterogeneous model and noticed that the elastic moduli varied slightly in the acetabular dome. Although not substantially variable in this healthy, non-pathological participant, heterogeneous bone models may be even more important when examining hip joints with various known pathologies (*e.g.*, femoroacetabular impingement, dysplasia, slipped capital femoral epiphysis), especially if the joint underwent osteoarthritic changes and subchondral bone remodelling [35, 41].

Our participant had an increased hip extension, during terminal stance, which resulted in prominent anterolateral hip joint stresses. Unlike previous finite element simulations, the joint contact forces that were implemented in this study were not acquired from instrumented prostheses data [7], which scaled bodyweight loading to the participant's activity; instead, hip contact forces were acquired from a musculoskeletal modelling simulation, which reflected joint loading predictions specific to our participant and activity [26]. The anterolateral stresses coincide with previous findings on anterior hip forces, during terminal stance and toe-off [24, 46, 47]. Lewis and associates (2010) indicated that muscle forces, together with ground reaction forces, contributed to substantially higher total forces during terminal stance phase; in which a greater hip extension resulted in elevated anterior hip joint force. Similarly, Wesseling and

associates' musculoskeletal model (2015) demonstrated a decreased hip contact force, during terminal stance, after reducing hip extension.

One of the limitations was the number of modelling parameters examined in this study. We selected conventionally used material modelling parameters from literature that simulated macroscopic effects of joint loading on cartilage contact stresses. It should be acknowledged that there are several other studies that implemented intricate modelling parameters and material properties, which posed other in-depth and purposeful research questions. This study also examined a single, healthy participant with no known lower-limb abnormalities, in efforts to compare parameterized material modelling parameters. Knowing that inter-subject variability is just as influential as parameterizing material properties [16], it would be interesting to examine the effects of each modelling parameter with a larger sample size or a group that could represent a patient-specific population. This would further confirm if a subject-specific, heterogeneous bone model could better predict symptomatic contact stresses.

The hip joint was imaged with 3-mm slices during MRI. Although this was a relatively large slice thickness, compared to CT imaging, the MRI was a high resolution sagittal sequence, adequate for assessing the cartilage thicknesses (in-plane pixel spacing of 0.469 mm). Similar to CT acquisition, MRI was also done in the supine position. To further assess the effects of hip morphologies on cartilage thickness, imaging during weight-bearing positions could be considered in the future [48], to incorporate the effects of natural postural position and loading.

Resultant hip joint loading was interpreted as hip contact forces applied to the femoral head, similar to load applications of Bergmann and associates' study (1993). Our hip joint contact forces were determined through static optimization and were marginally higher than forces measured from instrumented prostheses. However, differences in age, activity level, BMI, and pathology between our studied participant and participants from instrumented prostheses cohort (*i.e.*, older in age, moderate activity level, higher BMI, arthroplasty resulting from osteoarthritis) should be considered. The next step is to incorporate individual muscle contributions at their lines of action and through their wrapping points using a musculoskeletal model, which may yield higher resultant stresses, as opposed to a resultant net contact force at the hip joint center. Moreover, although it was not the purpose of this study, it would be interesting to select one combination of material modelling parameters, to further examine the effect of hip extension on anterior stresses during level walking [24]. This would lead to further

research in asymptomatic pathologies resulting in altered hip extension and pelvic range of motion, possibly delineating the associated risks with elevated anterior hip joint degeneration [46, 47].

There are several formal requirements that finite element simulations should meet to be deemed clinically applicable; which includes selecting and verifying the model parameters, as well as identifying the proper input parameters [44]. One of the ongoing challenges is the formulation of a robust finite element hip joint model that considers subject-specific parameters, hip joint loading, and geometric models, to predict adverse loading conditions [31]. From this study, a total of nine combinations of bone material parameters and soft tissue material properties were simulated and compared. Using the same geometries and hip joint loading parameters, for each combination of material properties, the differences in stress distributions and concentrations were relatively marginal (both visually and numerically). From the resulting similarities, the effects of simplified material modelling parameters leading to progressive joint degeneration has not yet been fully elucidated. The linear-elastic soft tissue models demonstrated the lowest variability in peak stress, while the cortical and trabecular bone assembly showed larger variability. It may be more feasible to implement either of these combinations for larger sample sizes, representative of healthy participant cohorts. Although the heterogeneous bone density model showed moderate variability, it showed the highest peak stress (with the hyperelastic soft tissues) and indicated more well-distributed stresses and secondary peaks. In combination with the non-linear, hyperelastic soft tissues, the heterogeneous bone model may be the most adequate to demonstrate inter-subject variability within a cohort or represent a patient-specific demographic with a known pathology or degenerative osteoarthritic changes. While there is variability to be expected with any combination of material properties and modelling parameters, it will always be important to understand relative differences between each combination and, if possible, account for these variabilities.

7.5 References

1. Abraham CL, Maas SA, Weiss JA, Ellis BJ, Peters CL, Anderson AE. A new discrete element analysis method for predicting hip joint contact stresses. *J Biomech*. 2013;46:1121-1127.
2. Anderson AE, Ellis BJ, Maas SA, Peters CL, Weiss JA. Validation of finite element predictions of cartilage contact pressure in the human hip joint. *J Biomech Eng*. 2008;130:051008.
3. Anderson AE, Ellis BJ, Maas SA, Weiss JA. Effects of idealized joint geometry on finite element predictions of cartilage contact stresses in the hip. *J Biomech*. 2010;43:1351-1357.
4. Ateshian GA, Henak CR, Weiss JA. Toward patient-specific articular contact mechanics. *J Biomech*. 2015;48:779-786.
5. Athanasiou KA, Agarwal A, Dzida FJ. Comparative study of the intrinsic mechanical properties of the human acetabular and femoral head cartilage. *J Orthop Res*. 1994;12:340-349.
6. Behrens BA, Nolte I, Wefstaedt P, Stukenborg-Colsman C, Bouguecha A. Numerical investigations on the strain-adaptive bone remodelling in the periprosthetic femur: influence of the boundary conditions. *Biomed Eng Online*. 2009;8:7.
7. Bergmann G, Graichen F, Rohlmann A. Hip joint loading during walking and running, measured in two patients. *J Biomech*. 1993;26:969-990.
8. Brand RA. Joint contact stress: a reasonable surrogate for biological processes? *Iowa Orthop J*. 2005;25:82-94.
9. Cardiff P, Karac A, Fitzpatrick D, Flavin R, Ivankovic A. Development of a Hip Joint Model for Finite Volume Simulations. *J Biomech Eng*. 2013;136:011006.
10. Chegini S, Beck M, Ferguson SJ. The effects of impingement and dysplasia on stress distributions in the hip joint during sitting and walking: a finite element analysis. *J Orthop Res*. 2009;27:195-201.
11. Day WH, Swanson SA, Freeman MA. Contact pressures in the loaded human cadaver hip. *J Bone Joint Surg Br*. 1975;57:302-313.
12. Ferguson SJ, Bryant JT, Ganz R, Ito K. The acetabular labrum seal: a poroelastic finite element model. *Clin Biomech (Bristol, Avon)*. 2000;15:463-468.
13. Ferguson SJ, Bryant JT, Ganz R, Ito K. The influence of the acetabular labrum on hip joint cartilage consolidation: a poroelastic finite element model. *J Biomech*. 2000;33:953-960.
14. Ferguson SJ, Bryant JT, Ito K. The material properties of the bovine acetabular labrum. *J Orthop Res*. 2001;19:887-896.
15. Garcia JJ, Cortes DH. A nonlinear biphasic viscohyperelastic model for articular cartilage. *J Biomech*. 2006;39:2991-2998.
16. Harris MD, Anderson AE, Henak CR, Ellis BJ, Peters CL, Weiss JA. Finite element prediction of cartilage contact stresses in normal human hips. *J Orthop Res*. 2012;30:1133-1139.
17. Hellwig FL, Tong J, Hussell JG. Hip joint degeneration due to cam impingement: a finite element analysis. *Comput Methods Biomech Biomed Engin*. 2016;19:41-48.
18. Henak CR, Abraham CL, Anderson AE, Maas SA, Ellis BJ, Peters CL, Weiss JA. Patient-specific analysis of cartilage and labrum mechanics in human hips with acetabular dysplasia. *Osteoarthritis Cartilage*. 2014;22:210-217.
19. Henak CR, Ateshian GA, Weiss JA. Finite element prediction of transchondral stress and strain in the human hip. *J Biomech Eng*. 2014;136:021021.
20. Henak CR, Carruth ED, Anderson AE, Harris MD, Ellis BJ, Peters CL, Weiss JA. Finite element predictions of cartilage contact mechanics in hips with retroverted acetabula. *Osteoarthritis Cartilage*. 2013;21:1522-1529.
21. Henak CR, Ellis BJ, Harris MD, Anderson AE, Peters CL, Weiss JA. Role of the acetabular labrum in load support across the hip joint. *J Biomech*. 2011;44:2201-2206.

22. Henak CR, Kapron AL, Anderson AE, Ellis BJ, Maas SA, Weiss JA. Specimen-specific predictions of contact stress under physiological loading in the human hip: validation and sensitivity studies. *Biomech Model Mechanobiol*. 2014;13:387-400.

23. Kurrat HJ, Oberländer W. The thickness of the cartilage in the hip joint. 1978;126:145-155.

24. Lewis CL, Sahrmann SA, Moran DW. Effect of hip angle on anterior hip joint force during gait. *Gait Posture*. 2010;32:603-607.

25. Macirowski T, Tepic S, Mann RW. Cartilage stresses in the human hip joint. *J Biomech Eng*. 1994;116:10-18.

26. Mantovani G, *Hip Joint Contact Load and Muscle Force in Femoroacetabular Impingement Population*, 2016, University of Ottawa: Ottawa. p. 182.

27. Mantovani G, Ng KCG, Lamontagne M. Regression Models to Predict Hip Joint Centers in Pathological Hip Population. *Gait Posture*. 2015;44:48-54.

28. Mechlenburg I, Nyengaard JR, Gelineck J, Soballe K. Cartilage thickness in the hip joint measured by MRI and stereology--a methodological study. *Osteoarthritis Cartilage*. 2007;15:366-371.

29. Mizrahi J, Solomon L, Kaufman B, Duggan T. An experimental method for investigating load distribution in the cadaveric human hip. 1981;63-B:610-613.

30. Ng KCG, Lamontagne M, Labrosse MR, Beaulé PE. Comparison of anatomical parameters of cam femoroacetabular impingement to evaluate hip joint models segmented from CT data. *Comput Methods Biomech Biomed Eng Imaging Vis*. 2016;1-10.

31. Ng KCG, Lamontagne M, Labrosse MR, Beaulé PE. Hip Joint Stresses Due to Cam-Type Femoroacetabular Impingement: A Systematic Review of Finite Element Simulations. *PLoS One*. 2016;11:e0147813.

32. Park S, Hung CT, Ateshian GA. Mechanical response of bovine articular cartilage under dynamic unconfined compression loading at physiological stress levels. *Osteoarthritis Cartilage*. 2004;12:65-73.

33. Radcliffe IA, Taylor M. Investigation into the affect of cementing techniques on load transfer in the resurfaced femoral head: a multi-femur finite element analysis. *Clin Biomech (Bristol, Avon)*. 2007;22:422-430.

34. Radin EL, Burr DB, Caterson B, Fyhrie D, Brown TD, Boyd RD. Mechanical determinants of osteoarthrosis. *Semin Arthritis Rheum*. 1991;21:12-21.

35. Radin EL, Paul IL, Tolkoff MJ. Subchondral bone changes in patients with early degenerative joint disease. *Arthritis Rheum*. 1970;13:400-405.

36. Ramos A, Simoes JA. Tetrahedral versus hexahedral finite elements in numerical modelling of the proximal femur. *Med Eng Phys*. 2006;28:916-924.

37. Rudman KE, Aspden RM, Meakin JR. Compression or tension? The stress distribution in the proximal femur. *Biomed Eng Online*. 2006;5:12.

38. Russell ME, Shivanna KH, Grosland NM, Pedersen DR. Cartilage contact pressure elevations in dysplastic hips: a chronic overload model. *J Orthop Surg Res*. 2006;1:6.

39. Schileo E, Dall'ara E, Taddei F, Malandrino A, Schotkamp T, Baleani M, Viceconti M. An accurate estimation of bone density improves the accuracy of subject-specific finite element models. *J Biomech*. 2008;41:2483-2491.

40. Speirs AD, Beaule PE, Ferguson SJ, Frei H. Stress distribution and consolidation in cartilage constituents is influenced by cyclic loading and osteoarthritic degeneration. *J Biomech*. 2014;47:2348-2353.

41. Speirs AD, Beaule PE, Rakhra KS, Schweitzer ME, Frei H. Increased acetabular subchondral bone density is associated with cam-type femoroacetabular impingement. *Osteoarthritis Cartilage*. 2013;21:551-558.

42. Taddei F, Schileo E, Helgason B, Cristofolini L, Viceconti M. The material mapping strategy influences the accuracy of CT-based finite element models of bones: an evaluation against experimental measurements. *Med Eng Phys*. 2007;29:973-979.

43. Unsworth A, Dowson D, Wright V. The Frictional Behavior of Human Synovial Joints—Part I: Natural Joints. 1975;97:369-376.

44. Viceconti M, Olsen S, Nolte LP, Burton K. Extracting clinically relevant data from finite element simulations. *Clin Biomech (Bristol, Avon)*. 2005;20:451-454.

45. von Eisenhart-Rothe R, Eckstein F, Muller-Gerbl M, Landgraf J, Rock C, Putz R. Direct comparison of contact areas, contact stress and subchondral mineralization in human hip joint specimens. *Anat Embryol (Berl)*. 1997;195:279-288.

46. Wesseling M, de Groote F, Meyer C, Corten K, Simon JP, Desloovere K, Jonkers I. Gait alterations to effectively reduce hip contact forces. *J Orthop Res*. 2015;33:1094-1102.

47. Wesseling M, Meyer C, de Groote F, Corten K, Simon JP, Desloovere K, Jonkers I. Gait alterations can reduce the risk of edge loading. *J Orthop Res*. 2016;34:1069-1076.

48. Wilson DR, McWalter EJ, Johnston JD. The measurement of joint mechanics and their role in osteoarthritis genesis and progression. *Rheum Dis Clin North Am*. 2013;39:21-44.

49. Yoshida H, Faust A, Wilckens J, Kitagawa M, Fetto J, Chao EY. Three-dimensional dynamic hip contact area and pressure distribution during activities of daily living. *J Biomech*. 2006;39:1996-2004.

IV Modelling of Clinically Relevant Scenarios

8 Increased Hip Joint Stresses Resulting from a Cam Deformity and Decreased Femoral Neck-Shaft Angle during Level Walking

K. C. Geoffrey Ng [1] | Giulia Mantovani [2] | Mario Lamontagne [2,1] | Michel R. Labrosse [1] | Paul E. Beaulé [3]

[1] Department of Mechanical Engineering | University of Ottawa | Ottawa, Ontario, Canada

[2] School of Human Kinetics | University of Ottawa | Ottawa, Ontario, Canada

[3] Division of Orthopaedic Surgery | University of Ottawa | Ottawa, Ontario, Canada

Contents of this chapter published as an article in *Clinical Orthopaedics and Related Research*® | August 2016

Ng KCG, Mantovani G, Lamontagne M, Labrosse MR, Beaulé PE, Hip Joint Stresses Resulting from a Cam Deformity and Femoral Neck-Shaft Angle during Level Walking. *Clin Orthop Relat Res*, 2016; In Press. DOI: 10.1007/s11999-016-5038-2

8.0 Abstract

Background: It is still unclear why many individuals with a cam morphology of the hip do not experience pain. It was recently reported that a decreased femoral neck-shaft angle may also be associated with hip symptoms. However, it is unclear what effects do different femoral neck-shaft angles have on hip joint stresses in symptomatic and asymptomatic individuals with cam morphology.

Questions/Purposes: We examined the effects of the cam morphology and femoral neck-shaft angle on hip stresses during walking by asking: (1) Are there differences in hip stress characteristics among symptomatic patients with cam morphology, asymptomatic individuals with cam morphology, and individuals without cam morphology? (2) What are the effects of high and low femoral neck-shaft angles on stresses?

Methods: Six participants were selected, from a larger cohort, and their cam morphology and femoral neck-shaft angle parameters were measured from CT data. Two participants were included in one of three groups: 1) symptomatic with a cam morphology, 2) asymptomatic with a cam morphology, 3) asymptomatic control with no cam morphology; with one participant having the highest femoral neck-shaft angle, whereas the other participant having the lowest, in each subgroup. Subject-specific finite element models were reconstructed and simulated during the stance phase, near push-off, to examine maximum shear stresses on the acetabular cartilage and labrum.

Results: The symptomatic group with cam morphology indicated high peak stresses (6.3–9.5 MPa), compared with the asymptomatic (5.9–7.0 MPa) and control groups (3.8–4.0 MPa). Differences in femoral neck-shaft angle influenced both symptomatic and asymptomatic groups; participants with the lowest femoral neck-shaft angles had higher peak stresses in their respective subgroups. There were no differences among control models.

Conclusions: The study suggests that individuals with a cam morphology and varus femoral neck angle are subject to higher mechanical stresses than those with a normal femoral neck angle. Individuals with a cam morphology and decreased femoral neck-shaft angle are likely to experience severe hip stresses. Although asymptomatic participants with cam morphology had elevated stresses, a higher femoral neck-shaft angle was associated with lower stresses. Future research should examine larger amplitudes of motion to assess adverse

8.1 Introduction

The pathomechanism of the cam-type hip morphology, which in some patients is associated with femoroacetabular impingement (FAI), has been intensely investigated to better understand anatomic and functional parameters associated with symptomatology. Cam deformity, characterized by an aspherical femoral head-neck junction, has been suggested as a cause of labral-chondral damage as well as an early cause for hip osteoarthritis [11, 17]. Several studies suggest that severe cam deformity, as defined by larger alpha angles, could indicate which individuals may be at risk of developing early hip pain and arthritis [1, 22]. Although many symptomatic individuals with a cam morphology experienced different hip kinematics, notably during level walking [21] and maximal squatting [23, 24], other individuals with a cam morphology may not experience any clinical signs or symptoms [2, 12, 13, 19, 22, 33, 45]. In addition to elevated alpha angles, it was recently noted that a decreased femoral neck-shaft angle might be indicative of early symptoms as well [13, 33, 34, 45]; however, it is unclear what combined effects a large cam morphology and decreased femoral neck-shaft angle have on resultant hip stresses. To our knowledge, no study has incorporated these subject-specific anatomic parameters with computational, finite element methods to determine the effects on mechanical hip stresses.

According to a recent systematic review on finite element simulations of cam FAI [36], there has been limited work pertaining to finite element simulations that examine cam FAI and, moreover, many of the previous studies used idealized hip geometries [8, 15] as opposed to models reconstructed from subject-specific imaging data. It has also been demonstrated that subchondral bone density is higher in individuals with a symptomatic or asymptomatic cam morphology [52, 53]; however, previous finite element simulations neglected subject-specific bone material properties. Previous finite element studies also attempted to delineate pathomechanics of cam FAI using hip reaction loads from instrumented hip prostheses [8, 15, 18] or from inverse dynamics [37]. However, inverse dynamics are limited to external and inertial forces, typically neglecting muscle activity [26, 54], whereas rigid body dynamics and musculoskeletal modeling include gravitational, inertial, and muscle forces to calculate joint contact loads.

Because elevated mechanical stresses in the subchondral bone may play a pathomechanical role in cam FAI [42, 52, 53], subject-specific input parameters (perhaps

including geometries, material properties, joint loading) are critical to adequately represent a patient demographic. It would also be necessary to examine hip stresses in individuals with an asymptomatic cam morphology to determine if stress magnitudes and distributions of these individuals are comparable to either an at-risk, symptomatic population or healthy control population without cam morphology. The purpose of this study therefore was to examine the combined effects of the cam morphology and femoral neck-shaft angle on hip stresses during level walking. We specifically addressed two research questions: (1) Are there any differences in hip stress characteristics among patients with cam morphology, asymptomatic individuals with cam morphology, and control individuals without cam morphology? (2) What are the effects of a high or low femoral neck-shaft angle on hip stresses for each respective subgroup?

8.2 Patients and Methods

Six male participants (n = 6, age = 32 ± 7 years, body mass index = 26 ± 3 kg/m^2), from a larger patient cohort (which consisted of 43 males [33]), were recruited through the senior orthopaedic surgeon's clinical practice (PEB). The cam morphology has been more prevalent in younger, athletic males [11]; therefore, the six participants in this study were male as well. Each participant underwent pelvic imaging using conventional CT scanners (Acquilion; Toshiba Medical Systems Corporation, Otawara, Japan; or Discovery CT750; GE Healthcare, Mississauga, Ontario, Canada) to confirm if they had a cam morphology, as indicated by either an axial 3:00 or radial 1:30 alpha angle greater than 50.5° or 60°, respectively [38, 44] (Figure 8.1). Participants were scanned in a supine position with a calibration phantom (Model 3; Mindways Software, Austin, TX, USA) placed under the lumbar vertebra for bone mineral densitometry. Participants who initially presented with clinical symptom, impingement sign, and a cam morphology on CT images were considered as symptomatic participants, who were then scheduled for surgery. The other participants were recruited as volunteers, who showed no hip pain, clinical impingement signs, and were unaware whether they had a cam morphology. From these volunteers, participants who showed a cam morphology on CT images but did not present with clinical signs or symptoms were considered as asymptomatic, whereas participants with no cam morphology and no clinical signs or symptoms were considered as control subjects. Each participant's alpha angles were assessed by a senior-level musculoskeletal radiologist (KSR), where for each symptomatic, asymptomatic, or control participant, the affected side was defined

by the hip with symptoms, higher alpha angle, or smaller alpha angle, respectively. Each participant's affected hip underwent subsequent MRI (MAGNETOM Symphony; Siemens Healthcare GmbH, Erlangen, Germany), to determine cartilage thicknesses and labral contours. Any participant with a history of a major lower limb injury or musculoskeletal abnormality was excluded.

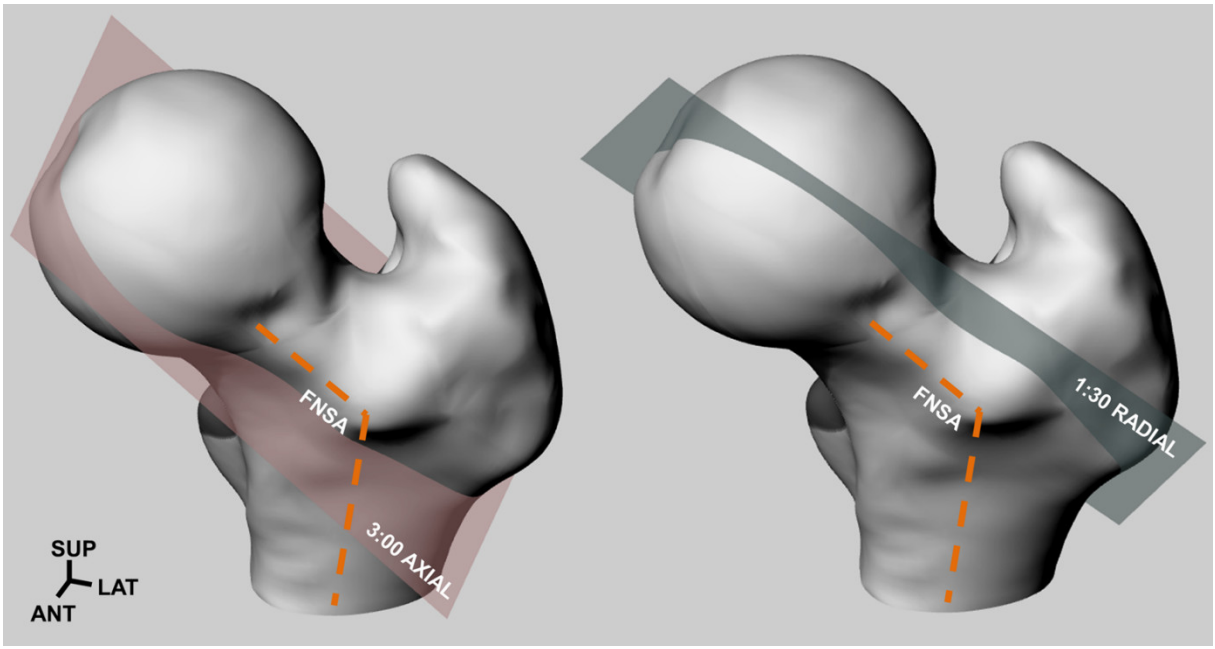

Figure 8.1. The cam morphology was determined by an alpha angle greater than 50.5° or 60° either in the 3:00 axial plane (left) or 1:30 radial plane (right), respectively. The femoral neck-shaft angle (FNSA) was also determined to examine the effects of a high and low femoral neck-shaft angle on each participant group.

In addition to the cam morphology, the femoral neck-shaft angle of each participant's affected hip was measured from their CT data [33], using a DICOM viewer (Onis 2.4; DigitalCore, Tokyo, Japan) to examine if the symptomatic group had a prominent decreased femoral neck-shaft angle, an anatomic characteristic associated with FAI symptomatology [33, 34] (Figure 8.1). Lateral center-edge angles were measured as well and confirmed to be normal (≤ 39°). Participants also completed pain questionnaires–Hip Disability and Osteoarthritis Outcome Score (HOOS) and WOMAC–to confirm symptoms. The pain questionnaires were used to assess any subjective differences in symptoms. We expected the symptomatic group to have lower pain questionnaire scores, compared to the asymptomatic and control groups (which should have scores near 100%). Based on the resultant anatomic and clinical indications, the larger cohort consisted of 12 symptomatic, 17 asymptomatic, and 14 control participants [33].

For this study, we selected two participants for each of the three groups from the larger cohort– one participant with the highest femoral neck-shaft angle and one with the lowest femoral neck-shaft angle for each of the symptomatic, asymptomatic, and control groups (Table 8.1). The study protocol was approved by the university and hospital research institute ethics boards. Participants provided informed consent before the study and all investigations were conducted ethically in conformity with research principles.

Table 8.1. Summary of clinical assessments and measured anatomical parameters for each symptomatic, asymptomatic, and control participant, with high (H) and low (L) femoral neck-shaft angle

Participant	Age (years)	BMI (kg/m^2)	HOOS Pain (%)	WOMAC Pain (%)	Axial 3:00 alpha angle (°)	Radial 1:30 alpha angle (°)	Femoral neck-shaft angle (°)
Symptomatic H	25	25	53	55	51	63	125
Symptomatic L	33	22	65	80	58	64	119
Asymptomatic H	28	27	100	100	52	66	134
Asymptomatic L	44	27	100	100	56	70	123
Control H	32	26	100	100	44	56	132
Control L	30	29	100	100	41	52	124

H = High femoral neck-shaft angle
L = Low femoral neck-shaft angle
HOOS = Hip Disability and Osteoarthritis Outcome Score
WOMAC = Western Ontario and McMaster Universities Arthritis Index

Before motion analysis, in efforts to minimize skin artifacts and pelvic misalignment during motion capture, surface radio-opaque markers were placed onto each participant's pelvic landmarks before CT imaging at the left and right anterosuperior iliac spines and posterosuperior iliac spines. Each participant performed level walking trials, at a self-selected pace, in the motion capture environment. Three-dimensional kinematics were recorded using a 10-camera motion capture system (MX-13; Vicon, Oxford, UK) with retroreflective markers placed on anatomic landmarks according to a modified Plug-in-Gait model [28]. Ground reaction forces of each participant's affected leg, during single stance, were captured using two stationary force plates (FP4060-08; Bertec, Columbus, OH, USA). The trajectories were filtered (Woltring, MSE = 15 mm^2) using motion analysis software (Nexus 1.8; Vicon) and ground reaction forces were filtered (zero-lag, fourth-order Butterworth, cut-off frequency 6 Hz) using numerical computational software (MATLAB R2014a; MathWorks, Nantick, MA, USA).

Muscle and hip contact forces were estimated using a musculoskeletal modeling program (OpenSim 3.1; SimTK, USA). We adapted a model, which consisted of the torso and lower body

segments [9], where the hip and lumbar spine were modelled as ball-and-socket joints, that contributed to a total of 23 degrees of freedom and 92 musculotendinous actuators [28]. Muscle forces were computed using a static optimization approach with a quadratic cost function [31] and resultant three-dimensional hip contact forces were calculated and expressed in the pelvic reference system [63].

Each participant's affected hip model was manually segmented from their CT data using image segmentation software (3D-Doctor 4.0; Able Software Corp, Lexington, MA, USA), including slices from the superior iliac crest to the proximal femur (Figure 8.2.A). The MRI was manually registered and centered on four control points of the target CT images, where the deepest width and depth of the acetabulum and the femoral head center were denoted as registration landmarks. The midpoint between the femoral and acetabular cartilages and their thicknesses were determined. The femoral cartilage, acetabular cartilage, and labrum were manually segmented. None of the participants indicated signs of osteoarthritis or joint space narrowing; therefore, cartilage was modeled as a smooth layer with no surface discrepancies. The segmented models were then resurfaced to reduce geometric artifacts using computer-aided design software (SolidWorks; Dassault Systèmes, Concord, MA, USA). Anatomic hip parameters of the resurfaced models were measured using computer-aided design software and compared with the original CT data, to confirm the accuracy of the resurfacing and modeling procedure [35].

Each participant's hip assembly was imported into finite element analysis software (ANSYS 12.1; ANSYS Inc, Canonsburg, PA, USA) and meshed with tetrahedral, SOLID187 elements. Bone material properties were based on subject-specific apparent density using the calibration phantom and quantitative mapping. Meshes were first imported into the bone density mapping software (Bonemat v3.1; Istituto Ortopedico Rizzoli, Bologna, Italy) and a density-elasticity relationship assigned unique elastic moduli to individual elements (Figure 8.2.B), for each individual participant model, based on the conversion from the densitometry calibration (ρ_{CT}) to the corrected density (ρ_{ash}), resulting in heterogeneous, isotropic bone models (Figure 8.2.C) [47, 56]. Cartilage and labrum were modeled as Neo-Hookean, hyperelastic materials [16, 40] with constant hydrostatic pressure (KEYOPT(6) = 1, hyperelasticity).

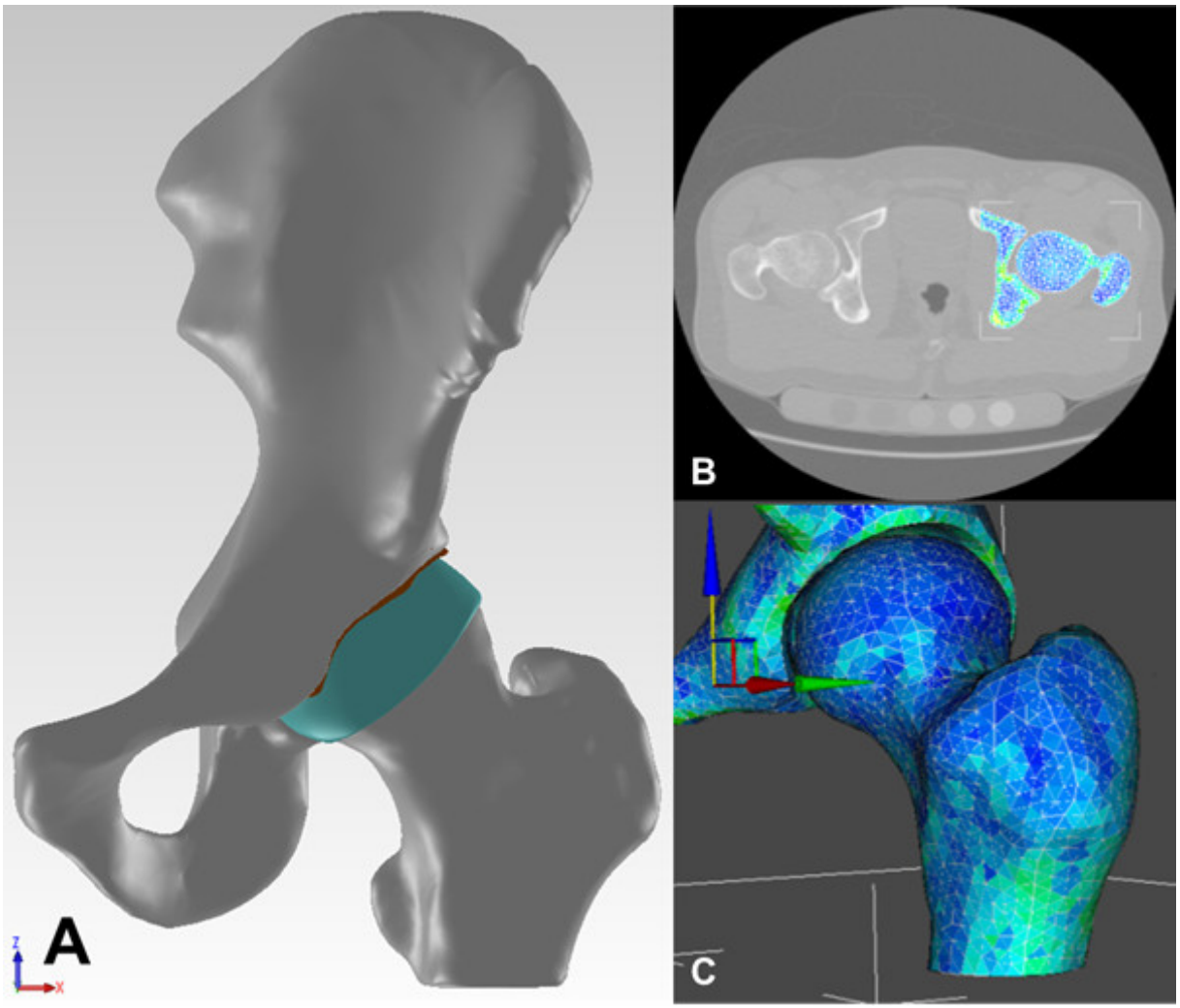

Figure 8.2. Frontal view of the segmented left hip assembly, from the superior iliac crest to the proximal diaphysis (**A**). The segmented model was resurfaced to reduce geometric artifacts and bone material properties were determined from and a density-elasticity relationship that assigned a unique elastic modulus to each individual element (**B**), that resulted in heterogeneous, isotropic bone models (**C**).

Bone and soft tissue models started with an element size of 3 and 2 mm, respectively, and were further refined to ensure mesh sensitivity. Mesh convergence was considered adequate if the change in stress magnitudes was less than 5%, with increasing element refinement. Unaveraged stresses were also compared with averaged integration point results, to ensure that the meshes were sufficiently refined. (The smallest resultant element size for the cartilage model were 0.22-0.74 mm.) Contacts between femoral and acetabular cartilages were modelled with a frictional coefficient of 0.01 [57]. Boundary conditions were fixed at the pubis symphysis and iliac crest (from anterior to posterior superior iliac spines) (Figure 8.3). The femur model was oriented using the kinematics data during the loading condition and was permitted to translate in

the loading direction [16, 37]. A quasistatic loading scenario, using the highest resultant hip forces during terminal stance, was selected for comparison with hip contact forces applied at the femoral head. Since cartilage may be most susceptible to shear stresses under quasi-static loading [27], maximum shear stresses were examined on each participant's acetabular cartilage and labrum to examine adverse loading conditions [15, 37]. A process flowchart from subject-specific input data to resultant hip stresses is summarized (Figure 8.4).

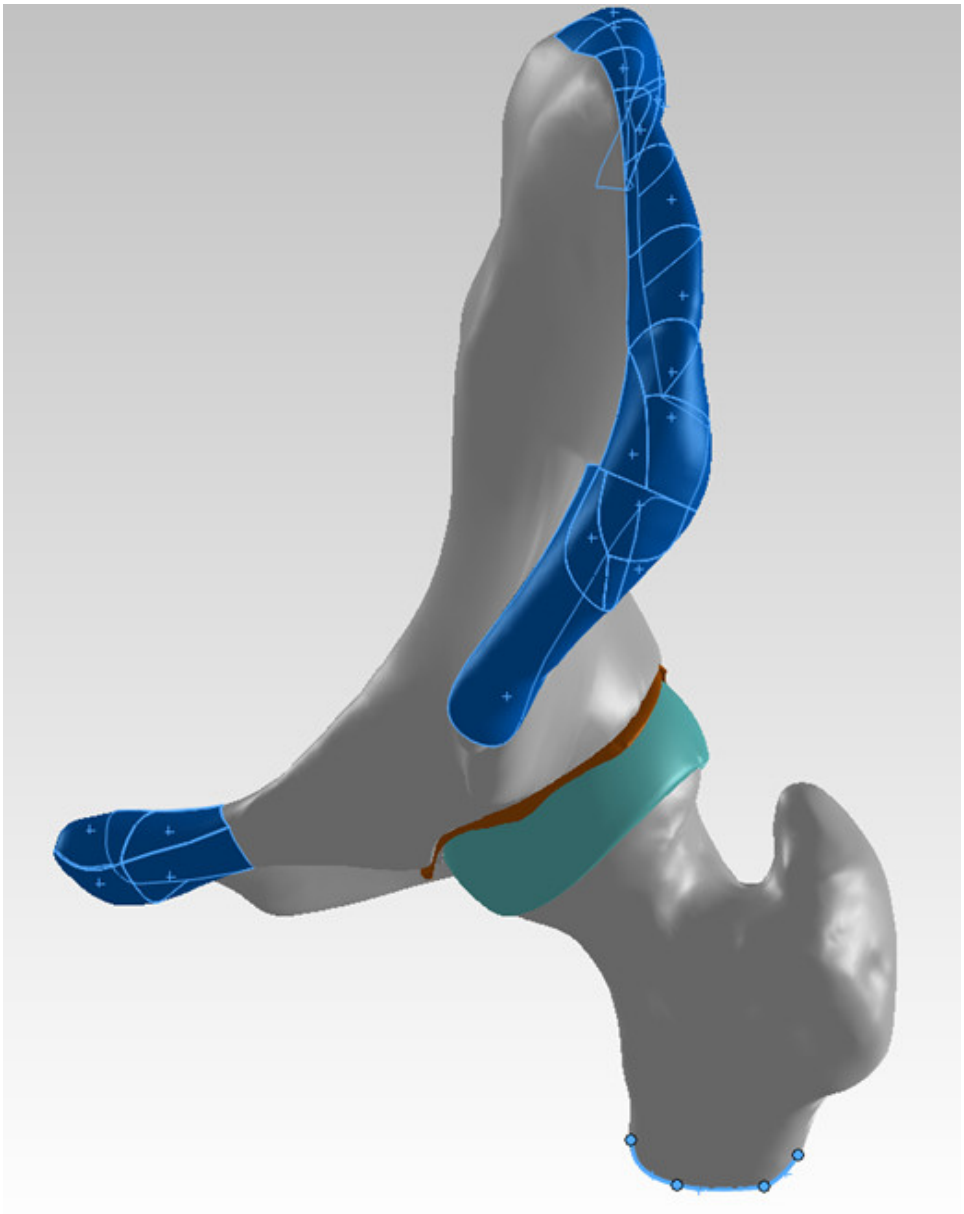

Figure 8.3. Boundary conditions were fixed at the pubis symphysis and iliac crest, from the anterior superior iliac spine to posterior superior iliac spine. The femur was oriented according to the kinematics data and was permitted to translate in the loading direction.

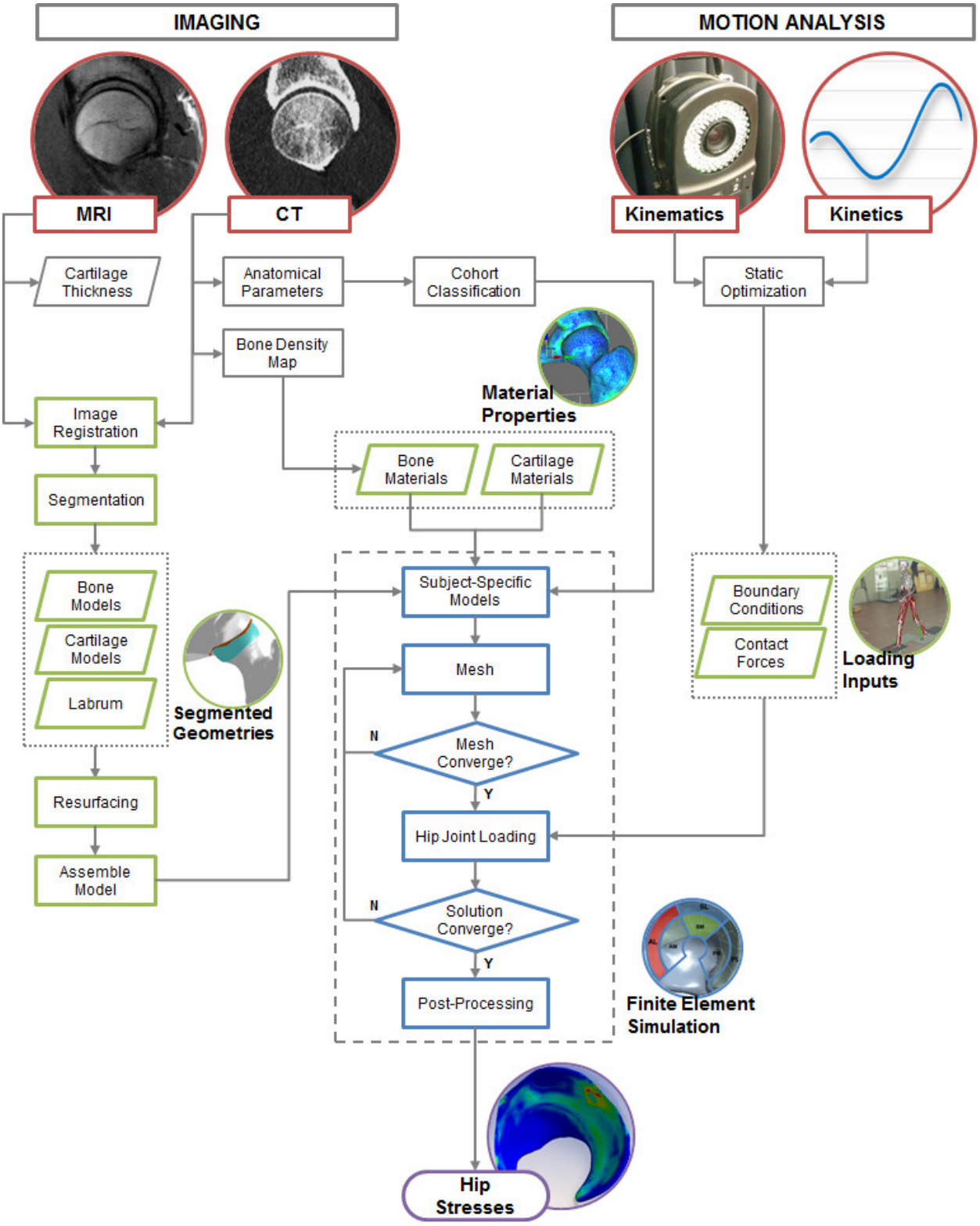

Figure 8.4. Process flowchart showing subject-specific input data used for the finite element simulations. The subject-specific hip geometries, material properties, and contact loads were combined and simulated to determine resultant hip stresses.

8.3 Results

The symptomatic and asymptomatic models showed higher maximum shear stresses than the controls. Both symptomatic participants indicated peak maximum shear stresses on the anterolateral cartilage (6.3–9.5 MPa), but also secondary posteroinferior stresses (Figure 8.5). Both asymptomatic participants showed moderate stress magnitudes in the superior and posterior cartilage (5.9–7.0 MPa), whereas the controls experienced the lowest stresses with more well-conforming contacts and dissipated distributions along the superior and posterior domes as well (3.8–4.0 MPa; Figure 8.5).

Differences in femoral neck-shaft angle influenced both cam morphology groups. The symptomatic participant with the lower femoral neck-shaft angle (119°) had the highest maximum shear stress in the anterolateral cartilage (9.5 MPa; Figure 8.6) with a high secondary peak stress in the posterior region (7.9 MPa) as well, whereas the symptomatic participant with the higher femoral neck-shaft angle (125°) showed a lower magnitude (6.3 MPa). The asymptomatic participant with the lowest femoral neck-shaft angle (123°) also had slightly higher peak stress (7.0 MPa) than the asymptomatic participant with the highest femoral neck-shaft angle (134°, 5.9 MPa). There were no substantial differences between the two controls.

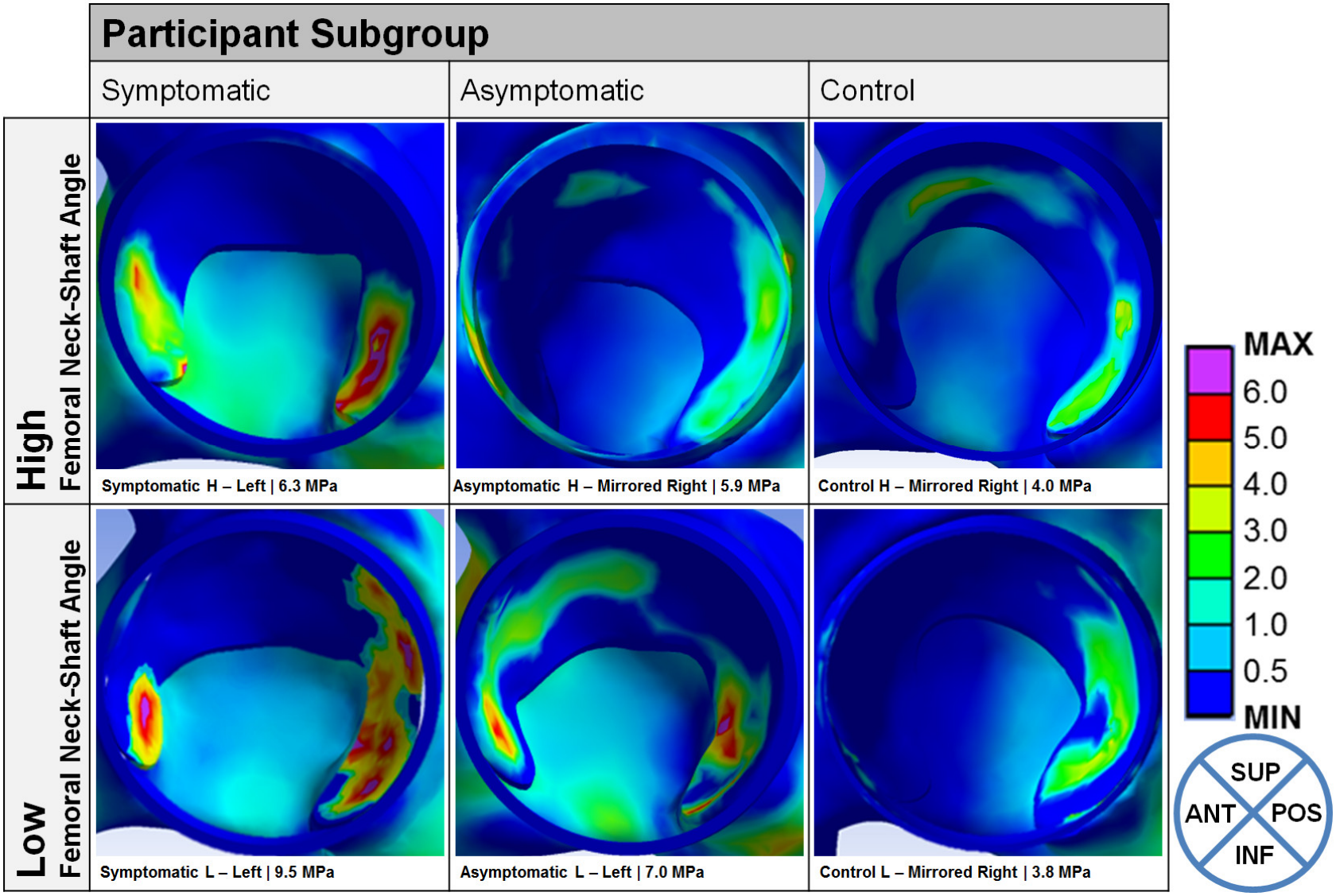

Figure 8.5. Sagittal view of the acetabular cartilage and labrum, from the resultant finite element simulations, showing the maximum shear stress distributions for each symptomatic, asymptomatic, and control participant with the highest (H = top row) and lowest (L = bottom row) femoral neck-shaft angle. The reference locations are denoted by anterior (ANT), posterior (POS), superior (SUP), and inferior (INF).

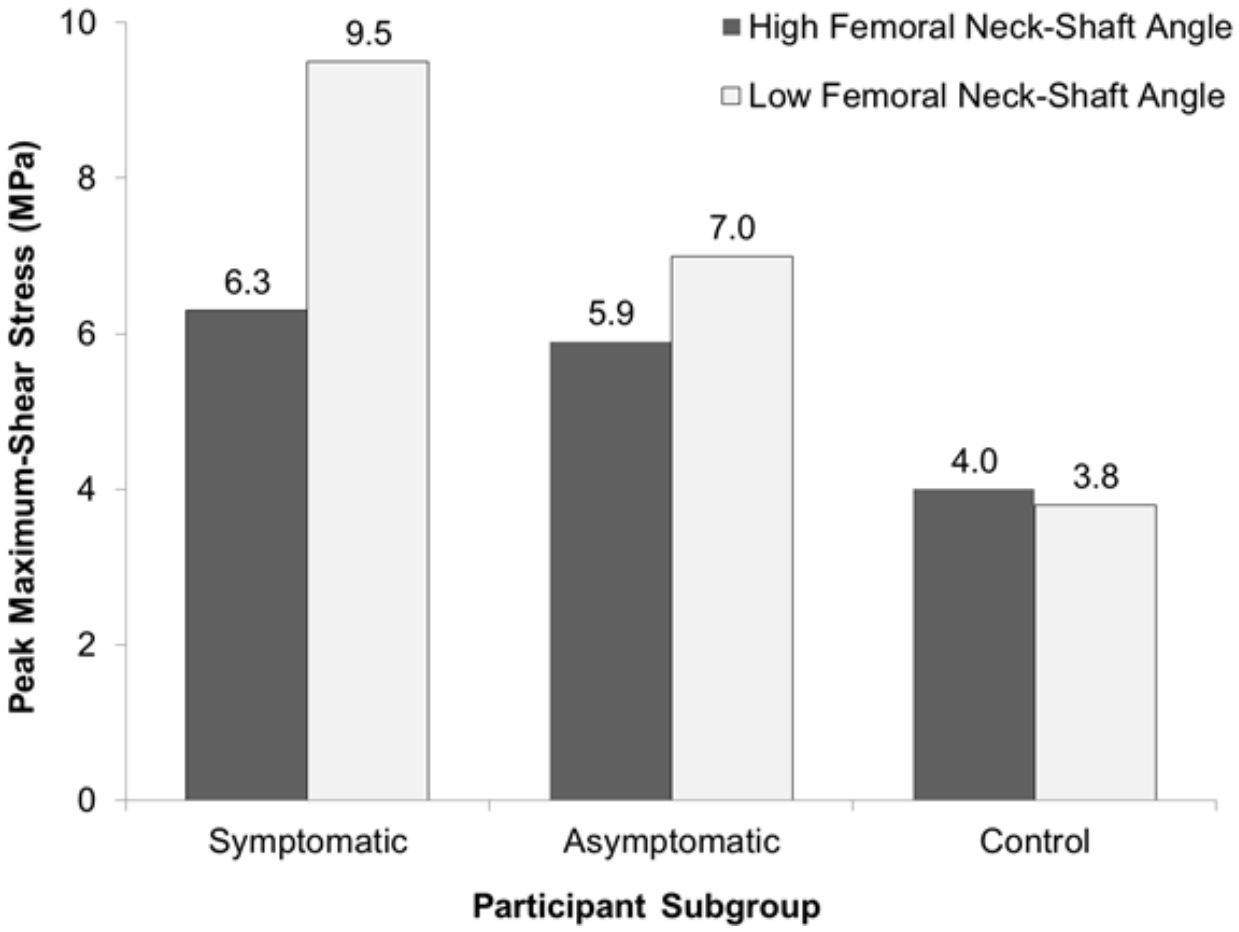

Figure 8.6. Graph indicating the peak maximum shear stress for each symptomatic, asymptomatic, and control participant with the highest and lowest femoral neck-shaft angle.

8.4 Discussion

It is unclear why certain individuals with cam deformities develop progressive degenerative changes and symptoms, whereas others remain asymptomatic for most of their lives [12, 19, 46, 55]. Gaining a better understanding of stresses in asymptomatic hips can provide critical insights into those who are at risk of arthritic changes. In an effort to address differences in the FAI population, we incorporated subject-specific anatomic parameters, geometries, material properties, and joint loading to determine if stresses resulting from an asymptomatic morphology share similarities with symptomatic or healthy individuals. We examined if decreased femoral neck-shaft angles could explain early symptoms resulting from adverse loading conditions. Although asymptomatic participants had elevated stresses, a higher femoral neck-shaft angle was associated with lower stresses despite a cam morphology.

Our study had certain limitations. First, there was slight overlap in femoral neck-shaft angles between the symptomatic and asymptomatic groups, that resulted in overlapping peak hip joint stresses as well. None of our symptomatic participants had a valgus neck to directly compare with upper limits of the asymptomatic and control groups (134° and 132°, respectively), whereas similarly, our asymptomatic and control participants did not have varus angles. The participants were selected from a larger cohort (n = 43), that examined differences in anatomical parameters between symptomatic, asymptomatic, and control participants [33]. From that study, the femoral neck-shaft angles of the asymptomatic (127 ± 3°; 123–134°) and control groups (128 ± 2°; 124–132°) were higher, in comparison with the symptomatic group (123 ± 2°; 119–125°; $\eta^2 = 0.496$, $p < 0.001$) [33]. It was interesting to note that higher stresses were not necessarily dependent on participant group or symptoms, but perhaps was more associated with femoral neck-shaft angle and a cam morphology. This might also further support the concept that a higher femoral neck-shaft angle decreases the risk of early symptoms [10, 33, 34, 49, 50]. We also accounted for the highest and lowest femoral neck-shaft angles in each group as opposed to examining the largest and smallest cam deformities.

Second, certain limitations were imposed by the small sample size. We captured the upper and lower neck angles, but a larger sample size would increase the robustness and differences among the subgroups, which may further delineate intersubject variability and correlate impingement severities with associated anatomical parameters (cam morphology and femoral neck-shaft angle). Due to this smaller sample size, we also did not match for BMI

between subgroups. We had a considerably small BMI range for each subgroup, thus were unable to observe the effects of varying BMI on hip joint stresses. It would be interesting to examine if varying BMIs would lead to higher hip joint stresses. Furthermore, since the cam morphology is prevalent males [11, 13], our larger cohort that we selected these participants from also consisted of male participants [33]. Future work to increasing the sample size and include female participants could examine the functional and anatomical variances.

Third, hip contact forces were also determined using static optimization [39, 41]. Previous studies indirectly validated and compared their results with contact forces from instrumented prostheses [7, 14, 26]. Our contact forces were marginally higher than those from instrumented prostheses, but differences in population characteristics, age, walking speed, and activity level should be considered [7, 25, 28, 58, 61].

Fourth, although we improved subject-specific bone material properties to examine FAI, we did not examine biphasic cartilage properties or consolidation, which should be considered in future studies along with dynamic responses [3, 27, 51]. Although subject-specific bone densities were mapped onto individual elements, resulting in heterogeneous bone models, another limitation may be the isotropic property. Isotropy is a conventional material property, when implementing subject-specific bone density mapping for heterogeneous components, however, future steps should consider anisotropic or orthotropic properties to simulate the material behavior or bone.

Fifth, capsular ligaments and muscle lines of action were not included in the model, because we focused on the contributions of the bony morphology toward adverse contact loading. Taut hip joint ligaments would properly seat the femoral head into the acetabulum at more neutral positions, but may restrain hip range of motion in individuals already with a cam morphology. However, knowing that capsular ligaments also play a vital role in minimizing edge loading [59, 60], poorly functioning ligaments may be unable to prevent adverse contact loading at higher amplitudes of motion. Therefore, it would be imperative to further examine the effects of the surrounding capsule on limiting adverse stresses and microinstability [20, 32].

Finally, we examined level walking and, although there were differences in cartilage stresses among the subgroups, we did not note any substantial subchondral bone stresses. The baseline bone densities, for each model, were within range of typical values for cortical and trabecular bones. There were no differences in elastic modulus between participants within a

subgroup. The symptomatic and asymptomatic participants had marginally higher elastic moduli than the control group, but no differences were observed on the subchondral bones. It would be important to examine other activities that require larger hip motions (*e.g.*, squatting, stair ascent/descent) to compare if elevated subchondral bone stresses are different among subgroups and delineate pathomechanical arthritic changes [29, 52, 53]. It is hypothesized that impinging motions may cause higher stresses, not only to the articulating cartilage, but also to the subchondral bone. This would further reinforce the theory that early subchondral bone adaptation may lead to secondary cartilage degeneration [42].

As mentioned, there was an overlap in femoral neck-shaft angles between the symptomatic and asymptomatic groups. The symptomatic cohort that we were selecting from did not have a high femoral neck-shaft angle and, similarly, the asymptomatic and control participants did not have low femoral neck-shaft angles for direct comparisons. The resultant consequence of these small differences has yet to be fully elucidated. The asymptomatic participants' moderate stresses were higher than the control subjects but were more evenly distributed than the symptomatic models. To our knowledge, no study has investigated hip contact stresses resulting from an asymptomatic cam morphology [36]. In comparison with one of the first finite element studies, Chegini and associates [8] examined cartilage stresses using an idealized ball-and-socket model parameterized to various cam and acetabular coverage morphologies, applying instrumented prosthesis loads. They reported no changes in stress as alpha angles were increased, which may be attributed to their idealized geometry. Our results for the control subjects were slightly higher than their control parameters (contact pressure = 2.57 ± 0.89 MPa); however, we included subject-specific geometries, bone material properties, and, more importantly, joint loading, which could have yielded a higher result. Another earlier study on FAI applied subject-specific intersegmental hip forces during maximal squat [37]. Our resultant contact stresses were within a reasonable range during the lower amplitude of hip motion, but cannot directly compare with the different squatting activity. The current study considered hip contact forces as opposed to intersegmental forces from inverse dynamics, thus improving the representation of hip contact stresses. Jorge and associates [18] found much higher cartilage contact pressures at higher amplitudes of hip motion. However, their study was limited to one male subject with a severe cam deformity (age = 27 years, alpha angle = 98°) matched with one healthy female control subject (age = 50 years, alpha angle = 48°). A recent study by

Hellwig and associates [15] also implemented idealized geometries and instrumented prosthesis loads during walking to compare one cam (alpha angle = 74°) with one control hip (alpha angle = 40°). Using a poroelastic, orthotropic cartilage model, they found peak contact pressures in the superior cartilage for the control hip (2.87 MPa). Peak pore pressure was also different between control (0.42 MPa, posterior cartilage) and FAI (3.76 MPa, anterosuperior cartilage). The authors remarked that their geometries were idealized for convergence.

In this study, the symptomatic and asymptomatic participants with low femoral neck-shaft angles had the highest resultant stresses in their respective subgroups. Both symptomatic participants and the asymptomatic participant with the lower femoral neck-shaft angle indicated anterolateral and posterior stress concentrations, which coincided very closely to known areas of cartilage damage [4-6], subchondral bone stiffening [53], and decreased proteoglycan content [29, 43] as a result of cam FAI. Elevated stresses of the symptomatic group could also be attributed to pre-existing chondrolabral damage, resulting in incongruent articulations and unfavorable contact mechanics. The control participant, with the lower femoral neck-shaft angle, showed more favorable contact mechanics, justifying that it could be a combination of both cam and neck angle parameters that contribute to adverse stresses. Although clinical assessment of the cam deformity is usually from multiplanar imaging, it does not provide a complete picture in regard to the likelihood for the onset of degenerative symptoms. Recent work by our group suggests that differences in peak stresses between the symptomatic and asymptomatic groups further supports that a decreased femoral neck-shaft angle may be an indicator of those at risk of developing early symptoms and onset of osteoarthritis [33, 34]. Also, in recent in vivo studies by Siebenrock and associates [49, 50], intertrochanteric varus osteotomies were performed on healthy ovine hips to reduce the femoral neck-shaft angle and experimentally induce mechanical cam impingement. This resulted in localized chondrolabral degeneration, comparable to progressive damage in human hips with FAI. The coxa vara construct seated the femoral head further into the acetabulum and brought the cam morphology closer to the anterolateral and anterosuperior labrum. This may predispose to early labral damage and perhaps explain why some asymptomatic individuals do not experience early symptoms. Although the cam morphology rarely impinges at lower amplitudes of motion, the effect of a lower femoral neck-shaft angle and shortened abductor may contribute to more adverse contact loading to stabilize the pelvis during level walking [58, 61, 62]. We retrospectively examined the participants'

terminal stance phase and remarked that both asymptomatic participants along with the control participant with high femoral neck-shaft angle all had higher hip extensions. Interestingly, both symptomatic individuals had small hip extensions during terminal stance, which may have been limited by capsular ligaments or perhaps indicate a protective mechanism to minimize anterior hip contact forces [25, 61]. This could be a neuromuscular adaptation mechanism to avoid pain by altering the direction and magnitude of the force vectors [30]. The unaffected, contralateral hip of the symptomatic group should be further investigated to confirm asymmetry and if compensatory load is applied onto the unaffected hip [48].

In conclusion, our study suggests that individuals with a cam morphology and varus neck angle may be subjected to elevated mechanical stresses. Although asymptomatic participants had elevated stresses, a higher femoral neck-shaft angle was associated with lower stresses despite a cam morphology. Thus, individuals with an asymptomatic cam morphology and low femoral neck-shaft angle may be at a greater risk of developing clinical signs and symptoms. Future studies will involve higher amplitudes of hip and pelvic motions as well as contact stresses at the underlying subchondral bone to better understand the contributions of various anatomic and functional parameters in individuals with a cam morphology.

8.5 References

1. Agricola R, Heijboer MP, Bierma-Zeinstra SM, Verhaar JA, Weinans H, Waarsing JH. Cam impingement causes osteoarthritis of the hip: a nationwide prospective cohort study (CHECK). *Ann Rheum Dis*. 2012;72:918-923.
2. Allen D, Beaule PE, Ramadan O, Doucette S. Prevalence of associated deformities and hip pain in patients with cam-type femoroacetabular impingement. *J Bone Joint Surg Br*. 2009;91:589-594.
3. Ateshian GA, Ellis BJ, Weiss JA. Equivalence between short-time biphasic and incompressible elastic material responses. *J Biomech Eng*. 2007;129:405-412.
4. Beaulé P, Hynes K, Parker G, Kemp K. Can the alpha angle assessment of cam impingement predict acetabular cartilage delamination? *Clin Orthop Relat Res*. 2012;470:3361-3367.
5. Beaule PE, Zaragoza E, Motamedi K, Copelan N, Dorey FJ. Three-dimensional computed tomography of the hip in the assessment of femoroacetabular impingement. *J Orthop Res*. 2005;23:1286-1292.
6. Beck M, Kalhor M, Leunig M, Ganz R. Hip morphology influences the pattern of damage to the acetabular cartilage: femoroacetabular impingement as a cause of early osteoarthritis of the hip. *J Bone Joint Surg Br*. 2005;87:1012-1018.
7. Bergmann G, Graichen F, Rohlmann A. Hip joint loading during walking and running, measured in two patients. *J Biomech*. 1993;26:969-990.
8. Chegini S, Beck M, Ferguson SJ. The effects of impingement and dysplasia on stress distributions in the hip joint during sitting and walking: a finite element analysis. *J Orthop Res*. 2009;27:195-201.
9. Delp SL, Loan JP, Hoy MG, Zajac FE, Topp EL, Rosen JM. An interactive graphics-based model of the lower extremity to study orthopaedic surgical procedures. *IEEE Trans Biomed Eng*. 1990;37:757-767.
10. Egea AJS, Valera M, Quiroga JMP, Proubasta I, Noailly J, Lacroix D. Impact of hip anatomical variations on the cartilage stress: A finite element analysis towards the biomechanical exploration of the factors that may explain primary hip arthritis in morphologically normal subjects. *Clin Biomech*. 2014;29:444-450.
11. Ganz R, Parvizi J, Beck M, Leunig M, Nötzli H, Siebenrock KA. Femoroacetabular impingement: a cause for osteoarthritis of the hip. *Clin Orthop Relat Res*. 2003;417:112-120.
12. Hack K, Di Primio G, Rakhra K, Beaule PE. Prevalence of cam-type femoroacetabular impingement morphology in asymptomatic volunteers. *J Bone Joint Surg Am*. 2010;92:2436-2444.
13. Hartofilakidis G, Bardakos NV, Babis GC, Georgiades G. An examination of the association between different morphotypes of femoroacetabular impingement in asymptomatic subjects and the development of osteoarthritis of the hip. *J Bone Joint Surg Br*. 2011;93:580-586.
14. Heller MO, Bergmann G, Kassi JP, Claes L, Haas NP, Duda GN. Determination of muscle loading at the hip joint for use in pre-clinical testing. *J Biomech*. 2005;38:1155-1163.
15. Hellwig FL, Tong J, Hussell JG. Hip joint degeneration due to cam impingement: a finite element analysis. *Comput Methods Biomech Biomed Engin*. 2016;19:41-48.
16. Henak CR, Ellis BJ, Harris MD, Anderson AE, Peters CL, Weiss JA. Role of the acetabular labrum in load support across the hip joint. *J Biomech*. 2011;44:2201-2206.
17. Ito K, Leunig M, Ganz R. Histopathologic features of the acetabular labrum in femoroacetabular impingement. *Clin Orthop Relat Res*. 2004;429:262-271.
18. Jorge JP, Simoes FM, Pires EB, Rego PA, Tavares DG, Lopes DS, Gaspar A. Finite element simulations of a hip joint with femoroacetabular impingement. *Comput Methods Biomech Biomed Engin*. 2014;17:1275-1284.
19. Jung KA, Restrepo C, Hellman M, AbdelSalam H, Morrison W, Parvizi J. The prevalence of cam-type femoroacetabular deformity in asymptomatic adults. *J Bone Joint Surg Br*. 2011;93:1303-1307.
20. Kalisvaart MM, Safran MR. Microinstability of the hip—it does exist etiology, diagnosis and treatment. *J Hip Preserv Surg*. 2015;2:123-135.

21. Kennedy MJ, Lamontagne M, Beaule PE. Femoroacetabular impingement alters hip and pelvic biomechanics during gait Walking biomechanics of FAI. *Gait Posture*. 2009;30:41-44.

22. Khanna V, Caragianis A, Diprimio G, Rakhra K, Beaule PE. Incidence of hip pain in a prospective cohort of asymptomatic volunteers: is the cam deformity a risk factor for hip pain? *Am J Sports Med*. 2014;42:793-797.

23. Lamontagne M, Brisson N, Kennedy MJ, Beaulé PE. Preoperative and postoperative lower-extremity joint and pelvic kinematics during maximal squatting of patients with cam femoro-acetabular impingement. *J Bone Joint Surg Am*. 2011;93:40-45.

24. Lamontagne M, Kennedy MJ, Beaule PE. The effect of cam FAI on hip and pelvic motion during maximum squat. *Clin Orthop Relat Res*. 2009;467:645-650.

25. Lewis CL, Sahrmann SA, Moran DW. Effect of hip angle on anterior hip joint force during gait. *Gait Posture*. 2010;32:603-607.

26. Lu TW, O'Connor JJ, Taylor SJ, Walker PS. Validation of a lower limb model with in vivo femoral forces telemetered from two subjects. *J Biomech*. 1998;31:63-69.

27. Macirowski T, Tepic S, Mann RW. Cartilage stresses in the human hip joint. *J Biomech Eng*. 1994;116:10-18.

28. Mantovani G, *Hip Joint Contact Load and Muscle Force in Femoroacetabular Impingement Population.* Ottawa, Canada: University of Ottawa; 2016:182.

29. McGuffin WS, Melkus G, Rakhra KS, Beaule PE. Is the contralateral hip at risk in patients with unilateral symptomatic cam femoroacetabular impingement? A quantitative T1rho MRI study. *Osteoarthritis Cartilage*. 2015;23:1337-1342.

30. Mendis MD, Wilson SJ, Hayes DA, Watts MC, Hides JA. Hip flexor muscle size, strength and recruitment pattern in patients with acetabular labral tears compared to healthy controls. *Man Ther*. 2014;19:405-410.

31. Modenese L, Phillips AM. Prediction of hip contact forces and muscle activations during walking at different speeds. *Multibody Syst Dyn*. 2012;28:157-168.

32. Myers CA, Register BC, Lertwanich P, Ejnisman L, Pennington WW, Giphart JE, LaPrade RF, Philippon MJ. Role of the acetabular labrum and the iliofemoral ligament in hip stability: an in vitro biplane fluoroscopy study. *Am J Sports Med*. 2011;39(Suppl):85S-91S.

33. Ng KCG, Lamontagne M, Adamczyk AP, Rakhra KS, Beaule PE. Patient-specific anatomical and functional parameters provide new insights into the pathomechanism of cam FAI. *Clin Orthop Relat Res*. 2015;473:1289-1296.

34. Ng KCG, Lamontagne M, Beaulé PE. Differences in anatomical parameters between the affected and unaffected hip in patients with bilateral cam-type deformities. *Clin Biomech*. 2016;33:13-19.

35. Ng KCG, Lamontagne M, Labrosse MR, Beaulé PE. Comparison of anatomical parameters of cam femoroacetabular impingement to evaluate hip joint models segmented from CT data. *Comput Methods Biomech Biomed Eng Imaging Vis.* 2016;In Press:1-10.

36. Ng KCG, Lamontagne M, Labrosse MR, Beaulé PE. Hip joint stresses due to cam-type femoroacetabular impingement: a systematic review of finite element simulations. *PLoS One*. 2016;11:e0147813.

37. Ng KCG, Rouhi G, Lamontagne M, Beaulé PE. Finite element analysis examining the effects of cam FAI on hip joint mechanical loading using subject-specific geometries during standing and maximum squat. *HSS J*. 2012;8:206-212.

38. Nötzli HP, Wyss TF, Stoecklin CH, Schmid MR, Treiber K, Hodler J. The contour of the femoral head-neck junction as a predictor for the risk of anterior impingement. *J Bone Joint Surg Br*. 2002;84:556-560.

39. Pandy MG. Computer modeling and simulation of human movement. *Annu Rev Biomed Eng*. 2001;3:245-273.

40. Park S, Hung CT, Ateshian GA. Mechanical response of bovine articular cartilage under dynamic unconfined compression loading at physiological stress levels. *Osteoarthritis Cartilage*. 2004;12:65-73.

41. Prilutsky BI, Zatsiorsky VM. Optimization-based models of muscle coordination. *Exerc Sport Sci Rev*. 2002;30:32-38.

42. Radin EL, Paul IL, Tolkoff MJ. Subchondral bone changes in patients with early degenerative joint disease. *Arthritis Rheum*. 1970;13:400-405.

43. Rakhra KS, Lattanzio PJ, Cardenas-Blanco A, Cameron IG, Beaule PE. Can T1-rho MRI detect acetabular cartilage degeneration in femoroacetabular impingement? A pilot study. *J Bone Joint Surg Br*. 2012;94:1187-1192.

44. Rakhra KS, Sheikh AM, Allen D, Beaule PE. Comparison of MRI alpha angle measurement planes in femoroacetabular impingement. *Clin Orthop Relat Res*. 2009;467:660-665.

45. Ranawat A, Schulz B, Baumbach S, Meftah M, Ganz R, Leunig M. Radiographic predictors of hip pain in femoroacetabular impingement. *HSS J*. 2011;7:115-119.

46. Rubin DA. Femoroacetabular impingement: fact, fiction, or fantasy? *AJR Am J Roentgenol*. 2013;201:526-534.

47. Schileo E, Dall'ara E, Taddei F, Malandrino A, Schotkamp T, Baleani M, Viceconti M. An accurate estimation of bone density improves the accuracy of subject-specific finite element models. *J Biomech*. 2008;41:2483-2491.

48. Shakoor N, Dua A, Thorp LE, Mikolaitis RA, Wimmer MA, Foucher KC, Fogg LF, Block JA. Asymmetric loading and bone mineral density at the asymptomatic knees of patients with unilateral hip osteoarthritis. *Arthritis Rheum*. 2011;63:3853-3858.

49. Siebenrock KA, Fiechter R, Tannast M, Mamisch TC, von Rechenberg B. Experimentally induced cam impingement in the sheep hip. *J Orthop Res*. 2013;31:580-587.

50. Siebenrock KA, Kienle KP, Steppacher SD, Tannast M, Mamisch TC, von Rechenberg B. Biochemical MRI predicts hip osteoarthritis in an experimental ovine femoroacetabular impingement model. *Clin Orthop Relat Res*. 2015;473:1318-1324.

51. Speirs AD, Beaule PE, Ferguson SJ, Frei H. Stress distribution and consolidation in cartilage constituents is influenced by cyclic loading and osteoarthritic degeneration. *J Biomech*. 2014;47:2348-2353.

52. Speirs AD, Beaule PE, Rakhra KS, Schweitzer ME, Frei H. Bone density is higher in cam-type femoroacetabular impingement deformities compared to normal subchondral bone. *Osteoarthritis Cartilage*. 2013;21:1068-1073.

53. Speirs AD, Beaule PE, Rakhra KS, Schweitzer ME, Frei H. Increased acetabular subchondral bone density is associated with cam-type femoroacetabular impingement. *Osteoarthritis Cartilage*. 2013;21:551-558.

54. Steele KM, Seth A, Hicks JL, Schwartz MS, Delp SL. Muscle contributions to support and progression during single-limb stance in crouch gait. *J Biomech*. 2010;43:2099-2105.

55. Sutter R, Dietrich TJ, Zingg PO, Pfirrmann CWA. How useful is the alpha angle for discriminating between symptomatic patients with cam-type femoroacetabular impingement and asymptomatic volunteers? *Radiology*. 2012;264:514-521.

56. Taddei F, Schileo E, Helgason B, Cristofolini L, Viceconti M. The material mapping strategy influences the accuracy of CT-based finite element models of bones: an evaluation against experimental measurements. *Med Eng Phys*. 2007;29:973-979.

57. Unsworth A, Dowson D, Wright V. The Frictional Behavior of Human Synovial Joints—Part I: Natural Joints. *J Lubric Techn-T ASME*. 1975;97:369-376.

58. Valente G, Taddei F, Jonkers I. Influence of weak hip abductor muscles on joint contact forces during normal walking: probabilistic modeling analysis. *J Biomech*. 2013;46:2186-2193.

59. van Arkel RJ, Amis AA, Cobb JP, Jeffers JR. The capsular ligaments provide more hip rotational restraint than the acetabular labrum and the ligamentum teres : an experimental study. *Bone Joint J*. 2015;97:484-491.

60. van Arkel RJ, Amis AA, Jeffers JR. The envelope of passive motion allowed by the capsular ligaments of the hip. *J Biomech*. 2015;48:3803-3809.

61. Wesseling M, de Groote F, Meyer C, Corten K, Simon JP, Desloovere K, Jonkers I. Gait alterations to effectively reduce hip contact forces. *J Orthop Res*. 2015;33:1094-1102.

62. Wesseling M, Meyer C, de Groote F, Corten K, Simon JP, Desloovere K, Jonkers I. Gait alterations can reduce the risk of edge loading. *J Orthop Res*. 2015;

63. Wu G, Siegler S, Allard P, Kirtley C, Leardini A, Rosenbaum D, Whittle M, D'Lima DD, Cristofolini L, Witte H, Schmid O, Stokes I. ISB recommendation on definitions of joint coordinate system of various joints for the reporting of human joint motion--part I: ankle, hip, and spine. International Society of Biomechanics. *J Biomech*. 2002;35:543-548.

9 Effects of Cam Femoroacetabular Impingement on Subchondral Bone Stresses during Squatting

K. C. Geoffrey Ng [1] | Giulia Mantovani [2] | Mario Lamontagne [2,1] | Michel R. Labrosse [1] | Paul E. Beaulé [3]

[1] Department of Mechanical Engineering | University of Ottawa | Ottawa, Ontario, Canada

[2] School of Human Kinetics | University of Ottawa | Ottawa, Ontario, Canada

[3] Division of Orthopaedic Surgery | University of Ottawa | Ottawa, Ontario, Canada

Contents of this chapter prepared as a manuscript for submission | March 2017

Ng KCG, Mantovani G, Lamontagne M, Labrosse MR, Beaulé PE, Effects of Cam-Type Femoroacetabular Impingement on Subchondral Bone Stresses during Squatting. 2017; Pending Submission.

9.0 Abstract

Objective: Examine the combined effects of the cam-type femoral head deformity and femoral neck-shaft angle on hip joint (cartilage, labrum, and subchondral bone) stresses, during squatting, in a symptomatic, asymptomatic, and control group.

Design: Six male participants were included, to represent three groups (symptomatic cam, asymptomatic cam, healthy control), with two participants per group – one with the highest femoral neck-shaft angle and one with the lowest. Each participant's finite element hip joint models were reconstructed from imaging data and assigned subject-specific bone material properties. Hip contact forces, during squatting, were determined and applied to the finite element models, to examine maximum shear stresses in the acetabular cartilage-labrum and subchondral bone.

Results: The cam groups experienced higher subchondral bone stresses than cartilage-labrum stresses. Both cam groups also had substantially higher subchondral bone stresses (symptomatic = 13.8–15.8 MPa, asymptomatic = 10.9–13.0 MPa), compared to the controls (6.4–6.5 MPa). The symptomatic and asymptomatic participants with low femoral neck-shaft angles had the highest cartilage and subchondral bone stresses, in their respective subgroups. The asymptomatic participant with low femoral neck-shaft angle demonstrated anterolateral subchondral bone stresses (123°, 13.0 MPa), similar to the symptomatic group.

Conclusions: The resultant subchondral bone stresses coincide with recent findings, where acetabular subchondral bone was denser in cam-type hips. Individuals with a cam deformity and varus neck orientation are subjected to elevated subchondral bone stresses, which would increase the risks of early clinical signs and degenerative process associated with FAI.

9.1 Introduction

Femoroacetabular impingement (FAI) is described as a pathomechanical failure process of the hip [14], attributed to an abnormal bone deformity – either due to an enlarged femoral head (cam-type), severe acetabular overcoverage (pincer-type), or a combination of both (mixed-type). Mechanical impingement is commonly experienced at higher extremes of hip motion, which can result in elevated hip joint stresses and precede early cartilage degeneration and osteoarthritis [1].

The cam deformity itself is an enlarged bony prominence over the femoral head-neck junction, characterizing an aspherical femoral head and elevated alpha angles [35, 37, 45]. Many individuals with cam FAI have can demonstrate restricted joint motions (*e.g.*, during level walking, stair ascent/descent, squatting) [22-24, 29, 40] and clinical signs of pain; however, several individuals with cam deformities never experience symptoms for much of their adult life [8, 16, 21]. The cause for concern for these asymptomatic individuals is that they are still susceptible to subchondral bone stiffening [36, 44] which may onset early cartilage degeneration [2, 5, 27].

It is possible that early pain symptoms in individuals with cam deformities may be attributed to trauma, injuries, or labral tears. It was recently observed that individuals with a cam deformity and a decreased femoral neck-shaft angle may be predisposed to symptoms of FAI [3, 17, 29, 30, 38]; however, it is still unknown what combined effects both parameters (cam deformity and neck angle) have on hip joint stresses.

In recent years, finite element methods were popularized to simulate cam FAI and examine resultant hip joint stresses [9, 18, 20, 34]. Previous simulations indicated that cam FAI experienced elevated stresses at higher amplitudes of motion (*e.g.*, sit-to-stand, squatting, deep flexion), in comparison with normal hips. However, there was a lack of subject-specificity in previous in silico studies, where many of the studies did not address subject-specific material properties or loading parameters to adequately represent participant groups and, moreover, a clinically defined asymptomatic population [32]. A recent study compared hip joint stresses due to symptomatic and asymptomatic cam morphologies, examining the instance of peak joint loading during level walking [33]. Although both symptomatic and asymptomatic cam morphologies demonstrated higher stresses than control hip, only marginal differences were observed between each participant's acetabular cartilage and subchondral bone. This lower subchondral bone stress could have been attributed to the smaller amplitude of walking motion.

Therefore, the purpose of this study was to investigate the combined effects of the cam deformity and femoral neck-shaft angle on hip joint stresses during squatting. Specifically, we examined acetabular cartilage-labrum and subchondral bone stresses in symptomatic, asymptomatic, and healthy individuals with high and low femoral neck-shaft angles.

9.2 Methods

9.2.1 Participants and Imaging

Six male participants (n = 6, age = 32 ± 7 years, BMI = 26 ± 3 kg/m^2), from a larger participant cohort, were selected for this study [29, 33]. In efforts to minimize skin artefacts and pelvic misalignments during motion capture, radio-opaque surface markers were placed onto each participant's left and right anterior superior iliac spines and posterior superior iliac spines prior to CT imaging [26]. Each participant was imaged using a conventional CT scanner, in a supine position (Acquilion, Toshiba Medical Systems Corporation, Markham, ON, Canada; or Discovery CT750, GE Healthcare, Mississauga, ON, Canada), imaging the iliac crest to the proximal diaphysis as well as the femoral condyles (512×512 resolution, slice thickness of 0.625 mm, 120 kVp, 200 mAs). A calibration phantom (Model 3, Mindways Software, Austin, TX, USA) was placed under the lumbar vertebra for bone densitometry and the natural lordosis was confirmed with a scout scan.

The CT data were reviewed by a senior musculoskeletal radiologist (KR) for a cam deformity, which was indicated by either an axial 3:00 or radial 1:30 alpha angle greater than 50.5° or 60°, respectively [29, 35, 37, 45] (Figure 8.1). Participants completed pain questionnaires – Hip Disability and Osteoarthritis Outcome Score (HOOS) and Western Ontario and McMaster Universities Arthritis Index (WOMAC) – to confirm symptoms. The participants who presented a cam deformity and clinical signs were considered as symptomatic; while the participants who indicated a cam deformity, but showed no clinical signs were considered as asymptomatic and the participants who did not have a cam deformity or clinical signs were considered as healthy controls. (Aside from the symptomatic participants, the remaining participants were unaware whether they had a cam deformity until after the data acquisition protocol.) For the symptomatic, asymptomatic, and control groups, the affected hip for comparison was the hip with clinical signs, larger cam deformity, and smaller cam deformity, respectively.

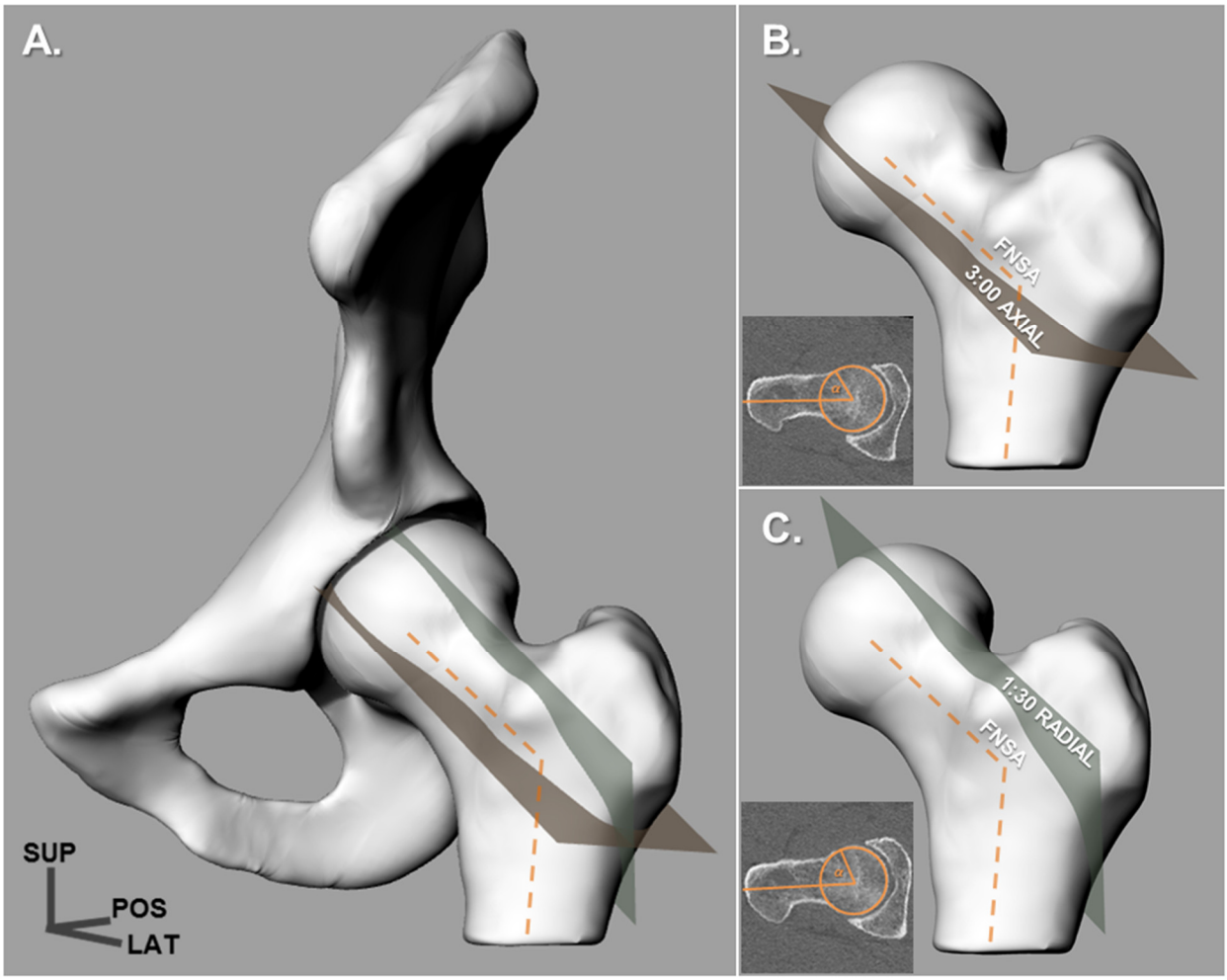

Figure 9.1. (**A**) Hip joint assembly, comprised of a segmented hemi-pelvis and proximal femur, indicating the alpha angle planes. Two planes were examined, to determine if the femoral head had a cam deformity: (**B**) the 3:00 axial plane observed if alpha angle exceeded 50.5°; and (**C**) the 1:30 radial plane observed if alpha angles exceeded 60° (small insets depicts CT image). The femoral neck-shaft angle (FNSA) was determined to examine the effects of neck angles on each group's acetabular cartilage and subchondral bone stresses.

The femoral neck-shaft angle was measured for each hip joint (Figure 8.1), using a DICOM viewer (Onis 2.4, DigitalCore, Tokyo, Japan), to confirm if the symptomatic group had a reduced neck angle [29, 30]. For each of the three participant groups, the participant with the largest femoral neck-shaft angle and participant with the smallest femoral neck-shaft angle were selected (Table 9.1). Each participant's affected hip underwent subsequent MRI (MAGNETOM Symphony, Siemens Healthcare GmbH, Erlangen, Germany), using a field strength of 1.5 T (384×384 resolution, slice thickness of 3 mm) to determine cartilage thicknesses and labral contours. Participants did not indicate other hip pathologies, major lower limb injuries, or other musculoskeletal abnormalities. The study protocol was approved by the university and hospital research institute ethics boards and participants provided informed consent prior to the investigations.

Table 9.1. Summary of clinical assessments and measured anatomical parameters for each symptomatic, asymptomatic, and control participant, with high (H) and low (L) femoral neck-shaft angle

Participant	Age (years)	BMI (kg/m^2)	HOOS Pain (%)	WOMAC Pain (%)	Axial 3:00 alpha angle (°)	Radial 1:30 alpha angle (°)	Femoral neck-shaft angle (°)
Symptomatic H	25	25	53	55	51	63	125
Symptomatic L	33	22	65	80	58	64	119
Asymptomatic H	28	27	100	100	52	66	134
Asymptomatic L	44	27	100	100	56	70	123
Control H	32	26	100	100	44	56	132
Control L	30	29	100	100	41	52	124

H = High femoral neck-shaft angle
L = Low femoral neck-shaft angle
HOOS = Hip Disability and Osteoarthritis Outcome Score
WOMAC = Western Ontario and McMaster Universities Arthritis Index

9.2.2 Segmentation and Modelling

Each participant's pelvis and femur bone models were manually segmented from CT data using segmentation software (3D-Doctor 4.0, Able Software Corp., Lexington, MA, USA). The MRI data were registered and centred on four control points of the target CT images, where the femoral head centre and the acetabulum's deepest width and depth were landmarks for registration (Figure 9.2.A). The midpoints between the femoral and acetabular cartilages were located on each slice to determine cartilage thicknesses; and the femoral cartilage, acetabular cartilage, and labrum were manually segmented. All segmented models were then resurfaced to

reduce geometric artefacts, using computer-aided design software (SolidWorks, Dassault Systèmes, Concord, MA, USA) (Figure 9.2.B). To confirm the accuracy of modelling procedure, anatomical hip joint parameters of the resurfaced models were measured using computer-aided design software and compared with the original CT data [31]. Soft tissues were modelled as smooth layers as none of the participants indicated osteoarthritis.

Hip joint models were imported into finite element analysis software (ANSYS 12.1, ANSYS Inc., Canonsburg, PA, USA) and meshed with tetrahedral, SOLID187 elements. The meshes were then imported into a bone density mapping program (Bonemat v3.1, Istituto Ortopedico Rizzoli, Bologna, Italy). A linear density-elasticity relationship assigned subject-specific elastic moduli to individual elements, based on the calibration phantom, resulting in heterogeneous, isotropic bone models [46] (Figure 9.2.C). Cartilage and labrum were modelled as Neo-Hookean, hyperelastic materials [19], with constant hydrostatic pressure. Articular cartilage contacts were modelled with a frictional coefficient of 0.01 [47]. Element sizes for the bone and soft tissue models started at 3 and 2 mm, respectively, and refined to ensure mesh sensitivity.

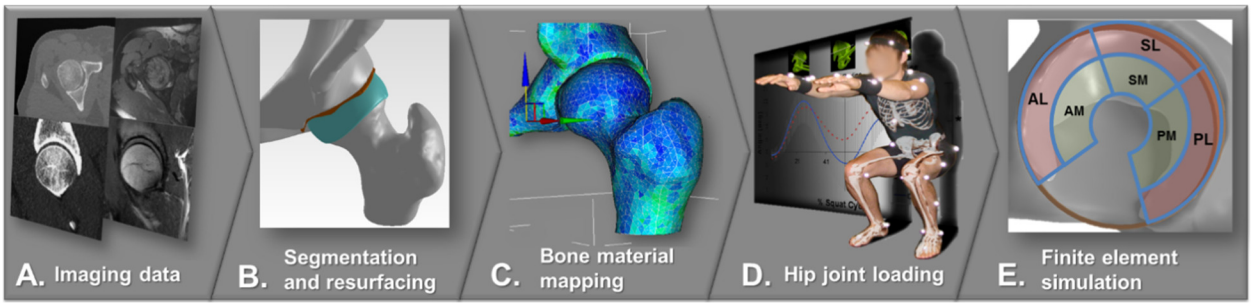

Figure 9.2. Summary of process showing subject-specific input data used for finite element simulations. (**A**) CT and MRI data were used for modelling; (**B**) hip joint models were segmented and resurfaced; (**C**) subject-specific bone material properties were mapped to each bone model; (**D**) squat loads were applied; and (**E**) simulated to determine resultant hip joint stresses on the acetabular cartilage, labrum, and subchondral bone.

9.2.3 Motion Analysis and Hip Joint Forces

Each participant performed maximal squatting trials in the motion capture environment (Figure 9.2.D), similar to previous squat protocols [28, 29, 34]. Three-dimensional kinematics were captured using ten infrared motion capture cameras (MX-13, Vicon, Oxford, UK) and retroreflective markers attached onto each participant's anatomical landmarks. The radio-opaque pelvis markers were replaced with retro-reflective markers and the motion trajectories were

filtered using motion analysis software (Woltring, MSE = 15 mm^2; Nexus 1.8, Vicon, Oxford, UK). Ground reaction forces were captured using two force plates (FP4060-08, Bertec, Columbus, OH, USA) and filtered using numerical computational software (zero-lag, 4^{th} order Butterworth, cut-off frequency 6Hz; MATLAB R2014a, MathWorks, Nantick, MA, USA). Hip contact forces were estimated using a musculoskeletal modelling program (OpenSim 3.1, SimTK, USA). The torso and lower-limb segments modelled the hips and lumbar as ball-and-socket joints, which contributed to 23 degrees of freedom and 92 musculotendon actuators [10, 25]. Muscle forces were determined using static optimization [28] and the resultant three-dimensional hip contact forces were expressed in the pelvic reference system [50].

9.2.4 Finite Element Simulation

Since each participant had a different squat depth and pelvic range of motion, a common quasi-static loading scenario was simulated to examine the mid-squat condition at 90° hip flexion, near 50% of leg length. In each finite element simulation, the hip contact forces were applied at the femoral head and boundary conditions were fixed at the pubis symphysis and superior iliac crest. Maximum shear stresses were examined on each participant's acetabular cartilage, labrum, and subchondral bone to examine adverse loading conditions (Figure 9.2.E). The femur was oriented per the squatting position and the sectioned plane of the proximal diaphysis was fixed to permit translation in the direction of loading [19, 33] (Figure 9.3). A flowchart from subject-specific input data to resultant hip joint stresses is summarized in (Figure 9.4).

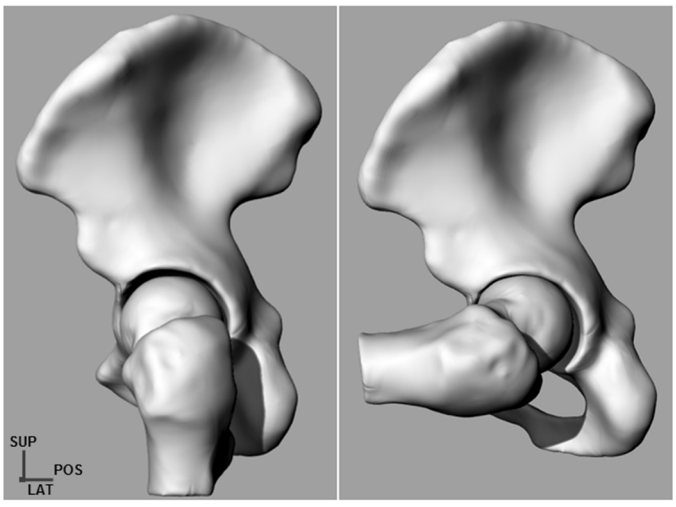

Figure 9.3. Sagittal view of the hip assembly during neutral position (left) and squatting position (right). The femur and pelvis models were oriented according to the mid-squat condition of 90° hip flexion near 50% of leg height.

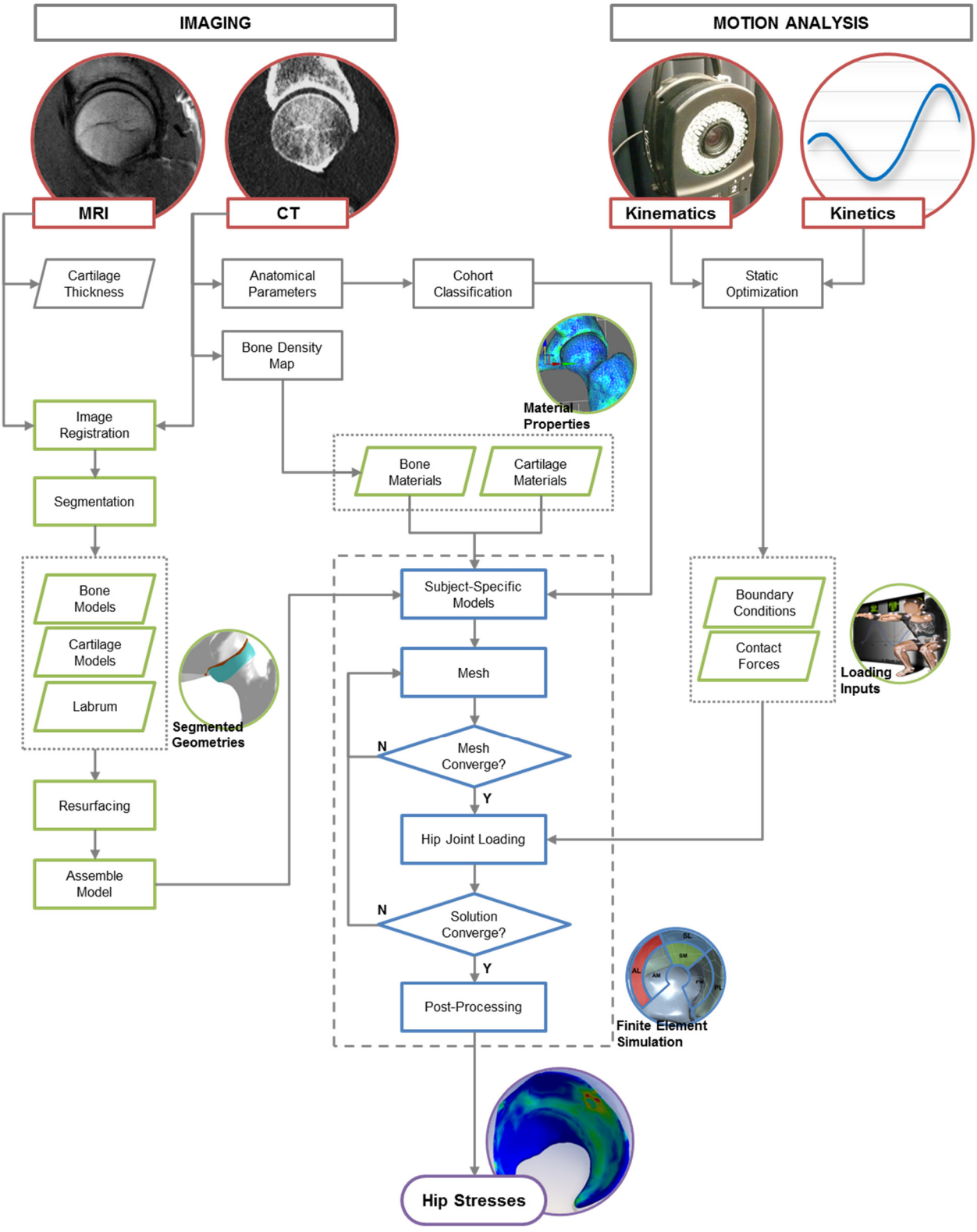

Figure 9.4. Summary of process showing subject-specific input data used for finite element simulations. (**A**) CT and MRI data were used for modelling; (**B**) hip joint models were segmented and resurfaced; (**C**) subject-specific bone material properties were mapped to each bone model; (**D**) squat loads were applied; and (**E**) simulated to determine resultant hip joint stresses on the acetabular cartilage, labrum, and subchondral bone.

9.3 Results

9.3.1 Cartilage and Labrum Stresses

Both symptomatic and asymptomatic groups had higher maximum shear stresses, compared to the controls. The symptomatic participant with low femoral neck-shaft angle showed the highest peak stress on the anterosuperior cartilage (119°, 10.4 MPa) with multiple stress concentrations in the posterior quadrant (Figure 8.5). The symptomatic participant with high femoral neck-shaft angle had a much lower peak stress at the anterolateral cartilage (125°, 7.4 MPa), with a prominent secondary posteroinferior stress concentration. Both asymptomatic participants had peak stresses on the anterolateral cartilage, with the lower femoral neck-shaft angle indicating a higher peak stress (123°, 7.5 MPa) compared to the higher femoral neck-shaft angle (134°, 6.9 MPa). Although there were no substantial differences in stress magnitudes between controls (5.9–6.2 MPa), the participant with high femoral neck-shaft angle showed more evenly dissipated stresses (Figure 8.5).

9.3.2 Subchondral Bone Stresses

Both cam deformity (symptomatic and asymptomatic) groups showed substantially higher stresses on the subchondral bone, than on the cartilage. Differences in femoral neck-shaft angle greatly influenced both cam deformity groups. The symptomatic participant with low femoral neck-shaft angle had the highest stress in the anterosuperior region (119°, 15.8 MPa), while the higher femoral neck-shaft angle resulted in a lower magnitude (125°, 13.8 MPa). Both symptomatic participants also indicated elevated secondary posterior stresses, perhaps due to contrecoup levering (Figure 9.6). The asymptomatic participants showed elevated anterolateral stresses; however, the participant with low femoral neck-shaft angle demonstrated an elevated anterosuperior stress, more similar to the symptomatic group and closer the acetabular rim (123°, 13.0 MPa). The asymptomatic participant with high femoral neck-shaft angle showed a slightly lower stress (134°, 10.9 MPa). Both control participants experienced lower, well-distributed stresses (6.4–6.5 MPa). For both cam deformity groups, peak subchondral bone stresses were substantially higher than their corresponding cartilage-labrum stresses (Figure 9.7); whereas for the control group, there were marginal differences between peak cartilage-labrum and subchondral bone stresses.

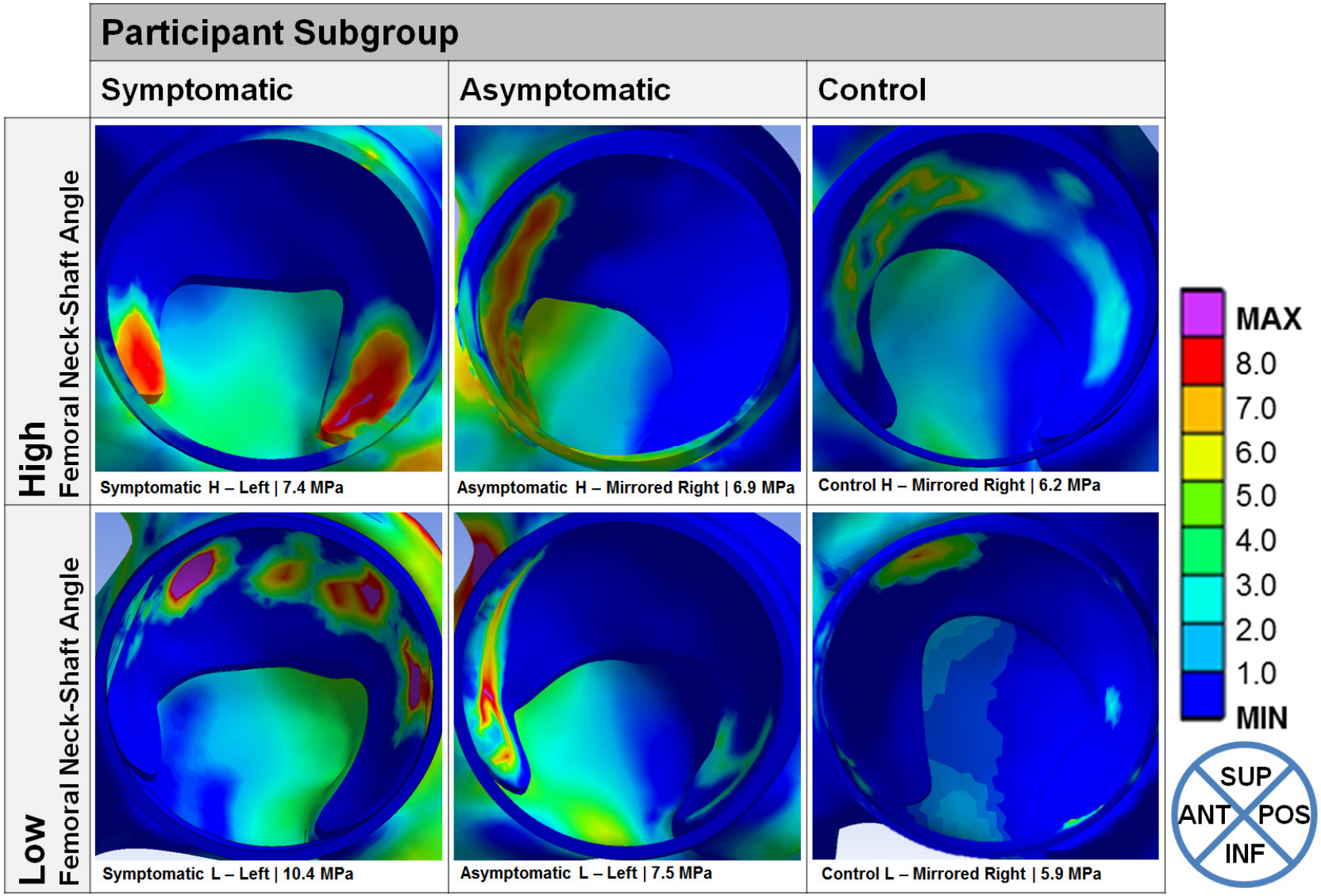

Figure 9.5. Sagittal view of the acetabular cartilage and labrum, from the resultant finite element simulations, showing the maximum shear stress distributions for each symptomatic, asymptomatic, and control participant with the highest (H = top row) and lowest (L = bottom row) femoral neck-shaft angle. The reference locations are denoted by anterior (ANT), posterior (POS), superior (SUP), and inferior (INF).

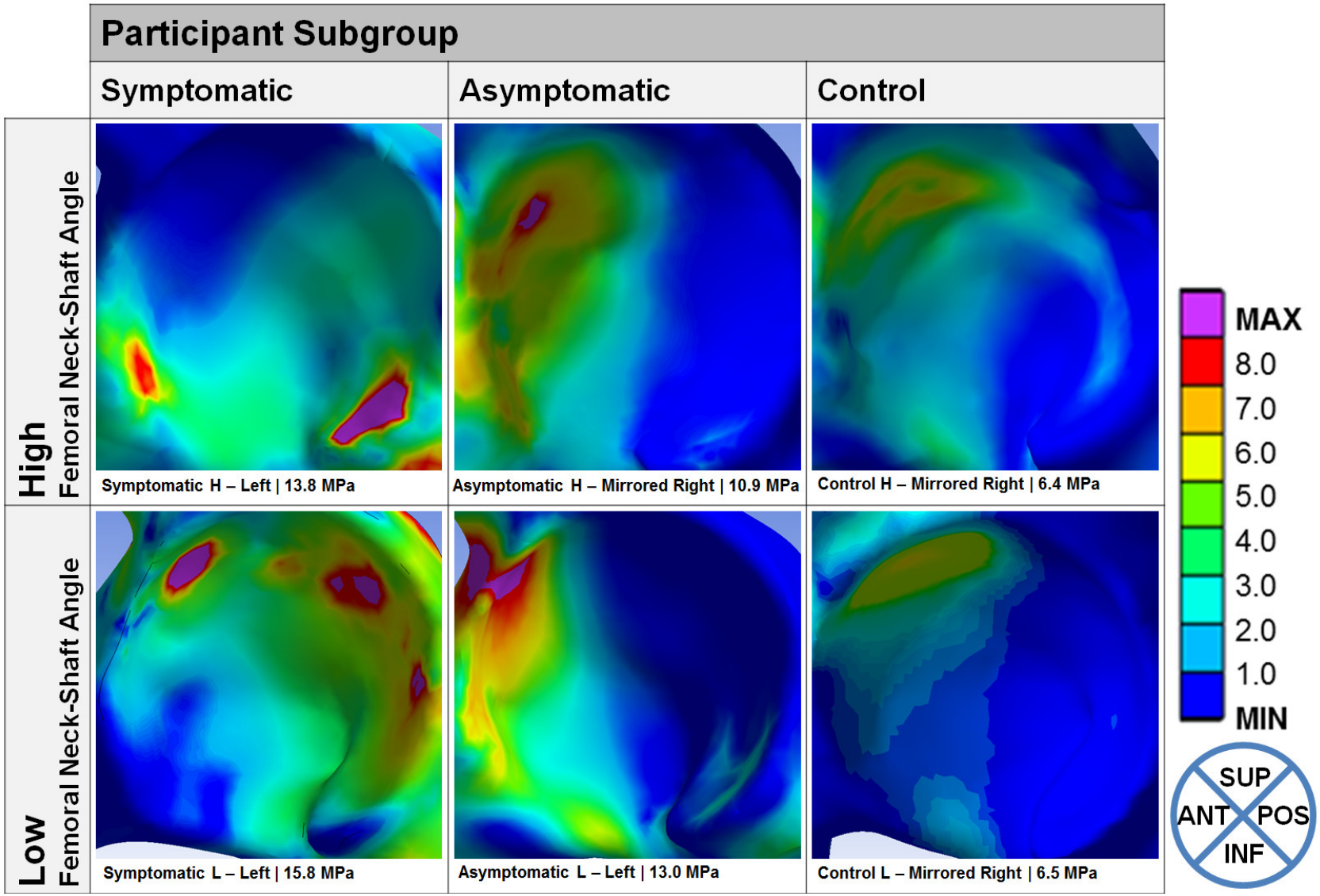

Figure 9.6. Sagittal view of the acetabular subchondral bone, showing the maximum shear stress distributions for each symptomatic, asymptomatic, and control participant with the highest (H – top row) and lowest (L – bottom row) femoral neck-shaft angle. The reference locations are denoted by anterior (ANT), posterior (POS), superior (SUP), and inferior (INF).

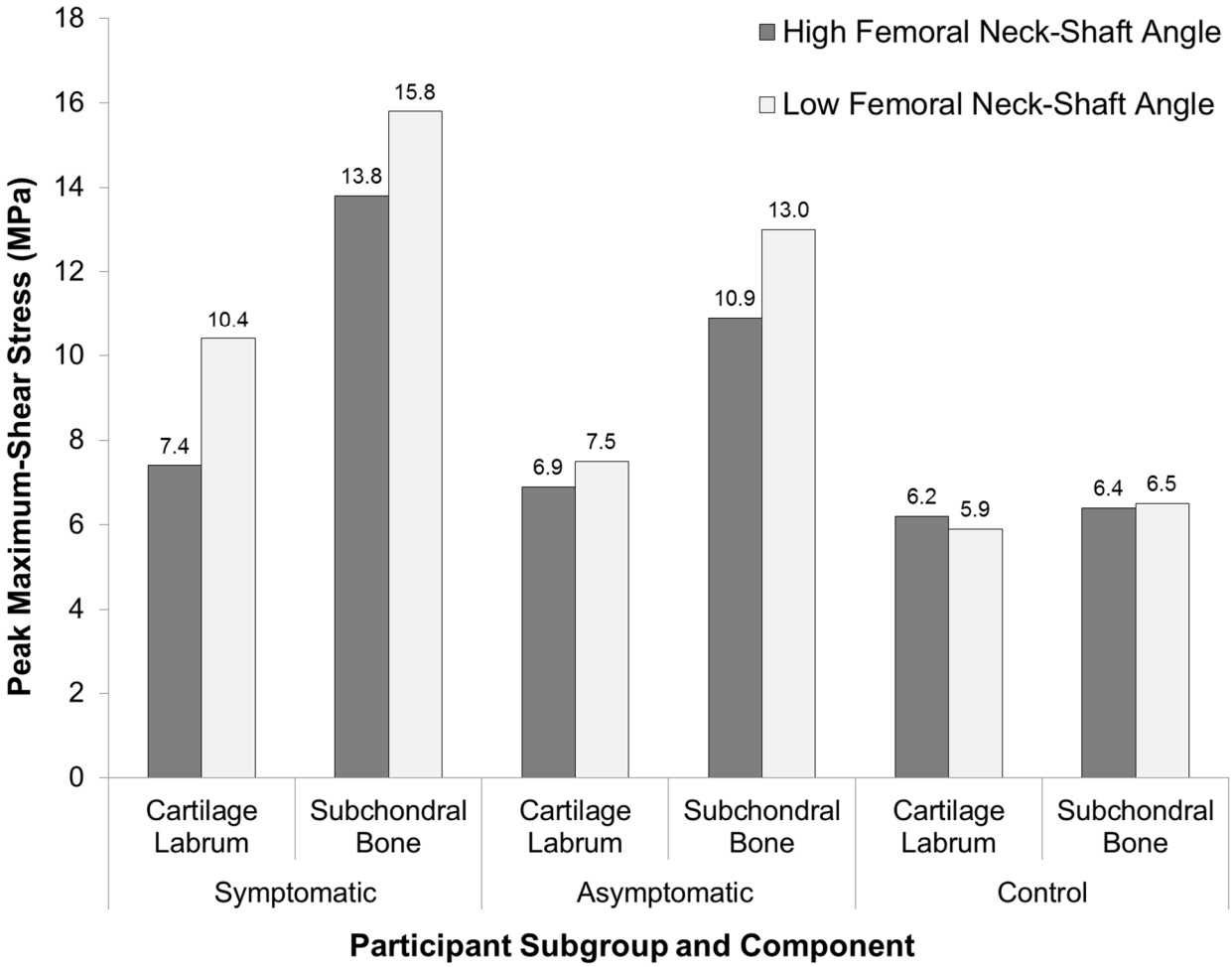

Figure 9.7. Peak maximum shear stress on the acetabular cartilage-labrum and subchondral bone, for each symptomatic, asymptomatic, and control participant, with the highest and lowest femoral neck-shaft angle.

9.4 Discussion

We implemented subject-specific hip joint geometries, bone material properties, and hip joint loading data to examine acetabular cartilage-labrum and subchondral bone stresses in symptomatic, asymptomatic, and control individuals with either a high or low femoral neck-shaft angle. Both cam deformity groups had slightly higher acetabular cartilage stresses, compared to the control group; however, the individuals with a cam deformity and low femoral neck-shaft angle had substantially high cartilage and subchondral bone stresses. The cam deformity groups' acetabular subchondral bone stresses were considerably higher than their associated cartilage stresses [34]. Interestingly, the asymptomatic participant with the high femoral neck-shaft angle demonstrated cartilage stresses that were marginally higher than the control group, but showed high subchondral bone stresses. These findings align very closely with recent studies, where acetabular subchondral bone was much denser in cam-type hips, regardless of clinical signs or symptoms [36, 44]. In addition, the asymptomatic participant with low femoral neck-shaft angle experienced subchondral bone stresses much more similar to the symptomatic group, which supports that early clinical signs and symptoms may be due to a decreased femoral neck-shaft angle [3, 17, 29, 30, 38]. To our knowledge, no study has investigated hip contact stresses in a clinically defined asymptomatic population, at an extreme range of motion [32].

A recent systematic review noted that several previous simulations on cam FAI implemented simplified geometric models to predict stresses, along with homogeneous bone material properties and instrumented prostheses loading data [32]. The first finite element simulation on FAI, by Chegini and associates (2009), reconstructed an idealized ball-and-socket model, parameterized to several cam and acetabular coverage morphologies, and applied instrumented prostheses forces for a stand-to-sit activity [9]. Although an indirect comparison of stress parameters, our cam deformity groups' peak cartilage-labrum stresses were similar to their reported large range of contact pressures (3.67 – 12.84 MPa) and von Mises stresses (9.7 – 27.2 MPa) for cam deformities with normal acetabular coverage. There was no report on subchondral bone stresses. In a previous study that examined acetabular subchondral bone stresses, due to cam FAI during maximal squatting [34], our peak maximum shear stresses for the cam deformity groups were within range of their values (13.4 – 16.9 MPa). The current study included a labrum model as well as subject-specific bone material properties and hip contact forces (as opposed to intersegmental forces from inverse dynamics), thus improving the representation of hip contact

stresses. Jorge and associates (2012) cam-type model also reported elevated peak contact pressures and von Mises stresses in the anterosuperior cartilage (11.6 and 14.4 MPa, respectively) and labrum (16.4 and 14.7 MPa, respectively), during deep flexion [20]. Their study was limited to one male subject, with a severe cam deformity (age = 27 years, alpha angle = 98°), matched with one female control subject (age = 50 years, alpha angle = 48°). Although previous finite element simulations were preliminary explorations of hip joint stresses due to cam FAI, none of the studies considered subject-specific bone material properties or the effects of femoral neck-shaft angles to adequately characterize subgroups. Previous studies also implemented either instrumented prosthesis loads or intersegmental reaction forces (from inverse dynamics) as opposed to hip joint contact forces (from static optimization and musculoskeletal modelling). In our earlier finite element study, that compared hip joint stresses between symptomatic, asymptomatic, and control individuals during level walking [33], the symptomatic group showed higher acetabular cartilage stresses (6.3 – 9.5 MPa), in comparison with asymptomatic (5.9 – 7.0 MPa) and control participants (3.8 – 4.0 MPa). Similarly, the symptomatic and asymptomatic participants with low femoral neck-shaft angles demonstrated higher peak cartilage stresses. However, from that earlier study, there were no differences between each participant's acetabular cartilage and subchondral bone stresses. The lower acetabular subchondral bone stresses could have been attributed to the smaller amplitude of motion (*i.e.*, walking motion reducing risks of impingement).

Our symptomatic participants exhibited multiple stress concentrations in the anterosuperior and posterior cartilage and subchondral bone, indicative of slight contrecoup stresses [5], and corresponded with regions of decreased proteoglycan content [2, 27]. Both symptomatic and asymptomatic groups indicated stress concentrations, which coincided to known areas of cartilage damage [4, 5] and subchondral bone stiffening [44]. Interestingly, both symptomatic participants had relatively low femoral neck-shaft angles, compared to the asymptomatic and control groups. The asymptomatic participant with low femoral neck-shaft angle (123°) had similar peak stresses as the symptomatic participant with high femoral neck-shaft angle (125°). This further supports that neck angle parameters, combined with cam deformity parameters, are influential discriminants to predict early symptoms of cam FAI [29, 30], and perhaps can further associate varus hips with elevated adverse stresses leading to early labral tears and clinical signs [3, 15, 17, 39].

A varus hip may also be more susceptible to shear loading across the physeal growth plate [13], which could predispose to slipped capital femoral epiphysis or cam FAI. In an earlier finite element study, by Fishkin and associates (2006), a single male model with slipped capital femoral epiphysis was parameterized to various femoral versions, directional varus loading, and bodyweight loading parameters [13]. The authors observed that varus loading conditions resulted in greater shear forces across the physis, which ultimately could increase slip risks. In another recent finite element study, Sánchez Egea and associates (2014) parameterized femoral neck-shaft (110 – 130°), femoral torsion (0 – 20°), and acetabular version angles (0 – 20°), examining anatomical variations leading to hip joint cartilage stresses during quasi-static walking loads [41]. Interestingly, their varus hip configuration (110°) also demonstrated higher stresses than their control model. However, their study parameterized one female model (age = 99 years, BMI = 23kg/m^2), taken from an existing database. More importantly, femoral head parameters did not consider any cam morphologies (*i.e.*, alpha angles and femoral head-neck offset), which could explain why peak stresses were centrally located in the acetabular cartilage, instead of the chondrolabral junction. In recent in vivo ovine studies, Siebenrock and associates (2013, 2015) performed intertrochanteric osteotomies on eight healthy sheep hips [42, 43]. Although the ovine femoral heads did not indicate cam-like deformities, the femoral neck-shaft angles were surgically decreased to induce mechanical impingement. The surgical procedure clearly reproduced varus neck angles and resulted in chondrolabral degeneration [42], similar to progressive hip joint degeneration in human hips with FAI [43]. The varus angle brought the lateral aspect of the femoral head closer to the labrum, predisposing to early labral damage and justifies why many asymptomatic individuals do not experience early symptoms.

In the greater spectrum of FAI research, previous work by our group showed noticeable differences in squatting mechanics, deep hip joint flexion, and pelvic range of motion, between symptomatic and control participants [23, 24, 29]. In this study, we selected a common squat depth (90° hip flexion, near 50% leg length) among all participants, to compare hip joint stresses at the same amplitude of motion. Although the asymptomatic and control participants could squat slightly deeper than half of their leg length, this instance was selected as the symptomatic participants were very near the maximal squat depth. Anatomically, a decreased neck angle can further position the greater and lesser trochanters more superiorly, which alters hip abductor muscle lengths, insertions, and functions [48]; as well as disrupting muscle wrapping around the

capsular ligaments [11, 49]. This should warrant further research to examine the roles of hip joint capsular ligaments and extra-articular tissues, with various neck orientations, to better understand the risks of edge loading during impinged motions.

There are limitations to consider and address for future research. We selected participants based on the maximum and minimum femoral neck-shaft angles, from our larger cohort, and did not base selections criteria on largest and smallest cam deformity parameters. None of our symptomatic participants had a valgus neck, to compare with the asymptomatic and control participants with high femoral neck-shaft angles (134° and 132°, respectively). However, this further supports that a higher femoral neck-shaft angle decreases the risk of early symptoms. A larger sample size would improve the robustness to correlate impingement severities with associated anatomical parameters (cam deformity and neck angle parameters). Furthermore, hip joint contact forces were determined from static optimization, as opposed to instrumented prostheses [6], thus were marginally higher. Differences in age, activity level, BMI, and hip pathology should be considered, when comparing hip contact forces from instrumented prostheses [25]. Also, muscle lines of action and capsular ligaments were not included in the model, as we examined on the effects of the bony cam deformity on adverse contact loading. Knowing that muscle loads contributes considerably to bone remodelling [12] and capsular ligaments may play a vital role in minimizing edge loading [49], it would be imperative to further examine the effects of the surrounding tissues on changes in hip contact forces and efforts to limit microinstability. Finally, soft tissue material properties were approximated, as we did not model biphasic cartilage properties. Future studies should consider poroelasticity to account for consolidation as well as integrating weight-bearing imaging to better characterize cartilage contact mechanics and understand the cartilage deformation [7].

Our study demonstrated that individuals with a cam deformity and varus neck angle are subjected to elevated subchondral bone stresses, which would increase the risks of early clinical signs and symptoms associated with FAI. Ultimately, the asymptomatic cam deformity can remain subclinical, while predisposing to early subchondral bone stiffening and progressive joint degeneration.

9.5 References

1. Agricola R, Heijboer MP, Bierma-Zeinstra SM, Verhaar JA, Weinans H, Waarsing JH. Cam impingement causes osteoarthritis of the hip: a nationwide prospective cohort study (CHECK). *Ann Rheum Dis*. 2012;72:918-923.
2. Anwander H, Melkus G, Rakhra KS, Beaule PE. T1rho MRI detects cartilage damage in asymptomatic individuals with a cam deformity. *J Orthop Res*. 2016;34:1004-1009.
3. Bardakos NV, Villar RN. Predictors of progression of osteoarthritis in femoroacetabular impingement: a radiological study with a minimum of ten years follow-up. *J Bone Joint Surg Br*. 2009;91:162-169.
4. Beaulé PE, Zaragoza E, Motamedi K, Copelan N, Dorey FJ. Three-dimensional computed tomography of the hip in the assessment of femoroacetabular impingement. *J Orthop Res*. 2005;23:1286-1292.
5. Beck M, Kalhor M, Leunig M, Ganz R. Hip morphology influences the pattern of damage to the acetabular cartilage: femoroacetabular impingement as a cause of early osteoarthritis of the hip. *J Bone Joint Surg Br*. 2005;87:1012-1018.
6. Bergmann G, Graichen F, Rohlmann A. Hip joint loading during walking and running, measured in two patients. *J Biomech*. 1993;26:969-990.
7. Buchan LL, Zhang H, Konan S, Heaslip I, Ratzlaff CR, Wilson DR. Open-MRI measures of cam intrusion for hips in an anterior impingement position relate to acetabular contact force. *J Orthop Res*. 2015;34:205-216.
8. Chakraverty JK, Sullivan C, Gan C, Narayanaswamy S, Kamath S. Cam and pincer femoroacetabular impingement: CT findings of features resembling femoroacetabular impingement in a young population without symptoms. *AJR Am J Roentgenol*. 2013;200:389-395.
9. Chegini S, Beck M, Ferguson SJ. The effects of impingement and dysplasia on stress distributions in the hip joint during sitting and walking: a finite element analysis. *J Orthop Res*. 2009;27:195-201.
10. Delp SL, Loan JP, Hoy MG, Zajac FE, Topp EL, Rosen JM. An interactive graphics-based model of the lower extremity to study orthopaedic surgical procedures. *IEEE Trans Biomed Eng*. 1990;37:757-767.
11. Domb BG, Shindle MK, McArthur B, Voos JE, Magennis EM, Kelly BT. Iliopsoas impingement: a newly identified cause of labral pathology in the hip. *HSS J*. 2011;7:145-150.
12. Fernandez J, Sartori M, Lloyd D, Munro J, Shim V. Bone remodelling in the natural acetabulum is influenced by muscle force-induced bone stress. *Int J Numer Method Biomed Eng*. 2014;30:28-41.
13. Fishkin Z, Armstrong DG, Shah H, Patra A, Mihalko WM. Proximal femoral physis shear in slipped capital femoral epiphysis--a finite element study. *J Pediatr Orthop*. 2006;26:291-294.
14. Ganz R, Parvizi J, Beck M, Leunig M, Nötzli H, Siebenrock KA. Femoroacetabular Impingement: A Cause for Osteoarthritis of the Hip. *Clin Orthop Rel Res*. 2003;417:112-120.
15. Guevara CJ, Pietrobon R, Carothers JT, Olson SA, Vail TP. Comprehensive morphologic evaluation of the hip in patients with symptomatic labral tear. *Clin Orthop Relat Res*. 2006;453:277-285.
16. Hack K, Di Primio G, Rakhra K, Beaule PE. Prevalence of cam-type femoroacetabular impingement morphology in asymptomatic volunteers. *J Bone Joint Surg Am*. 2010;92:2436-2444.
17. Hartofilakidis G, Bardakos NV, Babis GC, Georgiades G. An examination of the association between different morphotypes of femoroacetabular impingement in asymptomatic subjects and the development of osteoarthritis of the hip. *J Bone Joint Surg Br*. 2011;93:580-586.
18. Hellwig FL, Tong J, Hussell JG. Hip joint degeneration due to cam impingement: a finite element analysis. *Comput Methods Biomech Biomed Engin*. 2016;19:41-48.
19. Henak CR, Ellis BJ, Harris MD, Anderson AE, Peters CL, Weiss JA. Role of the acetabular labrum in load support across the hip joint. *J Biomech*. 2011;44:2201-2206.
20. Jorge JP, Simoes FM, Pires EB, Rego PA, Tavares DG, Lopes DS, Gaspar A. Finite element simulations of a hip joint with femoroacetabular impingement. *Comput Methods Biomech Biomed Engin*. 2014;17:1275-1284.

21. Jung KA, Restrepo C, Hellman M, AbdelSalam H, Morrison W, Parvizi J. The prevalence of cam-type femoroacetabular deformity in asymptomatic adults. *J Bone Joint Surg Br*. 2011;93:1303-1307.

22. Kennedy MJ, Lamontagne M, Beaule PE. Femoroacetabular impingement alters hip and pelvic biomechanics during gait Walking biomechanics of FAI. *Gait Posture*. 2009;30:41-44.

23. Lamontagne M, Brisson N, Kennedy MJ, Beaule PE. Preoperative and postoperative lower-extremity joint and pelvic kinematics during maximal squatting of patients with cam femoro-acetabular impingement. *J Bone Joint Surg Am*. 2011;93 Suppl 2:40-45.

24. Lamontagne M, Kennedy MJ, Beaule PE. The effect of cam FAI on hip and pelvic motion during maximum squat. *Clin Orthop Relat Res*. 2009;467:645-650.

25. Mantovani G, *Hip Joint Contact Load and Muscle Force in Femoroacetabular Impingement Population*, 2016, University of Ottawa: Ottawa. p. 182.

26. Mantovani G, Ng KCG, Lamontagne M. Regression Models to Predict Hip Joint Centers in Pathological Hip Population. *Gait Posture*. 2015;44:48-54.

27. McGuffin WS, Melkus G, Rakhra KS, Beaule PE. Is the contralateral hip at risk in patients with unilateral symptomatic cam femoroacetabular impingement? A quantitative T1rho MRI study. *Osteoarthritis Cartilage*. 2015;23:1337-1342.

28. Modenese L, Phillips AM. Prediction of hip contact forces and muscle activations during walking at different speeds. *Multibody Syst Dyn*. 2012;28:157-168.

29. Ng KCG, Lamontagne M, Adamczyk AP, Rakhra KS, Beaulé PE. Patient-specific anatomical and functional parameters provide new insights into the pathomechanism of cam FAI. *Clin Orthop Relat Res*. 2015;473:1289-1296.

30. Ng KCG, Lamontagne M, Beaulé PE. Differences in anatomical parameters between the affected and unaffected hip in patients with bilateral cam-type deformities. *Clin Biomech*. 2016;33:13-19.

31. Ng KCG, Lamontagne M, Labrosse MR, Beaulé PE. Comparison of anatomical parameters of cam femoroacetabular impingement to evaluate hip joint models segmented from CT data. *Comput Methods Biomech Biomed Eng Imaging Vis*. 2016;1-10.

32. Ng KCG, Lamontagne M, Labrosse MR, Beaulé PE. Hip Joint Stresses Due to Cam-Type Femoroacetabular Impingement: A Systematic Review of Finite Element Simulations. *PLoS One*. 2016;11:e0147813.

33. Ng KCG, Mantovani G, Lamontagne M, Labrosse MR, Beaulé PE. Increased Hip Stresses Resulting From a Cam Deformity and Decreased Femoral Neck-Shaft Angle During Level Walking. *Clin Orthop Relat Res*. 2016;In Press.

34. Ng KCG, Rouhi G, Lamontagne M, Beaulé PE. Finite Element Analysis Examining the Effects of Cam FAI on Hip Joint Mechanical Loading Using Subject-Specific Geometries During Standing and Maximum Squat. *HSS J*. 2012;8:206-212.

35. Nötzli HP, Wyss TF, Stoecklin CH, Schmid MR, Treiber K, Hodler J. The contour of the femoral head-neck junction as a predictor for the risk of anterior impingement. *J Bone Joint Surg Br*. 2002;84-B:556-560.

36. Radin EL, Paul IL, Tolkoff MJ. Subchondral bone changes in patients with early degenerative joint disease. *Arthritis Rheum*. 1970;13:400-405.

37. Rakhra KS, Sheikh AM, Allen D, Beaule PE. Comparison of MRI alpha angle measurement planes in femoroacetabular impingement. *Clin Orthop Relat Res*. 2009;467:660-665.

38. Ranawat A, Schulz B, Baumbach S, Meftah M, Ganz R, Leunig M. Radiographic Predictors of Hip Pain in Femoroacetabular Impingement. *HSS J*. 2011;7:115-119.

39. Redmond JM, Gupta A, Hammarstedt JE, Stake CE, Dunne KF, Domb BG. Labral injury: radiographic predictors at the time of hip arthroscopy. *Arthroscopy*. 2015;31:51-56.

40. Rylander JH, Shu B, Andriacchi TP, Safran MR. Preoperative and postoperative sagittal plane hip kinematics in patients with femoroacetabular impingement during level walking. *Am J Sports Med*. 2011;39 Suppl:36S-42S.

41. Sanchez Egea AJ, Valera M, Parraga Quiroga JM, Proubasta I, Noailly J, Lacroix D. Impact of hip anatomical variations on the cartilage stress: a finite element analysis towards the biomechanical exploration of the factors that may explain primary hip arthritis in morphologically normal subjects. *Clin Biomech*. 2014;29:444-450.

42. Siebenrock KA, Fiechter R, Tannast M, Mamisch TC, von Rechenberg B. Experimentally induced cam impingement in the sheep hip. *J Orthop Res*. 2013;31:580-587.

43. Siebenrock KA, Kienle KP, Steppacher SD, Tannast M, Mamisch TC, von Rechenberg B. Biochemical MRI predicts hip osteoarthritis in an experimental ovine femoroacetabular impingement model. *Clin Orthop Relat Res*. 2015;473:1318-1324.

44. Speirs AD, Beaule PE, Rakhra KS, Schweitzer ME, Frei H. Increased acetabular subchondral bone density is associated with cam-type femoroacetabular impingement. *Osteoarthritis Cartilage*. 2013;21:551-558.

45. Sutter R, Dietrich TJ, Zingg PO, Pfirrmann CWA. How Useful Is the Alpha Angle for Discriminating between Symptomatic Patients with Cam-type Femoroacetabular Impingement and Asymptomatic Volunteers? *Radiology*. 2012;264:514-521.

46. Taddei F, Cristofolini L, Martelli S, Gill HS, Viceconti M. Subject-specific finite element models of long bones: An in vitro evaluation of the overall accuracy. *J Biomech*. 2006;39:2457-2467.

47. Unsworth A, Dowson D, Wright V. The Frictional Behavior of Human Synovial Joints—Part I: Natural Joints. *J Lubric Techn-T ASME*. 1975;97:369-376.

48. Valente G, Taddei F, Jonkers I. Influence of weak hip abductor muscles on joint contact forces during normal walking: probabilistic modeling analysis. *J Biomech*. 2013;46:2186-2193.

49. van Arkel RJ, Amis AA, Cobb JP, Jeffers JR. The capsular ligaments provide more hip rotational restraint than the acetabular labrum and the ligamentum teres : an experimental study. *Bone Joint J*. 2015;97-B:484-491.

50. Wu G, Siegler S, Allard P, Kirtley C, Leardini A, Rosenbaum D, Whittle M, D'Lima DD, Cristofolini L, Witte H, Schmid O, Stokes I. ISB recommendation on definitions of joint coordinate system of various joints for the reporting of human joint motion--part I: ankle, hip, and spine. International Society of Biomechanics. *J Biomech*. 2002;35:543-548.

V Closing

10 Discussion

Summary | Clinical Implications | Limitations | Conclusion

10.0 Summary

In efforts to examine the effects of cam-type FAI on mechanical hip joint loading, this research program was structured to investigate the pathoanatomical influences on resultant hip joint stresses, using finite element modelling methods. From the systematic review of previous hip joint simulations of cam-type FAI (Chapter 2), specific gaps in the literature and three main areas for development were identified:

1. No consideration for anatomical parameters associated with FAI symptoms and very little emphasis on subject-specific hip joint geometries
2. No consideration for subject-specific bone material properties
3. No consideration for subject-specific hip joint loading parameters

Many of the previous models featured idealized, ball-and-cup, parametric geometries to predict stresses, and implemented homogeneous material properties and in vivo instrumented prostheses loading data. Therefore, the basis of this doctoral research was to formulate more subject-specific models, and to implement a participant cohort (comprised of symptomatic, asymptomatic, and control participants).

First, *Anatomical and Functional Characteristics* (Chapters 4 and 5) determined that the cohort's symptomatic participants had characteristically smaller femoral neck-shaft angles, in comparison with the asymptomatic and control participants. This was further confirmed in symptomatic participants who had bilateral cam deformities, where their asymptomatic (contralateral, unaffected) hip had a larger femoral neck-shaft angle and range of motion. The varus neck angle helped justify participant selection for the subsequent comparative analyses.

Secondly, the studies on *Determining Appropriate Modelling Characteristics* (Chapters 6 and 7) evaluated the accuracy of the large-scale anatomical parameters of the segmented models. This was important to confirm that the reconstructed geometries were representative of the original subject-specific imaging data. Moreover, various modelling parameters (geometric and material properties) were tested to compare the resultant hip joint stresses. The modelling parameters that were selected and compared, demonstrated marginal differences. The heterogeneous bone density models were selected and simulated, to provide more subject-specific representations of each participant cohort and the pathological hip.

Thirdly, the *Modelling of Clinically Relevant Scenarios* (Chapters 8 and 9) examined walking and squatting conditions, comparing the selected symptomatic, asymptomatic, and

control participants. Each of the three groups had one participant with the largest femoral neck-shaft angle (selected from the larger cohort) and one participant with the smallest femoral neck-shaft angle. The symptomatic participant with the low femoral neck-shaft angle demonstrated the highest stresses during walking and squatting. Interestingly, the asymptomatic participant with the low femoral neck-shaft angle showed slightly lower peak stresses, but indicated similar stress concentration on the acetabular cartilage and subchondral bone, during walking and squatting. There may be several anatomical and neuromuscular mechanisms that lead to progression of clinical signs. The results suggest that individuals with a cam deformity and varus neck angle are more at risk of developing early symptoms and labral damage. Table 10.1 summarizes each study (1, 2, 3), sub-study (A, B), and the important clinical findings.

Table 10.1. Summary of the conceptual framework and findings for each individual study (1, 2, 3) and components (A, B)

Study 1. Anatomical and Functional Characteristics	
A. Group classification	B. Affected vs. unaffected hip in symptomatic patients
• Parameters for classification were radial alpha angle, femoral neck-shaft angle, pelvic range of motion • Lower femoral neck-shaft angle associated with symptomatic hip	
Study 2. Determining Appropriate Modelling Characteristics	
A. Evaluation of 3D models	B. Comparison of material properties
• Segmented models and methods demonstrated strong reliability • Nonlinear hyperelastic cartilage models and subject-specific, heterogeneous bone models were examined	
Study 3. Modelling of Clinically Relevant Scenarios	
A. Loading during level walking	B. Loading during squatting
• Both symptomatic participants and the asymptomatic participant with low femoral neck-shaft angle indicated high stresses during walking and squatting • Participants with a cam deformity and low femoral neck-shaft angle demonstrated adverse loading conditions on the acetabular subchondral bone during squatting	

10.1 Clinical Implications

10.1.1 Varus Neck Angle

The symptomatic group had a significantly smaller femoral neck-shaft angle, which coincided with a few previous studies [10, 24, 48]. The discriminant function analysis determined that the femoral neck-shaft angle was the most significant discriminant, after radial alpha angle, to distinguish symptomatic from asymptomatic individuals. This was further observed in the individuals with bilateral cam deformities, but experienced symptoms on one side (affected side with lower femoral neck-shaft angle), while their contralateral side remained asymptomatic (unaffected side with normal femoral neck-shaft angle). Interestingly, some of the bilateral cam participants had larger alpha angles in their asymptomatic hips; which reiterated that mechanical impingement may be due to more than the bony cam deformity.

Anatomically, the varus angle positions the proximal femur's greater and lesser trochanters more superiorly (Figure 10.1). As a result, the femoral head is further seated into the acetabulum and would bring the cam deformity closer towards the anterosuperior labrum. Soft tissue attachments (capsular ligaments and musculotendons) on the two trochanters are also positioned slightly more superior and proximal to the pelvis. The greater trochanter of the femur acts as an attachment site for numerous muscles, including: gluteus medius and minimus, obturator internus and externus, gemelli, and piriformmis; while the lesser trochanter anchors the psoas major and iliacus muscles. Combined with a large cam deformity, this may lead to intra-articular impingement (from the bony deformity) and further extra-articular impingement (from the surrounding soft tissues).

In a previous biomechanical analysis of hip abductor function, Neumann (1989) suggested that the role of the abductor muscles should be considered in "closed-chained" perspectives (*e.g.*, during stance phase of level walking and during squatting), where load carriage should be typically avoided in cases where a symptomatic hip has a decreased internal moment arm [43]. In the case of coxa vara, although shortened hip abductors lengthens the internal moment arm (*i.e.*, hip joint centre to greater trochanter), the external moment arm (*i.e.*, hip joint centre to load of the overall bodyweight) remains the same, thus unable to balance and stabilize the pelvis [43, 61]. This may provoke adverse contact loading when trying to stabilize the pelvis in the frontal plane.

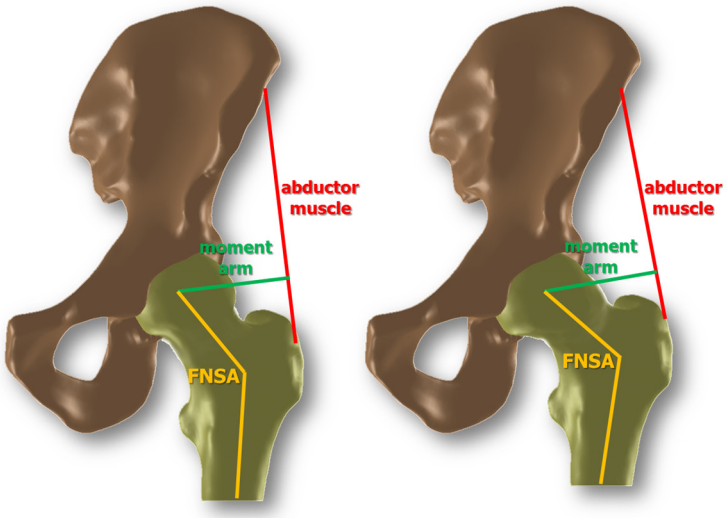

Figure 10.1. Hip assemblies for a femur with a normal femoral neck-shaft angle (FNSA) of 125° (**left**); and a smaller FNSA of 120° (**right**). The smaller neck angle shortened the abductor muscles and, combined with a cam deformity, was associated with symptoms and higher hip joint stresses.

From a spinopelvic perspective, a superiorly positioned lesser trochanter can also shorten iliopsoas and psoas major muscles [8, 13, 18]. Domb and associates (2011) reported cases of iliopsoas impingement leading to labral damage, due to smaller femoral neck-shaft angles [18]. A tighter psoas tendon may further induce adverse stresses to the anterior labrum (Figure 10.2), while restricting hip extension during walking and sagittal pelvic range of motion during squatting, as seen in Chapter 4 and in previous motion analyses [32, 33]. The tighter psoas, due to the varus neck, may be another causative factor as to why many symptomatic participants were unable to squat as low and experienced reduced sagittal pelvic range of motion.

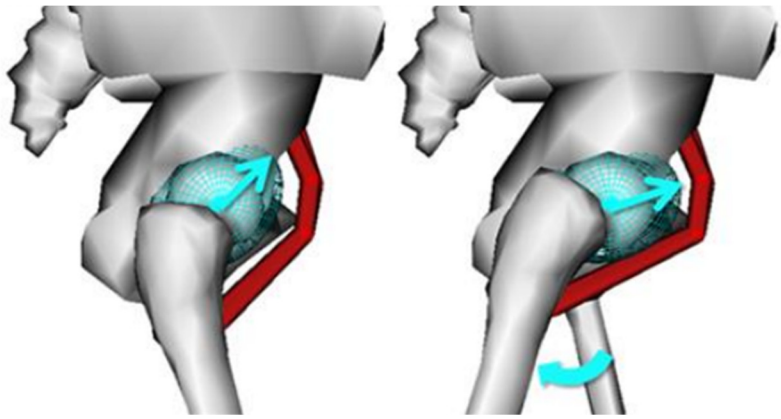

Figure 10.2. Sagittal view of the hip joint in a neutral position (**left**), with the iliopsoas further away from the anterior hip joint**;** and the hip joint in extension (**right**), where the iliopsoas may induce higher anterior forces and impingement. Reproduced with permission of University of Ottawa (Mantovani, 2016).

In addition to the previous suggestions that a lower femoral neck-shaft angle is associated with hip pain [8, 24, 48, 49], Siebenrock and associates (2013, 2015) recently examined the degenerative process of FAI in sheeps [53, 54]. This in vivo, animal study involved a surgical procedure to reduce the femoral neck-shaft angle to induce mechanical cam impingement (Figure 10.3). Ovine specimens were selected as they had aspherical femoral heads, similar to the characteristic shape of human cam morphologies They performed unilateral, intertrochanteric varus osteotomies on a group of 16 healthy sheeps, where the varus osteotomy seated the aspherical femoral head closer to the anterolateral and anterosuperior labrum. After short and long-term follow-up (sacrificed at 14, 22, 30, 38 weeks), they observed localized chondrolabral degeneration on the operated side, which were comparable to the progressive damage in human hips with cam FAI (Figure 10.4). Siebenrock and associates (2015) further confirmed the course of the ovine hips' degenerative process, measuring the cartilage biochemistry at 10 and 14 weeks, using predictive T2 and T2* imaging modalities [54].

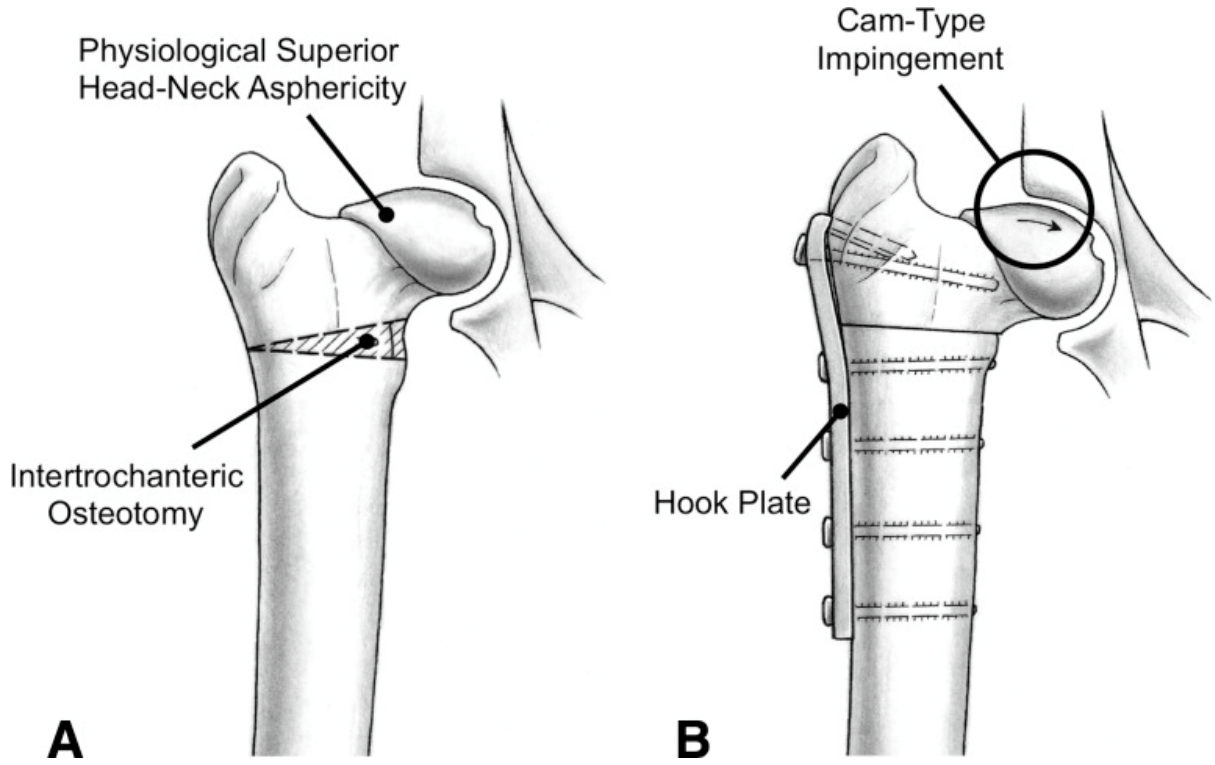

Figure 10.3. Siebenrock and associates (2015) examined the healthy sheep hip structure, as it had a naturally aspherical femoral head (A). An intertrochanteric varus osteotomy was performed to induce mechanical cam impingement (B), by medially rotating the femoral head-neck and closing a 15-degree wedge resection. Reproduced with permission of Springer (Siebenrock et al., 2015).

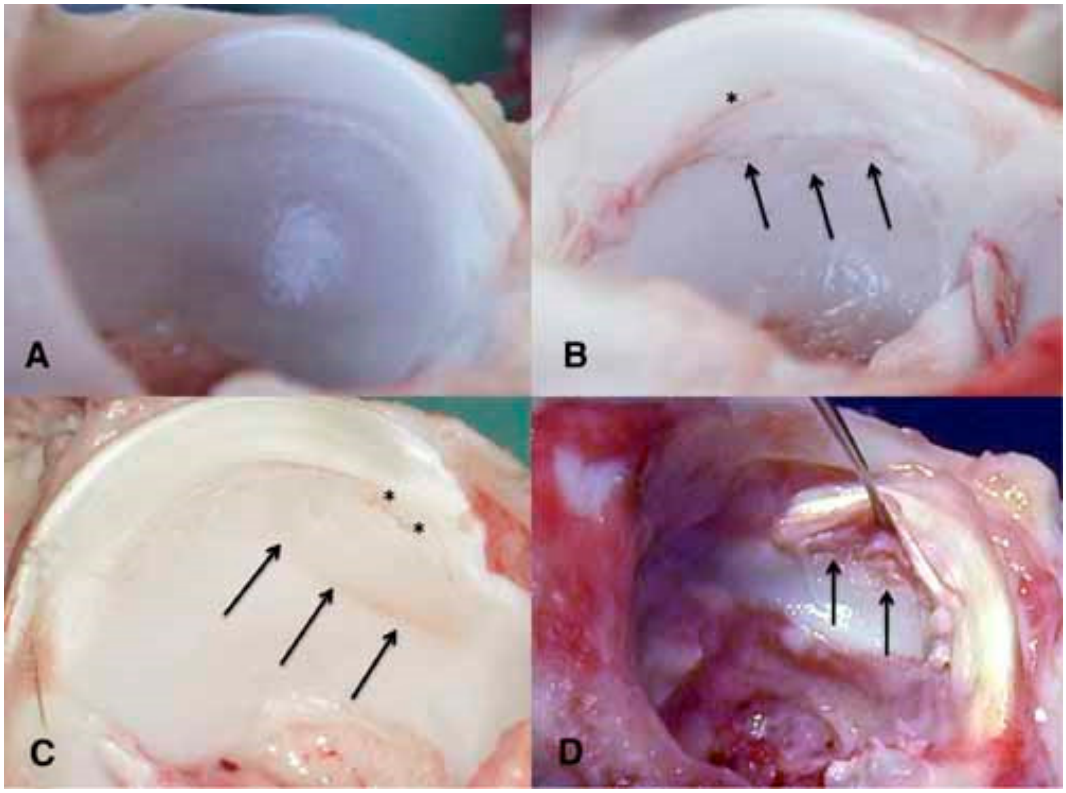

Figure 10.4. Siebenrock and associates' (2013) in vivo ovine study, comparing: (**A**) their macroscopic evaluation of a healthy, control sheep with normal cartilage; (**B**) development of lesions after 14 weeks of the varus osteotomy (black arrows denote malacia; star denotes longitudinal labral tear); (**C**) delamination of lesion (black stars) with carpet phenomena (black arrows) after 22 weeks; and (**D**) detached labrum, with malacia and cleavage lesions (black arrows) after 38 weeks. Reproduced with permission of John Wiley and Sons (Siebenrock et al., 2013).

10.1.2 Finite Element Methods

The importance of subject-specific hip joint simulations cannot be overstated, especially when examining clinical research questions. The finite element modelling parameters were selected to address previous concerns of subject-specificity, to better represent an individual's subject-specific anatomical geometries and bone material properties. First, subject-specific anatomy was a critical parameter to include in the finite element models, as the cam deformity and femoral neck-shaft angle were associated with symptomatic FAI. It was also important to include subject-specific cartilage thicknesses, to represent each cohort, since individuals with a cam morphology would naturally have slightly thinner cartilage layers, compared to control participants. Second, subject-specific bone material properties were necessary, since bone mineral densities differ between individuals with and without a cam morphology. Finally, subject-specific hip contact forces were important and reflected each participant's joint loading

mechanics. Interestingly, the symptomatic participants demonstrated lower hip contact forces, compared to the asymptomatic and control individuals. This indicates that hip joint stresses are likely less influenced by the magnitude of the force vector, but rather more influenced by the direction of the force vector. This also reiterates that the symptomatic participants demonstrated a neuromuscular compensatory mechanism, in efforts to avoid impingement and pain.

In efforts to extract clinically relevant data and results from finite element simulations, Viceconti and associates (2005) provided a guideline of issues to address, which included: model selection, proper parameter identification, inter-subject variability, verification, sensitivity analysis, and validation [64].

10.1.2.1 Model Selection

The intention of the selected model was to contribute to the understanding of adverse hip joint loading due to cam FAI. For the models to adequately represent a participant cohort, several subject-specific input parameters (*e.g.*, hip joint loading, geometries, and material properties specific to the participant or cohort) could be implemented to better predict the adverse loading conditions. The bone and soft tissue geometries were extracted from subject-specific imaging data and, along with the mesh refinement parameters and boundary conditions, were consistent for all simulations. For the quasi-static conditions, which simulated a specific instance during level walking (terminal stance) and mid-squat (90° of hip and knee flexion), conventional soft tissues properties were implemented. Cartilage was considered as a uniform, isotropic layer which was adequate for quasi-static, non-cyclic loading parameters [3, 4, 15, 23, 26-29, 50, 51, 68]. In combination with the hyperelastic soft tissues, heterogeneous bone models were implemented to demonstrate inter-subject variability within a cohort and to also represent a pathology-specific demographic. The effects of simplified material modelling parameters leading to progressive joint degeneration have not yet been fully elucidated.

10.1.2.2 Proper Parameter Identification and Inter-Subject Variability

As mentioned, the quasi-static simulations compared hip joint stresses at specific time points, during level walking (terminal stance) and mid-squat (90° of hip and knee flexion). For this, it was critical to identify the relevant independent variables to structure the comparative analyses. Differences in anatomical and functional parameters, between the participant groups

(symptomatic, asymptomatic, and control), established this basis for clinically relevant dependent variables. As an independent variable, the alpha angle parameter identified who were the individuals with the cam morphology; however, it was the neck angle parameters that established significant and clinical differences between those with or without symptoms.

For dependent variables, cartilage loss is a mediated process that has been linked to regions of elevated stresses, due to abnormal bone geometries [22, 42, 46]. As a dependent variable, maximum shear stresses were examined in each participant's acetabular cartilage, labrum, and subchondral bone [7, 35, 46], as it could indicate adverse loading leading to cartilage failure and across the cartilage-bone interface [7, 46]. More importantly, to contribute to the understanding of joint loading to the pathomechnical process, Ateshian and associates (2015) reported that the instantaenous response of shear stresses at the cartilage-bone interface was consistent with experimental observations [7]. Moreover, maximum shear stress has been typically measured to correlate with metrics observed for physical damage or metabolic change [7]. While there is variability to be expected with any combination of material properties and modelling parameters, it will always be important to understand relative differences between each combination of dependent variables and, if possible, account for these variabilities.

To account for inter-subject variability, each participant model had an individualized bone model, derived from a density-elasticity relationship. The heterogeneous bone models showed slightly more distinct secondary stress concentrations that corresponded with areas of denser bone, in comparison with the other conventional bone modelling parameters. This was more pertinent for the cross-sectional analysis – comparing subject-specific hip joint stresses within pathological groups. After retrospectively examining the bone density distributions, the elastic moduli were evidently different in the acetabular dome, demonstrating inter-subject variability (Figure 10.5). The symptomatic participants had marginally higher elastic moduli than the asymptomatic group; however, both cam deformity groups (symptomatic and asymptomatic groups) had higher acetabular elastic moduli than the control group, which coincided closely with previous analyses of acetabular subchondral bone density [58]. The symptomatic participant with low femoral neck-shaft angle had the highest elastic modulus values (~ 20 GPa), which reflected the osteoarthritic process of the stiffer subchondral bone and the elevated stresses in the acetabulum.

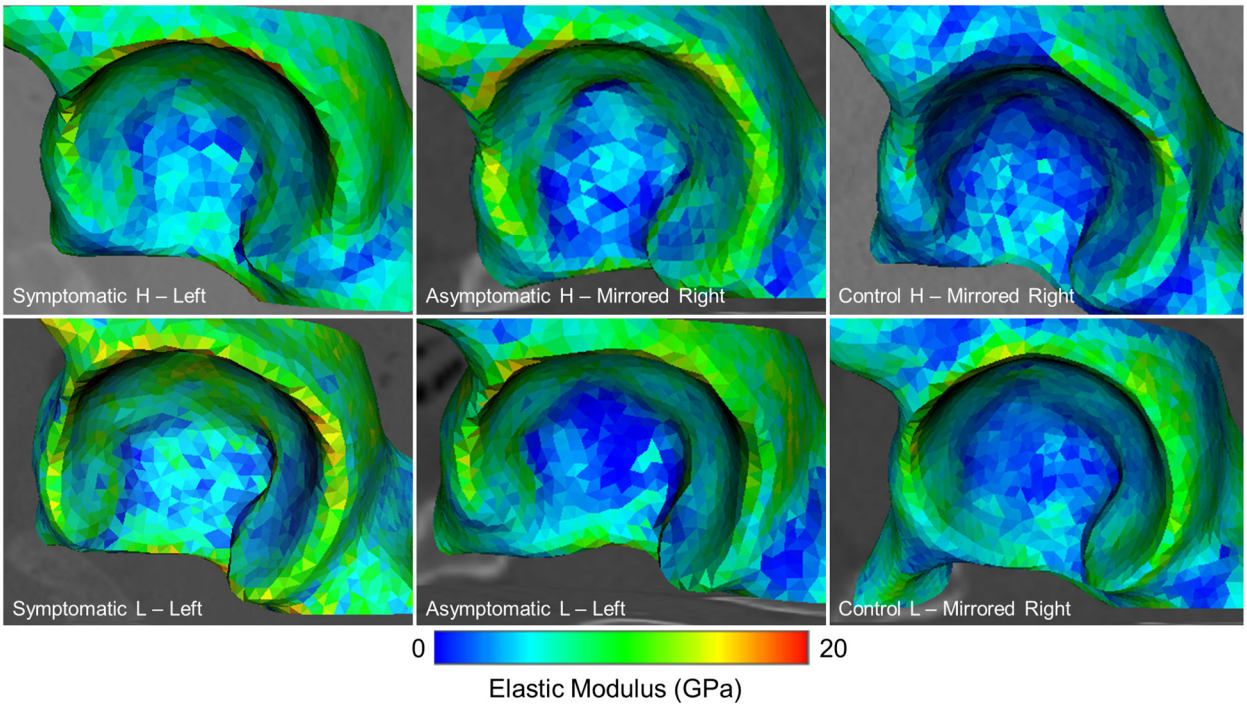

Figure 10.5. Sagittal view of each participant's acetabulum model, indicating the elastic modulus distribution. The symptomatic (**left**) and asymptomatic (**centre**) groups had higher elastic moduli than the control group (**right**), while the symptomatic participant with low femoral neck-shaft angle (**bottom left**) had the highest values.

10.1.2.3 Verification and Sensitivity Analysis

Verification ensures that the result approximates the underlying mathematical model [64]. The hip joint models were reconstructed from subject-specific imaging data and indicated slight discrepancies (from the Bland-Altman plots), but were consistent to be implemented in clinical orthopaedics [12]. The mesh for bone and soft tissue models started with a nominal element size of 3 and 2 mm, respectively, and then refined to ensure mesh insensitivity and convergence. Element sizes and counts were similar, for each of the bone and soft tissue models. For the nodal analysis, unaveraged stresses were confirmed to be within 5% of the averaged values at the integration points, to ensure that meshes were sufficiently refined [59]. Moreover, both iterative and direct solvers were tested and compared, to ensure that there were no inconsistencies.

10.1.2.4 Validity

As Viceconti and associates (2005) remarked, it is near impossible to fully validate a numerical model [64]. However, it is common to verify and validate results against previous similar studies

in literature. The implications of these comparisons are important as they permit a level of validation for how much "trust" there is in the results or if the finite element simulations yield any practical significance. The systematic review (Chapter 2) noted that previous FAI simulations used simplified geometries to predict stresses, along with homogeneous bone material properties and instrumented prostheses loading data. Furthermore, no study investigated hip contact stresses resulting from an asymptomatic cam morphology; thus, more importantly, no study differentiated between hips with a symptomatic cam deformity and an asymptomatic cam morphology.

The first reported finite element model on FAI, by Chegini and associates (2009), parameterized an idealized ball-and-socket model to various cam and acetabular coverage morphologies, and applied instrumented prosthesis loads [15]. During level walking, there were no changes in stress with varying alpha angles, which was likely due to their idealized geometry. Their control parameters were slightly lower (contact pressure = 2.57 ± 0.89 MPa), than results reported in this doctoral research; however, their model did not consider subject-specific geometries, bone material properties, and, more importantly, joint loading, which could have yielded a higher result. During squatting, the cam deformity groups' peak cartilage-labrum stresses were similar to their reported large range of contact pressures (3.67 – 12.84 MPa) and von Mises stresses (9.7 – 27.2 MPa) for cam deformities with normal acetabular coverage. There was no report on subchondral bone stresses.

Another earlier finite element study examined acetabular subchondral bone stresses, due to cam FAI during maximal squatting, but applied intersegmental hip forces [44]. The cam deformity groups' stresses were within range of their earlier values (13.4 – 16.9 MPa), however, the current study included a labrum model as well as subject-specific bone material properties and hip contact forces (as opposed to intersegmental forces from inverse dynamics), thus improving the representation of hip contact stresses.

Jorge and associates (2012) found much higher cartilage contact pressures during deep flexion, noticing elevated peak contact pressures and von Mises stresses in the anterosuperior cartilage (11.6 and 14.4 MPa, respectively) and labrum (16.4 and 14.7 MPa, respectively) [30]. Their study was limited to one male subject with a severe cam deformity (age = 27 years, alpha angle = 98°) matched with one healthy female control subject (age = 50 years, alpha angle = 48°). Another recent study by Hellwig and associates (2015) also implemented idealized geometries

and instrumented prosthesis loads during walking to compare one cam (alpha angle = 74°) with one control hip (alpha angle = 40°) [25]. Using a poroelastic, orthotropic cartilage model, they found peak contact pressures in the superior cartilage for the control hip (2.87 MPa). Peak pore pressure was also different between control (0.42 MPa, posterior cartilage) and FAI (3.76 MPa, anterosuperior cartilage). The authors remarked that their models were idealized for convergence [25]. It is also a common strategy to validate numerical models by comparing results with case controlled in vitro experiments. However, none of the previous finite element simulations on cam FAI validated their models using this approach. Although in vitro cadaveric studies involve physical testing of the biological tissues, there are numerous inherent limitations that may result in an incompatible solution.

To date, there has been no published in vitro cadaveric hip joint study that involved human hips with cam deformities. This makes direct validation, with previously established case controlled experiments, difficult. As mentioned earlier (Chapter 10.1.1 – Varus Neck Angle), Siebenrock and associates' (2013, 2015) in vivo studies examined the progression of hip joint degeneration in ovine hips with a cam deformity and varus neck angle [53, 54]. This is the closest study in vitro or in vivo study that considered the influence of additional anatomical parameters on joint degeneration; and aligns well with the results presented in this dissertation. In continuation with the aforementioned studies, Maquer and associates (2016) recently examined in vitro the effects of cam resection on ovine hips and found that fractures risks were only high with large osteochondroplasty procedures [37].

10.1.3 Effects of Cam FAI on Joint Stresses

From the finite element simulations on level walking and squatting, the cam deformity participants with low femoral neck-shaft angles had higher stresses in their respective subgroups. Both symptomatic participants and the asymptomatic participant with the lower femoral neck-shaft angle indicated anterolateral and posterior stress concentrations, which coincided very closely to known areas of cartilage damage. The symptomatic participants experienced multiple stress concentrations during squatting, in the anterosuperior and posterior cartilage and subchondral bone, which could have been indicative of slight contrecoup stresses [9], and corresponded with regions of decreased proteoglycan content [5, 39]. Interestingly, the asymptomatic participant with the high femoral neck-shaft angle demonstrated marginally higher

cartilage stresses than the control group, but showed high subchondral bone stresses during squatting. In addition, the asymptomatic participant with low femoral neck-shaft angle experienced subchondral bone stresses that were more similar to the symptomatic group [5, 58].

Comparing these results with clinical observations, Speirs and associates (2013) implemented the similar cohort (n = 36) of symptomatic, asymptomatic, and control participants (of 12 equally matched groups), to investigate acetabular subchondral bone density [58]. The anterosuperior bone density was much significantly higher for the symptomatic (14 – 38%) and asymptomatic groups (15 – 34%), compared to the controls. Interestingly, the asymptomatic group had higher bone mineral density values in the anterior rim section and anterosuperior midsection, compared to the symptomatic group (Figure 10.6). Moreover, bone mineral density correlated moderately with axial 3:00 alpha angle (R^2_{ALL} = 0.16) but had a stronger correlation with radial 1:30 alpha angle (R^2_{ALL} = 0.44).

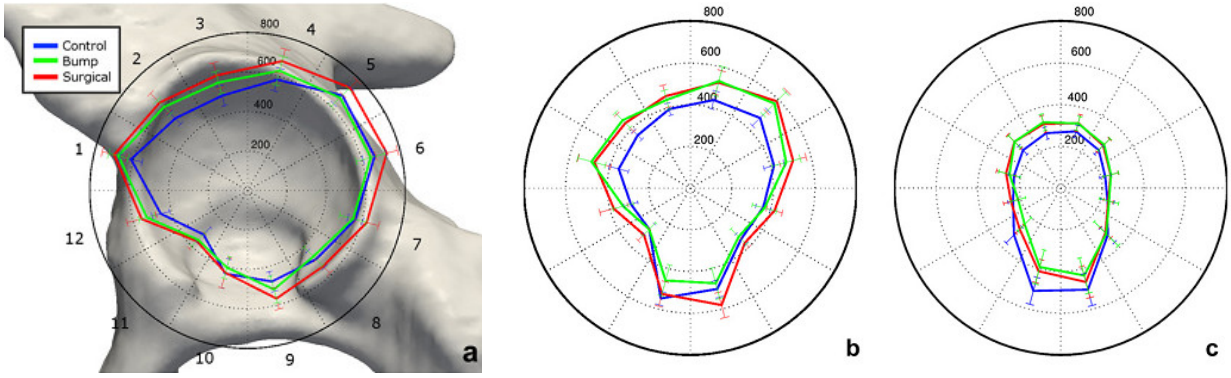

Figure 10.6. Sagittal view of Speirs and associates' (2013) acetabular bone mineral density plots of the symptomatic ("surgical", in red), asymptomatic ("bump", in green), and control groups (in blue), plotted on a left hip. Bone mineral density (mg/cc) was measured at: **A**) the level of the rim (lateral edge of the acetabulum); **B**) middle (midsection of the acetabular thickness); and **C**) medial wall. Reproduced with pending permission of Elsevier (Speirs et al., 2013).

In addition, recent publications demonstrated the capacity of T1ρ MRI to determine differences between normal hips and FAI [47], where relaxation time is inversely proportional to proteoglycan concentration. Using a similar cohort to this thesis study, McGuffin and associates (2015) studied 19 individuals with bilateral cam deformities and found no differences in proteoglycan depletion between their affected (symptomatic) hip and their unaffected (asymptomatic, contralateral) hip, indicating that there is still an increased risk of cartilage degeneration, regardless of hip pain [39]. Comparing relaxation times, the closest comparison

was in the anterolateral quadrant and the affected hip (mean = 31.7 ms, range = 29.6 – 34.0 ms) was only marginally higher than the unaffected side (mean = 29.1, range = 26.2 – 31.9 ms; p = 0.089). Anwander and associates (2016) then compared 20 asymptomatic individuals with a cam deformity to 16 healthy individuals, using T1ρ MRI [5]. Again, asymptomatic cam hips had a longer relaxation time (34.0 ± 4.6 ms) than control hips (31.3 ± 3.2 ms; p = 0.050). In this case, alpha angles did not correlate with relaxation time; which may further support that the size of the cam deformity alone does not lead to a depletion of proteoglycan or to the progression of symptoms.

Although the cam deformity rarely impinges at lower amplitudes of motion, the combined effect with a lower femoral neck-shaft angle and shortened abductor may contribute to more adverse contact loading to stabilize the pelvis. Elevated hip joint stresses of symptomatic individuals could be attributed to pre-existing chondrolabral damage, resulting in incongruent articulations and unfavorable contact mechanics. The control participant in this study, with the lower femoral neck-shaft angle, showed more favorable contact mechanics, which again may justify that a combination of both cam and neck angle parameters (among others) may contribute to adverse stresses.

During level walking, both asymptomatic participants along with the control participant with high femoral neck-shaft angle all had larger hip extensions. Both symptomatic individuals had smaller hip extensions during terminal stance, which could have been limited by capsular ligaments or perhaps indicated a protective mechanism to minimize anterior hip contact forces [34, 65]. Interestingly, the symptomatic participants had lower hip joint contact forces, in comparison with the other two groups. In terms of the anatomical structure, the varus neck and higher trochanters resulted in a shortened iliofemoral ligament and different iliopsoas wrapping. This could also be a neuromuscular adaptation mechanism to avoid pain by altering the direction and magnitude of the force vectors [40]. Lewis and associates (2010) determined that a greater hip extension resulted in elevated anterior hip joint force [34]; while Wesseling and associates' musculoskeletal model (2015) also showed lower hip contact forces, during terminal stance, after reducing hip extension [65]. Wesseling and associates' (2016) subsequent study on hip implants suggested that increasing hip abduction would decrease contact forces; while decreasing hip extension, during terminal stance, would further result in lower risks of edge loading [66].

Furthermore, there have been suggestions that subclinical slipped capital femoral epiphysis (SCFE) and the abnormal head-neck extension can lead to the growth of the cam deformity [1, 17, 21, 55]. A varus hip could lead a hip to higher shear loading across the physeal growth plate, which could further predispose to SCFE or cam FAI [20]. In an earlier finite element study, by Fishkin and associates (2006), a single male model with slipped capital femoral epiphysis was parameterized to various femoral versions, directional varus loading, and bodyweight loading parameters [20]. Varus loading conditions resulted in higher shear forces across the physeal plate, ultimately increasing the risk of slippage. In another study by Sánchez Egea and associates (2014), a finite element model was parameterized with various femoral neck-shaft (110 – 130°), femoral torsion (0 – 20°), and acetabular version angles (0 – 20°), to examine the effects of anatomical variations on hip joint cartilage stresses, during quasi-static walking loads [52]. In comparison with the results from this dissertation, their varus configuration (110°) demonstrated higher stresses than their control model (Figure 10.7); though their study parameterized one female model (age = 99 years, BMI = 23 kg/m^2), taken from an existing database. Moreover, femoral head parameters were not considered (*i.e.*, alpha angles and femoral head-neck offset), which could explain why peak stresses were centrally located in the acetabular cartilage, instead of the chondrolabral junction.

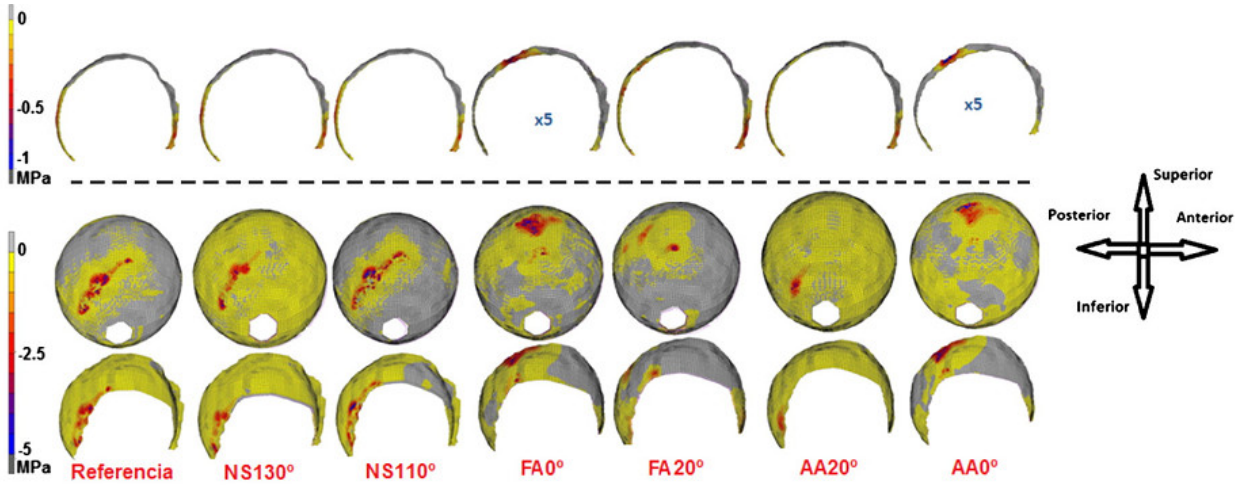

Figure 10.7. Sánchez Egea and associates' (2014) finite element study that compared a normal hip condition (Referencia) and parameterized femoral neck-shaft (NS), femoral anteversion (FA), and acetabular anteversion (AA) angles, examining stress distributions in the labrum (**top row**), femoral cartilage (**middle**), and acetabular cartilage (**bottom**). The varus neck configuration (NS110°) resulted in higher and very localized stresses across the posterosuperior quadrants. Reproduced with permission of Elsevier (Sánchez Egea et al., 2014).

In Buchan and associates' (2015) work, 12 cadaveric hips with cam morphology were loaded and examined using open MRI [14]. It was not reported if the specimens experienced symptomatic impingement. The hip joint specimens were placed in two positions: 1) supine and 2) anterior impingement; and imaged using a T1-weighted sequence. After imaging, the iliofemoral capsular ligament and ligamentum teres were excised, to access the hip joint capsule. Contact pressure sensors (K-Scan 4400, Tekscan, Boston, MA, USA), designed for the acetabular socket's convexity-concavity articulation, were mounted onto the lunate surface. The hip specimens were manually moved to simulate passive anterior impingement. From this work, hips with the cam morphology demonstrated a higher level of intrusion into the cartilage space [14]. Interestingly, their hip with a combination of a cam morphology, coxa vara, acetabular retroversion, and femoral neck osteophytes had the highest contact forces (Figure 10.8), in comparison with all the other hips. The authors reported that two hip specimens were excluded from their study, as the cam deformity was severely large combined with a varus neck, which resulted in dislocations.

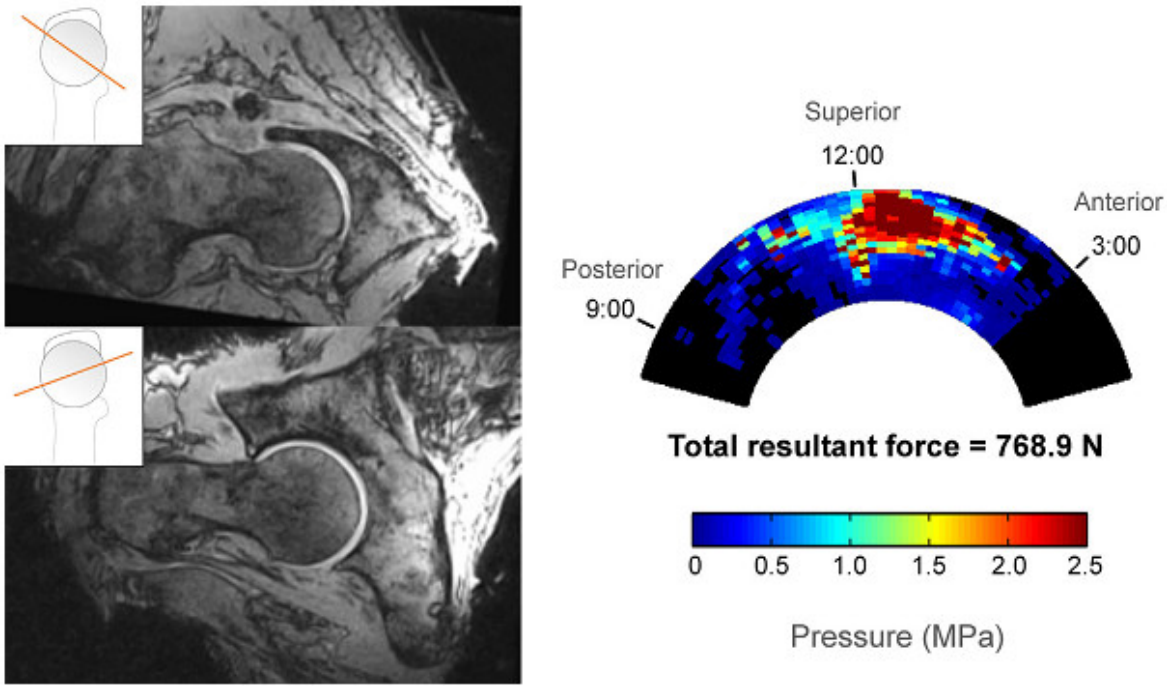

Figure 10.8. Buchan and associates' (2015) hip joint specimen with a combination of a large cam morphology, varus neck angle, acetabular retroversion, and anterior neck osteophytes. The impingement test resulted in a severe cam intrusion (**top left**) and contact with the anterior labrum (**bottom left**). Moreover, the total resultant contact force, measured from the contact pressure sensors, were the highest among their collected specimens (**right**). The resultant stresses, from the impingement test, was concentrated in the anterosuperior quadrant. Reproduced with permission of John Wiley and Sons (Buchan et al., 2015).

10.2 Limitations

10.2.1 Participant Demographics

One general limitation that affected all three studies was that the cohort consisted of a male-dominant population, as the cam deformity is statistically prevalent in men. The inclusion of females could introduce variances in anatomical structure and squat kinematics. Therefore, an additional study to examine sex-differences could elucidate whether the pathomechanics of FAI is specific to sex. Age differences may also have been a limitation since cartilage and labral damage not only depends on the size of the deformity, but may also increase with age. Although our symptomatic group was slightly older, age differences were not significant and there were a few older symptomatic participants who performed deeper squats and wider pelvic motions.

Furthermore, many of the patients who presented themselves to the senior orthopaedic surgeon, with unilateral hip pain, were younger males. It may have been possible that these patients were exposed to strenuous physical activities during skeletal maturation, predisposing them to cam deformities. Their persisting clinical symptoms and pain over time may have been attributed to the recurring mechanical impingement, leading to symptomatic chondrolabral damage or subchondral bone stiffening. The subsequent recruitment process of the asymptomatic participants required seeking volunteers who could fulfill the sex-, age-, BMI-matching criteria. As result, several of the asymptomatic volunteers (with and without a cam morphology) were male, young, and average in BMI (characteristic of the young, athletic, male population).

Although it was determined that the sample sizes were adequate for the anatomical measurements, a larger sample size would further increase predictive power. For the finite element simulations, certain limitations were imposed by the small sample size. The participants with the highest and lowest neck angles were selected for simulation, but a larger sample size would increase the robustness and differences among the subgroups, which may help to further delineate intersubject variability and correlate impingement severities with associated anatomical parameters (cam morphology and femoral neck-shaft angle).

It is possible that the participants' walking and squatting motions (squat depth and pelvic range of motion) were limited by pain. However, during any of the required task, participants were asked if they experienced any discomfort or pain during the motion, and none of the patients stated that pain limited their walking or squatting capacity. It is possible that the pace of

the walking or squatting motion may have affected the loading dynamics of the cam deformity onto the articulating surfaces. Although none of the patients had evidence of osteoarthritis on imaging data, there are still numerous possible causes of limited squat (*e.g.*, apprehension by the participant to avoid pain, neuromuscular inability, extra-articular impingement). Another limitation was the use of pain to help classify the different groups.

10.2.2 Anatomical Parameters

One of the limitations was the number of CT parameters considered. Since the focus was on cam-type FAI, common recurring parameters of the proximal femur were selected, as opposed to the acetabulum. To fully understand the relationship among joint structures, clinical signs, and the role of acetabular orientation on joint kinematics, an extensive study of the morphological parameters associated with the acetabulum (*e.g.*, lateral center-edge angle, retroversion index, subtended angles, acetabular crossover locations and coverage) may be needed in the future, along with a 3D shape analysis of the cam deformity. These additional anatomical parameters could be considered to further compare symmetry between the affected and unaffected sides, in individuals with bilateral cam deformities. A next step could be to examine the relationship between the acetabular coverage and the femoral head-neck deformity and its influences on range of motions. Moreover, additional anatomical spinopelvic parameters should be measured, to examine their potential influence on anterior hip joint pain and restricted sagittal range of motion. This could also help further differentiate symptomatic from asymptomatic hips.

10.2.3 Modelling Parameters

To evaluate the geometric 3D hip joint models, the anatomical measurements adhered to the 2D measurement methods as closely as possible (*i.e.*, circle-fitting to reconstruct a geometric centroid). The intention was to model large-scale anatomical parameters of the femoral head-neck and acetabulum and compare anatomical measurements that were used in clinical practice. According to our Bland-Altman analyses, it was slightly more difficult to assess asymptomatic participants, suggesting the need for more thorough understanding of the anatomical indicators of osteoarthritis to classify the asymptomatic population. Apart from the alpha angles, there were no other established anatomical thresholds to characterize asymptomatic individuals. The Bland Altman analyses' limits of agreement were deemed reasonable, based on our clinical application

[12], with mean differences centered on zero. A few underestimations should be expected with CT measurements. When doubt arises with the segmented models and in clinical practice, any measured hip joint parameter with an intermethod ICC near or below 0.75 should be repeated. If the intermethod ICC still falls below 0.75 after the repeated observation, the model could be re-segmented to ensure that the models are accurate geometric representations.

From the MRI data, the hip was imaged with 3-mm slices and although this was a relatively large slice thickness, compared to CT imaging, the MRI was a high resolution sagittal sequence, adequate for assessing the cartilage thicknesses (in-plane pixel spacing of 0.469 mm). Both the CT and MRI acquisitions were done in the supine position. To further assess the effects of hip morphologies on cartilage thickness, imaging during weight-bearing positions could be considered in the future [67], to incorporate the effects of natural postural position and loading.

In terms of the material modelling parameters, a notable limitation was the number of parameters examined in this study. Conventionally used material modelling parameters from literature were selected to simulate the macroscopic effects of joint loading on cartilage contact stresses. This study also examined a single, healthy participant with no known lower-limb abnormalities, in efforts to compare parameterized material modelling parameters. Knowing that inter-subject variability may be just as influential as parameterizing material properties [23], it would be interesting to examine the effects of each modelling parameter with a larger sample size or a group that could represent a patient-specific population. This would further confirm if a subject-specific, heterogeneous bone model could better predict symptomatic contact stresses. There are several previous studies that implemented intricate modelling parameters and material properties, which posed other in-depth and purposeful research questions.

Although there was an improvement with implementing subject-specific bone material properties to examine FAI, biphasic cartilage properties or permeability were not considered. Cartilage consolidation should be further considered in future studies along with dynamic responses [6, 35, 57]. Although subject-specific bone densities were mapped onto individual elements, resulting in heterogeneous bone models, another limitation may be the isotropic properties used. Isotropy is a conventional material property, when implementing subject-specific bone density mapping for heterogeneous components, however, future steps should consider anisotropic or orthotropic properties to simulate the material behavior or bone.

Although higher maximum shear stresses may be associated with increased subchondral bone density [58) as well as potentially higher risks of hip joint degeneration [39, 46], it is not known if cumulative stress or damage can play a role in the osteoarthritic process. In addition to incorporating dynamic responses in future studies, a cumulative stress metric should be considered to further examine the damage threshold in the cartilage.

Resultant hip joint loading was interpreted as hip contact forces applied to the femoral head, similar to load applications of Bergmann and associates' study (1993). Hip joint contact forces implemented in this dissertation were determined through static optimization and were marginally higher than forces measured from instrumented prostheses [36]. It should be acknowledged that there are large variances in age, activity level, BMI, and pathology between the participants studied in this work and participants with instrumented prostheses (*i.e.*, older in age, moderate activity level, higher BMI, arthroplasty resulting from osteoarthritis). A subsequent step could be to incorporate individual muscle contributions at their lines of action and through their wrapping points using a musculoskeletal model, which may yield higher resultant stresses, as opposed to a resultant net contact force at the hip joint center. As discussed earlier (Chapter 10.1.1 – Varus Neck Angle), subject-specific muscle wrapping and lines of actions (*e.g.*, femoroacetabular abductors and rotators due to varus neck angle; tightened psoas and anterior hip pain, due to pelvic tilt and varus neck angle), can help further delineate differences between symptomatic and asymptomatic individuals [63].

10.2.4 Clinical Simulations

The resultant simulations carry certain limitations. Only quasi-static conditions during level walking (peak force during terminal stance) and during squatting (mid-squat condition) were examined and compared. There are numerous other activities of daily living that could have been implemented for simulation, such as: stairs ascent and descent, sit-to-stand and stand-to sit, incline ramp up and decline ramp down; however, standard gait analysis was selected as it was common movement of interest. Furthermore, squatting requires a larger combined range of hip motions; and it was selected for comparison as it previously revealed differences between symptomatic patients and healthy, control individuals [33].

In terms of the selected participants, the individual with the highest and the individual with the lowest femoral neck-shaft angle were selected for each subgroup. Due to the

characteristically varus angle of the symptomatic group, there was an overlap in femoral neck-shaft angles between the symptomatic and asymptomatic groups (*i.e.*, more varus necks of the symptomatic group, compared to the normal range of neck angles of the asymptomatic group). None of the symptomatic participants had a valgus neck to directly compare with upper limits of the asymptomatic and control groups (134° and 132°, respectively), whereas similarly, our asymptomatic and control participants did not have varus angles. The consequence of these small differences has yet to be fully elucidated. The slight overlap in femoral neck-shaft angles between the symptomatic and asymptomatic groups also showed overlapping peak hip joint stresses. It was interesting to note that higher stresses were not necessarily dependent on participant group or symptoms, but were perhaps associated with femoral neck-shaft angle and cam morphology. In addition, we also accounted for the highest and lowest femoral neck-shaft angles in each group as opposed to examining the largest and smallest cam deformities. The baseline bone densities for each model were within range of typical values for cortical and trabecular bones. There were no differences in elastic modulus between participants within a subgroup, but the symptomatic and asymptomatic participants had marginally higher elastic moduli than the control group.

In addition to the muscle lines of actions, capsular ligaments were not included in the model in the modelling and simulations. Although the focus was on the contributions of the bony morphology toward adverse contact loading, the study of ligament contributions towards contact mechanics would be instructive. Taut hip joint ligaments could properly seat the femoral head into the acetabulum at more neutral positions, but may restrain hip range of motion in individuals with a cam morphology. Knowing that muscle loads contributes considerably to bone remodelling [11, 19] and knowing that capsular ligaments also play a vital role in minimizing edge loading [62], poorly functioning ligaments may be unable to prevent adverse contact loading at higher amplitudes of motion. Thus, further examination of the surrounding capsule on limiting adverse stresses and microinstability is warranted [31, 38, 41, 56, 60].

10.2.5 Effects of Surgical Correction

The post-operative effects (after open surgical dislocation or arthroscopic cam resection) of the symptomatic patients were not examined. It was recently reported that surgically resecting the cam deformity can delay the pathomechanical process of subchondral bone stiffening [16]. One

of the next steps, part of the ongoing research program, is to compare the hip joint stresses before and after surgical correction, to determine if there are any improvements to the hip joint stresses.

The results from this dissertation may further challenge the perspectives of joint preservation surgery. In a case where a patient who underwent an ineffective cam resection (to reduce pain or delay the pathomechanical process), an intertrochanteric osteotomy could be considered, to correct the varus neck. Alternatively, femoral neck lengthening can be considered for hips with superiorly positioned greater trochanters, to lengthen the abductor muscles [2]. Moreover, in the scenario of tightened iliopsoas, due to coxa vara, an alternative psoas release could be considered, to alleviate anterior hip joint stresses [18]. The long-term results of the combined surgeries would need to be further investigated, to fully understand any effects on microinstability of the hip joint.

In any case, non-invasive and non-surgical methods should always be considered first. If no labral tear or short-term cartilage damage was experienced, it would be a question of pain management for the individual and lengthening the hip abductors and iliopsoas. This non-invasive, muscular strengthening approach could be implemented prior to any long-term degenerative or arthritic changes.

10.3 Conclusion

With the ultimate goal to understand the pathomechanisms of cam FAI, the collective sub-studies and the iterative design process of the finite element models presented a modelling approach to the analysis of cam FAI, by integrating more subject-specific data to investigate mechanical stresses corresponding to areas of articulating cartilage damage and subchondral bone adaptation. In efforts to preserve the natural hip joint, understanding that anatomical parameters can play an important role in the onset of hip symptomatology is critical to help identify those who are at greater risk of earlier onset of irreversible damage.

An early theory, proposed by our research group,[1] suggested that the cam morphology could subject the hip joint to early bone adaptation. This early research question asked if bone remodelling, secondary to mechanical stimulus, could play a role in the degenerative process [45]. At the time, there was still no clear understanding of how additional anatomical parameters could contribute to symptoms and mechanical hip joint loading, aside from the cam morphology. Nevertheless, the early ideas brought into the discussion the question of how the hip could be subjected to adverse loading conditions, directly to the bone, from the cam effect.

Multidisciplinary efforts to characterize FAI remain to be warranted. To help delineate focal sub-studies and improve the understanding of cam FAI, this dissertation identified gaps in the literature. Upon closer observations, adverse hip joint stresses were less likely due to the actual magnitudes of the applied forces, but instead were more likely due to the combination of the cam deformity, varus neck angle, and subject-specific bone material properties, which could have affected the resultant mechanical loading directions and contact mechanics. With this in mind, anatomical and functional parameters will be crucial to help distinguish asymptomatic individuals and should be implemented towards developing screening programs – in efforts to predict hips that will be at risk of early symptoms. The combined effects of the cam morphology and varus neck may induce higher stresses into the subchondral bone during larger hip motions. This would increase the likelihood of early pain associated with FAI. Although it is possible that an asymptomatic cam deformity can remain subclinical, while predisposing to early subchondral bone stiffening, hips with an asymptomatic morphology and varus neck angle may be at greater risks of labral tears and degeneration.

---

[1] Ng KCG, Rouhi G, Lamontagne M, Beaulé PE. The mechanisms that initiate femoroacetabular impingement – can Wolff's law explain FAI? In proceedings of *Bioengineering 08*. 2008. Imperial College London, UK.

Ongoing research will examine the functional outcomes of asymptomatic participants, to observe how different natural histories and the role of soft tissues (*i.e.*, capsular ligaments and muscles) will influence the progression of symptoms. In efforts to delay surgery and preserve the inherent stability of the native hip, physical examinations and additional anatomical parameters (*i.e.*, femoral neck angles and cam deformity parameters) should be observed early, prior to the onset of symptoms. With the decreased neck angle in mind, other treatment options such as physiotherapy, abductors and psoas muscle training and recruitment strategies should be considered.

Although the research question of "*what are the effects of cam FAI on mechanical hip joint loading?*" is still elusive, the overall benefit taken from the present research work is the characterization of the pathoanatomical aspects associated with cartilage damage and the clarification of the causal relationship between FAI and the prevalence of osteoarthritis. A better understanding of the interaction between the joint morphology, function, and mechanical stimuli could possibly lead to an improved screening process to detect the progression of a cam FAI and provide clinicians the indications on where initial chondrolabral or cartilage damage could occur. Early recognition could help reduce hip osteoarthritis cases and, thus the number of hip arthroplasty surgeries.

10.4 References

1. Albers CE, Steppacher SD, Haefeli PC, Werlen S, Hanke MS, Siebenrock KA, Tannast M. Twelve percent of hips with a primary cam deformity exhibit a slip-like morphology resembling sequelae of slipped capital femoral epiphysis. *Clin Orthop Relat Res*. 2015;473:1212-1223.
2. Albers CE, Steppacher SD, Schwab JM, Tannast M, Siebenrock KA. Relative femoral neck lengthening improves pain and hip function in proximal femoral deformities with a high-riding trochanter. *Clin Orthop Relat Res*. 2015;473:1378-1387.
3. Anderson AE, Ellis BJ, Maas SA, Peters CL, Weiss JA. Validation of finite element predictions of cartilage contact pressure in the human hip joint. *J Biomech Eng*. 2008;130:051008.
4. Anderson AE, Ellis BJ, Maas SA, Weiss JA. Effects of idealized joint geometry on finite element predictions of cartilage contact stresses in the hip. *J Biomech*. 2010;43:1351-1357.
5. Anwander H, Melkus G, Rakhra KS, Beaule PE. T1rho MRI detects cartilage damage in asymptomatic individuals with a cam deformity. *J Orthop Res*. 2016;34:1004-1009.
6. Ateshian GA, Ellis BJ, Weiss JA. Equivalence between short-time biphasic and incompressible elastic material responses. *J Biomech Eng*. 2007;129:405-412.
7. Ateshian GA, Henak CR, Weiss JA. Toward patient-specific articular contact mechanics. *J Biomech*. 2015;48:779-786.
8. Bardakos NV. Hip impingement: beyond femoroacetabular. *J Hip Preserv Surg*. 2015;2:206-223.
9. Beck M, Kalhor M, Leunig M, Ganz R. Hip morphology influences the pattern of damage to the acetabular cartilage: femoroacetabular impingement as a cause of early osteoarthritis of the hip. *J Bone Joint Surg Br*. 2005;87:1012-1018.
10. Bedi A, Dolan M, Leunig M, Kelly BT. Static and Dynamic Mechanical Causes of Hip Pain. *Arthroscopy*. 2011;27:235-251.
11. Bitsakos C, Kerner J, Fisher I, Amis AA. The effect of muscle loading on the simulation of bone remodelling in the proximal femur. *J Biomech*. 2005;38:133-139.
12. Bland JM, Altman DG. Applying the right statistics: analyses of measurement studies. *Ultrasound Obstet Gynecol*. 2003;22:85-93.
13. Blankenbaker DG, Tuite MJ, Keene JS, del Rio AM. Labral injuries due to iliopsoas impingement: can they be diagnosed on MR arthrography? *AJR Am J Roentgenol*. 2012;199:894-900.
14. Buchan LL, Zhang H, Konan S, Heaslip I, Ratzlaff CR, Wilson DR. Open-MRI measures of cam intrusion for hips in an anterior impingement position relate to acetabular contact force. *J Orthop Res*. 2015;34:205-216.
15. Chegini S, Beck M, Ferguson SJ. The effects of impingement and dysplasia on stress distributions in the hip joint during sitting and walking: a finite element analysis. *J Orthop Res*. 2009;27:195-201.
16. Dang T, Beaulé PE, Frei H, Speirs A. Acetabular Bone Density Decreases Following Surgical Correction of FAI Deformities. In proceedigs of *Orthopaedic Research Society Annual Meeting*. 2016. Orlando, FL, USA.
17. Dodds MK, McCormack D, Mulhall KJ. Femoroacetabular impingement after slipped capital femoral epiphysis: does slip severity predict clinical symptoms? *J Pediatr Orthop*. 2009;29:535-539.
18. Domb BG, Shindle MK, McArthur B, Voos JE, Magennis EM, Kelly BT. Iliopsoas impingement: a newly identified cause of labral pathology in the hip. *Hss J*. 2011;7:145-150.
19. Fernandez J, Sartori M, Lloyd D, Munro J, Shim V. Bone remodelling in the natural acetabulum is influenced by muscle force-induced bone stress. *Int J Numer Method Biomed Eng*. 2014;30:28-41.
20. Fishkin Z, Armstrong DG, Shah H, Patra A, Mihalko WM. Proximal femoral physis shear in slipped capital femoral epiphysis--a finite element study. *J Pediatr Orthop*. 2006;26:291-294.
21. Goodman DA, Feighan JE, Smith AD, Latimer B, Buly RL, Cooperman DR. Subclinical slipped capital femoral epiphysis. Relationship to osteoarthrosis of the hip. *J Bone Joint Surg Am*. 1997;79:1489-1497.

22. Gregory JS, Waarsing JH, Day J, Pols HA, Reijman M, Weinans H, Aspden RM. Early identification of radiographic osteoarthritis of the hip using an active shape model to quantify changes in bone morphometric features: can hip shape tell us anything about the progression of osteoarthritis? *Arthritis Rheum*. 2007;56:3634-3643.

23. Harris MD, Anderson AE, Henak CR, Ellis BJ, Peters CL, Weiss JA. Finite element prediction of cartilage contact stresses in normal human hips. *J Orthop Res*. 2012;30:1133-1139.

24. Hartofilakidis G, Bardakos NV, Babis GC, Georgiades G. An examination of the association between different morphotypes of femoroacetabular impingement in asymptomatic subjects and the development of osteoarthritis of the hip. *J Bone Joint Surg Br*. 2011;93:580-586.

25. Hellwig FL, Tong J, Hussell JG. Hip joint degeneration due to cam impingement: a finite element analysis. *Comput Methods Biomech Biomed Engin*. 2016;19:41-48.

26. Henak CR, Abraham CL, Anderson AE, Maas SA, Ellis BJ, Peters CL, Weiss JA. Patient-specific analysis of cartilage and labrum mechanics in human hips with acetabular dysplasia. *Osteoarthritis Cartilage*. 2014;22:210-217.

27. Henak CR, Anderson AE, Weiss JA. Subject-specific analysis of joint contact mechanics: application to the study of osteoarthritis and surgical planning. *J Biomech Eng*. 2013;135:021003.

28. Henak CR, Ateshian GA, Weiss JA. Finite element prediction of transchondral stress and strain in the human hip. *J Biomech Eng*. 2014;136:021021.

29. Henak CR, Carruth ED, Anderson AE, Harris MD, Ellis BJ, Peters CL, Weiss JA. Finite element predictions of cartilage contact mechanics in hips with retroverted acetabula. *Osteoarthritis Cartilage*. 2013;21:1522-1529.

30. Jorge JP, Simoes FM, Pires EB, Rego PA, Tavares DG, Lopes DS, Gaspar A. Finite element simulations of a hip joint with femoroacetabular impingement. *Comput Methods Biomech Biomed Engin*. 2014;17:1275-1284.

31. Kalisvaart MM, Safran MR. Microinstability of the hip—it does exist etiology, diagnosis and treatment. 2015;2:123-135.

32. Lamontagne M, Brisson N, Kennedy MJ, Beaule PE. Preoperative and postoperative lower-extremity joint and pelvic kinematics during maximal squatting of patients with cam femoro-acetabular impingement. *J Bone Joint Surg Am*. 2011;93 Suppl 2:40-45.

33. Lamontagne M, Kennedy MJ, Beaule PE. The effect of cam FAI on hip and pelvic motion during maximum squat. *Clin Orthop Relat Res*. 2009;467:645-650.

34. Lewis CL, Sahrmann SA, Moran DW. Effect of hip angle on anterior hip joint force during gait. *Gait Posture*. 2010;32:603-607.

35. Macirowski T, Tepic S, Mann RW. Cartilage stresses in the human hip joint. *J Biomech Eng*. 1994;116:10-18.

36. Mantovani G, *Hip Joint Contact Load and Muscle Force in Femoroacetabular Impingement Population*, 2016, University of Ottawa: Ottawa. p. 182.

37. Maquer G, Burki A, Nuss K, Zysset PK, Tannast M. Head-Neck Osteoplasty has Minor Effect on the Strength of an Ovine Cam-FAI Model: In Vitro and Finite Element Analyses. *Clin Orthop Relat Res*. 2016;

38. Martin HD, Savage A, Braly BA, Palmer IJ, Beall DP, Kelly B. The function of the hip capsular ligaments: a quantitative report. *Arthroscopy*. 2008;24:188-195.

39. McGuffin WS, Melkus G, Rakhra KS, Beaule PE. Is the contralateral hip at risk in patients with unilateral symptomatic cam femoroacetabular impingement? A quantitative T1rho MRI study. *Osteoarthritis Cartilage*. 2015;23:1337-1342.

40. Mendis MD, Wilson SJ, Hayes DA, Watts MC, Hides JA. Hip flexor muscle size, strength and recruitment pattern in patients with acetabular labral tears compared to healthy controls. *Man Ther*. 2014;19:405-410.

41. Myers CA, Register BC, Lertwanich P, Ejnisman L, Pennington WW, Giphart JE, LaPrade RF, Philippon MJ. Role of the acetabular labrum and the iliofemoral ligament in hip stability: an in vitro biplane fluoroscopy study. *Am J Sports Med*. 2011;39 Suppl:85S-91S.

42. Neogi T. Clinical significance of bone changes in osteoarthritis. *Ther Adv Musculoskelet Dis*. 2012;4:259-267.

43. Neumann DA. Biomechanical analysis of selected principles of hip joint protection. *Arthritis Care Res*. 1989;2:146-155.

44. Ng KCG, Rouhi G, Lamontagne M, Beaule PE. Finite Element Analysis Examining the Effects of Cam FAI on Hip Joint Mechanical Loading Using Subject-Specific Geometries During Standing and Maximum Squat. *HSS J*. 2012;8:206-212.

45. Ng KCG, Rouhi G, Lamontagne M, Beaulé PE. The mechanisms that initiate femoroacetabular impingement – can Wolff's law explain FAI? In proceedings of *Bioengineering 08*. 2008. Imperial College London, UK.

46. Radin EL, Burr DB, Caterson B, Fyhrie D, Brown TD, Boyd RD. Mechanical determinants of osteoarthrosis. *Semin Arthritis Rheum*. 1991;21:12-21.

47. Rakhra KS, Lattanzio PJ, Cardenas-Blanco A, Cameron IG, Beaule PE. Can T1-rho MRI detect acetabular cartilage degeneration in femoroacetabular impingement?: a pilot study. *J Bone Joint Surg Br*. 2012;94:1187-1192.

48. Ranawat A, Schulz B, Baumbach S, Meftah M, Ganz R, Leunig M. Radiographic Predictors of Hip Pain in Femoroacetabular Impingement. *HSS J*. 2011;7:115-119.

49. Redmond JM, Gupta A, Hammarstedt JE, Stake CE, Dunne KF, Domb BG. Labral injury: radiographic predictors at the time of hip arthroscopy. *Arthroscopy*. 2015;31:51-56.

50. Rudman KE, Aspden RM, Meakin JR. Compression or tension? The stress distribution in the proximal femur. *Biomed Eng Online*. 2006;5:12.

51. Russell ME, Shivanna KH, Grosland NM, Pedersen DR. Cartilage contact pressure elevations in dysplastic hips: a chronic overload model. *J Orthop Surg Res*. 2006;1:6.

52. Sanchez Egea AJ, Valera M, Parraga Quiroga JM, Proubasta I, Noailly J, Lacroix D. Impact of hip anatomical variations on the cartilage stress: a finite element analysis towards the biomechanical exploration of the factors that may explain primary hip arthritis in morphologically normal subjects. *Clin Biomech*. 2014;29:444-450.

53. Siebenrock KA, Fiechter R, Tannast M, Mamisch TC, von Rechenberg B. Experimentally induced cam impingement in the sheep hip. *J Orthop Res*. 2013;31:580-587.

54. Siebenrock KA, Kienle KP, Steppacher SD, Tannast M, Mamisch TC, von Rechenberg B. Biochemical MRI predicts hip osteoarthritis in an experimental ovine femoroacetabular impingement model. *Clin Orthop Relat Res*. 2015;473:1318-1324.

55. Siebenrock KA, Wahab KH, Werlen S, Kalhor M, Leunig M, Ganz R. Abnormal extension of the femoral head epiphysis as a cause of cam impingement. *Clin Orthop Relat Res*. 2004;54-60.

56. Smith MV, Costic RS, Allaire R, Schilling PL, Sekiya JK. A biomechanical analysis of the soft tissue and osseous constraints of the hip joint. *Knee Surg Sports Traumatol Arthrosc*. 2014;22:946-952.

57. Speirs AD, Beaule PE, Ferguson SJ, Frei H. Stress distribution and consolidation in cartilage constituents is influenced by cyclic loading and osteoarthritic degeneration. *J Biomech*. 2014;47:2348-2353.

58. Speirs AD, Beaule PE, Rakhra KS, Schweitzer ME, Frei H. Increased acetabular subchondral bone density is associated with cam-type femoroacetabular impingement. *Osteoarthritis Cartilage*. 2013;21:551-558.

59. Sussman T, Bathe KJ. Studies of finite element procedures - stress band plots and the evaluation of finite element meshes. *Eng Comput*. 1986;3:178-191.

60. Tibor LM, Leunig M. The pathoanatomy and arthroscopic management of femoroacetabular impingement. *Bone Joint Res*. 2012;1:245-257.

61. Valente G, Taddei F, Jonkers I. Influence of weak hip abductor muscles on joint contact forces during normal walking: probabilistic modeling analysis. *J Biomech*. 2013;46:2186-2193.

62. van Arkel RJ, Amis AA, Jeffers JR. The envelope of passive motion allowed by the capsular ligaments of the hip. *J Biomech*. 2015;48:3803-3809.

63. van Arkel RJ, Modenese L, Phillips AT, Jeffers JR. Hip abduction can prevent posterior edge loading of hip replacements. *J Orthop Res*. 2013;31:1172-1179.

64. Viceconti M, Olsen S, Nolte LP, Burton K. Extracting clinically relevant data from finite element simulations. *Clin Biomech (Bristol, Avon)*. 2005;20:451-454.

65. Wesseling M, de Groote F, Meyer C, Corten K, Simon JP, Desloovere K, Jonkers I. Gait alterations to effectively reduce hip contact forces. *J Orthop Res*. 2015;33:1094-1102.

66. Wesseling M, Meyer C, de Groote F, Corten K, Simon JP, Desloovere K, Jonkers I. Gait alterations can reduce the risk of edge loading. *J Orthop Res*. 2016;34:1069-1076.

67. Wilson DR, McWalter EJ, Johnston JD. The measurement of joint mechanics and their role in osteoarthritis genesis and progression. *Rheum Dis Clin North Am*. 2013;39:21-44.

68. Yoshida H, Faust A, Wilckens J, Kitagawa M, Fetto J, Chao EY. Three-dimensional dynamic hip contact area and pressure distribution during activities of daily living. *J Biomech*. 2006;39:1996-2004.

VI Appendix

A List of Contributions

Recognitions | Published | Submitted | Presented

Studies related to cam-type FAI during the course of the doctoral research program

Recognitions

- Best Teaser Presentation – Orthopaedics Research Society – 2016
  Hip Joint Stresses due to the Cam Deformity and Femoral Neck-Shaft Angles during Level-Walking
- Clinical Biomechanics Award Finalist – International Society of Biomechanics – 2015
  Differences in Anatomical Parameters between the Affected and Unaffected Hip in Patients with Bilateral Cam-Type Deformities
- Award for Most Outstanding Student Paper in the Academic Stream – Canadian Medical and Biological Engineering Society – 2013
  Three-dimensional modelling and squat depth to examine geometric hip joint parameters of cam femoroacetabular impingement
- Poster Award – University of Ottawa Graduate Studies and Engineering and Research Day – 2013
  Hip joint stresses before and after corrective surgery for cam FAI

Journals

Published (in order of thesis chapters)

1. Ng KCG, Lamontagne M, Labrosse MR, Beaulé PE. Hip Joint Stresses Due to Cam-Type Femoroacetabular Impingement: A Systematic Review of Finite Element Simulations. *PLoS One*. 2016;11:e0147813.
2. Ng KCG, Lamontagne M, Adamczyk AP, Rakhra KS, Beaulé PE. Patient-specific anatomical and functional parameters provide new insights into the pathomechanism of cam FAI. *Clin Orthop Relat Res*. 2015;473:1289-1296.
3. Ng KCG, Lamontagne M, Beaulé PE. Differences in anatomical parameters between the affected and unaffected hip in patients with bilateral cam-type deformities. *Clin Biomech*. 2016;33:13-19.
4. Ng KCG, Labrosse MR, Beaulé PE, Lamontagne M. 2016. Comparison of Anatomical Parameters of Cam FAI from CT Images and from Segmented Three-Dimensional Models. *Comput Methods Biomech Biomed Eng Imaging Vis*. 2016;1-10.
5. Ng KCG, Mantovani G, Lamontagne M, Labrosse MR, Beaulé PE. 2016. Increased Hip Stresses Resulting From a Cam Deformity and Decreased Femoral Neck-Shaft Angles During Level Walking. *Clin Orthop Relat Res*. 2017;475:998-1008.

Submitted (in order of thesis chapters)

6. Ng KCG, Labrosse MR, Beaulé PE, Lamontagne M. Comparison of Hip Joint Stresses from Conventional Material Modelling Parameters. Prepared for submission. 2017.

7. Ng KCG, Mantovani G, Lamontagne M, Labrosse MR, Beaulé PE. Effects of Cam-Type Femoroacetabular Impingement on Subchondral Bone Stresses during Squatting. Prepared for submission. 2017.

Additional

8. Mantovani G, Ng KCG, Lamontagne M. Regression Models to Predict Hip Joint Centers in Pathological Hip Population. *Gait Posture*. 2015;48-54.

Book Chapter

9. Lamontagne M, Ng KCG, Mantovani G, Catelli DS. *Biomechanics of Femoroacetabular Impingement*. In: Doral MN, Karlsson J (Eds). Sports Injuries. Springer Berlin Heidelberg: 2016; 1-14.

Conferences

Podiums

10. Ng KCG, Lamontagne M, Catelli DS, Beaulé PE. 2016. Do Anatomical Parameters of Cam FAI Influence Hip Joint Mechanics during Level Walking? In Proceedings of the 71st Canadian Orthopaedics Association Annual Meeting.
11. Ng KCG, Mantovani G, Lamontagne M, Labrosse MR, Beaulé PE. 2016. Hip Joint Stresses due to the Cam Deformity and Femoral Neck-Shaft Angles during Level-Walking. In Proceedings of the Orthopaedic Research Society 2016 Annual Meeting. Orlando, FL, USA.
12. Beaulé PE, Ng KCG, Lamontagne M. 2016. Effects of cam impingement on bone during squatting. In Proceedings of the Bernese Hip Symposium 2016. Berne, Switzerland.
13. Ng KCG, Lamontagne M, Beaulé PE. 2015. Differences in Anatomical Parameters between the Affected and Unaffected Hip in Patients with Bilateral Cam-Type Deformities. In Proceedings of the International Society of Biomechanics Conference 2015. Glasgow, Scotland.
14. Mantovani G, Ng KCG, Beaulé PE, Lamontagne M. 2015. Hip Joint Centre Models in FAI Population. In Proceedings of the International Society of Biomechanics Conference 2015. Glasgow, Scotland.
15. Ng KCG, Mantovani G, Lamontagne M, Labrosse MR, Beaulé PE. 2015. Hip Joint Stresses in Individuals with an Asymptomatic Cam Deformity during Level-Walking. In Proceedings of the Orthopaedic Research Society 2015 Annual Meeting. Las Vegas, NV, USA.
16. Ng KCG, Lamontagne M, Adamczyk AP, Rakhra KS, Beaulé PE. 2014. Discriminant Function Analysis Using Radiographic and Biomechanical Parameters in Determining At-Risk Patients with a Cam Deformity. In Proceedings of the Orthopaedic Research Society 2014 Annual Meeting. New Orleans, LA, USA.

17. Beaulé PE, Ng KCG, Lamontagne M. 2014. Biomechanical and radiographic parameters predicting symptomatic FAI. In Proceedings of the Bernese Hip Symposium 2014. Berne, Switzerland.
18. Ng KCG, Lamontagne M, Beaulé PE. 2013. Discriminant function analysis using radiographic and squat depth parameters to classify cam femoroacetabular impingement. In Proceedings of the International Society of Biomechanics Conference 2013. Natal, Brazil.
19. Ng KCG, Dwyer KD, Varin D, Lamontagne M. 2013. Comparing squat kinematics and kinetics using subject-specific pelvis landmarks and hip joint centres from CT data. In Proceedings of the International Society of Biomechanics Conference 2013. Natal, Brazil.
20. Ng KCG, Dwyer KD, Lamontagne M, Beaulé PE. 2013. Hip Joint Geometry and Squat Depth to Classify Cam FAI. In Proceedings of the 68th Canadian Orthopaedic Association Annual Meeting. Winnipeg, MB, Canada.
21. Ng KCG, Lamontagne M, Labrosse MR, Beaulé PE. 2013. Three-dimensional modelling and squat depth to examine geometric hip joint parameters of cam femoroacetabular impingement. In Proceedings of the 36th Canadian Medical and Biological Engineering Society Conference. Ottawa, ON, Canada.

Posters

22. Ng KCG, Mantovani G, Lamontagne M, Labrosse MR, Beaulé PE. 2016. Hip Joint Stresses due to the Cam Deformity and Femoral Neck-Shaft Angles during Level-Walking. In Proceedings of the Orthopaedic Research Society 2016 Annual Meeting. Orlando, FL, USA.
23. Ng KCG, Mantovani G, Lamontagne M, Labrosse MR, Beaulé PE. 2016. The Effects of Cam Femoroacetabular Impingement on Subchondral Bone Stresses during Squatting. In Proceedings of the Orthopaedic Research Society 2016 Annual Meeting. Orlando, FL, USA.
24. Ng KCG, Labrosse MR, Beaulé PE, Lamontagne M. 2014. Comparison of anatomical parameters of cam femoroacetabular impingement from CT images and from segmented three-dimensional models. In Proceedings of the 7th World Congress of Biomechanics. Boston, MA, USA.
25. Lamontagne M, Ng KCG, Labrosse MR, Dwyer KD, Beaulé PE. 2013. Correlation between physical examination and pain questionnaires with radiographic parameters of cam FAI. In Proceedings of the 8th Combined Meeting of Orthopaedics Research Societies. Venice, Italy.
26. Ng KCG, Lamontagne M, Labrosse MR, Beaulé PE, 2013. Finite element analysis to examine the hip joint stresses before and after corrective FAI surgery. In Proceedings of the Orthopaedic Research Society 2013 Annual Meeting. San Antonio, TX, USA.
27. Ng KCG, Lamontagne M, Beaulé PE. 2012. Finite Element Model of Cam FAI: Examining the Stress Distributions on the Cartilage and Acetabulum during a Squat Motion. Exhibit in Proceedings of the 2012 Annual Meeting of the American Academy of Orthopaedic Surgeons. San Francisco, CA, USA.

Non-Refereed

28. Ng KCG, Lamontagne M, Labrosse MR. 2016. Examining the Influences of Cam-Type Femoroacetabular Impingement on Mechanical Hip Joint Loading. In Proceedings of MCG Seminars 2016. University of Ottawa, Ottawa, ON, Canada.
29. Ng KCG, Mantovani G, Lamontagne M, Labrosse MR, Beaulé PE. 2014. Hip Joint Stresses in Individuals with an Asymptomatic Cam Deformity during Level-Walking. In Proceedings of Hans K. Uhthoff Day 2015. The Ottawa Hospital, Ottawa, ON, Canada.
30. Ng KCG, Lamontagne M, Labrosse MR, Beaulé PE. 2014. Correlation between physical examination and questionnaires with anatomical parameters of cam FAI. In Proceedings of Hans K. Uhthoff Day 2014. The Ottawa Hospital, Ottawa, ON, Canada.
31. Mantovani G, Ng KCG, Lamontagne M, Beaulé PE. 2014. Correlation between anatomical parameters of cam FAI and muscle activity during squatting. In Proceedings of Hans K. Uhthoff Day 2014. The Ottawa Hospital, Ottawa, ON, Canada.
32. Ng KCG, Lamontagne M, Labrosse MR, Beaulé PE. 2013. Hip joint stresses before and after corrective surgery for cam FAI. Poster at the 7th Annual Graduate Studies and Engineering Research Day. University of Ottawa, Ottawa, ON, Canada.
33. Ng KCG, Lamontagne M, Labrosse MR, Rakhra KS, Beaulé PE. 2013. Discriminant function analysis using geometric hip joint and squat depth parameters to classify cam FAI. In Proceedings of Hans K. Uhthoff Day 2013. The Ottawa Hospital, Ottawa, ON, Canada.
34. Lamontagne M, Ng KCG, Beaulé PE. 2013. Anatomical and functional characterization of femoroacetabular impingement. Proceedings in the Let People Move Institute Symposium. Perugia, Italy.
35. Adamczyk AP, Ng KCG, Lamontagne M, Beaulé PE. 2013. Discriminant functional analysis of radiographic parameters in determining at-risk patients with a cam deformity. Poster at the 2013 Faculty of Medicine Research Day. The Ottawa Hospital, Ottawa, ON, Canada.
36. Ng KCG, Lamontagne M, Labrosse MR, Beaulé PE. 2012. Stress distributions in the hip before and after corrective FAI surgery. Proceedings in Hans K. Uhthoff Day 2012. The Ottawa Hospital, Ottawa, ON, Canada.

B Ethics

Ottawa Health Science Network Research Ethics Board / Conseil d'éthique de la recherche du Réseau de science de la santé d'Ottawa

RE: Protocol# - 2009537-01H **Femoroacetabular Impingement: Correlating Hip Morphology to Changes in Cartilage and Subchondral Bone**

Renewal Expiry Date - 16 August, 2016

I am pleased to inform you that your Annual Renewal Request was reviewed by the Ottawa Health Science Network Research Ethics Board (OHSN-REB) and is approved. No changes, amendments or addenda may be made in the protocol or the consent form without the OHSN-REB's review and approval.

Renewal is valid for a period of one year. Approximately one month prior to that time, a single renewal form should be sent to the REB office.

The OHSN-REB acknowledges that recruitment is closed and the study end date has been extended to August 2016.

OHSN-REB complies with the membership requirements and operates in compliance with the Tri-Council Policy Statement: Ethical Conduct for Research Involving Humans; the International Conference on Harmonization - Good Clinical Practice: Consolidated Guideline; the provisions of the Personal Health Information Protection Act 2004; and the Food and Drug Act of Health Canada and its applicable Regulations.

The OHSN-REB has reviewed and approved the clinical trial protocol and informed consent form for the trial which is to be conducted by the qualified investigator named above at the specified clinical trial site. This approval and the views of this Research Ethics Board have been documented in writing.

C Mechanical Properties

Material Tensors

Orthotropic properties representing different elastic responses to loads in the XYZ directions, can be represented by nine elastic constants in the constitutive equation:

$$\begin{matrix}\varepsilon_{xx}\\ \varepsilon_{yy}\\ \varepsilon_{zz}\\ \varepsilon_{yz}\\ \varepsilon_{zx}\\ \varepsilon_{xy}\end{matrix} = \begin{matrix}\frac{1}{E_x} & \frac{v_{yx}}{E_y} & \frac{v_{zx}}{E_z} & 0 & 0 & 0\\ \frac{v_{xy}}{E_x} & \frac{1}{E_y} & \frac{v_{zy}}{E_z} & 0 & 0 & 0\\ \frac{v_{xz}}{E_x} & \frac{v_{yz}}{E_y} & \frac{1}{E_z} & 0 & 0 & 0\\ 0 & 0 & 0 & \frac{1}{2G_{yz}} & 0 & 0\\ 0 & 0 & 0 & 0 & \frac{1}{2G_{zx}} & 0\\ 0 & 0 & 0 & 0 & 0 & \frac{1}{2G_{xy}}\end{matrix} \begin{matrix}\sigma_{xx}\\ \sigma_{yy}\\ \sigma_{zz}\\ \sigma_{yz}\\ \sigma_{zx}\\ \sigma_{xy}\end{matrix} \qquad \text{Equation C.1}$$

where E represents the elastic modulus, G represents the shear modulus, and v represents Poisson's ratio. The subscripts indicate the applied normal plane and coordinate direction, respectively. The orthotropic material model is different from the isotropic model, where the elastic modulus, shear modulus, and Poisson's ratio are independent of direction, as seen by:

$$\begin{matrix}\varepsilon_{xx}\\ \varepsilon_{yy}\\ \varepsilon_{zz}\\ \varepsilon_{yz}\\ \varepsilon_{zx}\\ \varepsilon_{xy}\end{matrix} = \frac{1}{E}\begin{matrix}1 & v & v & 0 & 0 & 0\\ v & 1 & v & 0 & 0 & 0\\ v & v & 1 & 0 & 0 & 0\\ 0 & 0 & 0 & 1+v & 0 & 0\\ 0 & 0 & 0 & 0 & 1+v & 0\\ 0 & 0 & 0 & 0 & 0 & 1+v\end{matrix} \begin{matrix}\sigma_{xx}\\ \sigma_{yy}\\ \sigma_{zz}\\ \sigma_{yz}\\ \sigma_{zx}\\ \sigma_{xy}\end{matrix} \qquad \text{Equation C.2}$$

where only two constants are needed. Various models for the articular cartilage have also been implemented in the past. Some researchers have exploited the biphasic property of cartilage considering cartilage as a poroelastic material. However, in studies looking at the articular cartilage as a whole-body layer, as opposed to focusing on the fluid exudation and intermittent hydrostatic pressures, a simplified isotropic property has often been implemented. Since quasi-static loading involves non-cyclic loads, time-dependent and viscoelastic behaviours can also be ignored.

Mechanical Stress Analysis

Many computational finite element programs provide various nodal and element solution tools for post-processing analysis. The von Mises stress analysis is frequently used to calculate nodal solutions to examine the loading conditions and equivalent stresses in the component. The corresponding failure criterion considers the squared differences of the principal stresses, then compares the equivalent stress with the material's yield stress, as stated by:

$$\frac{1}{2}[(\sigma_1 \quad \sigma_2)^2 + (\sigma_2 \quad \sigma_3)^2 + (\sigma_3 \quad \sigma_1)^2] \leq {\sigma_y}^2 \qquad \text{Equation C.3}$$

where σ_1, σ_2, σ_3 represent the principal stresses and σ_y represents the yield stress. By taking the equilibrium state of a material's distortion energy into account, the von Mises failure theory acts as a conservative failure criterion and is often used for assessing ductile engineering materials. Thus, it may be questionable to determine von Mises stresses in the innominate structure, since the hip assembly comprises of quasi-brittle bone tissues.

Alternatively, a maximum shear stress analysis can provide a less conservative account for principal stresses. Theoretically, the maximum shear stress analysis (Tresca's failure criterion) considers the differences between the maximum and minimum principal stresses. The failure criterion would require for one half of the difference between the principal stresses to be less than the yield shear stress.

Although the maximum shear stress analysis is another conventional failure criterion for ductile materials, it is less conservative in comparison with von Mises criterion. Moreover, since cartilage is mostly under shear stress, it may be more suitable to examine adverse hip loading conditions by considering principal stresses and resultant maximum shear stresses. As described in Radin and associates' work (1991), maximum shear stresses could indicate risks of adverse loading conditions leading to cartilage failure and across the cartilage-bone interface.[2]

[2] Radin EL, Burr DB, Caterson B, Fyhrie D, Brown TD, Boyd RD. Mechanical determinants of osteoarthrosis. Semin Arthritis Rheum. 1991;21:12-21.

D Bibliography

Abraham CL, Maas SA, Weiss JA, Ellis BJ, Peters CL, Anderson AE. A new discrete element analysis method for predicting hip joint contact stresses. *J Biomech*. 2013;46:1121-1127.

Agricola R, Heijboer MP, Bierma-Zeinstra SM, Verhaar JA, Weinans H, Waarsing JH. Cam impingement causes osteoarthritis of the hip: a nationwide prospective cohort study (CHECK). *Ann Rheum Dis*. 2012;72:918-923.

Agricola R, Heijboer MP, Ginai AZ, Roels P, Zadpoor AA, Verhaar JA, Weinans H, Waarsing JH. A Cam Deformity Is Gradually Acquired During Skeletal Maturation in Adolescent and Young Male Soccer Players: A Prospective Study With Minimum 2-Year Follow-up. *Am J Sports Med*. 2014.

Agricola R, Waarsing JH, Thomas GE, Carr AJ, Reijman M, Bierma-Zeinstra SM, Glyn-Jones S, Weinans H, Arden NK. Cam impingement: defining the presence of a cam deformity by the alpha angle: data from the CHECK cohort and Chingford cohort. *Osteoarthritis Cartilage*. 2014;22:218-225.

Albers CE, Steppacher SD, Haefeli PC, Werlen S, Hanke MS, Siebenrock KA, Tannast M. Twelve percent of hips with a primary cam deformity exhibit a slip-like morphology resembling sequelae of slipped capital femoral epiphysis. *Clin Orthop Relat Res*. 2015;473:1212-1223.

Albers CE, Steppacher SD, Schwab JM, Tannast M, Siebenrock KA. Relative femoral neck lengthening improves pain and hip function in proximal femoral deformities with a high-riding trochanter. *Clin Orthop Relat Res*. 2015;473:1378-1387.

Allen D, Beaule PE, Ramadan O, Doucette S. Prevalence of associated deformities and hip pain in patients with cam-type femoroacetabular impingement. *J Bone Joint Surg Br*. 2009;91:589-594.

Alonso-Rasgado T, Jimenez-Cruz D, Bailey CG, Mandal P, Board T. Changes in the stress in the femoral head neck junction after osteochondroplasty for hip impingement: A finite element study. *J Orthop Res*. 2012;30:1999-2006.

Anderson AE, Ellis BJ, Maas SA, Peters CL, Weiss JA. Validation of finite element predictions of cartilage contact pressure in the human hip joint. *J Biomech Eng*. 2008;130:051008.

Anderson AE, Ellis BJ, Maas SA, Weiss JA. Effects of idealized joint geometry on finite element predictions of cartilage contact stresses in the hip. *J Biomech*. 2010;43:1351-1357.

Anderson LA, Peters CL, Park BB, Stoddard GJ, Erickson JA, Crim JR. Acetabular cartilage delamination in femoroacetabular impingement. Risk factors and magnetic resonance imaging diagnosis. *J Bone Joint Surg Am*. 2009;91:305-313.

Anwander H, Melkus G, Rakhra KS, Beaule PE. T1rho MRI detects cartilage damage in asymptomatic individuals with a cam deformity. *J Orthop Res*. 2016;34:1004-1009.

Apprich S, Mamisch TC, Welsch GH, Bonel H, Siebenrock KA, Kim YJ, Trattnig S, Dudda M. Evaluation of articular cartilage in patients with femoroacetabular impingement (FAI) using T2* mapping at different time points at 3.0 Tesla MRI: a feasibility study. *Skeletal Radiol*. 2012;41:987-995.

Arbabi E, Chegini S, Boulic R, Tannast M, Ferguson SJ, Thalmann D. Penetration depth method--novel real-time strategy for evaluating femoroacetabular impingement. *J Orthop Res*. 2010;28:880-886.

Ateshian GA, Ellis BJ, Weiss JA. Equivalence between short-time biphasic and incompressible elastic material responses. *J Biomech Eng*. 2007;129:405-412.

Ateshian GA, Henak CR, Weiss JA. Toward patient-specific articular contact mechanics. *J Biomech*. 2015;48:779-786.

Athanasiou KA, Agarwal A, Dzida FJ. Comparative study of the intrinsic mechanical properties of the human acetabular and femoral head cartilage. *J Orthop Res*. 1994;12:340-349.

Audenaert EA, Baelde N, Huysse W, Vigneron L, Pattyn C. Development of a three-dimensional detection method of cam deformities in femoroacetabular impingement. *Skeletal Radiol*. 2011;40:921-927.

Audenaert EA, Mahieu P, Pattyn C. Three-dimensional assessment of cam engagement in femoroacetabular impingement. *Arthroscopy*. 2011;27:167-171.

Ayeni O, Chu R, Hetaimish B, Nur L, Simunovic N, Farrokhyar F, Bedi A, Bhandari M. A painful squat test provides limited diagnostic utility in CAM-type femoroacetabular impingement. *Knee Surg Sports Traumatol Arthrosc*. 2013.

Banerjee P, Mclean CR. Femoroacetabular impingement: a review of diagnosis and management. 2011;4:23-32.

Bardakos NV, Villar RN. Predictors of progression of osteoarthritis in femoroacetabular impingement: a radiological study with a minimum of ten years follow-up. *J Bone Joint Surg Br*. 2009;91:162-169.

Barton C, Salineros MJ, Rakhra KS, Beaule PE. Validity of the alpha angle measurement on plain radiographs in the evaluation of cam-type femoroacetabular impingement. *Clin Orthop Relat Res*. 2011;469:464-469.

Basso T, Klaksvik J, Syversen U, Foss OA. Biomechanical femoral neck fracture experiments--a narrative review. *Injury*. 2012;43:1633-1639.

Beaulé PE. Femoroacetabular impingement: current status of diagnosis and treatment: editorial comment. *Clin Orthop Relat Res*. 2009;467:603-604.

Beaulé P, Hynes K, Parker G, Kemp K. Can the Alpha Angle Assessment of Cam Impingement Predict Acetabular Cartilage Delamination? *Clin Orthop Rel Res*. 2012;470:3361-3367.

Beaulé PE, Kim YJ, Rakhra KS, Stelzeneder D, Brown TD. New frontiers in cartilage imaging of the hip. *Instr Course Lect*. 2012;61:253-262.

Beaulé PE, Zaragoza E, Motamedi K, Copelan N, Dorey FJ. Three-dimensional computed tomography of the hip in the assessment of femoroacetabular impingement. *J Orthop Res*. 2005;23:1286-1292.

Beck M, Kalhor M, Leunig M, Ganz R. Hip morphology influences the pattern of damage to the acetabular cartilage: femoroacetabular impingement as a cause of early osteoarthritis of the hip. *J Bone Joint Surg Br*. 2005;87:1012-1018.

Beck M, Leunig M, Parvizi J, Boutier V, Wyss D, Ganz R. Anterior femoroacetabular impingement: part II. Midterm results of surgical treatment. *Clin Orthop Relat Res*. 2004;67-73.

Bedi A, Dolan M, Leunig M, Kelly BT. Static and Dynamic Mechanical Causes of Hip Pain. *Arthroscopy*. 2011;27:235-251.

Bedi A, Thompson M, Uliana C, Magennis E, Kelly BT. Assessment of range of motion and contact zones with commonly performed physical exam manoeuvers for femoroacetabular impingement (FAI): what do these tests mean? *Hip Int*. 2013;23 Suppl 9:S27-34.

Behrens BA, Nolte I, Wefstaedt P, Stukenborg-Colsman C, Bouguecha A. Numerical investigations on the strain-adaptive bone remodelling in the periprosthetic femur: influence of the boundary conditions. *Biomed Eng Online*. 2009;8:7.

Bergmann G, Deuretzbacher G, Heller M, Graichen F, Rohlmann A, Strauss J, Duda GN. Hip contact forces and gait patterns from routine activities. *J Biomech*. 2001;34:859-871.

Bergmann G, Graichen F, Rohlmann A. Hip joint loading during walking and running, measured in two patients. *J Biomech*. 1993;26:969-990.

Bergmann G, Graichen F, Rohlmann A, Bender A, Heinlein B, Duda GN, Heller MO, Morlock MM. Realistic loads for testing hip implants. 2010;20:65-75.

Bitsakos C, Kerner J, Fisher I, Amis AA. The effect of muscle loading on the simulation of bone remodelling in the proximal femur. J Biomech. 2005;38:133-139.

Bland JM, Altman DG. Applying the right statistics: analyses of measurement studies. *Ultrasound Obstet Gynecol*. 2003;22:85-93.

Bland JM, Altman DG. A note on the use of the intraclass correlation coefficient in the evaluation of agreement between two methods of measurement. *Comput Biol Med*. 1990;20:337-340.

Bland JM, Altman DG. Statistical methods for assessing agreement between two methods of clinical measurement. *Lancet*. 1986;1:307-310.

Blankenbaker DG, Tuite MJ, Keene JS, del Rio AM. Labral injuries due to iliopsoas impingement: can they be diagnosed on MR arthrography? *AJR Am J Roentgenol*. 2012;199:894-900.

Bombardier C, Hawker G, Mosher D, *The Impact of Arthritis in Canada: Today and Over the Next 30 Years*, 2011, Arthritis Alliance of Canada.

Botser IB, Ozoude GC, Martin DE, Siddiqi AJ, Kuppuswami S, Domb BG. Femoral anteversion in the hip: comparison of measurement by computed tomography, magnetic resonance imaging, and physical examination. *Arthroscopy*. 2012;28:619-627.

Bouma HW, Hogervorst T, Audenaert E, Krekel P, van Kampen PM. Can combining femoral and acetabular morphology parameters improve the characterization of femoroacetabular impingement? Clin Orthop Relat Res. 2015;473:1396-1403.

Brand RA. Joint contact stress: a reasonable surrogate for biological processes? *Iowa Orthop J*. 2005;25:82-94.

Brisson N, Lamontagne M, Kennedy MJ, Beaulé PE. The effects of cam femoroacetabular impingement corrective surgery on lower-extremity gait biomechanics. *Gait Posture*. 2013;37:258-263.

Buchan LL, Zhang H, Konan S, Heaslip I, Ratzlaff CR, Wilson DR. Open-MRI measures of cam intrusion for hips in an anterior impingement position relate to acetabular contact force. *J Orthop Res*. 2015;34:205-216.

Buchanan TS, Lloyd DG, Manal K, Besier TF. Estimation of muscle forces and joint moments using a forward-inverse dynamics model. *Med Sci Sports Exerc*. 2005;37:1911-1916.

Buchanan TS, Lloyd DG, Manal K, Besier TF. Neuromusculoskeletal modeling: estimation of muscle forces and joint moments and movements from measurements of neural command. *J Appl Biomech*. 2004;20:367-395.

Cadet ER, Babatunde OM, Gorroochurn P, Chan AK, Stancato-Pasik A, Brown M, Johnson S, Kaiser PB, Gardner TR, Ayeni OR. Inter- and intra-observer agreement of femoroacetabular impingement (FAI) parameters comparing plain radiographs and advanced, 3D computed tomographic (CT)-generated hip models in a surgical patient cohort. *Knee Surg Sports Traumatol Arthrosc*. 2014;1-8.

Cardiff P, Karac A, Fitzpatrick D, Flavin R, Ivankovic A. Development of a Hip Joint Model for Finite Volume Simulations. *J Biomech Eng*. 2013;136:011006.

Carter DR, Hayes WC. The compressive behavior of bone as a two-phase porous structure. *J Bone Joint Surg Am*. 1977;59:954-962.

Casartelli NC, Bizzini M, Maffiuletti NA, Lepers R, Leunig M. Rehabilitation and return to sport after bilateral open surgery for femoroacetabular impingement in a professional ice hockey player: A case report. Phys Ther Sport. 2014.

Chakraverty JK, Sullivan C, Gan C, Narayanaswamy S, Kamath S. Cam and pincer femoroacetabular impingement: CT findings of features resembling femoroacetabular impingement in a young population without symptoms. *AJR Am J Roentgenol*. 2013;200:389-395.

Chegini S, Beck M, Ferguson SJ. The effects of impingement and dysplasia on stress distributions in the hip joint during sitting and walking: a finite element analysis. *J Orthop Res*. 2009;27:195-201.

Clohisy JC, Baca G, Beaule PE, Kim YJ, Larson CM, Millis MB, Podeszwa DA, Schoenecker PL, Sierra RJ, Sink EL, Sucato DJ, Trousdale RT, Zaltz I. Descriptive epidemiology of femoroacetabular impingement: a North American cohort of patients undergoing surgery. *Am J Sports Med*. 2013;41:1348-1356.

Clohisy JC, Knaus ER, Hunt DM, Lesher JM, Harris-Hayes M, Prather H. Clinical presentation of patients with symptomatic anterior hip impingement. *Clin Orthop Relat Res*. 2009;467:638-644.

Clohisy JC, McClure JT. Treatment of anterior femoroacetabular impingement with combined hip arthroscopy and limited anterior decompression. *Iowa Orthop J*. 2005;25:164-171.

Clohisy JC, St John LC, Schutz AL. Surgical treatment of femoroacetabular impingement: a systematic review of the literature. *Clin Orthop Relat Res*. 2010;468:555-564.

Cohen J. Statistical Power Analysis for the Behavioural Sciences. 2nd ed. Hillsdale, NJ. Lawrence Erlbaum Associates. 1988.

Couteau B, Hobatho MC, Darmana R, Brignola JC, Arlaud JY. Finite element modelling of the vibrational behaviour of the human femur using CT-based individualized geometrical and material properties. *J Biomech*. 1998;31:383-386.

Crowninshield RD, Brand RA. A physiologically based criterion of muscle force prediction in locomotion. *J Biomech*. 1981;14:793-801.

Dandachli W, Islam SU, Liu M, Richards R, Hall-Craggs M, Witt J. Three-dimensional CT analysis to determine acetabular retroversion and the implications for the management of femoro-acetabular impingement. *J Bone Joint Surg Br*. 2009;91:1031-1036.

Dandachli W, Ul Islam S, Tippett R, Hall-Craggs MA, Witt JD. Analysis of acetabular version in the native hip: comparison between 2D axial CT and 3D CT measurements. *Skeletal Radiol*. 2011;40:877-883.

Dang T, Beaulé PE, Frei H, Speirs A. Acetabular Bone Density Decreases Following Surgical Correction of FAI Deformities. In proceedings of *Orthopaedic Research Society Annual Meeting*. 2016. Orlando, FL, USA.

Davis RB, Ounpuu S, Tyburski D, Gage JR. A gait analysis data collection and reduction technique. *Hum Mov Sci*. 1991;10:575-587.

Davy DT, Kotzar GM, Brown RH, Heiple KG, Goldberg VM, Heiple KG, Jr., Berilla J, Burstein AH. Telemetric force measurements across the hip after total arthroplasty. *J Bone Joint Surg Am*. 1988;70:45-50.

Day WH, Swanson SA, Freeman MA. Contact pressures in the loaded human cadaver hip. *J Bone Joint Surg Br*. 1975;57:302-313.

de Sa D, Urquhart N, Philippon M, Ye JE, Simunovic N, Ayeni OR. Alpha angle correction in femoroacetabular impingement. *Knee Surg Sports Traumatol Arthrosc*. 2014;22:812-821.

Delp SL, Anderson FC, Arnold AS, Loan P, Habib A, John CT, Guendelman E, Thelen DG. OpenSim: open-source software to create and analyze dynamic simulations of movement. *IEEE Trans Biomed Eng*. 2007;54:1940-1950.

Delp SL, Loan JP, Hoy MG, Zajac FE, Topp EL, Rosen JM. An interactive graphics-based model of the lower extremity to study orthopaedic surgical procedures. *IEEE Trans Biomed Eng*. 1990;37:757-767.

Dodds MK, McCormack D, Mulhall KJ. Femoroacetabular impingement after slipped capital femoral epiphysis: does slip severity predict clinical symptoms? *J Pediatr Orthop*. 2009;29:535-539.

Doherty M, Courtney P, Doherty S, Jenkins W, Maciewicz RA, Muir K, Zhang W. Nonspherical femoral head shape (pistol grip deformity), neck shaft angle, and risk of hip osteoarthritis: a case-control study. *Arthritis Rheum*. 2008;58:3172-3182.

Domb BG, Shindle MK, McArthur B, Voos JE, Magennis EM, Kelly BT. Iliopsoas impingement: a newly identified cause of labral pathology in the hip. *HSS J*. 2011;7:145-150.

Dudda M, Albers C, Mamisch T, Werlen S, Beck M. Do Normal Radiographs Exclude Asphericity of the Femoral Head-Neck Junction? *Clin Orthop Relat Res*. 2009;467:651-659.

Dwyer KD, *The Effect of Femoroacetabular Deformity on Lower-Limb Joint Biomechanics during Daily Functional Tasks*, in *School of Human Kinetics*2014, University of Ottawa: Ottawa. p. 109.

Eijer H, Myers SR, Ganz R. Anterior femoroacetabular impingement after femoral neck fractures. *J Orthop Trauma*. 2001;15:475-481.

Ejnisman L, Philippon M, Lertwanich P, Pennock A, Herzog M, Briggs K, Ho C. Relationship Between Femoral Anteversion and Findings in Hips With Femoroacetabular Impingement. *Orthopedics*. 2013;36:e293-300.

Erdemir A, McLean S, Herzog W, van den Bogert AJ. Model-based estimation of muscle forces exerted during movements. *Clin Biomech (Bristol, Avon)*. 2007;22:131-154.

Ergen FB, Vudali S, Sanverdi E, Dolgun A, Aydingoz U. CT assessment of asymptomatic hip joints for the background of femoroacetabular impingement morphology. *Diagn Interv Radiol*. 2013;

Fabricant PD, Fields KG, Taylor SA, Magennis E, Bedi A, Kelly BT. The effect of femoral and acetabular version on clinical outcomes after arthroscopic femoroacetabular impingement surgery. J Bone Joint Surg Am. 2015;97:537-543.

Ferguson SJ, Bryant JT, Ganz R, Ito K. The acetabular labrum seal: a poroelastic finite element model. *Clin Biomech (Bristol, Avon)*. 2000;15:463-468.

Ferguson SJ, Bryant JT, Ganz R, Ito K. An in vitro investigation of the acetabular labral seal in hip joint mechanics. *J Biomech*. 2003;36:171-178.

Ferguson SJ, Bryant JT, Ganz R, Ito K. The influence of the acetabular labrum on hip joint cartilage consolidation: a poroelastic finite element model. *J Biomech*. 2000;33:953-960.

Fernandez J, Sartori M, Lloyd D, Munro J, Shim V. Bone remodelling in the natural acetabulum is influenced by muscle force-induced bone stress. *Int J Numer Method Biomed Eng*. 2014;30:28-41.

Fishkin Z, Armstrong DG, Shah H, Patra A, Mihalko WM. Proximal femoral physis shear in slipped capital femoral epiphysis--a finite element study. *J Pediatr Orthop*. 2006;26:291-294.

Fornaro J, Székely G, Harders M, *Semi-automatic Segmentation of Fractured Pelvic Bones for Surgical Planning*, in *Biomedical Simulation*, F. Bello and S. Cotin, Editors. 2010, Springer Berlin Heidelberg. p. 82-89.

Fu M, Xiang S, Zhang Z, Huang G, Liu J, Duan X, Yang Z, Wu P, Liao W. The biomechanical differences of rotational acetabular osteotomy, Chiari osteotomy and shelf procedure in developmental dysplasia of hip. *BMC Musculoskelet Disord*. 2014;15:47.

Ganz R, Leunig M, Leunig-Ganz K, Harris WH. The etiology of osteoarthritis of the hip: an integrated mechanical concept. *Clin Orthop Relat Res*. 2008;466:264-272.

Ganz R, Parvizi J, Beck M, Leunig M, Nötzli H, Siebenrock KA. Femoroacetabular Impingement: A Cause for Osteoarthritis of the Hip. *Clin Orthop Rel Res*. 2003;417:112-120.

Garcia JJ, Cortes DH. A nonlinear biphasic viscohyperelastic model for articular cartilage. *J Biomech*. 2006;39:2991-2998.

Genda E, Iwasaki N, Li G, MacWilliams BA, Barrance PJ, Chao EY. Normal hip joint contact pressure distribution in single-leg standing--effect of gender and anatomic parameters. *J Biomech*. 2001;34:895-905.

Gilles B, Christophe FK, Magnenat-Thalmann N, Becker CD, Duc SR, Menetrey J, Hoffmeyer P. MRI-based assessment of hip joint translations. *J Biomech*. 2009;42:1201-1205.

Goodman DA, Feighan JE, Smith AD, Latimer B, Buly RL, Cooperman DR. Subclinical slipped capital femoral epiphysis. Relationship to osteoarthrosis of the hip. *J Bone Joint Surg Am*. 1997;79:1489-1497.

Gosvig KK, Jacobsen S, Palm H, Sonne-Holm S, Magnusson E. A new radiological index for assessing asphericity of the femoral head in cam impingement. *J Bone Joint Surg Br*. 2007;89:1309-1316.

Gregory JS, Waarsing JH, Day J, Pols HA, Reijman M, Weinans H, Aspden RM. Early identification of radiographic osteoarthritis of the hip using an active shape model to quantify changes in bone morphometric features: can hip shape tell us anything about the progression of osteoarthritis? *Arthritis Rheum*. 2007;56:3634-3643.

Guevara CJ, Pietrobon R, Carothers JT, Olson SA, Vail TP. Comprehensive morphologic evaluation of the hip in patients with symptomatic labral tear. Clin Orthop Relat Res. 2006;453:277-285.

Gupta AK, Abrams GD, Nho SJ. What's New in Femoroacetabular Impingement Surgery: Will We Be Better in 2023? *Sports Health*. 2014;6:162-170.

Hack K, Di Primio G, Rakhra K, Beaule PE. Prevalence of cam-type femoroacetabular impingement morphology in asymptomatic volunteers. *J Bone Joint Surg Am*. 2010;92:2436-2444.

Haider I, Speirs A, Alnabelseya A, Beaule PE, Frei H. Femoral subchondral bone properties of patients with cam-type femoroacetabular impingement. *Osteoarthritis Cartilage*. 2016;24:1000-1006.

Hallgren KA. Computing inter-rater reliability for observational data: an overview and tutorial. *Tutor Quant Methods Psychol*. 2012;8:23-34.

Hamner SR, Seth A, Delp SL. Muscle contributions to propulsion and support during running. *J Biomech*. 2010;43:2709-2716.

Harris MD, Anderson AE, Henak CR, Ellis BJ, Peters CL, Weiss JA. Finite element prediction of cartilage contact stresses in normal human hips. *J Orthop Res*. 2012;30:1133-1139.

Harris MD, Datar M, Whitaker RT, Jurrus ER, Peters CL, Anderson AE. Statistical shape modeling of cam femoroacetabular impingement. *J Orthop Res*. 2013;31:1620-1626.

Harris MD, Kapron AL, Peters CL, Anderson AE. Correlations between the alpha angle and femoral head asphericity: Implications and recommendations for the diagnosis of cam femoroacetabular impingement. *Eur J Radiol*. 2014;83:788-796.

Harris MD, Reese SP, Peters CL, Weiss JA, Anderson AE. Three-dimensional quantification of femoral head shape in controls and patients with cam-type femoroacetabular impingement. *Ann Biomed Eng*. 2013;41:1162-1171.

Harris WH. Etiology of osteoarthritis of the hip. *Clin Orthop Relat Res*. 1986;20-33.

Hartofilakidis G, Bardakos NV, Babis GC, Georgiades G. An examination of the association between different morphotypes of femoroacetabular impingement in asymptomatic subjects and the development of osteoarthritis of the hip. *J Bone Joint Surg Br*. 2011;93:580-586.

Haviv B, O'Donnell J. Arthroscopic treatment for symptomatic bilateral cam-type femoroacetabular impingement. Orthopedics. 2010;33:874.

Heller MO, Bergmann G, Deuretzbacher G, Durselen L, Pohl M, Claes L, Haas NP, Duda GN. Musculo-skeletal loading conditions at the hip during walking and stair climbing. *J Biomech*. 2001;34:883-893.

Hellwig FL, Tong J, Hussell JG. Hip joint degeneration due to cam impingement: a finite element analysis. *Comput Methods Biomech Biomed Engin*. 2015;1-8.

Henak CR, Abraham CL, Anderson AE, Maas SA, Ellis BJ, Peters CL, Weiss JA. Patient-specific analysis of cartilage and labrum mechanics in human hips with acetabular dysplasia. *Osteoarthritis Cartilage*. 2014;22:210-217.

Henak CR, Anderson AE, Weiss JA. Subject-specific analysis of joint contact mechanics: application to the study of osteoarthritis and surgical planning. *J Biomech Eng*. 2013;135:021003.

Henak CR, Ateshian GA, Weiss JA. Finite element prediction of transchondral stress and strain in the human hip. *J Biomech Eng*. 2014;136:021021.

Henak CR, Carruth ED, Anderson AE, Harris MD, Ellis BJ, Peters CL, Weiss JA. Finite element predictions of cartilage contact mechanics in hips with retroverted acetabula. *Osteoarthritis Cartilage*. 2013;21:1522-1529.

Henak CR, Ellis BJ, Harris MD, Anderson AE, Peters CL, Weiss JA. Role of the acetabular labrum in load support across the hip joint. *J Biomech*. 2011;44:2201-2206.

Henak CR, Kapron AL, Anderson AE, Ellis BJ, Maas SA, Weiss JA. Specimen-specific predictions of contact stress under physiological loading in the human hip: validation and sensitivity studies. *Biomech Model Mechanobiol*. 2014;13:387-400.

Henriksen K, Neutzsky-Wulff AV, Bonewald LF, Karsdal MA. Local communication on and within bone controls bone remodeling. *Bone*. 2009;44:1026-1033.

Hunt MA, Guenther JR, Gilbart MK. Kinematic and kinetic differences during walking in patients with and without symptomatic femoroacetabular impingement. *Clin Biomech (Bristol, Avon)*. 2013;28:519-523.

Ilizaliturri VM, Jr., Orozco-Rodriguez L, Acosta-Rodriguez E, Camacho-Galindo J. Arthroscopic treatment of cam-type femoroacetabular impingement: preliminary report at 2 years minimum follow-up. *J Arthroplasty*. 2008;23:226-234.

Information CIfH, *Hip and Knee Replacements in Canada: Canadian Joint Replacement Registry 2014 Annual Report*, 2014: Ottawa, Ontario.

Ito K, Minka MA, 2nd, Leunig M, Werlen S, Ganz R. Femoroacetabular impingement and the cam-effect. A MRI-based quantitative anatomical study of the femoral head-neck offset. *J Bone Joint Surg Br*. 2001;83:171-176.

Jaberi FM, Parvizi J. Hip pain in young adults: femoroacetabular impingement. *J Arthroplasty*. 2007;22:37-42.

Jorge JP, Simoes FM, Pires EB, Rego PA, Tavares DG, Lopes DS, Gaspar A. Finite element simulations of a hip joint with femoroacetabular impingement. *Comput Methods Biomech Biomed Engin*. 2014;17:1275-1284.

Jung KA, Restrepo C, Hellman M, AbdelSalam H, Morrison W, Parvizi J. The prevalence of cam-type femoroacetabular deformity in asymptomatic adults. *J Bone Joint Surg Br*. 2011;93:1303-1307.

Kadaba MP, Ramakrishnan HK, Wootten ME. Measurement of lower extremity kinematics during level walking. *J Orthop Res*. 1990;8:383-392.

Kahlenberg CA, Han B, Patel RM, Deshmane PP, Terry MA. Time and Cost of Diagnosis for Symptomatic Femoroacetabular Impingement. 2014;2.

Kalisvaart MM, Safran MR. Microinstability of the hip—it does exist etiology, diagnosis and treatment. *J Hip Preserv Surg*. 2015;2:123-135.

Kang AC, Gooding AJ, Coates MH, Goh TD, Armour P, Rietveld J. Computed tomography assessment of hip joints in asymptomatic individuals in relation to femoroacetabular impingement. *Am J Sports Med*. 2010;38:1160-1165.

Kang Y, Engelke K, Kalender WA. A new accurate and precise 3-D segmentation method for skeletal structures in volumetric CT data. *IEEE Trans Med Imaging*. 2003;22:586-598.

Kappe T, Kocak T, Reichel H, Fraitzl CR. Can femoroacetabular impingement and hip dysplasia be distinguished by clinical presentation and patient history? Knee Surg Sports Traumatol Arthrosc. 2012;20:387-392.

Kapron AL, Anderson AE, Aoki SK, Phillips LG, Petron DJ, Toth R, Peters CL. Radiographic prevalence of femoroacetabular impingement in collegiate football players: AAOS Exhibit Selection. *J Bone Joint Surg Am*. 2011;93:1-10.

Kassarjian A, Brisson M, Palmer WE. Femoroacetabular impingement. *Eur J Radiol*. 2007;63:29-35.

Kennedy MJ, Lamontagne M, Beaule PE. Femoroacetabular impingement alters hip and pelvic biomechanics during gait Walking biomechanics of FAI. *Gait Posture*. 2009;30:41-44.

Kim WY, Hutchinson CE, Andrew JG, Allen PD. The relationship between acetabular retroversion and osteoarthritis of the hip. *J Bone Joint Surg Br*. 2006;88:727-729.

Khanna V, Caragianis A, Diprimio G, Rakhra K, Beaule PE. Incidence of hip pain in a prospective cohort of asymptomatic volunteers: is the cam deformity a risk factor for hip pain? *Am J Sports Med*. 2014;42:793-797.

Klaue K, Durnin CW, Ganz R. The acetabular rim syndrome. A clinical presentation of dysplasia of the hip. *J Bone Joint Surg Br*. 1991;73:423-429.

Konan S, Rayan F, Haddad FS. Is the frog lateral plain radiograph a reliable predictor of the alpha angle in femoroacetabular impingement? *J Bone Joint Surg Br*. 2010;92:47-50.

Kurrat HJ, Oberländer W. The thickness of the cartilage in the hip joint. 1978;126:145-155.

Kutty S, Schneider P, Faris P, Kiefer G, Frizzell B, Park R, Powell J. Reliability and predictability of the centre-edge angle in the assessment of pincer femoroacetabular impingement. 2012;36:505-510.

Lamontagne M, Brisson N, Kennedy MJ, Beaule PE. Preoperative and postoperative lower-extremity joint and pelvic kinematics during maximal squatting of patients with cam femoro-acetabular impingement. *J Bone Joint Surg Am*. 2011;93 Suppl 2:40-45.

Lamontagne M, Brisson N, Kennedy MJ, Beaulé PE. Preoperative and Postoperative Lower-Extremity Joint and Pelvic Kinematics During Maximal Squatting of Patients with Cam Femoro-Acetabular Impingement. *J Bone Joint Surg*. 2011;93:40-45.

Lamontagne M, Kennedy MJ, Beaule PE. The effect of cam FAI on hip and pelvic motion during maximum squat. *Clin Orthop Relat Res*. 2009;467:645-650.

Larson CM, Giveans MR. Arthroscopic management of femoroacetabular impingement: early outcomes measures. *Arthroscopy*. 2008;24:540-546.

Laude F, Boyer T, Nogier A. Anterior femoroacetabular impingement. *Joint Bone Spine*. 2007;74:127-132.

Lavigne M, Parvizi J, Beck M, Siebenrock KA, Ganz R, Leunig M. Anterior femoroacetabular impingement: part I. Techniques of joint preserving surgery. *Clin Orthop Relat Res*. 2004;61-66.

Lee J, Koh D, Ong CN. Statistical evaluation of agreement between two methods for measuring a quantitative variable. *Comput Biol Med*. 1989;19:61-70.

Lenaerts G, Bartels W, Gelaude F, Mulier M, Spaepen A, Van der Perre G, Jonkers I. Subject-specific hip geometry and hip joint centre location affects calculated contact forces at the hip during gait. *J Biomech*. 2009;42:1246-1251.

Leunig M, Beaule PE, Ganz R. The concept of femoroacetabular impingement: current status and future perspectives. *Clin Orthop Relat Res*. 2009;467:616-622.

Leunig M, Ganz R. [Femoroacetabular impingement. A common cause of hip complaints leading to arthrosis]. *Unfallchirurg*. 2005;108:9-10, 12-17.

Lewis CL, Sahrmann SA, Moran DW. Effect of hip angle on anterior hip joint force during gait. *Gait Posture*. 2010;32:603-607.

Li R, Chow M. Evaluation of reproducibility for paired functional data. 2005;93:81-101.

Li X, Yankeelov TE, Peterson TE, Gore JC, Dawant BM. Automatic nonrigid registration of whole body CT mice images. *Med Phys*. 2008;35:1507-1520.

Liechti EF, Ferguson SJ, Tannast M. Protrusio acetabuli: Joint loading with severe pincer impingement and its theoretical implications for surgical therapy. *J Orthop Res*. 2014;

Lin LI. A concordance correlation coefficient to evaluate reproducibility. Biometrics. 1989;45:255-268.

Liu H, Zhao J, Dai N, Qian H, Tang Y. Improve accuracy for automatic acetabulum segmentation in CT images. *Biomed Mater Eng*. 2014;24:3159-3177.

Lloyd DG, Besier TF. An EMG-driven musculoskeletal model to estimate muscle forces and knee joint moments in vivo. *J Biomech*. 2003;36:765-776.

Lohan DG, Seeger LL, Motamedi K, Hame S, Sayre J. Cam-type femoral-acetabular impingement: is the alpha angle the best MR arthrography has to offer? *Skeletal Radiol*. 2009;38:855-862.

Lu TW, O'Connor JJ, Taylor SJ, Walker PS. Validation of a lower limb model with in vivo femoral forces telemetered from two subjects. *J Biomech*. 1998;31:63-69.

Macirowski T, Tepic S, Mann RW. Cartilage stresses in the human hip joint. *J Biomech Eng*. 1994;116:10-18.

Mantovani G, *Hip Joint Contact Load and Muscle Force in Femoroacetabular Impingement Population*, 2016, University of Ottawa: Ottawa. p. 182.

Mantovani G, Lamontagne M. How Different Marker Sets Affect Joint Angles in Inverse Kinematics Framework. *J Biomech Eng*. 2017;139:1-7.

Mantovani G, Ng KCG, Lamontagne M. Regression Models to Predict Hip Joint Centers in Pathological Hip Population. *Gait Posture*. 2015;44:48-54.

Maquer G, Burki A, Nuss K, Zysset PK, Tannast M. Head-Neck Osteoplasty has Minor Effect on the Strength of an Ovine Cam-FAI Model: In Vitro and Finite Element Analyses. *Clin Orthop Relat Res*. 2016;

Martin HD, Savage A, Braly BA, Palmer IJ, Beall DP, Kelly B. The function of the hip capsular ligaments: a quantitative report. *Arthroscopy*. 2008;24:188-195.

Mast NH, Impellizzeri F, Keller S, Leunig M. Reliability and agreement of measures used in radiographic evaluation of the adult hip. *Clin Orthop Relat Res*. 2011;469:188-199.

McGuffin WS, Melkus G, Rakhra KS, Beaule PE. Is the contralateral hip at risk in patients with unilateral symptomatic cam femoroacetabular impingement? A quantitative T1rho MRI study. *Osteoarthritis Cartilage*. 2015;23:1337-1342.

Mechlenburg I, Nyengaard JR, Gelineck J, Soballe K. Cartilage thickness in the hip joint measured by MRI and stereology--a methodological study. *Osteoarthritis Cartilage*. 2007;15:366-371.

Mendis MD, Wilson SJ, Hayes DA, Watts MC, Hides JA. Hip flexor muscle size, strength and recruitment pattern in patients with acetabular labral tears compared to healthy controls. *Man Ther*. 2014;19:405-410.

Menschik F. The hip joint as a conchoid shape. *J Biomech*. 1997;30:971-973.

Meyer DC, Beck M, Ellis T, Ganz R, Leunig M. Comparison of six radiographic projections to assess femoral head/neck asphericity. *Clin Orthop Relat Res*. 2006;445:181-185.

Mizrahi J, Solomon L, Kaufman B, Duggan T. An experimental method for investigating load distribution in the cadaveric human hip. 1981;63-B:610-613.

Modenese L, Phillips AM. Prediction of hip contact forces and muscle activations during walking at different speeds. *Multibody Syst Dyn*. 2012;28:157-168.

Monazzam S, Bomar JD, Agashe M, Hosalkar HS. Does femoral rotation influence anteroposterior alpha angle, lateral center-edge angle, and medial proximal femoral angle? A pilot study. *Clin Orthop Relat Res*. 2013;471:1639-1645.

Morgan EF, Bayraktar HH, Keaveny TM. Trabecular bone modulus-density relationships depend on anatomic site. *J Biomech*. 2003;36:897-904.

Murray RO. The aetiology of primary osteoarthritis of the hip. *Br J Radiol*. 1965;38:810-824.

Myers CA, Register BC, Lertwanich P, Ejnisman L, Pennington WW, Giphart JE, LaPrade RF, Philippon MJ. Role of the acetabular labrum and the iliofemoral ligament in hip stability: an in vitro biplane fluoroscopy study. *Am J Sports Med*. 2011;39(Suppl):85S-91S.

Myers SR, Eijer H, Ganz R. Anterior femoroacetabular impingement after periacetabular osteotomy. *Clin Orthop Relat Res*. 1999;93-99.

Nepple JJ, Riggs CN, Ross JR, Clohisy JC. Clinical presentation and disease characteristics of femoroacetabular impingement are sex-dependent. *J Bone Joint Surg Am*. 2014;96:1683-1689.

Neogi T. Clinical significance of bone changes in osteoarthritis. *Ther Adv Musculoskelet Dis*. 2012;4:259-267.

Neumann DA. Biomechanical analysis of selected principles of hip joint protection. *Arthritis Care Res*. 1989;2:146-155.

Ng KCG, Lamontagne M, Adamczyk AP, Rakhra KS, Beaulé PE. Patient-specific anatomical and functional parameters provide new insights into the pathomechanism of cam FAI. *Clin Orthop Relat Res*. 2015;473:1289-1296.

Ng KCG, Lamontagne M, Beaulé PE. Differences in anatomical parameters between the affected and unaffected hip in patients with bilateral cam-type deformities. *Clin Biomech*. 2016;33:13-19.

Ng KCG, Lamontagne M, Labrosse MR, Beaulé PE. Comparison of anatomical parameters of cam femoroacetabular impingement to evaluate hip joint models segmented from CT data. *Comput Methods Biomech Biomed Eng Imaging Vis.* 2016;In Press:1-10.

Ng KCG, Lamontagne M, Labrosse MR, Beaulé PE. Hip joint stresses due to cam-type femoroacetabular impingement: a systematic review of finite element simulations. *PLoS One*. 2016;11:e0147813.

Ng KCG, Mantovani G, Lamontagne M, Labrosse MR, Beaulé PE. Increased Hip Stresses Resulting From a Cam Deformity and Decreased Femoral Neck-Shaft Angle During Level Walking. *Clin Orthop Relat Res*. 2016;In Press.

Ng KCG, Rouhi G, Lamontagne M, Beaulé PE. Finite Element Analysis Examining the Effects of Cam FAI on Hip Joint Mechanical Loading Using Subject-Specific Geometries During Standing and Maximum Squat. *HSS J*. 2012;8:206-212.

Ng KCG, Rouhi G, Lamontagne M, Beaulé PE. The mechanisms that initiate femoroacetabular impingement – can Wolff's law explain FAI? In proceedings of *Bioengineering 08*. 2008. Imperial College London, UK.

Nötzli HP, Wyss TF, Stoecklin CH, Schmid MR, Treiber K, Hodler J. The contour of the femoral head-neck junction as a predictor for the risk of anterior impingement. *J Bone Joint Surg Br*. 2002;84-B:556-560.

Nouh MR, Schweitzer ME, Rybak L, Cohen J. Femoroacetabular impingement: can the alpha angle be estimated? *AJR Am J Roentgenol*. 2008;190:1260-1262.

Nussbaumer S, Leunig M, Glatthorn JF, Stauffacher S, Gerber H, Maffiuletti NA. Validity and test-retest reliability of manual goniometers for measuring passive hip range of motion in femoroacetabular impingement patients. *BMC Musculoskelet Disord*. 2010;11:194.

Pandy MG. Computer modeling and simulation of human movement. *Annu Rev Biomed Eng*. 2001;3:245-273.

Park S, Hung CT, Ateshian GA. Mechanical response of bovine articular cartilage under dynamic unconfined compression loading at physiological stress levels. *Osteoarthritis Cartilage*. 2004;12:65-73.

Philippon M, Schenker M, Briggs K, Kuppersmith D. Femoroacetabular impingement in 45 professional athletes: associated pathologies and return to sport following arthroscopic decompression. *Knee Surg Sports Traumatol Arthrosc*. 2007;15:908-914.

Pollard TC, Villar RN, Norton MR, Fern ED, Williams MR, Murray DW, Carr AJ. Genetic influences in the aetiology of femoroacetabular impingement: a sibling study. *J Bone Joint Surg Br*. 2010;92:209-216.

Pollard TC, Villar RN, Norton MR, Fern ED, Williams MR, Simpson DJ, Murray DW, Carr AJ. Femoroacetabular impingement and classification of the cam deformity: the reference interval in normal hips. *Acta Orthop*. 2010;81:134-141.

Preininger B, Schmorl K, von Roth P, Winkler T, Matziolis G, Perka C, Tohtz S. Femoral Offset (3D) in Patients without Osteoarthritis - Index Values from 200 Hip Joints. *Open Orthop J*. 2012;6:578-581.

Prilutsky BI, Zatsiorsky VM. Optimization-based models of muscle coordination. *Exerc Sport Sci Rev*. 2002;30:32-38.

Radcliffe IA, Taylor M. Investigation into the affect of cementing techniques on load transfer in the resurfaced femoral head: a multi-femur finite element analysis. *Clin Biomech (Bristol, Avon)*. 2007;22:422-430.

Radin EL, Burr DB, Caterson B, Fyhrie D, Brown TD, Boyd RD. Mechanical determinants of osteoarthrosis. *Semin Arthritis Rheum*. 1991;21:12-21.

Radin EL, Paul IL, Tolkoff MJ. Subchondral bone changes in patients with early degenerative joint disease. *Arthritis Rheum*. 1970;13:400-405.

Rakhra KS, Lattanzio PJ, Cardenas-Blanco A, Cameron IG, Beaule PE. Can T1-rho MRI detect acetabular cartilage degeneration in femoroacetabular impingement? A pilot study. *J Bone Joint Surg Br*. 2012;94:1187-1192.

Rakhra KS, Sheikh AM, Allen D, Beaule PE. Comparison of MRI alpha angle measurement planes in femoroacetabular impingement. *Clin Orthop Relat Res*. 2009;467:660-665.

Ramos A, Simoes JA. Tetrahedral versus hexahedral finite elements in numerical modelling of the proximal femur. *Med Eng Phys*. 2006;28:916-924.

Ranawat A, Schulz B, Baumbach S, Meftah M, Ganz R, Leunig M. Radiographic Predictors of Hip Pain in Femoroacetabular Impingement. *HSS J*. 2011;7:115-119.

Ratzlaff C, Simatovic J, Wong H, Li L, Ezzat A, Langford D, Esdaile JM, Kennedy C, Embley P, Caves D, Hopkins T, Cibere J. Reliability of hip examination tests for femoroacetabular impingement. *Arthritis Care Res (Hoboken)*. 2013;65:1690-1696.

Redmond JM, Gupta A, Hammarstedt JE, Stake CE, Dunne KF, Domb BG. Labral injury: radiographic predictors at the time of hip arthroscopy. Arthroscopy. 2015;31:51-56.

Reynolds D, Lucas J, Klaue K. Retroversion of the acetabulum. A cause of hip pain. *J Bone Joint Surg Br*. 1999;81:281-288.

Roels P, Agricola R, Oei E, Weinans H, Campoli G, Zadpoor AA. Mechanical factors explain development of cam-type deformity. *Osteoarthritis Cartilage*. 2014;

Rothenfluh E, Zingg P, Dora C, Snedeker JG, Favre P. Influence of resection geometry on fracture risk in the treatment of femoroacetabular impingement: a finite element study. *Am J Sports Med*. 2012;40:2002-2008.

Rubin DA. Femoroacetabular impingement: fact, fiction, or fantasy? *AJR Am J Roentgenol*. 2013;201:526-534.

Rudman KE, Aspden RM, Meakin JR. Compression or tension? The stress distribution in the proximal femur. *Biomed Eng Online*. 2006;5:12.

Russell ME, Shivanna KH, Grosland NM, Pedersen DR. Cartilage contact pressure elevations in dysplastic hips: a chronic overload model. *J Orthop Surg Res*. 2006;1:6.

Rylander JH, Shu B, Andriacchi TP, Safran MR. Preoperative and postoperative sagittal plane hip kinematics in patients with femoroacetabular impingement during level walking. *Am J Sports Med*. 2011;39 Suppl:36S-42S.

Sanchez Egea AJ, Valera M, Quiroga JMP, Proubasta I, Noailly J, Lacroix D. Impact of hip anatomical variations on the cartilage stress: A finite element analysis towards the biomechanical exploration of the factors that may explain primary hip arthritis in morphologically normal subjects. *Clin Biomech*. 2014;29:444-450.

Sartori M, Reggiani M, Lloyd DG, Pagello E. A neuromusculoskeletal model of the human lower limb: towards EMG-driven actuation of multiple joints in powered orthoses. *IEEE Int Conf Rehabil Robot*. 2011;2011:5975441.

Schileo E, Dall'ara E, Taddei F, Malandrino A, Schotkamp T, Baleani M, Viceconti M. An accurate estimation of bone density improves the accuracy of subject-specific finite element models. *J Biomech*. 2008;41:2483-2491.

Schileo E, Taddei F, Malandrino A, Cristofolini L, Viceconti M. Subject-specific finite element models can accurately predict strain levels in long bones. *J Biomech*. 2007;40:2982-2989.

Shakoor N, Dua A, Thorp LE, Mikolaitis RA, Wimmer MA, Foucher KC, Fogg LF, Block JA. Asymmetric loading and bone mineral density at the asymptomatic knees of patients with unilateral hip osteoarthritis. *Arthritis Rheum*. 2011;63:3853-3858.

Shrout PE, Fleiss JL. Intraclass correlations: uses in assessing rater reliability. *Psychol Bull*. 1979;86:420-428.

Siebenrock KA, Fiechter R, Tannast M, Mamisch TC, von Rechenberg B. Experimentally induced cam impingement in the sheep hip. *J Orthop Res*. 2013;31:580-587.

Siebenrock KA, Kienle KP, Steppacher SD, Tannast M, Mamisch TC, von Rechenberg B. Biochemical MRI predicts hip osteoarthritis in an experimental ovine femoroacetabular impingement model. *Clin Orthop Relat Res*. 2015;473:1318-1324.

Siebenrock KA, Wahab KH, Werlen S, Kalhor M, Leunig M, Ganz R. Abnormal extension of the femoral head epiphysis as a cause of cam impingement. *Clin Orthop Relat Res*. 2004;54-60.

Smith MV, Costic RS, Allaire R, Schilling PL, Sekiya JK. A biomechanical analysis of the soft tissue and osseous constraints of the hip joint. *Knee Surg Sports Traumatol Arthrosc*. 2014;22:946-952.

Sparks DR, Beason DP, Etheridge BS, Alonso JE, Eberhardt AW. Contact pressures in the flexed hip joint during lateral trochanteric loading. *J Orthop Res*. 2005;23:359-366.

Speirs AD, Beaule PE, Ferguson SJ, Frei H. Stress distribution and consolidation in cartilage constituents is influenced by cyclic loading and osteoarthritic degeneration. *J Biomech*. 2014;47:2348-2353.

Speirs AD, Beaule PE, Rakhra KS, Schweitzer ME, Frei H. Bone density is higher in cam-type femoroacetabular impingement deformities compared to normal subchondral bone. *Osteoarthritis Cartilage*. 2013;21:1068-1073.

Speirs AD, Beaule PE, Rakhra KS, Schweitzer ME, Frei H. Increased acetabular subchondral bone density is associated with cam-type femoroacetabular impingement. *Osteoarthritis Cartilage*. 2013;21:551-558.

Standaert CJ, Manner PA, Herring SA. Expert opinion and controversies in musculoskeletal and sports medicine: femoroacetabular impingement. *Arch Phys Med Rehabil*. 2008;89:890-893.

Steele KM, Seth A, Hicks JL, Schwartz MS, Delp SL. Muscle contributions to support and progression during single-limb stance in crouch gait. *J Biomech*. 2010;43:2099-2105.

Stulberg S, Cordell L, Harris WH, Ramsey P, MacEwen G. *Unrecognized childhood disease: A major cause of idiopathic osteoarthritis of the hip.* in *Third Open Scientific Meeting of The Hip Society*. 1975. St. Louis, MO.

Sussman T, Bathe KJ. Studies of finite element procedures - stress band plots and the evaluation of finite element meshes. *Eng Comput*. 1986;3:178-191.

Sutter R, Dietrich TJ, Zingg PO, Pfirrmann CWA. How Useful Is the Alpha Angle for Discriminating between Symptomatic Patients with Cam-type Femoroacetabular Impingement and Asymptomatic Volunteer*Radiology*. 2012;264:514-521.

Tabachnick BG, Fidell LS. *Using Multivariate Statistics*. 5th ed. Boston, MA, USA: Pearson Education, Inc; 2007.

Taddei F, Cristofolini L, Martelli S, Gill HS, Viceconti M. Subject-specific finite element models of long bones: An in vitro evaluation of the overall accuracy. *J Biomech*. 2006;39:2457-2467.

Taddei F, Martelli S, Reggiani B, Cristofolini L, Viceconti M. Finite-element modeling of bones from CT data: sensitivity to geometry and material uncertainties. *IEEE Trans Biomed Eng*. 2006;53:2194-2200.

Taddei F, Schileo E, Helgason B, Cristofolini L, Viceconti M. The material mapping strategy influences the accuracy of CT-based finite element models of bones: an evaluation against experimental measurements. *Med Eng Phys*. 2007;29:973-979.

Tannast M, Mistry S, Steppacher SD, Reichenbach S, Langlotz F, Siebenrock KA, Zheng G. Radiographic analysis of femoroacetabular impingement with Hip2Norm-reliable and validated. *J Orthop Res*. 2008;26:1199-1205.

Tannast M, Siebenrock KA, Anderson SE. Femoroacetabular Impingement: Radiographic Diagnosis—What the Radiologist Should Know. *AJR Am J Roentgenol*. 2007;188:1540-1552.

Taylor WR, Roland E, Ploeg H, Hertig D, Klabunde R, Warner MD, Hobatho MC, Rakotomanana L, Clift SE. Determination of orthotropic bone elastic constants using FEA and modal analysis. *J Biomech*. 2002;35:767-773.

Tibor LM, Leunig M. The pathoanatomy and arthroscopic management of femoroacetabular impingement. *Bone Joint Res*. 2012;1:245-257.

Tomazevic D, Likar B, Slivnik T, Pernus F. 3-D/2-D registration of CT and MR to X-ray images. *IEEE Trans Med Imaging*. 2003;22:1407-1416.

Tonnis D, Heinecke A. Acetabular and femoral anteversion: relationship with osteoarthritis of the hip. J Bone Joint Surg Am. 1999;81:1747-1770.

Unsworth A, Dowson D, Wright V. The Frictional Behavior of Human Synovial Joints—Part I: Natural Joints. 1975;97:369-376.

Valente G, Taddei F, Jonkers I. Influence of weak hip abductor muscles on joint contact forces during normal walking: probabilistic modeling analysis. *J Biomech*. 2013;46:2186-2193.

van Arkel RJ, Amis AA, Cobb JP, Jeffers JR. The capsular ligaments provide more hip rotational restraint than the acetabular labrum and the ligamentum teres : an experimental study. *Bone Joint J*. 2015;97:484-491.

van Arkel RJ, Amis AA, Jeffers JR. The envelope of passive motion allowed by the capsular ligaments of the hip. *J Biomech*. 2015;48:3803-3809.

Viceconti M, Olsen S, Nolte LP, Burton K. Extracting clinically relevant data from finite element simulations. *Clin Biomech (Bristol, Avon)*. 2005;20:451-454.

von Eisenhart-Rothe R, Eckstein F, Muller-Gerbl M, Landgraf J, Rock C, Putz R. Direct comparison of contact areas, contact stress and subchondral mineralization in human hip joint specimens. *Anat Embryol (Berl)*. 1997;195:279-288.

Wei HJ, Liang HC, Lee MH, Huang YC, Chang Y, Sung HW. Construction of varying porous structures in acellular bovine pericardia as a tissue-engineering extracellular matrix. *Biomaterials*. 2005;26:1905-1913.

Wesseling M, de Groote F, Meyer C, Corten K, Simon JP, Desloovere K, Jonkers I. Gait alterations to effectively reduce hip contact forces. *J Orthop Res*. 2015;33:1094-1102.

Wesseling M, Meyer C, de Groote F, Corten K, Simon JP, Desloovere K, Jonkers I. Gait alterations can reduce the risk of edge loading. *J Orthop Res*. 2016;34:1069-1076.

Wilson DR, McWalter EJ, Johnston JD. The measurement of joint mechanics and their role in osteoarthritis genesis and progression. *Rheum Dis Clin North Am*. 2013;39:21-44.

Wu G, Siegler S, Allard P, Kirtley C, Leardini A, Rosenbaum D, Whittle M, D'Lima DD, Cristofolini L, Witte H, Schmid O, Stokes I. ISB recommendation on definitions of joint coordinate system of various joints for the reporting of human joint motion--part I: ankle, hip, and spine. International Society of Biomechanics. *J Biomech*. 2002;35:543-548.

Yoshida H, Faust A, Wilckens J, Kitagawa M, Fetto J, Chao EY. Three-dimensional dynamic hip contact area and pressure distribution during activities of daily living. *J Biomech*. 2006;39:1996-2004.